Physiological role of AMPAR nanoscale organization at basal state and during synaptic plasticities

Benjamin Compans

université de BORDEAUX

THÈSE PRÉSENTÉE

POUR OBTENIR LE GRADE DE

DOCTEUR DE

L'UNIVERSITÉ DE BORDEAUX

ÉCOLE DOCTORALE DES SCIENCES DE LA VIE ET DE LA SANTE

SPÉCIALITÉ NEUROSCIENCES

Par Benjamin COMPANS

Rôle physiologique de l'organisation des récepteurs AMPA à l'échelle nanométrique à l'état basal et lors des plasticités synaptiques

Sous la direction de : Eric Hosy

Soutenue le 19 Octobre 2017

Membres du jury

Stéphane Oliet	Directeur de Recherche CNRS	Président
Jean-Louis Bessereau	PU/PH Université de Lyon	Rapporteur
Sabine Levi	Directeur de Recherche CNRS	Rapporteur
Ryohei Yasuda	Directeur de Recherche Max Planck Florida Institute	Examinateur
Yukiko Goda	Directeur de Recherche Riken Brain Science Institute	Examinateur
Daniel Choquet	Directeur de Recherche CNRS	Invité

Interdisciplinary Institute for NeuroSciences (IINS)

CNRS UMR 5297

Université de Bordeaux Centre Broca Nouvelle-Aquitaine
146 Rue Léo Saignat
33076 Bordeaux (France)

Résumé

Le cerveau est formé d'un réseau complexe de neurones responsables de nos fonctions cognitives et de nos comportements. Les neurones reçoivent *via* des contacts spécialisés nommés « synapses », des signaux d'autres neurones. Le rôle de la synapse est de convertir le signal électrique du neurone afférent en un signal chimique, *via* la libération de neurotransmetteurs. Ce signal chimique est ensuite retransformé par le neurone cible en signal électrique suite à l'activation de récepteurs aux neurotransmetteurs. Cependant, un neurone reçoit des milliers de signaux codés de manière spatio-temporelle venant de divers neurones. Le mécanisme par lequel les neurones reçoivent, intègrent et transmettent ces informations est très complexe et n'est toujours pas parfaitement compris.

Dans les synapses excitatrices, les récepteurs AMPA (AMPARs) sont responsables de la transmission synaptique rapide. Les récents développements en microscopie de super résolution ont permis à la communauté scientifique de changer la vision de la transmission synaptique. Une première avancée fait suite à l'observation que les AMPARs ne sont pas distribués de façon homogène dans les synapses, mais sont organisés en nanodomaines de ~ 80 nm de diamètre contenant ~ 20 récepteurs. Ce contenu est un facteur important pour déterminer l'amplitude de la réponse synaptique. En raison de la basse affinité des AMPARs pour le glutamate, un AMPAR ne peut être activé que lorsqu'il est situé dans une zone de ~ 150 nm en face du site de libération des neurotransmetteurs. Récemment, il a été montré que les nanodomaines d'AMPARs sont situés en face de ces sites de libération, formant des nano-colonnes trans-synaptiques à l'état basal. Cette organisation précise à l'échelle nanométrique semble être un facteur clé dans l'efficacité de la transmission synaptique. Une autre avancée a été l'observation que les AMPARs diffusent à la surface des neurones et sont immobilisés à la synapse pour participer à la transmission synaptique. L'échange dynamique entre le pool diffusif d'AMPARs et les récepteurs immobilisés dans les nanodomaines participe au maintien de l'efficacité de la réponse synaptique lors de stimulations à hautes fréquences.

L'objectif de ma thèse a été de déterminer le rôle des paramètres indiqués ci-dessus sur les propriétés de la transmission synaptique, à l'état basal et au cours de phénomènes dits de plasticité synaptique. Tout d'abord, nous avons identifié le rôle crucial de la Neuroligine dans l'alignement des nanodomaines d'AMPARs avec les sites de libération du glutamate. En plus de cela, nous avons mis en évidence l'impact de cet alignement sur l'efficacité de la transmission synaptique en perturbant celui-ci. En parallèle, nous avons démontré que les AMPARs désensibilisés sont plus mobiles à la membrane plasmatique que les récepteurs ouverts ou fermés, et ce, en raison d'une diminution de leur affinité pour les sites d'immobilisation synaptiques. Nous avons montré que ce mécanisme permettait aux synapses de récupérer plus rapidement de la désensibilisation et d'assurer la fidélité de la transmission synaptique lors de stimulations à hautes fréquences. Enfin, les synapses peuvent moduler leurs intensités de réponse grâce à des mécanismes de plasticité synaptique à long terme, et plus particulièrement, la dépression à long terme (LTD) qui correspond à un affaiblissement durable de ce poids synaptique. La LTD est importante dans certains processus cognitifs et pour la flexibilité comportementale, car elle semble liée à un mécanisme de tri sélectif des synapses en fonction de leur activité. À la suite des découvertes précédentes concernant le rôle de la nano-organisation dynamique des AMPARs pour réguler le poids et la fiabilité de la transmission synaptique, j'ai décidé d'étudier leur rôle dans l'affaiblissement et la sélection des synapses. J'ai découvert que la quantité d'AMPAR par nanodomaine diminue rapidement et durablement. Cette première phase semble due à une augmentation de l'internalisation des AMPARs. Dans un deuxième temps, la mobilité des AMPARs augmente suite à une réorganisation moléculaire de la synapse. Ce changement de mobilité des AMPARs permet aux synapses déprimées de maintenir leur capacité à répondre aux signaux neuronaux à hautes fréquences. Ainsi, nous proposons que l'augmentation de la mobilité des AMPARs au cours de la LTD permet de transmettre une réponse fidèle dans les synapses stimulées à hautes fréquences et donc de sélectivement les maintenir tout en éliminant les synapses inactives.

Mots clés : transmission synaptique, récepteurs AMPA, organisation synaptique, microscopie à super-résolution, plasticité synaptique

Abstract

The brain is a complex network of interconnected neurons responsible for all our cognitive functions and behaviors. Neurons receive inputs at specialized contact zones named synapses which convert an all or none electrical signal to a chemical one, through the release of neurotransmitters. This chemical signal is then turned back in a tunable electrical signal by receptors to neurotransmitters. However, a single neuron receives thousands of inputs coming from several neurons in a spatial- and temporal-dependent manner. The precise mechanism by which neurons receive, integrate and transmit these synaptic inputs is highly complex and is still not perfectly understood.

At excitatory synapses, AMPA receptors (AMPARs) are responsible for the fast synaptic transmission. With the recent developments in super-resolution microscopy, the community has changed its vision of synaptic transmission. One breakthrough was the discovery that AMPARs are not randomly distributed at synapses but are organized in nanodomains of ~80 nm of diameter containing ~20 receptors. This content is an important factor since it will determine the intensity of the synaptic response. Due to their mM affinity for glutamate, AMPARs can only be activated when located in an area of ~150 nm in front of the neurotransmitter release site. Recently, AMPAR nanodomains have been shown to be located in front of glutamate release sites and to form trans-synaptic nanocolumns at basal state. Thus, the nanoscale organization of AMPARs regarding release sites seems to be a key parameter for the efficiency of synaptic transmission. Another breakthrough in the field was the observation that AMPARs diffuse at the cell surface and are immobilized at synapses to participate to synaptic transmission. The dynamic exchange between AMPAR diffusive pool and the receptors immobilized into the nanodomains participates to maintain the efficiency of synaptic response upon high-frequency stimulation.

The overall aim of my PhD has been to determine the role of each above listed parameters on the intimate properties of synaptic transmission both at basal state and during synaptic plasticity. First, we identified the crucial role of Neuroligin in the alignment of AMPAR nanodomains with glutamate release sites. In addition, we managed to break this alignment to understand its impact on synaptic transmission properties. In parallel, we demonstrated that, due to a decrease in their affinity for synaptic traps, desensitized AMPARs diffuse more at the plasma membrane than opened or closed receptors. This mechanism allows synapses to recover faster from desensitization and ensure the fidelity of synaptic transmission upon high-frequency release of glutamate. Finally, synapses can modulate their strength through long-term synaptic plasticity, in particular, Long-Term Depression (LTD) corresponds to a long-lasting weakening of synaptic strength and is thought to be important in some cognitive processes and behavioral flexibility through synapse selective elimination. Following the previous discoveries about the impact of AMPAR dynamic nano-organization at synapses on the regulation of the synaptic transmission strength and reliability, I decided to investigate their role in the weakening of synapses. I found that AMPAR nanodomain content drops down rapidly and this depletion lasts several minutes to hours. The initial phase seems to be due to an increase of endocytosis events, but in a second phase, AMPAR mobility is increased following a reorganization of the post-synaptic density. This change in mobility allows depressed synapses to maintain their capacity to answer to high-frequency inputs. Thus, we propose that LTD-induced increase in AMPAR mobility allows to conduct a reliable response in synapses under high-frequency stimulation and thus to selectively maintain them while eliminating the inactive ones.

Keywords: synaptic transmission, AMPA receptors, synaptic organization, super-resolution microscopy, synaptic plasticity

Acknowledgments / Remerciements

Je tiens tout d'abord à remercier l'ensemble des membres de mon jury de thèse pour le temps consacré à évaluer mon travail de thèse.

Je souhaite tout particulièrement remercier **Eric Hosy**, mon directeur de thèse, pour son soutien tout au long de ces quatre dernières années. Tu as pris le risque de me prendre en thèse après deux rencontres et je suis très heureux d'avoir fait le choix de travailler avec toi. Tu m'as permis d'évoluer tout au long de cette thèse passant d'un « piou » qui avait besoin d'être secoué à un « PIOU » qui avait compris l'importance de se prendre en main pour arriver au bout de cette thèse. Encore plus important, ton soucis de mon bien-être et des gens que tu encadres de façon générale, a rendu cette expérience agréable à vivre au quotidien. Donc encore une fois un grand merci pour ce partage exceptionnel qu'il soit purement scientifique ou personnel.

Je voudrais également exprimer toute ma reconnaissance à **Daniel Choquet** pour m'avoir accueilli au sein de son équipe de recherche. Merci pour la confiance dont tu fais preuve pour que les gens de ton équipe puissent travailler dans les meilleures conditions possibles. Cette confiance est certainement un des facteurs qui rend la vie de laboratoire au sein de ton équipe si agréable et la science plus facile.
Un grand merci à l'ensemble de l'équipe. Merci à Matthieu, Françoise, David, Rémi et Christelle pour leur présence et les discussions toujours enrichissantes. Merci également à Sara, Magalie, Léa, Emeline et Charlotte pour votre bonne humeur quotidienne, tous ces moments partagés au labo et en dehors. Merci à Julien Dupuis qui m'a suivi depuis mon stage de M1 et qui y est pour beaucoup dans l'initiation de cette thèse et pour ses nombreux conseils.
Merci également à tous les copains hors du labo (en essayant de n'oublier personne) : Freddo, Romain, Nono, Sab, Momo, Jerem, Seb, Emilie, Simon, Adrien, Max et Sosso, Alex et Mathieu.

Cette thèse ne serait pas aussi enrichissante sans des compagnons d'aventure extraordinaires, à savoir le PhD Crew. Donc merci à **Thomas** chaud chaud chaud patate, Captain **Corey**, Crazy **Mat**, **Anaïs**, **Laetitia** et **Charline**. Ces quatre années à évoluer et à traverser les mêmes épreuves ont été beaucoup plus facile ensemble … notamment la session x-fit.

Enfin, un gigantesque MERCI à **Julia, Nat', Mélanie, Amandine,** et **Andy** pour tous ces moments extraordinaires passés à vos côtés. Merci aussi de m'avoir poussé chaque jour au cours de cette thèse pour que je trouve un meilleur équilibre. Votre soutien et votre amitié permanents ont été d'une inestimable aide durant ces quatre dernières années et le seront encore pendant longtemps. Merci aussi à Fab', Romain, Gégé et Baptiste pour tous ces moments partagés.

Finalement, je tiens à dire merci à mes parents pour avoir toujours tout fait pour que j'arrive là où j'en suis et d'avoir toujours cru en mes capacités. Je sais que ça n'a pas toujours été facile mais j'espère que vous serez fiers de cet aboutissement. Merci aussi Pierre pour ton soutien régulier et éternel.

La connaissance s'acquiert par l'expérience, tout le reste n'est que de l'information.
Einstein

Abbreviations

ABP: AMPAR Binding Protein

AIS: Axon Initial Segment

AMPAR: α-Amino-3-hydroxy-5-Methyl-isoxazole-Propionic Acid Receptor

AP: Action Potential

AP2: Adaptor Protein 2

ATP: Adenosine TriPhosphate

AZ: Active Zone

Ca^{2+}: Calcium

CaMKII: Ca^{2+}/Calmodulin-dependent protein Kinase II

CNS: Central Nervous System

CP-AMPAR: Calcium-Permeable AMPAR

CTD: C-Terminal Domain

CTZ: Cyclothiazide

DIV: Day *In Vitro*

d-STORM: direct-Stochastic Optical Reconstruction Microscopy

EC50: half maximal Effective Concentration

EM: Electron Microscopy

EPSC: Excitatory Post-Synaptic Current

fEPSP: field-Excitatory Post-Synaptic Potential

GABA: γ-Amino-Butyric Acid

GKAP: Guanylate-Kinase-Associated Protein

GRIP: Glutamate Receptor Interacting Protein

GSK3: Glycogen Synthase Kinase-3

iGluRs: ionotropic Glutamate Receptors

IPSC: Inhibitory Post-Synaptic Current

KAR: Kainate Receptor

LBD: Ligand-Binding Domain

LTD: Long-Term Depression

LTP: Long-Term Potentiation

MAGUK: Membrane-Associated Guanylate Kinase

mEPSC: miniature Excitatory Post-Synaptic Current

mGluR: metabotropic Glutamate Receptor

NMDAR: N-Methyl-D-Aspartate Receptor

NSF: N-ethylmaleimide-Sensitive Factor

NTD: N-Terminal Domain

P2XR: Purinergic P2X Receptor

PALM: Photo-Activated Localization Microscopy

PICK1: Protein Interacting with C Kinase 1

PKC: Protein Kinase C

PLC: PhosphoLipase C

Pr: release probability

PP1: Protein Phosphatas 1

PP2B: Protein Phosphatase 2B or Calcineurin

PPD: Paired-Pulse Depression

PSD: Post-Synaptic Density

Q: Quantum of response

QD: Quantum Dot

RIM: Rab3-Interacting Molecule

RIM-BP: RIM-Binding Protein

SMLM: Single Molecule Localization Microscopy

SNARE: Soluble N-ethylmaleimide-sensitive-factor Attachment protein Receptor

SPT: Single-Particle Tracking

STED: Stimulated-Emission Depletion microscopy

STF: Short-Term Facilitation

STD: Short-Term Depression

STDP: Spike Timing-Dependent Plasticity

STP: Short-Term Plasticity

TARP: Transmembrane AMPAR Regulatory Protein

TMD: TransMembrane Domain

u-PAINT: universal-Point Accumulation for Imaging in Nanoscale Topography

VGCC: Voltage-Gated Calcium Channel

Table of contents

INTRODUCTION

The brain is a highly complex organ composed of ~100 billion neurons, each one connected to thousands of neuronal partners. How these neurons interact and communicate with each other to enable our behaviors, our thoughts and our memories is one of the main questions in biology. The brain is organized in several regions which have to exchange information to accomplish their various tasks. These circuits established within and between regions are highly studied and quite well identified. However, each region has its own organization as a network of interconnected and diverse neuronal and non-neuronal cells. Although non-neuronal cells are 10 times more numerous than neurons in the **C**entral **N**ervous **S**ystem (CNS), neurons are considered as the functional unit of the brain. Neurons exist in all shapes, sizes and electrical properties. Nevertheless, they all share the same principle of functioning to communicate. The transfer of information occurs at the highly specialized contact zones between two neurons named synapses (Forster and Sherrington, 1897; Ramon y Cajal, 1909). Post-synaptic neurons receive quanta of chemical information through release of neurotransmitters from pre-synaptic neurons. They convert them into small and tunable electrical signals via the receptors for neurotransmitters (inputs). Thus, the synaptic transmission can be broken down into neurotransmitter release from a pre-synaptic element or axonal bouton, diffusion of neurotransmitters across the synaptic cleft and activation of neurotransmitter receptors located on the post-synaptic element. In the CNS, there are three main types of synapses: (i) excitatory synapses for which the glutamate is the principal neurotransmitter, (ii) inhibitory synapses for which both **γ**-**A**mino-**B**utyric **A**cid (GABA) and glycine are the neurotransmitters and (iii) the neuromodulatory synapses which are of various types depending on the neuromodulator. Neurotransmitters are stored into vesicles in the pre-synapse and diffuse in the synaptic cleft once released to activate post-synaptic receptors. Binding of neurotransmitters to their specific receptors triggers currents through the post-synaptic plasma membrane, creating an **E**xcitatory or **I**nhibitory **P**ost-**S**ynaptic **C**urrent (EPSC or IPSC respectively). This signal will then propagates to the soma and be integrated in a spatial- and temporal-dependent manner. This summation of synaptic inputs will be able to generate or not an **A**ction **P**otential (AP) (output) in order to transfer the processed information to other neurons.

Briefly, APs are generated after somatic integration in a region called the **A**xon **I**nitial **S**egment (AIS) (Häusser et al., 1995; Stuart and Sakmann, 1994; Stuart et al., 1997). If the different inputs (excitatory and/or inhibitory) received from pre-synaptic neurons produced a depolarization of the post-synaptic neuron sufficient to reach a threshold, an AP will be generated in an all-or-none manner to transfer the signal to other neurons. Once the electrical

signal is created at the AIS, it propagates along the axon to reach all synapses where the information can be transferred to other neurons.

Even if multiple modifications of the AIS are responsible for the modulation of AP threshold (Grubb and Burrone, 2010), the initial neuronal input comes from synapses. The fidelity or adaptability of synaptic responses is one of the main key of network properties. Through my PhD, I have been working on the understanding of the impact of the molecular organization and dynamic of neurotransmitter receptors on both the reliability and the adaptability of the excitatory synaptic transmission.

Chapter 1
The excitatory synaptic transmission

1. The synapse

The excitatory synapse is formed by the association of a pre-synaptic axonal bouton containing vesicles filled with glutamate and a post-synaptic protrusion named dendritic spine. During spine formation, an extension of the dendrite termed filopodia is created to sense a pre-synaptic partner. Once the partner has been found, the filopodia is stabilized through interaction of adhesion proteins such as Neuroligin which binds to its pre-synaptic partner Neurexin to form a trans-synaptic complex. Then, both cellular elements recruit the molecular machinery necessary to form functional synapses (Goda and Davis, 2003). The pre- and post-synaptic membranes are separated by ~20 nm of synaptic cleft. At this contact zone, the pre-synapse organizes an area specialized in the regulation of the neurotransmitter vesicular release named **A**ctive **Z**one (AZ). It faces a post-synaptic area named **P**ost-**S**ynaptic **D**ensity (PSD) that is enriched in various proteins rendering it electron-dense as seen by electron microscopy (EM) (**Figure 1**). The PSD size varies from 200 to 800 nm of diameter and from 30 to 60 nm of thickness (Harris et al., 2013; Schikorski and Stevens, 1997; Walker et al., 2017). Spines vary greatly in their dimensions across brain regions, from 0.2-0.8 µm in the hippocampus to almost 1 mm at the Calyx of Held. As neuronal function is to integrate and deliver a simple signal to the network, neurons constantly regulate the number of pre-synaptic inputs they receive. Indeed, spines are remarkably dynamic, changing size, shape, and orientation over timescales of seconds to minutes and of hours to days as observed with live imaging studies. This structural plasticity of spine selects between useful and over numerous synapses and thus impacts the total number of synapses participating to the network activity. Neurons receive thousands of inputs coming from several pre-synaptic neurons which can burst synchronously or not. The **number of activated synapses (N)** during the transfer of information between neurons is a crucial parameter for the spatial and temporal integration of synaptic inputs and is tightly controlled all along the neuron life.

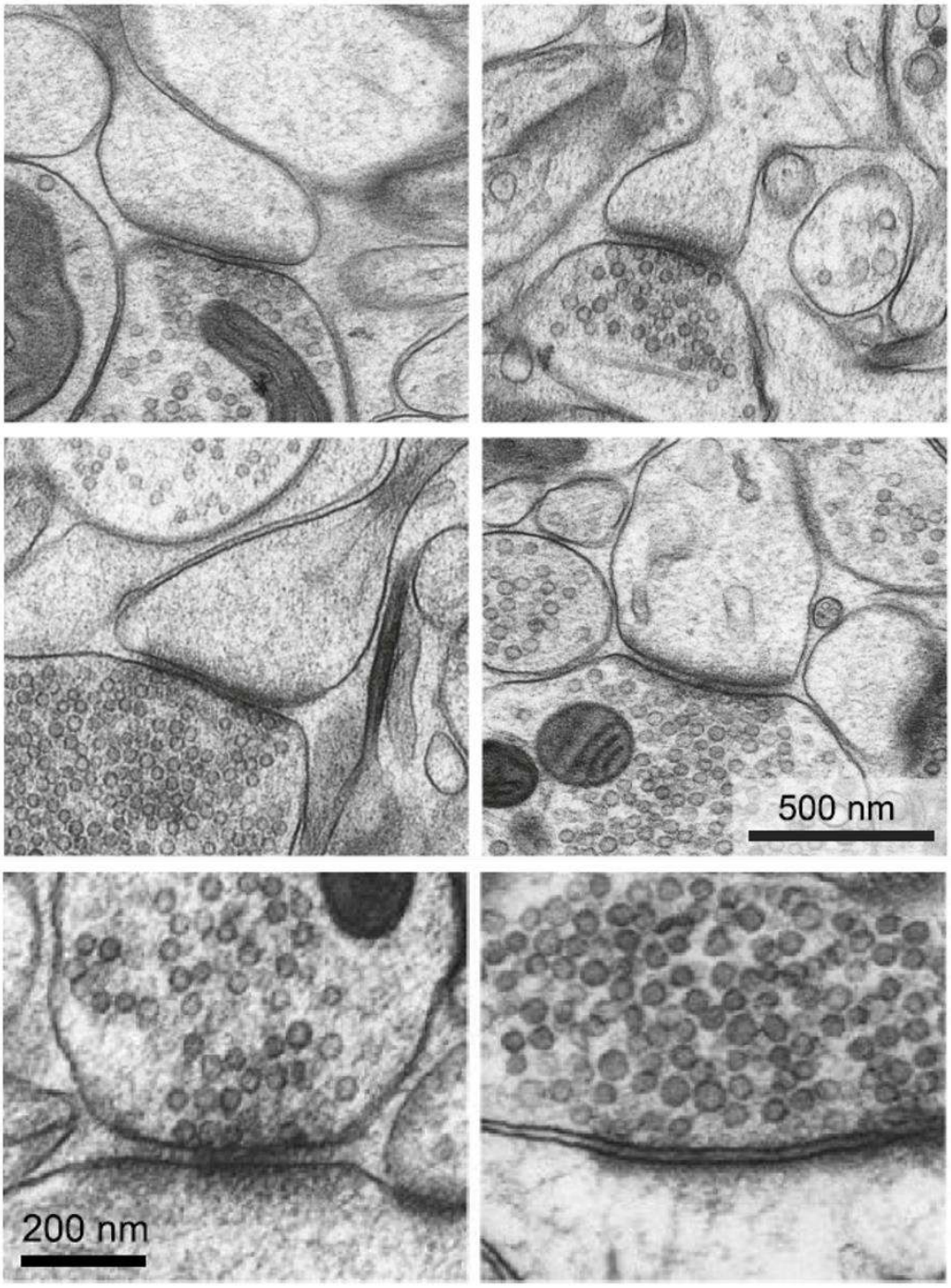

Figure 1. Cryo-EM images of CNS excitatory synapse. The pre-synaptic bouton is filled with glutamate containing vesicles which can be docked at the Active Zone which faces the Post-Synaptic Density. (From Korogod et al 2015)

2. The pre-synapse

a. Molecular organization of the axonal bouton

The pre-synaptic element formed by the axonal bouton is characterized by its high density of neurotransmitter-containing vesicles. In the 1950s, EM revealed the asymmetric organization of synapses with one compartment enriched in ~40-nm-diameter vesicles which contain neurotransmitters (Gray, 1959; Palay, 1956; Palay and Palade, 1955; De Robertis and Bennett, 1955). Synaptic vesicles are clustered into the pre-synaptic bouton and despite the fact that their organization seems to be random, three pools of vesicles can be distinguished depending on their functions. Half of the vesicles belongs to the "recycling pool" as they are able to exocytose neurotransmitters upon moderate stimulation. A part of those recycling vesicles are docked at the AZ and are thus ready to be exocytosed. This second fraction of vesicles belongs to the "readily releasable pool". Finally, the second half of synaptic vesicles forms the "reserve pool" which is left unreleased even after strong stimulation (Denker and Rizzoli, 2010; Rizzoli and Betz, 2005). The release of glutamate contained in synaptic vesicle is restricted to the AZ which contains the necessary machinery for vesicle exocytosis. The AZ has four main functions: (i) dock and prime the readily releasable pool of synaptic vesicles, (ii) recruit voltage-gated calcium channels (VGCCs) to synchronize excitation with glutamate release, (iii) localize the release of neurotransmitters in front of the PSD via trans-synaptic proteins, and (iv) organize and reorganize the pre-synapse during basal transmission and synaptic plasticity (Harris et al., 2013; Südhof, 2012).

Glutamate release at excitatory synapses depends on the fusion of synaptic vesicles with the plasma membrane through a complex mechanism which requires the action of several proteins at specific locations (**Figure 2**). The fusion between glutamatergic vesicles and the pre-synaptic membrane is operated by the SNARE (**S**oluble **N**-ethylmaleimide-sensitive-factor **A**ttachment protein **Re**ceptor) complex which tightens after the influx of Ca^{2+}, sensed by the vesicular protein synaptotagmin (Jahn and Fasshauer, 2012; Zhou et al., 2017a). Within the cytosol, several laboratories have shown using EM that synaptic vesicles are linked by filaments mainly composed of actin and myosin. Those filaments are thought to play a role in the structural organization of the pre-synapse but also in the mobilization and docking of synaptic vesicles. A role in the recycling of exocytosed vesicles has also been shown (Cole et al., 2016; Doussau and Augustine, 2000; Miki et al., 2016; Sankaranarayanan et al., 2003). Additionally,

Bassoon and Piccolo are the main pre-synaptic scaffolding proteins associated with the AZ which guide synaptic vesicles from the backfield to the AZ and are responsible for their clustering into the pre-synapse (Mukherjee et al., 2010; Südhof, 2012; Tom Dieck et al., 1998; Waites et al., 2011).

Functionally, the **R**ab3-**I**nteracting **M**olecule (RIM) has been identified as a key protein to regulate vesicle release. RIM is implicated in vesicle docking and priming through its interaction with Rab3 present at the vesicle surface. It also involved in the recruitment of VGCCs to the AZ, linking Ca^{2+} channels to docked vesicles (Geppert et al., 1997; Kaeser et al., 2011; Schoch et al., 2002). Its deletion causes a decrease in the number of docked vesicles, a decrease of calcium (Ca^{2+}) influx into the pre-synapse and an impairment of neurotransmitter release (Kaeser et al., 2011). At the AZ, RIM forms a complex with **RIM-B**inding **P**roteins (RIM-BP) to optimize the organization of the machinery for fast release (Acuna et al., 2015; Grauel et al., 2016). Interestingly, it has been shown that VGCC, mostly $Ca_v2.1$ (P/Q-type) and $Ca_v2.2$ (N-type) are recruited to the AZ by binding simultaneously RIM and RIM-BP. The deletion of both RIM and RIM-BP depletes VGCC within the pre-synapse, eliminates the tethering and priming of synaptic vesicles, and abolishes glutamate release (Acuna et al., 2016).

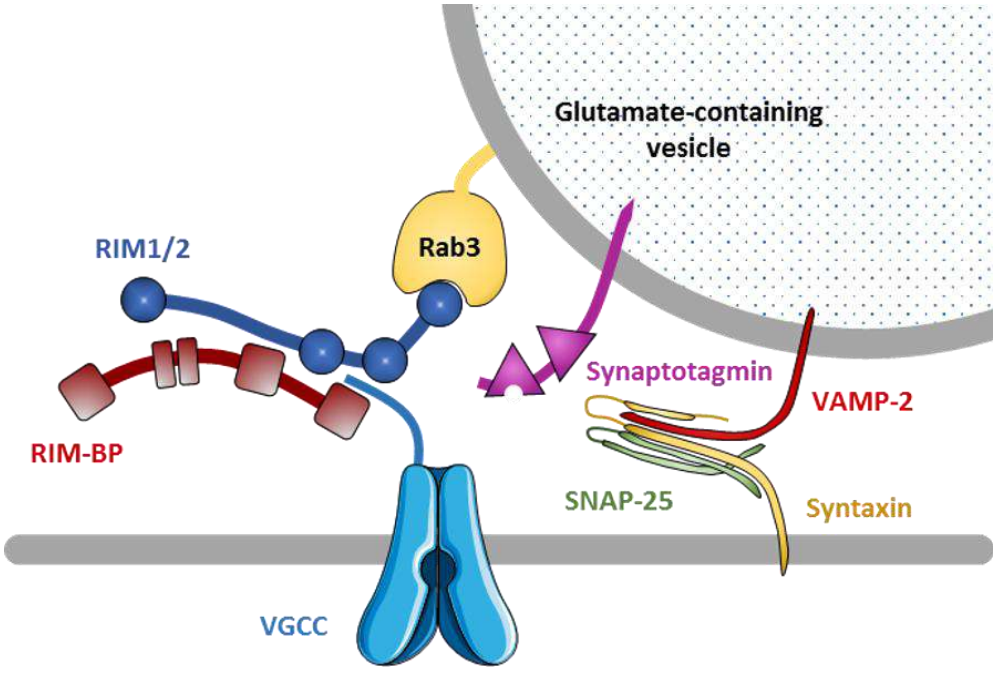

Figure 2. Glutamate release machinery. Glutamate-containing vesicle is docked at the active zone by the interaction in one hand between vesicular Rab3 and RIM1/2 RIM-BP complex and in the other hand by the SNARE complex (VAMP2, Syntaxin and SNAP-25). VGCC are transiently immobilized at the docking site by interacting with RIM1/2 and RIM-BP to allow a local influx of calcium which will be sense by Synaptotagmin to trigger the fusion of the vesicle with the plasma membrane and thus release glutamate in the synaptic cleft.

b. Pre-synaptic organization tunes synaptic transmission

In parallel to the first observation of the pre-synapse organization in the 1950s, Katz demonstrated that neurotransmitter release was at the origin of the post-synaptic electrical response (Fatt and Katz, 1951; Huxley, 2002). After confirming the notion of the AP threshold during electrical stimulation, he showed that this AP triggers the action of neurotransmitters on the post-synaptic element and introduced the notion of "quantum of action". The smallest quanta is equal to a miniature spontaneous post-synaptic current and the synaptic response is composed of a sum of quantal units (Del Castillo and Katz, 1954; Fatt and Katz, 1951). Later on, it has been shown by coupling electrophysiological recordings and EM that a single quanta is the result of a single vesicle release event at the AZ (Heuser et al., 1979). It is well known that each quanta is independent of one another and that the number of quanta released upon AP stimulation is dependent on the **release probability (P_r)** of single vesicles. This P_r coupled to the previously defined N (number of activated synapse) is a key parameter of the efficacy of neuron communication.

The P_r is highly sensitive to extracellular Ca^{2+} and Mg^{2+} concentrations (Del Castillo and Katz, 1954; McLachlan, 1978; Scimemi and Diamond, 2012). Several studies have shown that the organization of the pre-synaptic release machinery plays a role in the Pr of synaptic vesicles. Consequently, the understanding of the precise organization and regulation of this release machinery is crucial. The recent use of super-resolution microscopy start to enlighten the molecular organization of the glutamate release sites (Dani et al., 2010; Glebov et al., 2017; Tang et al., 2016). To summarize, the AZ is precisely organized to optimize the release of glutamate at specific sites. The main parameter of this organization which affect the P_r is undeniably the recruitment of VGCC at these release sites. Indeed, for neurotransmitter release to occur, the intracellular Ca^{2+} concentration must reach a threshold determined by Ca^{2+} sensors responsible for the vesicular fusion, such as synaptotagmin. The bulk of Ca^{2+} in the axonal bouton reaches about 500 nM following an AP. However the Ca^{2+} concentration required for the release is estimated to be as high as 10 µM. Such high concentration is likely to be reached only in close vicinity of the VGCC. Thus, the localization of Ca^{2+} influx through VGCC regarding docked vesicles appears crucial in the neurotransmitter release process. VGCC are enriched in the AZ and are recruited at release sites by interacting with RIM and RIM-BP (Acuna et al., 2015, 2016; Grauel et al., 2016; Südhof, 2012). A tight coupling (10-20 nm) of VGCC with the release machinery can be observed at some central synapses (Branco and Staras, 2009). A single channel opening triggers vesicular fusion and P_r is uniform across

docked vesicles as long as the distribution of VGCC is random and that the density of VGCC is superior to the one of docked vesicles (Schneider et al., 2015; Scimemi and Diamond, 2012). The absence of this tight coupling by knocking-down RIM-BP for example, triggers a decrease of P_r and a decrease of evoked EPSC (Grauel et al., 2016). Inversely, the increase of SNARE complex assembly increase the calcium-affinity of release and so the P_r (Acuna et al., 2014). Finally, VGCCs have been shown to be highly mobile while confined into the AZ. Intracellular calcium chelation decreases this mobility and strongly influences P_r (Ermolyuk et al., 2013; Schneider et al., 2015). Glutamate release can vary within and across synapses depending on the precise organization of AZs, and influences the input of post-synapses.

3. The post-synapse

a. Glutamate receptors

The post-synapse aims to convert the chemical signals coming from the pre-synapse via glutamate release into tunable electrical signals. To this end, the post-synapse accumulates receptor proteins which are activated by glutamate binding. These receptors can be either ionotropic glutamate receptors (iGluRs) or metabotropic glutamate receptors (mGluRs). iGluRs are ligand-gated ion channels that mediate most of the excitatory neurotransmission. Glutamate-binding triggers the opening of the channel pore, allowing charged ions to diffuse down to their chemical and electrical gradients. The three major classes of iGluRs have been named relatively to their specific agonist: α-**A**mino-3-hydroxy-5-**M**ethyl-isoxazole-**P**ropionic **A**cid **R**eceptors (AMPARs), **N**-**M**ethyl-**D**-**A**spartate **R**eceptors (NMDARs) and **Ka**inate **R**eceptors (KARs) (Lodge, 2009). AMPARs are responsible for the fast synaptic transmission and mainly mediate Na+/K+ currents and will be further detailed in chapter 2. NMDARs differ from AMPARs in several important manners. At rest, the ion channel of NMDARs is blocked by Mg^{2+}. This Mg^{2+} block is released when the post-synaptic membrane is sufficiently depolarized, after AMPAR activation for example. Therefore NMDARs do not participate significantly in basal synaptic transmission and are rather considered as coincidence detectors for pre- and post-synaptic activity. The second feature which marks a difference between AMPARs and NMDARs is the permeability of NMDARs to Ca^{2+} ions. Even if some AMPARs are calcium-permeable (CP-AMPARs), NMDARs play a key role at synapses to activate many intracellular calcium-dependent cascades. This calcium permeability of NMDARs gives them a central role in the modification of synaptic strength referred as synaptic plasticity which relies on calcium-dependent mechanisms. Finally, NMDARs differ by their gating mode. They are

activated by glutamate with a high affinity but require in parallel the presence of a co-agonist which is either glycine or D-serine. They present relatively slow activation kinetics, implicating them more in long-term signaling than directly in the electrical fast synaptic transmission. The KARs seem more implicated as regulators of synaptic transmission than as real direct effectors, but their exact role is still poorly understood (Traynelis et al., 2010)

In addition to the role of iGluRs on synaptic transmission, mGluRs modulate synaptic EPSCs by their presence at both sides of the synapse. Indeed, mGluRs family is composed of eight different receptors (mGluR1-8) which can be localized at the pre- or post-synaptic membrane, mainly outside of the synaptic cleft. Their functions are multiple as they convert glutamate release into protein G responses, leading to complex and various transduction signaling pathways according to the mGluR subtype. Their roles depend on their composition, threshold of activation and partners but they are implicated in synapse maturation, plasticity, and calcium homeostasis (Ferraguti and Shigemoto, 2006).

These various receptors present a highly variable affinity for glutamate, from the nM range for NMDARs to the mM range for AMPARs. This mean that their localization regarding glutamate release site will determine their level of activation. This glutamate receptor nanoscale organization inside the post-synapse is tightly regulated to control synaptic efficiency, through the vast amount of scaffolding proteins forming the PSD.

b. Organization of the Post-Synaptic Density

The core of the post-synapse is composed of thousands of scaffolding proteins tightly organized to form the PSD. They are involved in the synaptic development, in basal synaptic transmission and play a key role in synaptic plasticity. Among them, the deeper part of the PSD is mainly composed of Homer, Shank and **G**uanylate-**K**inase-**A**ssociated **P**rotein (GKAP), while the **M**embrane-**A**ssociated **GU**anylate **K**inases (MAGUK) family proteins seem highly concentrated closer to the post-synaptic membrane (**Figure 3**).

The main members of synaptic MAGUK proteins are PSD-95, PSD-93, SAP97 and SAP102. PSD-95 plays a primary role in the PSD organization because (i) it accumulates before and is located closer to the post-synaptic membrane compared to other PSD proteins, (ii) its level of expression affects synapse maturation and strength, (iii) spine shrinkage or pruning is correlated with a decrease of synaptic PSD-95 (Chen et al., 2011; El-Husseini et al., 2000; Woods et al., 2011). However, it has been suggested that the absence of PSD-95 could be

compensated by the other members of the MAGUK family as they display a large homology (Elias et al., 2006; Levy et al., 2015). As a central scaffolding protein of the excitatory PSD, PSD-95 is composed of series of protein interaction domains enabling the clustering of various synaptic proteins. PSD-95, as the other MAGUKs, has three PDZ domains, a SH3 domain and a **G**uanylate-**K**inase (GK) like domain (Okabe, 2007; Sheng and Kim, 2011). PSD-95 is able to recruit and stabilize several synaptic proteins at the post-synaptic membrane mainly through its PDZ domains. For instance, the first two PDZ domains, working as a tandem (Sainlos et al., 2011), play a crucial role in the organization of the two main glutamate receptors (AMPARs and NMDARs) at synapses. On its N-terminal part, PSD-95 can be anchored to the post-synaptic membrane via the palmitoylation of two cysteine residues (El-Husseini et al., 2002; Fukata et al., 2013). PSD-95 is thought to have two conformations, a C-shaped and an extended configurations depending on its palmitoylation and phosphorylation state, so on its synaptic localization (Chen et al., 2011; Fukata et al., 2013; Nakagawa et al., 2004; Nelson et al., 2013a).

In order to ensure its scaffolding role, PSD-95 is highly stable at synapses with a low turnover rate as demonstrated by FRAP experiments (Kuriu et al., 2006; Sharma et al., 2006). Once PSD-95 is anchored at synapses in an open conformation, its interaction domains are outstretched, allowing interactions to several proteins crucial for synaptic transmission as glutamate receptors or adhesion proteins. First of all, PSD-95 stabilizes NMDARs at synapses via a direct interaction between the last four amino acids of the C-terminal domain of GluN2 subunit of NMDAR and the first two PDZ domains of PSD-95 (Groc et al., 2004, 2006). PSD-95 has also been identified as one of the main organizer of AMPARs. Briefly, although AMPAR subunits own a PDZ-binding motif, they are unable to interact directly with PSD-95. Indeed, it has been shown in the team that truncation of the C-terminal domain of GluA2 subunit of AMPAR does not impact its surface diffusion or synaptic stabilization but only affects its expression at the cell surface (Bats et al., 2007). GluA C-terminal domain is important for several functions of AMPAR, but not for its interaction with PSD-95. AMPAR interacts with PSD-95 through an intermediate, identified as the **T**ransmembrane **A**MPAR **R**egulatory **P**roteins (TARPs; (Bats et al., 2007; Chen et al., 2000; Nicoll, 2006; Schnell et al., 2002)). More details on the role of AMPAR associated proteins are given in chapters 2 and 3. To conclude, the PSD is not an unstructured aggregate of scaffolding proteins, but it follows tight organization rules which are still not understood. For example, PSD-95 presents multiple phosphorylation sites, each targeted by kinases or phosphatases that are activated during synaptic development, maturation or plasticity. They regulate PSD-95 nanoscale organization

and its interactions with proteins. This complex structure will be able to organize acutely the various glutamate receptors and so to define synaptic transmission properties.

The precise molecular organization of both scaffolding proteins and glutamate receptors regarding the release site determines the number of receptors activated during a synaptic input. This property named **Q for quantum of response** corresponds to the single unit of synaptic transmission and can be regulated by the neuron both in term of intensity and kinetics, all along the synaptic timelife.

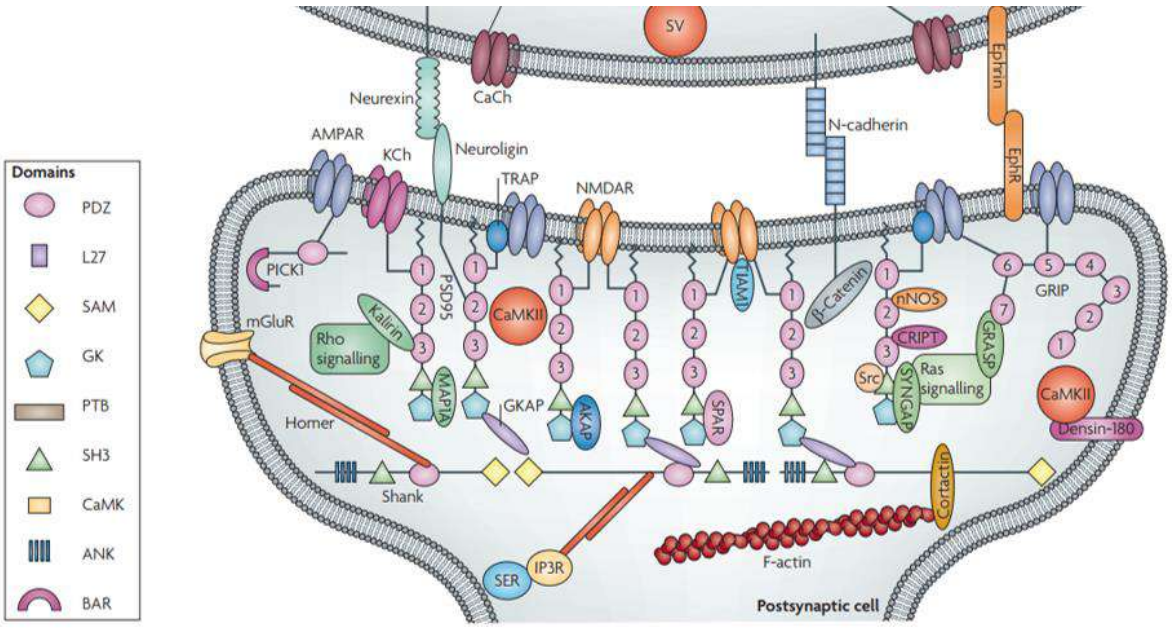

Figure 3. General scheme of molecular organization of the PSD of excitatory synapses. From Feng and Zhang 2009

4. Synaptic input integration – the NPQ

Previous chapters briefly present an overview of basic knowledge on the principal components of the synaptic transmission. These components are coordinated to regulate and define the inputs received by the post-synaptic neuron when pre-synaptic inputs are delivered. The **N** corresponds to the number of activated synapses. The pre-synapse regulates the amount of released glutamate but more importantly, the probability of this release to occur following an AP ($\mathbf{P_r}$). Finally, the organization and the composition of glutamate receptor complexes determine the post-synaptic quantum of synaptic response (**Q**).

This vision differs partly from the initial quantal theory of synaptic transmission of Katz. Indeed in 1954, Katz suggested that synaptic current intensity (i) at muscle results from the combination between the number of released neurotransmitter molecules per vesicle, called "quantal content" (q), the probability (p) of the synapse to release a vesicle and the overall number of stimulated release site (n) such as i = n.p.q (Del Castillo and Katz, 1954; McLachlan, 1978).

Concerning the N, studies about the pre-synaptic organization and release mechanism shifted our vision from a single bouton with multiple unorganized release sites to bouton with single (or two) well defined active zone and docking sites (Auger and Marty, 2000; Chen et al., 2004; Pulido and Marty, 2017; Tang et al., 2016). Still, some exceptions exist such as the mossy fiber and the calyx of Held axonal boutons which contain several AZs. This means that **N** corresponds to the number of synapses, belonging to the same post-synaptic neuron, which are activated by a single information input. This N is controlled by mechanisms of structural plasticity which can suppress or create synapses during network reshuffling (Holtmaat and Svoboda, 2009; Moser et al., 1994; Yang et al., 2009; Zhou et al., 2017b; Zuo et al., 2005).

The $\mathbf{P_r}$ concept is unchanged even if we know now that it can be modulated during short-term and long-term plasticity.

The most revisited concept is the q. Initially it has been defined as the number of glutamate molecules per vesicle. This was based on a vision of fixed and homogenously distributed glutamate receptors at the synaptic surface. Yet, the neurotransmitter content appears to be quite stable from one vesicle to another (Franks et al., 2002; Heine et al., 2008; Lisman et al., 2007a; Raghavachari and Lisman, 2004). In addition, recent works demonstrated that glutamate receptor complexes are not homogenously organized inside the synapse. They can change their composition and thus modulate their glutamate affinity and their conductance. In this condition, q is not only a pre-synaptic property but relies mainly on the quantity of glutamate receptors

inside the synapse, their proper organization, their location regarding the release site, and their molecular composition.

As described previously, the generation of an AP output from the AIS depends on a temporal and spatial integration of synaptic signals. Thus, the intensity the somatic current (I) depends on the number of activated synapses/release sites (N), the probability of vesicular release (P_r) at each stimulated release site and the quantum of response (Q) such as $I = N.P_r.Q$ (**Figure 4**).

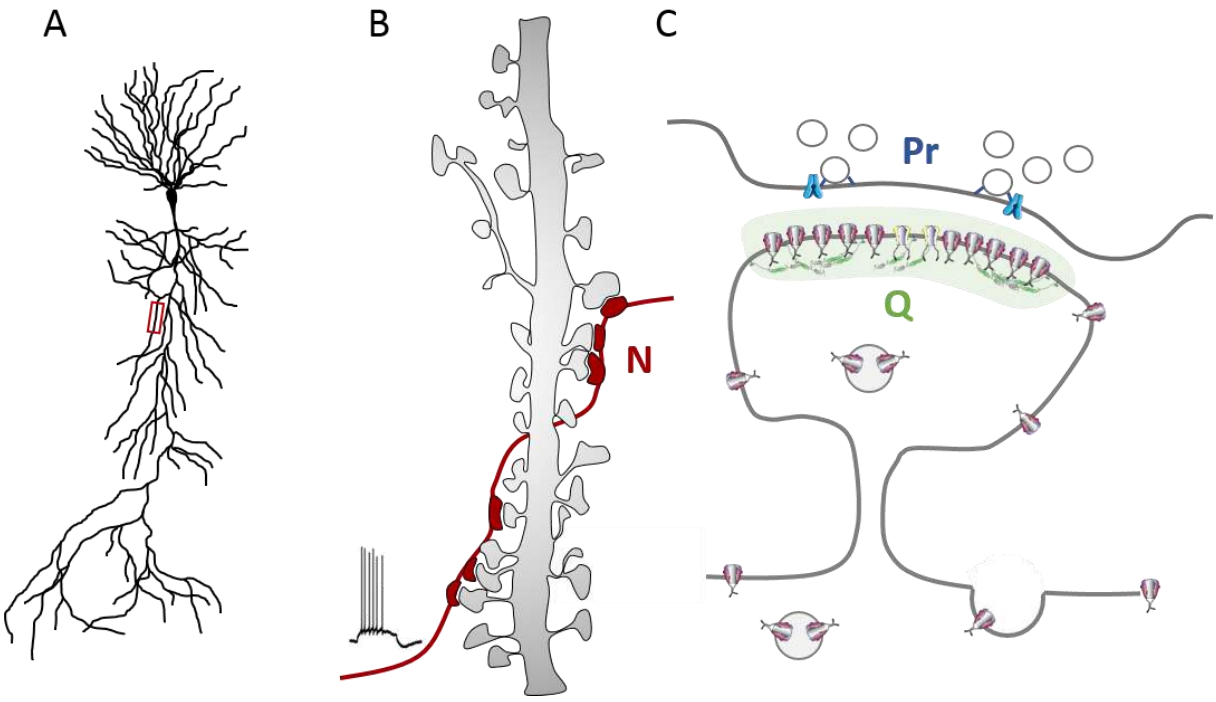

Figure 4. The NPQ paradigm. (A) CA1 pyramidal neuron. A dendritic segment (red rectangle) is detailed in the panel B. (B) Dendritic segment (grey) with spines . A single axon (red) coming from another neuron connect several time the dendritic segment forming synapses. When APs arrive in the axonal boutons it activates the **N** synapses formed with the CA1 pyramidal neuron. (C) Structure of a synapse with in the pre-synaptic vesicles, which can be docked through the molecular release machinery and can be released when an AP arrives at the axonal bouton with a certain probability (**Pr**). In front are located glutamatergic receptors. Their density, composition and location will determine the quantum of response **Q**.

5. Dendritic integration

The properties of diffusion of the synaptic inputs across the dendritic shaft from synapses to the soma aim to modulate/integrate those signals to generate or not an AP output at the AIS. Thus, the capacity of synaptic inputs to trigger an AP output depends on how they are modified effectively before reaching the AIS.

Early mathematical models investigated the role of the dendritic arborization on the input/output relationship, showing that dendrites attenuate and filter synaptic potentials as they propagate to the soma, thus influencing their effects on AP output generation (Rall, 1962). This model, called the cable theory for dendrites, took advantage of the fact that dendrites resemble electrical cables, and therefore borrowed from existing equations developed to describe signal propagation in undersea telegraph lines ("cable theory"). The relevant electrical properties include the specific membrane resistivity (Rm), the specific membrane capacitance (Cm) and the internal axial resistance (Ri). Because Ri increases as a function of length and Cm increases as a function of membrane area, distal synaptic signals will experience more amplitude and kinetic filtering than proximal ones (Magee, 2000; Rall, 1962). Such a system would be highly "undemocratic" with proximal synapses having a stronger influence in the generation of axonal outputs than distal synapses. While it can be thought that distal synapses are only involved in local processing and do not impact axonal outputs, several studies support a model of "dendritic democracy" (Häusser, 2001; Magee, 2000; Sjostrom et al., 2008) (**Figure 5**). Most of the experimental evidences obtained so far indicate that input-output relationship is independent of input location. It has been shown using mainly localized release of caged glutamate that the amplitude of the evoked current measured at the soma is independent of the site of glutamate release within synapses receiving inputs from the same fibers (i.e. Schaffer collateral-CA1 synapses) (Pettit and Augustine, 2009). This result has been confirmed using dual whole-cell patch clamp recordings in combination with localized minimal stimulations (Magee and Cook, 2000). This suggest that neuronal properties exist to counterbalance the filtering effect of the dendrite such that all inputs are received by the soma independently of their location within the dendritic arborization and for a same layer of axonal projections, and *at fine* restore a "democratic" system.

Two features can affect the input-output relationship. The first one concerns the electrical properties of dendrites, either due to the morphology of the dendritic arborization (passive properties) or through the impact of voltage-gated ion channels and local dendritic excitability

(active properties). The second feature concerns directly the synaptic inputs, meaning that a neuron can adapt its synaptic strength in function of their localization on the dendritic tree.

By measuring synaptic inputs directly in the dendrite, near the synaptic input site, Magee and Cook obtained evidences of a synaptic scaling of distal synapses regarding proximal ones. This suggests that synaptic strength can be control at the synaptic level to shape the input-output relationship independently of the synaptic location (Häusser, 2001; Magee and Cook, 2000). The first possibility of such scaling is that distal synapses release more glutamate molecule per vesicle or more vesicles per release event. However, there is so far no evidence defending this possibility. The organization of the post-synapse is a more expected possibility to control the synaptic strength. Several studies report a gradual increase of glutamate receptor content and neurotransmitter-evoked calcium signals when the synapse-to-soma distance increase (Menon et al., 2013; Smith et al., 2003; Walker et al., 2017).

To conclude, at basal state, the relationship between synaptic inputs and the somatic integrated signal is modulated by two main components, the intrinsic synaptic properties governed by the NPQ rules, and the dendritic and somatic integration/transmission properties. Both can be modulated either by modulation of the NPQ through events called structural and synaptic plasticity or by modification of dendritic and somatic excitability due to a phenomenon called intrinsic plasticity.

In the following chapters, we will focus more particularly on plastic events regulating the NPQ properties. They correspond to short-term or long-term modifications of one or more of these parameters due to specific input properties. As these synaptic properties concern more directly the fast synaptic transmission, which implicates AMPARs more than NMDARs or KARs, I will introduce our current knowledge concerning AMPAR complex composition and the role of their precise organization at synapses on basal synaptic transmission before going back to the concept of synaptic plasticity.

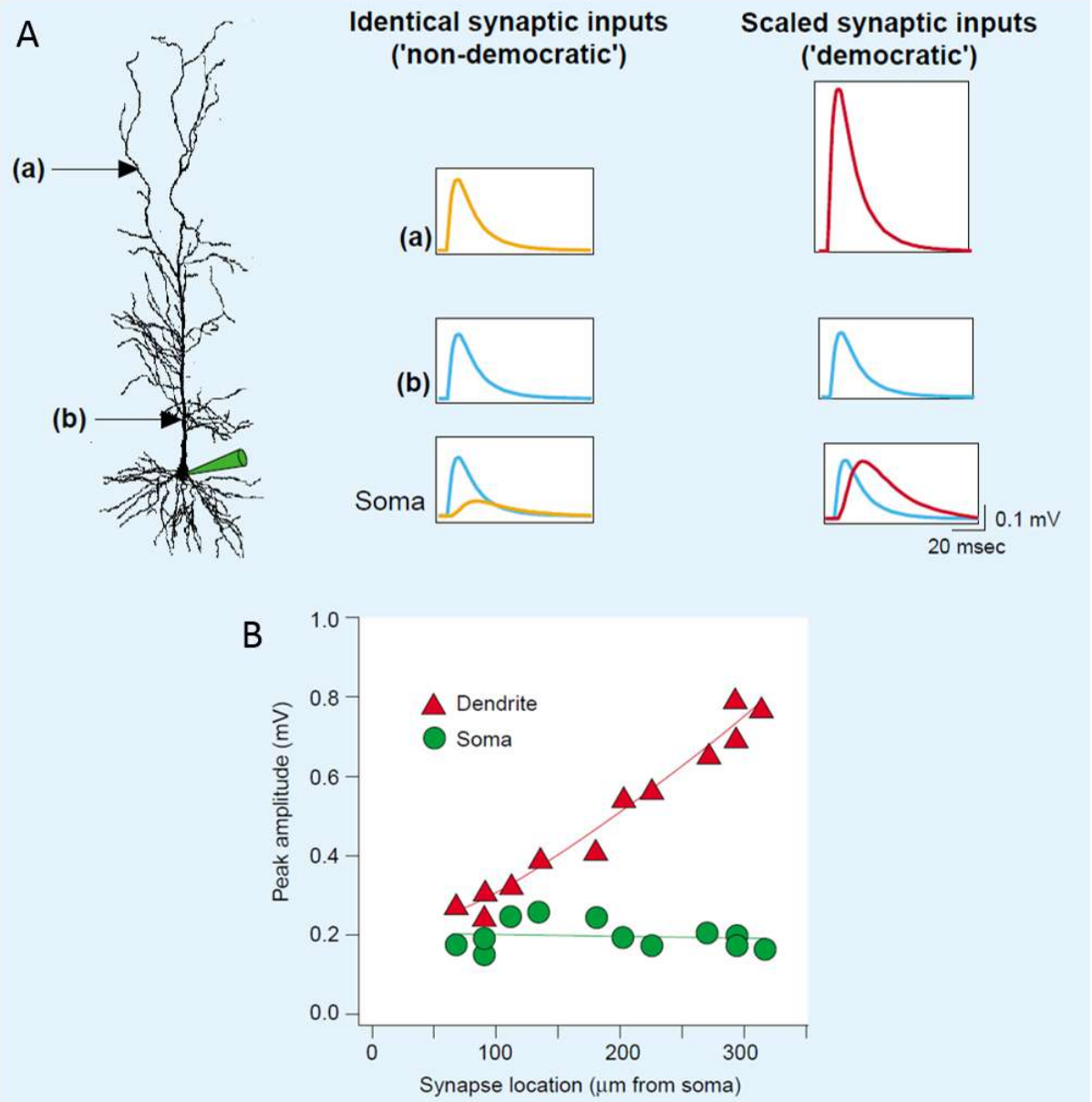

Figure 5. Dendritic integration. (A) Compensation of dendritic filtering. A schematic reconstruction of a CA1 pyramidal neuron where (a) and (b) indicate distal and proximal synapses respectively. The middle panel presents a "non democratic" system in which both distal and proximal have identical synaptic inputs and produces very different EPSP sizes at the soma due to dendritic filtering. The right panel corresponds to a dendritic democracy in which synaptic inputs are scaled depending on the synaptic location, allowing them to have the same somatic peak amplitude. (B) Synaptic strength measured at the soma is independent of the synaptic location across the dendritic arborization. Evoked EPSPs recorded at the dendrite near the synaptic site (triangle) or at the soma (circles). Adapted from Hausser 2001

Chapter 2

AMPAR-dependent synaptic transmission

1. AMPAR structure

AMPARs are tetrameric cation channels that mediate fast excitatory synaptic transmission upon glutamate binding. AMPAR assemblies are complex signaling machines that function as homo- or heterotetramers built from combinations of four subunits, GluA1-4. Each subunit differs in its contribution to channel kinetics, ion selectivity and receptor trafficking properties. AMPARs show a widespread distribution in the brain, as expected from their key role in excitatory transmission. GluA1, GluA2 and GluA3 are enriched in most of the CNS regions on the contrary to GluA4 that is abundant in the cerebellum (Schwenk et al., 2014).

Each AMPAR subunit comprises about 900 amino acids and has a molecular weight of about 100 kDa (Hollmann and Heinemann, 1994). They are coded by their own genes but share ~70 % amino acid sequence identity. They display a unique modular architecture as each subunit consists of four distinct domains: an extracellular **N**-**T**erminal **D**omain (NTD, also referred to as ATD for **A**mino-**T**erminal **D**omain), a **L**igand-**B**inding **D**omain (LBD), a **T**rans**M**embrane **D**omain (TMD) that forms the pore of the ion channel, and a cytoplasmic **C**-**T**erminal **D**omain (CTD) (**Figure 6**). The CTD varies in length between subunits and plays an important role in AMPAR trafficking. Indeed, this CTD is subject to various activity-dependent post-translational modifications impacting synaptic strength. AMPAR TMD is formed by four hydrophobic domains: M1, M3 and M4 which cross the lipid bilayer, while M2 faces the cytoplasm as a reentering loop that forms part of the channel pore. The LBD is formed of two segments (S1 and S2) which initiate conformational changes upon glutamate binding (Armstrong et al., 2006). Since LBDs of adjacent subunits dimerize back-to-back via their upper S1 lobes, closure of the clamshell around glutamate causes separation of the lower S2 lobes, transmitting forces to the TMD and triggering opening of the channel pore (Greger et al., 2017; Mayer, 2006; Twomey et al., 2017a). The NTD encompasses 50 % of the receptor mass and reaches midway into the synaptic cleft where it can interact with other synaptic proteins such as N-cadherin (Jin et al., 2009). The NTD which present a similar clamshell organization as the LBD is a main actor in the assembly of AMPAR subunit dimers before they interact to form a tetramer through their LBD domains. Moreover, the NTD undergoes major conformational

changes during AMPAR desensitization (Dürr et al., 2014; Herguedas et al., 2016; Jin et al., 2009).

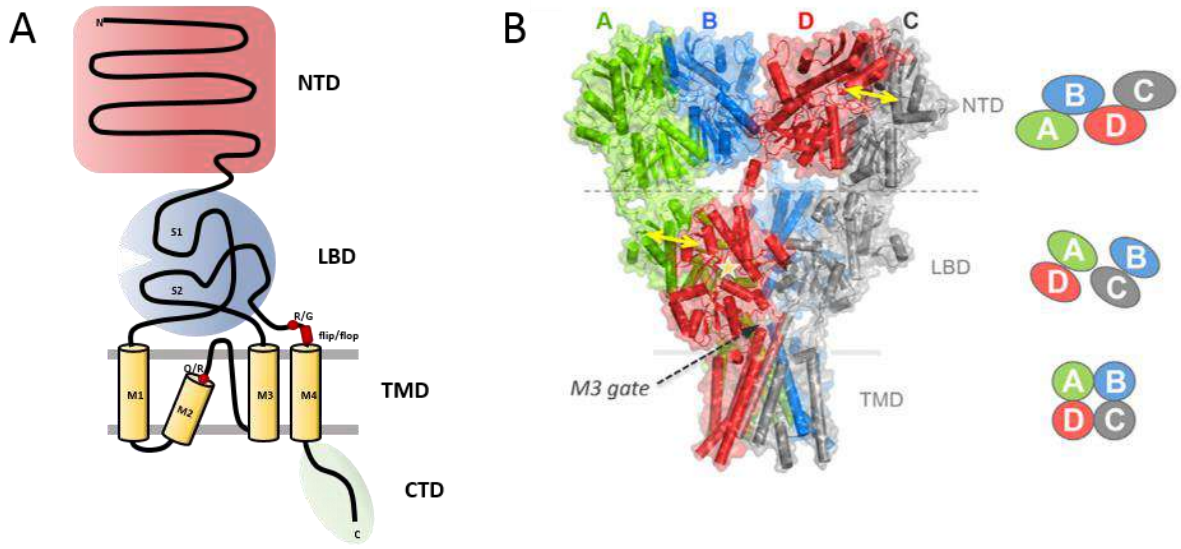

Figure 6. Structure of AMPAR subunits. The panel A corresponds to a schematic representation of a GluA subunit of AMPAR, showing the 4 distinct domains (NTD, LBD, TMD and CTD) as well as the post-transcriptional modification sites (red). The panel B corresponds to the structure of AMPAR and showing the organization of the 4 subunits (A, B, C and D) (from Greger et al 2017).

Each subunit brings a specificity in term of gating properties. Another level of variability is due to various post-transcriptional modifications (**Figure 6A**). Briefly, receptors present a flip/flop alternative splicing in a 38 amino acid region located just before the M4 segment and this activity-dependent alternative splicing affects the channel gating kinetics and pharmacological properties (Penn et al., 2012). In addition, AMPARs display post-transcriptional processing or mRNA editing. Maybe the most important one concerns specifically GluA2 subunit. Its M2 segment contains a Q/R (Glutamine Q to Arginine R) mRNA editing site. This post-transcriptional modification renders GluA2-containing AMPARs impermeable to calcium, reduces AMPAR channel conductance and open probability (Derkach et al., 2007; Greger et al., 2017). This editing occurs during brain development and ~99 % of GluA2 subunits are edited in the adult CNS. Finally, a last editing site is present in GluA2-4 subunits just before the flip/flop domain. This second mRNA editing site switches an Arginine (R) to a Glycine (G). Most of expressed subunits are in the editing form. This editing affect AMPAR gating kinetics, subunit assembly and trafficking (Greger et al., 2017; Penn et al., 2012).

2. AMPAR currents

AMPARs present a low affinity for glutamate with a half-maximal effective concentration (EC_{50}) of ~0.5 mM compare to NMDARs which has a nanomolar range affinity for glutamate. When exposed to a pulse of 1 mM glutamate a current is generated with a rapid rise time of 100-600 µs (Raghavachari and Lisman, 2004). This reflects the very fast binding/activation kinetic and high opening probability of AMPARs (**Figure 7A**).

The single channel conductance is highly variable, from <1 pS to ~30 pS, because of AMPAR subunit composition, RNA editing and alternative splicing (Swanson et al., 1997), but also due to the number of glutamate molecules that bound to the receptor. Two glutamate molecules must bind the receptor to open it, and then the channel conductance increases proportionally to the number of bound glutamate (**Figure 7B**). The more efficient is the agonist, the more frequently the receptor will occupy the high-conductance state (Rosenmund, 1998). This particularity underlines the importance of AMPAR localization regarding glutamate release sites, independently of the AMPAR composition to determine the synaptic response intensity (Q value).

Once open, receptors deactivate rapidly following clearance of synaptic glutamate. The deactivation occurs in ~2.5 ms and is probably sufficient to explain the termination of AMPAR-mediated EPSC. Indeed, glutamate is cleared from the synaptic cleft in few hundreds of µs following a single vesicle release (Colquhoun et al., 1992; Raghavachari and Lisman, 2004). During high frequency release or strong stimulation, if glutamate is not cleared rapidly enough, AMPAR channel closes rapidly and the receptor enters in a desensitized state which lasts for tens to hundreds of ms. The desensitized state corresponds to a conformational state of the receptor in which glutamate can still bind to the receptor but the channel is closed (Dürr et al., 2014; Sun et al., 2002). First characterized by Katz on acetylcholine receptor, further studies have shown that desensitization is a functionally important phenomenon that occurs in most ligand-gated ion channels. Desensitization of AMPAR has been shown to occur in presence of saturating concentration of agonist (glutamate, AMPA and quisqualate). However, subsequent experiments have shown that desensitization is effectively promoted by much lower glutamate concentration than required for activation while recovery from desensitization proceeds at a rate at least 10-fold slower than deactivation (Colquhoun et al., 1992; Trussell and Fischbach, 1989; Trussell et al., 1988). While debated, desensitization appears to play a role in the regulation of synaptic strength on a synapse-specific basis, especially during high-frequency stimuli (Constals et al., 2015; Koike-Tani et al., 2008; Otis et al., 1996).

On a conformational point of view, crystallography and cryo-EM imaging has shown that AMPAR undergoes multiple massive conformational changes of NTD and LBD during desensitization (Armstrong et al., 2006; Chen, Shanshuang; Yan Zhao, Yuhang (Steven) Wang, Mrinal Shekhar, Emad Tajkhorshid, 2017; Dürr et al., 2014; Twomey et al., 2017b) (**Figure 7C**)**.** The simple model where AMPAR is closed, opened and get desensitized appears to be more complex. It has been shown that AMPAR displays different stages of channel opening depending on the number of bound glutamate molecules leading to several desensitized states (Meyerson et al., 2014; Robert and Howe, 2003). This structural complexity relies on AMPAR composition, regulation by post-translational modification and interactome, leading to a more complex view of how AMPARs participate to the integration of synaptic inputs.

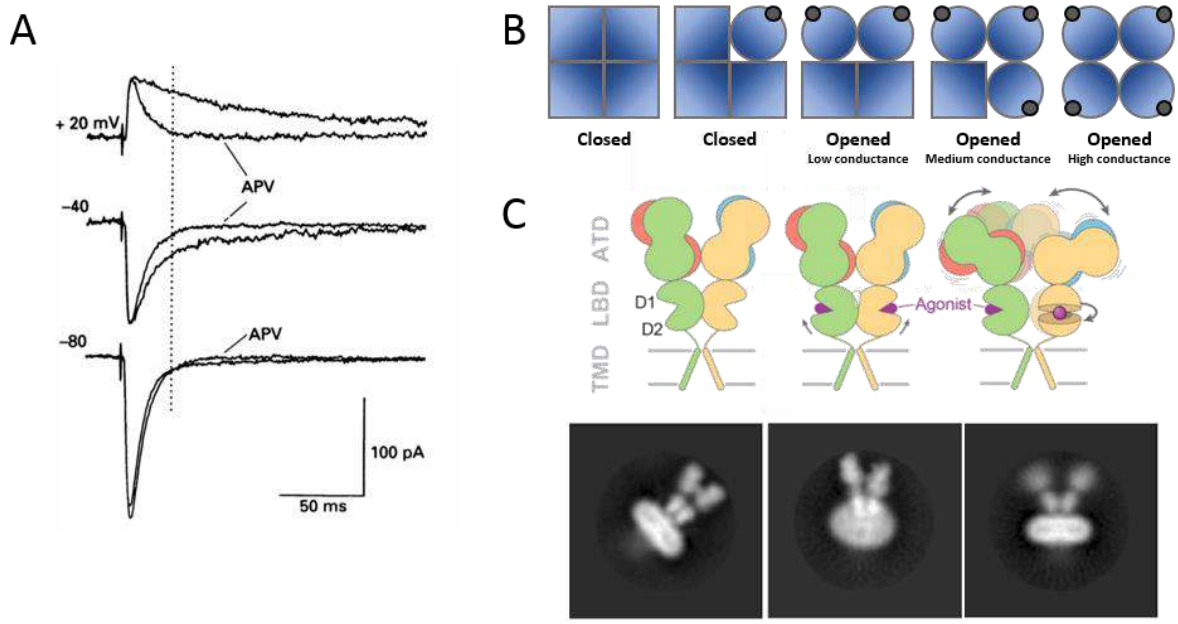

Figure 7. AMPAR gating properties. (A) Excitatory post-synaptic current are mainly mediated by AMPAR at resting potential (-70 mV). The contribution of NMDAR is almost null as shown by the similar EPSC obtained in the presence of NMDAR blocker (APV) at -70 mV (From Hestrin et al 1990). (B) Activation of AMPAR requires at least two bound glutamate (black circle). Activation of more subunits (Blue square) opens the channel to a higher conductance level. (C) AMPAR conformational states: close (left), open (middle) and desensitized (right) in schematic representation or cryo-EM visualization (Durr et al 2014 & Chen et al 2017)

3. AMPAR assembly and macromolecular complex

Most of AMPARs are synthetized in the soma. To form a mature receptor, four subunits need to assemble together in a dimer-to-dimer process. In the CNS, the majority of AMPARs

exists as heterotetramers and most of them contain edited GluA2 subunits, restricting Ca^{2+} permeability. The first assembly as dimer is attributed to NTD affinities while the tetramer formation and stabilization is attributed to LBD and TMD interactions. Regarding the dimer assembly, GluA1 NTD has an affinity for GluA2 NTD that is >200-fold stronger than for another GluA1 NTD. The effect of these affinity differences in the hippocampus where GluA1-3 subunits are expressed results in the assembly of almost exclusively GluA1/GluA2 (~80 %) and GluA2/GluA3 (< 20%) heterotetramers (Lu et al., 2009). Still, the presence of low level of homotetrameric GluA1 (CP-AMPARs) has been observed. While their contribution to basal synaptic transmission is unlikely to occur, a role during synaptic plasticity has been reported since they could allow a better control of calcium influx that is at the origin of those mechanisms (Huganir and Nicoll, 2013; Sanderson et al., 2016).

In the CNS, AMPAR are almost never isolated from their assembly to their synaptic localization where they mediate synaptic transmission. They are described as a macromolecular complexes comprising various auxiliary proteins (Schwenk et al., 2012). The receptor core could be surrounded by up to four members of four distinct families of membrane proteins: the TARPs (γ-2, γ-3, γ-4, γ-5, γ-7, γ-8 (Jackson and Nicoll, 2011; Tomita et al., 2003)), the **c**or**ni**chon **h**omologs 2 and 3 (CNIH2, 3 (Schwenk et al., 2009)), GSG1L protein (Schwenk et al., 2012; Twomey et al., 2017b) and Shisa family (CKAMP44/Shisa9 and Shisa6 (Engelhardt et al., 2010; Karataeva et al., 2014; Klaassen et al.)) (**Figure 8A**). A definition of AMPAR auxiliary protein based on three criteria has been proposed by Tomita's lab: (i) to be a non-pore forming subunit, (ii) to have a direct and stable interaction with the pore-forming subunits, and (iii) to modulate AMPAR trafficking and/or biophysical properties (Yan and Tomita, 2012). The composition of the AMPAR macromolecular complex is highly dynamic, changing across brain regions, during development or in response to neuronal activity, thus giving another level of variability compared to single channel properties. While it appears evident that the presence of this bench of proteins around AMPAR regulates its trafficking, its synaptic localization and its gating properties, the precise role of each one remains unclear. Due to the redundant role of the various auxiliary proteins in AMPAR trafficking and gating, it is difficult to understand the precise role of each in region where several members of the same family are expressed. However, regarding TARP γ-2 (stargazin) which is the most characterized, several interesting results regarding the regulation of AMPAR functions have been obtained.

Briefly, the first result has been obtained by Roger Nicoll's group on Stargazer mice (mice lacking γ-2). They showed that in the cerebellum where stargazin is the main TARP, neurons

display an intense decrease of the surface AMPAR level, suggesting a role of stargazin in AMPAR trafficking and surface expression (Chen et al., 2000). However, it has been recently hypothesized that this suppression of AMPARs in the cerebellum of the stargazer mouse was not only due to the suppression of stargazin but also to the over-activity of γ-7 which favors AMPAR endocytosis (Bats et al., 2012). Other studies have demonstrated that the interaction between stargazin PDZ-binding motif and PSD-95 allows the anchoring of AMPAR at synapses (**Figure 8B**) (Bats et al., 2007; Opazo et al., 2010; Sainlos et al., 2011; Schnell et al., 2002). As previously reported (chapter 1), AMPAR seems unable to interact directly with PSD-95. Bats *et al.* demonstrated that the loss of interaction between stargazin and PSD-95 impairs AMPAR immobilization and accumulation at synapses and leads to a decrease of synaptic transmission. This regulation of AMPAR mobility and synaptic anchoring is dependent on synaptic activity and phosphorylation state of stargazin. Schematically, the phosphorylation level of the stargazin cytoplasmic tail controls its interaction with the negative charge of the lipid bilayer. An increase in the phosphorylation level outstretches the tail and favors interaction with the anchored PSD-95 (Hafner et al., 2015; Sumioka et al., 2011; Tomita et al., 2005a). Finally, stargazin does not only impact AMPAR trafficking and stabilization at synapses but also tunes AMPAR synaptic responses by slowing channel deactivation and desensitization (Jackson and Nicoll, 2011; Tomita et al., 2005b). (**Figure 8C**)

Similar regulations are introduced to AMPAR complex by the other auxiliary proteins. Moreover, it has been reported that endogenous AMPAR currents seem dependent on the presence of a combination of at least two different associated proteins (Gill et al., 2011; Kato et al., 2010). This clearly reveals that synaptic current properties are due to the highly regulated combination between AMPAR composition, post-translational modifications, position regarding glutamate release, and presence of various regulatory proteins. Until now, a clear view of AMPAR complex composition in various brain areas and the physiological effect of such variability on the synaptic transmission properties are far to be understood.

4. AMPAR synaptic location

Once assembled, AMPARs are transported to the plasma membrane. Most of the neo-synthesized receptors travel from the soma through active vesicular transport. It has been described that AMPARs can also be synthesized locally in endoplasmic reticulum located in the dendritic shaft, just above dendritic spines (Greger and Esteban, 2007). The precise localization of AMPAR surface delivery remains debated as some studies report that it occurs

exclusively in extra-synaptic regions on the dendritic shaft, while other studies claim that it can also occur in spines. Following their exocytosis, AMPARs diffuse to synapse where their number, localization and regulation will be critical for the synaptic input integration. The recent advances in our understanding of AMPAR nanoscale organization at synapses and its role in tuning synaptic transmission (Q value) are presented in the following chapter.

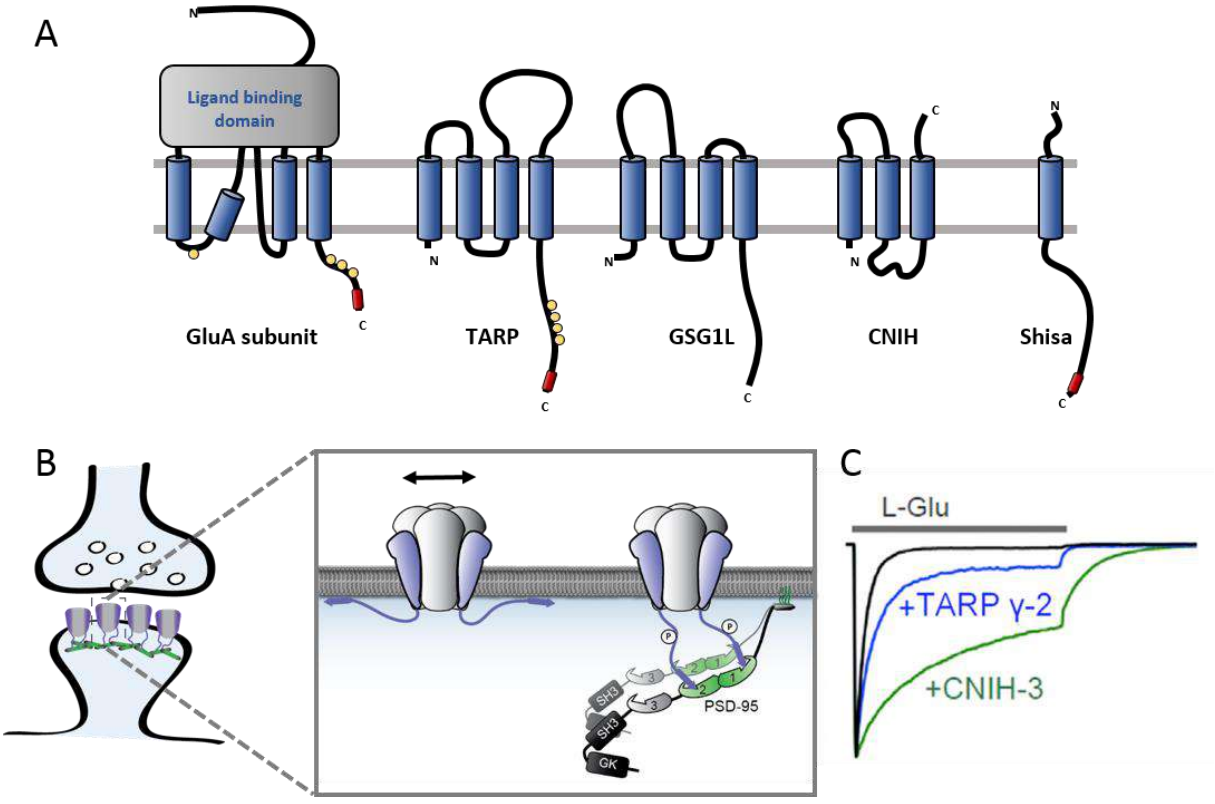

Figure 8. AMPAR macromolecular complex. (A) Schematic structure of GluA subunit of AMPAR (left) and of the four families of AMPAR auxiliary proteins. (B) AMPAR (grey) is immobilized by the interaction between stargazin (blue) and PSD-95 PDZ domains (green) when stargazin C-terminal tail is phosphorylated (C) Biophysical properties of AMPAR are impacted by the presence of auxiliary proteins (from Greger et al 2017).

Chapter 3

Molecular regulation of synaptic transmission

Neurophotonics

Neurophotonics.SPIEDigitalLibrary.org

Review on the role of AMPA receptor nano-organization and dynamic in the properties of synaptic transmission

Benjamin Compans
Daniel Choquet
Eric Hosy

SPIE.

Benjamin Compans, Daniel Choquet, Eric Hosy, "Review on the role of AMPA receptor nano-organization and dynamic in the properties of synaptic transmission," *Neurophoton.* **3**(4), 041811 (2016), doi: 10.1117/1.NPh.3.4.041811.

Neurophotonics 3(4), 041811 (Oct–Dec 2016)

REVIEW

Review on the role of AMPA receptor nano-organization and dynamic in the properties of synaptic transmission

Benjamin Compans,[a,b] Daniel Choquet,[a,b,c,*] and Eric Hosy[a,b]
[a]University of Bordeaux, Interdisciplinary Institute for Neuroscience, UMR 5297, Bordeaux F-33000, France
[b]Interdisciplinary Institute for Neuroscience, CNRS, UMR 5297, Bordeaux F-33000, France
[c]University of Bordeaux, Bordeaux Imaging Center, UMS 3420 CNRS, US4 INSERM, France

Abstract. Receptor trafficking and its regulation have appeared in the last two decades to be a major controller of basal synaptic transmission and its activity-dependent plasticity. More recently, considerable advances in super-resolution microscopy have begun deciphering the subdiffraction organization of synaptic elements and their functional roles. In particular, the dynamic nanoscale organization of neurotransmitter receptors in the postsynaptic membrane has recently been suggested to play a major role in various aspects of synapstic function. We here review the recent advances in our understanding of alpha-amino-3-hydroxy-5-méthyl-4-isoxazolepropionic acid subtype glutamate receptors subsynaptic organization and their role in short- and long-term synaptic plasticity. [DOI: 10.1117/1.NPh.3.4.041811]

Keywords: receptor trafficking; synaptic plasticity; super-resolution microscopy.

Paper 16041SSVRR received Jun. 21, 2016; accepted for publication Oct. 19, 2016; published online Nov. 15, 2016.

1 Introduction

The fundamental building block of neuron-to-neuron communication is the synapse, a micrometer size organelle, where the membranes of two cells come in close apposition to favor information transfer. Our deep understanding of this structure, named for the first time in 1897 by Foster and Sherrington, has evolved in parallel with the development of new technologies. Most of the main conceptual advances in our understanding of synaptic organization and function have originated from new imaging developments. Based on the new silver staining developed by Camillo Golgi, Cajal[1] demonstrated that nerve cells are not continuous but contiguous, invalidating the cable theory of the nervous system. At the same time, he introduced the notion that a synapse is composed of three independent compartments: the presynapse, the postsynapse, and the space between them: the synaptic cleft. This organization remained hypothetical until the first precise image of a synapse was obtained in parallel in the 1950s by two laboratories using electron microscopy.[2,3] The first image of a synapse revealed an asymmetric organization, with one compartment enriched in ∼50 nm sized vesicle.[2,4,5] This discovery and the demonstration one year later that these vesicles contained neurotransmitters,[5] coupled to Katz's electrophysiological recordings of unitary postsynaptic voltage changes, established most of the basis for our current knowledge of the mechanisms of synaptic transmission.[6,7] The presynapse releases a "quantum" of neurotransmitters in the synaptic cleft due to discrete vesicle fusion, triggering a reproducible postsynaptic current. Despite the large number of newly available techniques, our present vision of the synapse is not very different from the one described by Palay, even though the invention of the patch-clamp technique offered a more robust way to measure synaptic currents[8] and the revolution in genomics and proteomics allowed to allocate proteins, their interactions, and structures, into the various synaptic compartments. From the cloning of the first glutamate receptor in 1994[9] and the identification of PSD-95 as the main scaffold element of the postsynaptic density,[10–12] to the extensive proteomic characterization of synaptic elements,[13–16] it is probably safe to say that by now, most protein constituents of the synapse have been identified. However, as detailed below, we still do not fully understand how synapses work and many shadow zones remain.

An important misconception in shaping our original understanding of synaptic transmission was the omission of dynamic regulation at various levels. Indeed, since 1973 and the discovery of the concept of synaptic plasticity by Bliss and Lomo, new dynamic levels of regulation of synaptic transmission have regularly been identified. From this moment, synaptic transmission is accepted as a dynamic mechanism, which can be modified through plastic events on both short and long terms to adapt the synaptic transmission to various types of received inputs.[17–20]

The expansion of neuroscience research during the 1990s led to an intense debate over the role of both the pre- and the postsynapse in those plastic events. Short-term plasticity has been usually attributed to presynaptic modifications. Briefly, when action potentials arrive in the 1- to 100-Hz range, calcium levels accumulate over time in the presynaptic terminal, leading to a time-dependent increase in the release probability, which is responsible for short-term paired-pulse facilitation.[21] This dogma is still valid in spite of the identification of some postsynaptic components in the regulation of short-term synaptic depression, such as alpha-amino-3-hydroxy-5-méthyl-4-isoxazolepropionic acid (AMPA) receptor (AMPAR) desensitization and more recently AMPAR lateral diffusion (see Sec. 2.1).

Concerning long-term plasticity, the debate has been more pronounced. The main evidence suggesting a presynaptic mechanism came from the observation that the synaptic failure

*Address all correspondence to: Daniel Choquet, E-mail: daniel.choquet@u-bordeaux.fr

rate decreases following the induction of long-term potentiation (LTP).[22–24] But other studies suggest that postsynaptic modifications, such as AMPAR over-accumulation, were sufficient to induce LTP.[25–28] Various recent studies demonstrate that the reality lies in-between. Postsynaptically, changes in the number and composition of AMPAR complexes have been observed by uncaging and fluorescence imaging experiments. Moreover, some synapses are able to unsilence following potentiation protocols by accumulating AMPAR.[29–31] On the other hand, retrograde signaling via endocannabinoids indicates that the presynapse is also affected by long-term plasticity and, until now, the existence of a possible increase in glutamate content inside vesicles, or the change of release probability has not been ruled out.[32,33]

This review paper focuses mainly on postsynaptic organization and modifications, but it is important to constantly keep in mind that pre- and postsynapses are intrinsically connected and coregulated. We will focus on changes that occur on the postsynaptic side of the synapse, which indeed are now recognized as playing a central role in plasticity at many synapses, including the Schaeffer collaterals and CA1 pyramidal cells of the hippocampus, arguably the best studied synapse in terms of plasticity phenomenon.

Modifications in postsynaptic properties have been proposed early to account for plasticity of synaptic transmission.[34–36] These modifications have been attributed both to the changes in glutamatergic receptor properties[26,37–39] and the modification in AMPAR numbers at the postsynapse.[30,35,40,41] The changes in AMPAR number have been initially attributed solely to endocytic and exocytic processes.[42–46] It has been demonstrated that exocytosis of AMPAR is essential for induction of LTP.[44] But an important remaining question was how do AMPARs travel from the exocytosed vesicle to the synapse? The first use of single-particle tracking, the ancestor of super-resolution microscopy, revealed that AMPAR can diffuse at the plasma-membrane (as all transmembrane proteins, and in particular all neurotransmitter receptors) and exchange between synaptic and extrasynaptic sites.[47–49] The application of the revolutionary single-particle and single-molecule-tracking approaches has granted access to understanding the behavior of single proteins. After a series of first steps based on imaging latex beads, then organic dyes and semiconductor quantum dots, the last decade has seen a large development of super-resolution imaging techniques largely based on massively increasing the throughput of single-molecule detection assays, offering a new vision of synapse organization.

2 New Vision of the Synapse

2.1 *Nonsaturation of Postsynaptic AMPARs by Glutamate Release*

The conceptualization of the synapse as being composed of a presynaptic compartment dedicated to calcium-dependent neurotransmitter release and a postsynaptic compartment harboring a stable number of receptors has long been sufficient to define a functional model of synaptic transmission. Within such a framework, long-term plasticity is explained by presynaptic modification of release probability and potential changes in the glutamate content per vesicle, and by postsynaptic increases or decreases in the total amount of AMPAR inside the PSD. Our view of the number of AMPAR present in a given PSD has evolved importantly over the years. One of the initial paper, based on electron microscopy, described a "sharp decrease of receptor density at the edge of the membrane specialization (the PSD), which demonstrates that at a given level of glutamate only a well-defined number of receptors can be activated."[50] Even if glutamate diffuses out of the cleft, a much lower density of receptors will be reached, probably contributing little to the synaptic current. Then, improvement in fluorescence microscopy and electron microscopy labeling and glutamate uncaging started to better estimate the number of AMPAR inside the synapse, with an amount of around 100 receptors per synapse.[51–53] A paradox appeared when the number of AMPAR per PSD was compared to the effective amplitude of miniature currents, which reports a lower amplitude than expected even by taking into account the low affinity of AMPAR for glutamate.

The first answer to this paradox has been brought by the Richard Tsien Laboratory, when they demonstrated that a single glutamate vesicle release into the synaptic cleft was not able to saturate all postsynaptic AMPARs.[54] This work has then been confirmed by other laboratories, even if the real saturation level of AMPAR inside the synapse during endogenous activity is still not perfectly defined.[55–59] Indeed, experimental studies of glutamate diffusion into the synaptic cleft suggest that under the release site, glutamate can reach a concentration of around 1 to 5 mM within a couple 100 μs following vesicle release.[57,58,60–62] Computing and modeling, based largely on Monte Carlo simulations, allowed to estimate the width of the synaptic area, where glutamate concentration is sufficient to activate AMPAR. Due to the strong cooperativity of AMPAR activation and the rapid dissipation of glutamate, AMPAR seems to be activated only onto an area of around 100 to 150 nm full width at half maximum (FWHM) in front of the release site.[55,56,59,62,63] These conclusions partly change our conception of what could be the synaptic quantum of response. Indeed, initially a quantum was considered as the number of glutamate molecules per vesicle. Models now show that the amplitude of synaptic responses depends not only on the presynaptic quantum but also on the clustering level of AMPARs and their position with respect to the release site (Fig. 1).[55,59,64,65]

2.2 *Lateral Diffusion of AMPARs as a Mechanism to Control AMPAR Density at the Synapse*

Although the concept of a fluid mosaic membrane has been proposed since 1972 by Singer and Nicholson,[66] and that the application of the FRAP technique has demonstrated a rapid exchange via Brownian lateral diffusion of the various membrane constituents,[67,68] it is only since the early 2000s, with the improvement of single-particle tracking techniques, that lateral diffusion has started to be considered as a nonnegligible physiological parameter, particularly in neuronal cells. Precursor studies were performed by Mu Ming Poo's Lab on the acetylcholine receptor, showing its diffusion in the extrasynaptic membrane of muscle cells and introducing the diffusion trap model.[68–70] A few years later, many laboratories, including Sheetz's to study adhesion molecules and biomechanical forces and Kusumi's to understand diffusion properties of membrane proteins and lipids, have used and improved single-particle tracking techniques.[71–73] In 2001, for the first time, our group together with Antoine Triller applied single-particle tracking techniques on neurons to reveal and analyze the properties of the mobility of an inhibitory neurotransmitter receptor.[74]

One year later, we published the characterization of AMPAR surface mobility.[47] The use of single-particle tracking drastically

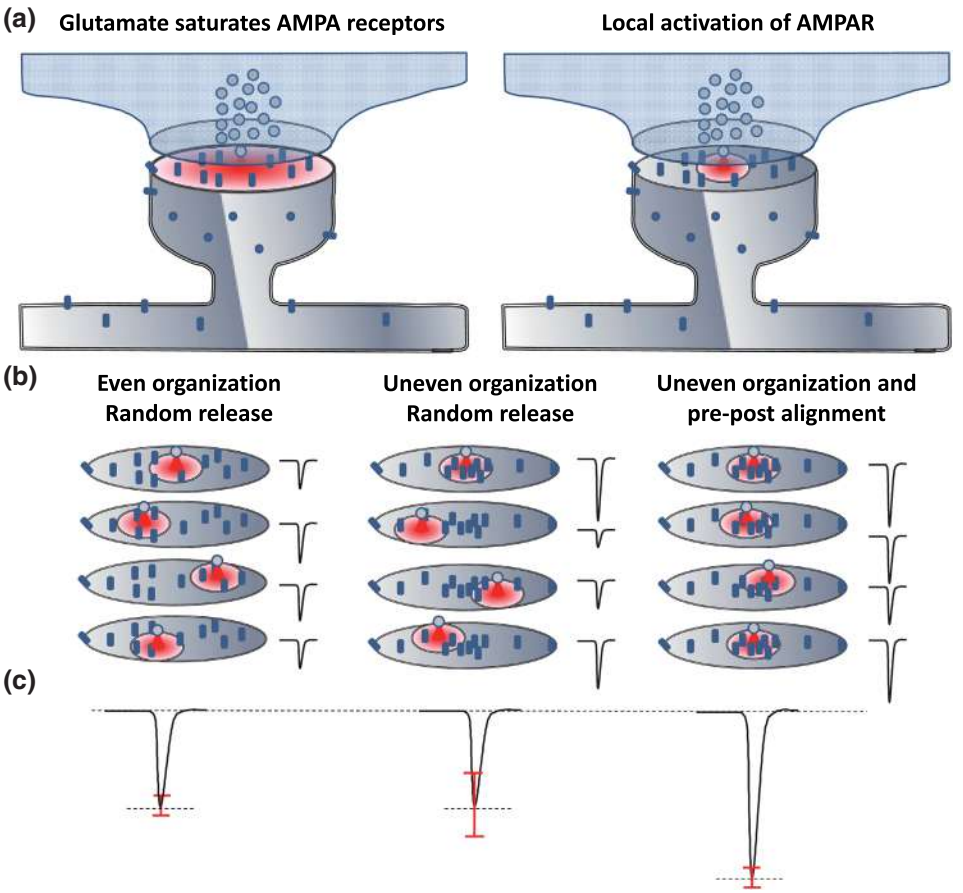

Fig. 1 Toward a new vision of the synapse. (a) Scheme of synapse, the area where AMPAR can be activated by glutamate after release of a presynaptic vesicle is represented in red. Previously, synaptic receptor in the synapse was thought to be saturated, in 1920s experiments from several laboratories demonstrated that AMPAR are likely activated only on a 100- to 150-nm diameter area due to their low affinity.[55,56,59,62] (b) Effect of AMPAR organization and release site localization on the variability of AMPAR responses. Following the discovery of the nonsaturation of synaptic AMPAR, modeling studies identified three hypothesis represented here. From left to right: even organization of AMPAR and random release, clustered AMPAR and random release, clustered organization and release in front of the cluster. The corresponding average and variability of miniature EPSC in function of AMPAR organization are represented in (c).

changed our vision of AMPAR dynamic and organization inside synapses. The dogma that neurotransmitter receptors were immobile at synapses, their number in the PSD being affected only by endo- and exocytosis, was proven wrong. Indeed, various experiments revealed that AMPARs constantly alternate between fast Brownian diffusion and confined motion.[47,49] Each receptor may adopt successively both of these behaviors, and activity regulates the time spent in one or the other diffusive state.[49,75–78] Importantly, these experiments revealed the presence of specific and saturable binding sites for AMPAR inside the synapse.

The following years in the field have been dedicated to identify which molecular mechanisms are responsible for the AMPAR trapping at synapses. Unraveling the nature of the traps was intimately linked to the initial progress in genome sequencing and decoding and then the improvement in high throughput and sensitive proteomic technique.[79–82] For example, Letts et al.[83] cloned gamma2, a protein belonging to the calcium channel family that when mutated triggered hereditary epilepsy in mice. Two years later, gamma2 (also named stargazin) has been identified as the first AMPAR regulatory protein, implicated in both their cellular traffic to the membrane, the regulation of their electrophysiological properties and responsible for their synaptic trapping.[84,85] These studies demonstrated that AMPARs do not travel alone, but they are part of a macromolecular complex composed of many different auxiliary proteins. The composition of these complexes is highly dynamic and varies across different brain regions and during neuronal activity.[86] So far, the AMPAR complex proteome is composed of >30 different proteins, mainly transmembrane ones. It includes the receptor core, formed by tetramers of the pore forming GluA1-4 subunits[9,87] and of various associated proteins belonging mainly to three families of membrane proteins: the transmembrane AMPA regulatory proteins (TARPs γ-2, γ-3, γ-4, γ-7, and γ-8,[88]), the cornichon, (CNIH2 and CNIH3,[81,89]), and the shisa family (Shisa9/CKAMP44 and Shisa6,[82,90,91]) [Fig. 2(a)]. The precise role of each auxiliary subunit is not well established, even if many studies using knock-out mice or protein mutations have tried to clarify the impact of some AMPAR associated proteins on synaptic function both at basal state and during plastic events.

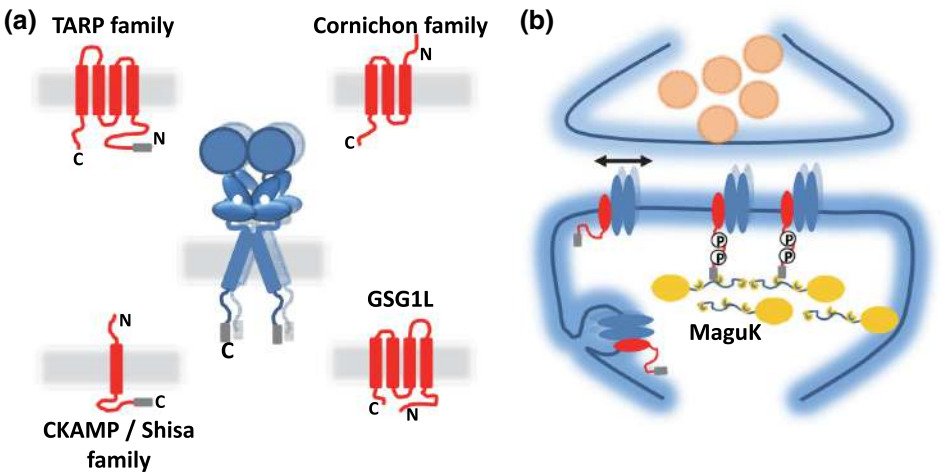

Fig. 2 Scheme of the molecular organization of AMPAR content. (a) Representation of the AMPAR (as a tetrameric structure) and of the various identified auxiliary proteins structure. (b) Schematic representation of an example of molecular AMPAR complex stabilization inside synapse. The phosphorylation of the cytoplasmic tail of stargazin favors its orientation to the cytosol, increasing its interactions with scaffolding proteins, and so immobilizing the AMPAR complex.[92,93,94] Nonphosphorylated complexes present a higher lateral surface mobility.

The most studied auxiliary proteins belong to the family of the TARPs, which include stargazin (TARP γ-2), the canonical member of this family. Stargazin is important for the trapping of AMPARs inside the synapse and more particularly to the MAGUK proteins present inside the PSD (such as PSD95[84,92]). The loss of interaction between the TARP and the scaffold, as shown using a c-terminus truncation mutant of stargazin that cannot bind PSD95 (delta-C mutant), impairs AMPAR accumulation at synapses, decreasing the amplitude of the synaptic response.[95] Single-particle tracking video microscopy demonstrated that the dynamic interaction between stargazin and PSD-95 regulates the exchange of AMPARs by lateral diffusion between extrasynaptic and synaptic compartments.[95] Those exchanges are controlled mostly by the phosphorylation state of the TARP[92,93,96] [Fig. 2(b)]. The disruption of this interaction using competing divalent ligands reduces AMPAR synaptic function and decreases the trapping of AMPAR at synapses.[97] Interestingly, competing for the TARP-PSD95 interaction could suppress only half of the synaptic responses, suggesting that other interactions might be at play to stabilize AMPAR at synapses.

Little is known about the role of other TARPs on AMPAR lateral diffusion and immobilization at the PSD. TARP γ-7, mainly expressed in the cerebellum, seems to be also involved in the regulation of AMPAR anchoring inside the synapse,[98,99] and TARP γ-8, mainly expressed in the hippocampus and in the cortex, seems to control AMPAR number at the plasma membrane and extrasynaptic localization,[100] even if its role in anchoring to PSD-95 is still controversial.[100,101]

The literature is less abundant concerning the auxiliary proteins that do not belong to the TARP family, and for the moment, a clear vision of their physiological and molecular role is still lacking. The cornichon protein seems to be able to form a tripartite interaction with AMPAR and TARP.[102] This interaction could stabilize AMPAR/TARP complex and act on AMPAR gating properties.[89] Initially, the shisa family members had been identified as a regulator of the biophysical properties of AMPARs[82,90,91,103] but recently, Klaassen et al.[91] demonstrated that they also play a role in anchoring AMPAR. All those studies pointed to the existence of a tight coupling between the regulation of AMPAR gating properties and their diffusion/trapping behavior. Despite extensive research on the role of the different auxiliary protein on AMPAR properties, heavy work is still needed to determine the contribution of the AMPAR complex composition variability into the multiplicity of synaptic response properties observed in the different central nervous system areas.

Even if the precise role of each AMPAR auxiliary subunit is not clear, previous studies have shown that they play a crucial role in both the lateral diffusion and the synaptic organization of AMPAR, thus regulating the synaptic transmission efficiency. Most of these experiments used quantum dot or FRAP experiments, limiting the access to a high number of individual molecule properties. The emergence of new high-density live super-resolution techniques with higher throughput will now allow better characterization of the role of each auxiliary protein in AMPAR organization and diffusion properties.

2.3 *Postsynaptic Nano-Organization*

As mentioned above, studies in the early 2000s questioned the existence of a putative sub-PSD organization of postsynaptic proteins.[54,56,59] Unfortunately, optical microscopy is limited by diffraction to 300 nm, rendering it impossible to decipher AMPAR organization with a precision higher than the PSD size. First attempts at describing this organization have been performed using single-particle tracking with quantum dots. In these conditions, random second to minute time scale immobilization of AMPAR in the PSD was reported, revealing a potential local subsynaptic organization.[76] But it is only the recent application of the new super-resolution microscopy techniques on AMPAR that succeeded to reveal the AMPAR nano-organization inside synapses.[64,65,104–106]

In the last decade, new microscopy techniques have been developed to bypass the diffraction limit, such as structured illumination microscopy, stimulated emission depletion (STED), and single-molecule localization microscopy, including photo-activated localization microscopy (PALM), universal point

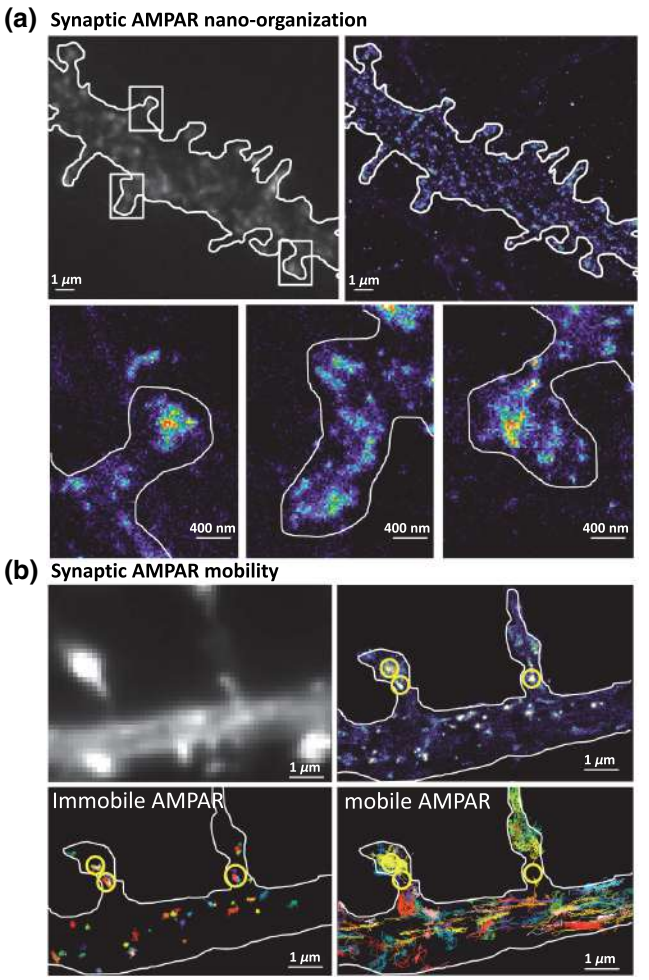

Fig. 3 Example of AMPAR nano-organization and lateral mobility. (a) Image of conventional fluorescence images and high-resolution d-STORM of AMPAR organization on a dendrite (upper part), with zoom on three synapses, where clusters can be easily distinguished (lower part). (b) Image of conventional fluorescence images and high-resolution u-PAINT of AMPAR lateral mobility on a dendrite (upper part). In the lower part are represented individual AMPAR trajectories of immobile receptors (left panel), which are mainly presented inside nanoclusters (yellow circle), and mobile receptors (right panel), which are enriched out of the nanoclusters.

accumulation in nanoscale topography (u-PAINT), and stochastic optical reconstruction microscopy (STORM).[107–115] These techniques allow observation of biological samples with 10- to 100-nm spatial resolution. The improvement in labeling techniques, fluorescent probes, and optical parameters has led to major improvements in this field and opened the possibility today to perform multicolor three-dimensional (3-D) image acquisitions at tens of nanometer resolution,[116–120] in tissue,[121–124] or even *in vivo*.[125–128] This improvement in super-resolution imaging also led to the development of high-density single-particle tracking at the nanoscale. The most used approach is arguably sptPALM,[114] which allows tracking target proteins genetically fused with photoswitchable fluorescent proteins. More recently, the development of u-PAINT allowed for the first time to track a high density of endogenous membrane proteins and to build super-resolved images of native proteins in real time by stochastic labeling.[110]

The emergence of those super-resolution imaging techniques and their application in neuroscience allows a better understanding of the dynamic distribution of synaptic proteins at the nanoscale. In 2010, for the first time, STORM on fixed olfactory bulb slices was performed to map the organization of various pre- and postsynaptic scaffolding proteins.[122] A few years later, three papers using different complementary super-resolution techniques were published and tackled the question of the nano-organization of postsynaptic AMPARs and PSD-95.[64,65,105]

Using a combination of super-resolution techniques, on fixed or living hippocampal cultured neurons, Nair et al. focused on AMPAR's dynamic nano-organization. Using u-PAINT and sptPALM, they tracked AMPARs at high density and showed for the first time the presence at synapses of AMPARs nanodomains. They observed that AMPARs are immobilized in fixed hotspots and are mobile between those. Super-resolution imaging on fixed cells (u-PAINT, PALM, dSTORM, and STED), as well as electron microscopy, confirmed the presence of one to three 80 nm clusters per synapse containing 20 to 25 receptors each (Fig. 3). Those AMPAR nanodomains can be stable for tens of minutes at the synapse as shown by time lapse sptPALM.[65] On the other hand, MacGillavry et al.[64] studied the dynamic organization of PSD-95-mEOS by PALM and sptPALM and showed the presence of one 80-nm clusters per synapse. Fukata et al.[105] via an elegant approach, observed ~150-nm cluster of the palmitoylated form of PSD-95 tagged using for the first time a genetically encoded antibody sensitive to palmitoylated form of PSD95 and imaged by STED microscopy. Nair et al. also investigated the organization of PSD-95 fused to mEOS by PALM and found ~150-nm clusters. While the presence of PSD-95 cluster is observed by the three groups, the number of clusters is still controversial since MacGillavry et al. observed one cluster per PSD (<10% of PSDs contain more than one PSD-95 cluster), whereas Fukata et al. and Nair et al. observed between one to four cluster per PSD depending of the PSD size (~40% of PSDs contain more than one PSD-95 cluster). Recently, Blanpied's group reported an average of two nanoclusters of endogenous PSD-95 per synapse.[129] In brain slices, these PSD95 subclusters have been recently reported as well, and both Broadhead et al. and Tang et al. found that 20% to 40% of PSDs contain more than one PSD-95 nanocluster, on PSD95 mEOS or GFP knock-in mice or endogenous PSD 95, respectively.[104,129]

Due to the large number of laboratories that have reported the postsynaptic nano-organization of PSD95 and AMPAR, this new concept discovered 3 years ago is now being currently accepted. One important question regarding this synaptic organization has been answered recently by the work of Blanpied's Lab, demonstrating the presence of presynaptic–postsynaptic nanocolumns.[129]

It is optically challenging to realize multiple color experiments at the nanoscale because of drift during acquisition, or achromatisms, and so on. The solution they used was to couple a new cluster detection method based on tessellation[130] and cross-correlation analysis to determine if two proteins are organized better than random. Tang et al. applied this analysis type on dual 3-D-dSTORM images to observe presynaptic scaffolding proteins as regulating synaptic membrane exocytosi (RIM)1/2 and the main postsynaptic scaffolding protein, PSD-95. RIM is known to play an important role in synaptic-vesicle docking through its interaction with MUNC13, which recruits calcium-channels.[131–133] Tang et al. observed that RIM1/2 presents a clustered organization identical to PSD95 nanoclusters in both

size and number of clusters. On the contrary, MUNC13 is more broadly distributed, and Bassoon seems randomly organized.[129]

Tang et al.[129] demonstrated that presynaptic clusters of RIM1/2 are mainly aligned in front of postsynaptic clusters of PSD95. This study provides evidence for the existence of transsynaptic nanocolumns which coorganize the presynaptic machinery for glutamate release with the postsynaptic AMPAR nanodomains. This new concept reveals a molecular level of organization between pre- and postsynapses unexpected 20 years ago, which likely notably improves the efficiency of synaptic transmission. The molecular component responsible for this presynaptic–postsynaptic alignment remains to be identified. Deciphering the parameters that determine their regulation during physiological processes as maturation and plasticities will be important. Multiple candidates have been identified, such as neurexin/neuroligin, N-cadherin, leucine rich repeat transmembrane, or synCAM, but the relevant molecules are still unknown.[134–137]

The physiological impact of such an organization of the postsynaptic compartment on synaptic transmission properties was then investigated by using modeling. MacGillavry et al. used Monte Carlo simulation to determine the effect of the localization of glutamate release on uniform or clustered distribution of AMPARs and showed that the release of glutamate on AMPARs cluster increases the amplitude of mEPSCs compared to an "off cluster" release or release on a "uniform" distribution.[64] Based on the same model, Nair et al.[65] determined the impact not only of AMPAR density inside clusters, but also of the intercluster distance and cluster to release site distance on synaptic responses. Monte Carlo simulations suggested that all these parameters strongly impact the amplitude of mEPSCs. The density of AMPARs was the most sensitive parameter. On the contrary, a certain tolerance of a couple of tens of nanometer with respect to mEPSC amplitude was observed with respect to the location of the glutamate release site. Indeed, mEPSCs amplitude decreased only when the release site was at least 100 nm away from the nanodomain center.

In spines containing more than one AMPAR nanodomain, the average intercluster distance was measured of 450 nm, with only 20% of clusters closer than 250 nm from one another. Monte Carlo simulations showed that when glutamate was released on top of a nanodomain, the second nanodomain is not activated if the intercluster distance is larger than 300 nm, revealing a certain independence of each nanodomain.[65]

Experimentally, Nair et al. partly destabilized nanodomains to investigate the experimental importance of such an organization on synaptic properties. PSD-95 is one of the main organizers of AMPAR at synapses and two color super-resolution imaging of PSD-95 and AMPAR suggests a colocalization of both proteins. Knocking-down PSD-95 led to a 21% decrease of AMPAR number per nanodomain, which was correlated with a 20% decrease in mEPSCs amplitude. This correlation between nanodomain content in AMPAR and the amplitude of synaptic transmission suggests that AMPAR nanodomains could be responsible for the postsynaptic quantum of synaptic response.

This discovery of AMPAR nano-organization coupled to the concept of lateral diffusion changes our vision of the synaptic organization and function, but raises multiple questions. The previously reported studies present a new vision of the synapse at its stable state, but synapses are plastic organelles, able to adapt both to short- and long-term stimulation. Hence, one can postulate that modifications of AMPAR nanoscale organization could underlie various forms of synaptic plasticity. Many studies have brought indications of the molecular rearrangements taking place during plasticity at the whole synapse—diffraction limited—level; we now need to fuse these studies with the concept of lateral diffusion and nanoclustering of AMPAR to deliver a new vision of synaptic transmission regulation during plastic events.

3 Activity Regulates the Dynamic Nano-Organization of AMPARs

3.1 *Importance of the Dynamic Nano-Organization of AMPARs for Short-Term Plasticity*

Neurons are able to adapt their synaptic response at high frequency as a function of the previously received stimuli. Indeed, the amplitude of a second response is highly dependent on the delay that separates it from the first one. This mechanism, called short-term plasticity, has been abundantly described because it varies as a function of the type of neuron, the maturation status of the synapses, and so on and determines the capacity of the neuron to integrate and either filter or amplify the received signal.[138] Until recently, regulation of paired pulse responses has solely been attributed to presynaptic modifications of transmitter release or AMPAR desensitization. Presynaptic short-term plasticity mechanisms largely involve variations in presynaptic calcium buffering capacities or availability of transmitter filled vesicles for release. If release probability is boosted by the first stimulus, this leads to paired pulse facilitation, whereas if release probability decreases, it leads to paired pulse depression. Postsynaptic AMPAR desensitization also participates in paired pulse depression at synapses with high release probability.[139–141] However, it has been generally thought that at most synapses, and in particular at the Schaffer collateral-CA1 cell synapses, AMPAR desensitization does not participate in short-term plasticity.[142] Generally, the impact of AMPAR desensitization on paired pulse synaptic responses is observed to be surprisingly lower than expected with respect to the AMPAR biophysical properties observed in heterologous systems.[143]

The introduction of the concept of AMPAR lateral mobility in 2002 brought a new potentially important parameter.[47] Indeed, the speed of the mobile receptors, around 0.1 to 1 $\mu m^2 s^{-1}$, is compatible with the temporality of paired pulse synaptic events. In 2008, a role for AMPAR lateral mobility in tuning the rate of recovery from paired pulse depression was proposed. Heine et al. showed that the blockade of AMPAR lateral mobility through antibody crosslinking largely decreases the amplitude of the second synaptic response, promoting paired-pulse depression.[77] The general idea underlying this study was that as AMPAR constantly diffuse inside synapses, their speed allows them to cross the PSD within tens of milliseconds. Thus, during a paired pulse response with an interstimulus interval in the tens of ms range, a significant amount of AMPAR can be spatially exchanged. After a first glutamate release, all receptors, and so among them the desensitized one, could thus be replaced by naïve receptors from adjacent regions. This could allow a faster recovery from synaptic depression. The conclusion of this work was that AMPAR lateral mobility could contribute to improve the synaptic response to high-frequency stimulation.

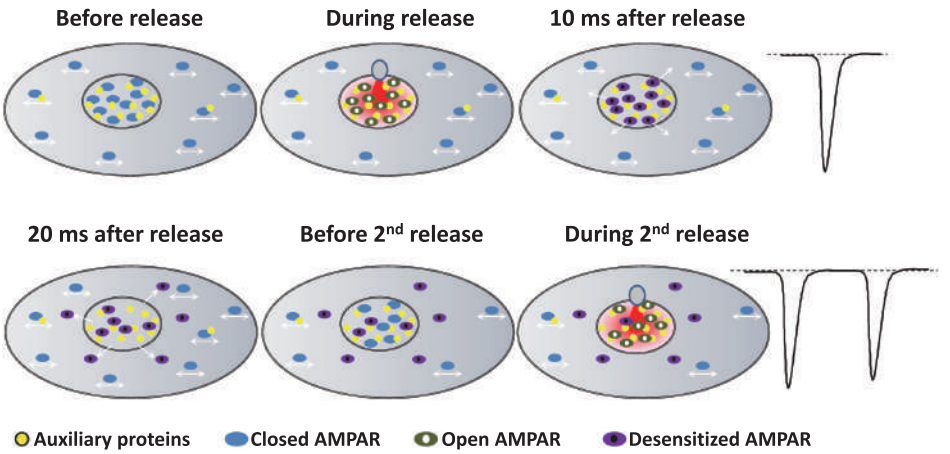

Fig. 4 Chronological scheme of the role of AMPAR lateral mobility on short-term paired pulse response. Before release, all receptors are closed, part of them are trapped inside clusters, the other diffusing freely. Just after release, if release happens on clusters, receptors in an area of 150 nm around the release site get opened and then rapidly desensitized, leading to classical synaptic currents. Rapidly, part of desensitized receptors unbind from their auxiliary proteins and diffuse out of the release site. Diffusive closed receptors can be trapped by the free auxiliary proteins, renewing the naïve AMPAR content inside the cluster. When a second release happens, part of receptors desensitized by the first release have diffused out of the area facing the release site, and most receptors under the release are in a closed state, available for activation by the second release. This conformational-dependent lateral mobility favors a sustained synaptic response at high release frequency.

The role of AMPAR diffusion on paired pulse responses could be even stronger if only desensitized receptors would diffuse out of the release site, whereas naïve receptors would replace them. Several studies reported that glutamate tends to increase AMPAR mobility,[49,144] without clearly identifying the underlying molecular mechanism. Using conformational mutants and drug applications, Constals et al. demonstrated that desensitized receptors are more diffusive than opened or closed receptors.[75] Glutamate induced unbinding, or at least uncoupling, between AMPARs and its main auxiliary protein stargazin has been described since 2004.[145,146] The use of genetic fusion between AMPAR and stargazin and biochemical experiments confirmed that the glutamate-dependent mobility increase was due to a loss of affinity of desensitized receptors for their auxiliary proteins.[75] This loss of AMPAR-TARP interaction is important for the recovery observed during paired-pulse depression experiments[75] (Fig. 4). Other auxiliary proteins may also play a role in the recovery from depression, such as Shisa6, which traps AMPAR into synapses and prevents desensitization during synaptic activity.[91]

A model emerged from these studies, in which AMPARs are immobilized inside nanodomains by interacting with auxiliary proteins and scaffolding proteins. The first release of glutamate activates AMPAR, which then quickly desensitize. The associated conformational changes trigger an increase in AMPAR mobility, freeing them from TARP induced immobilization. The freely diffusive closed receptors can be specifically trapped at these free trapping sites, allowing a renewing of AMPAR inside the nanocluster in the tens of milliseconds. This specific glutamate-induced mobility of desensitized AMPAR can be at the root of the receptor turnover essential for fidelity of fast synaptic transmission.[75] Such a model reconciles the role of AMPAR desensitization with their experimentally measured weak impact on paired pulse responses. A prediction of these results is that regulation of AMPAR mobility could adapt neuronal responses to bursting activity. It will be, therefore, of interest to determine the impact of AMPAR mobility on tuning network activity.

3.2 *Long-Term Plasticity*

While we described above how synapses can modify their short-term responses, it has also been described half a century ago that they can regulate their responses on the long term. These mechanisms, called long-term plasticity, seem at least in part, to be at the basis of information storage and memory.[18–20,34] It is now well established that these learning and memory mechanisms are mediated in large part by long lasting changes in the AMPAR mediated synaptic responses. The most thoroughly characterized examples of such synaptic plasticity are LTP and long-term depression (LTD).[18,34]

Since these first seminal papers, many laboratories worked to decipher the molecular mechanisms responsible for those events. It is now clear that LTP and LTD require the exocytosis and the endocytosis of AMPARs, respectively. These mechanisms trigger a regulation of the total amount of AMPAR at the cell surface. However, we previously described that the post-synapse is dynamically nano-organized and that both the dynamic and the organization of AMPAR regulate synaptic transmission properties. Recently, Monte Carlo-based simulation described the multiple molecular parameters that could lead to a potentiation.[63] Those simulations revealed that an increase in AMPAR clustering inside nanodomains, or an increase in the number of AMPAR per nanodomain, or an improvement of the alignment between presynaptic release sites and AMPAR clusters, could trigger an increase in AMPAR response amplitude. Surprisingly, these models suggested that a 50% potentiation in synaptic current necessitates either a 100% to 200% increase in AMPAR number at the synapses, or only a modest increase in the AMPARs density into nanodomains.[63,65] Based on those simulations and the discovery of the trapping of AMPAR into nanodomains, it is possible to postulate that

LTP could be due to an increase in the density of AMPAR and/or an increase of the nanodomain size, or an improvement in the alignment between the presynaptic glutamate release site and the postsynaptic nanodomain. The use of super-resolution microscopy being quite recent in the field, this hypothesis has not been yet investigated, but previous studies could help us to support or invalidate some of these hypotheses.

First, regarding the hypothesis of an increase in AMPAR density inside nanodomains during LTP, d-STORM experiments allowed to determine that 20 to 25 receptors are contained inside a nanodomain.[65,106,130] Structural properties of AMPARs indicate that an individual homomeric GluA2 AMPAR has a width of around 15 nm, at its N-terminal domain.[87] Even if some other studies determined that heteromeric GluA2/GluA3 AMPARs have a more compact NTD in an "O-shape,"[147] an estimation of around 15 nm taking into account the presence of the various auxiliary proteins should be close to the reality, leading to an estimated area of 0.0002 μm^2 per receptor.[148,149] The surface of a nanodomain is around 0.008 μm^2, corresponding to a diameter of 100 nm.[65] Based on mathematical compacting optimization calculation, a maximum of 35 receptors can be contained inside a single nanodomain.[150] Considering the molecular arrangement inside the membrane as a nearly optimal organization, justified by the ability of AMPAR to exchange inside the nanodomain, we can conclude that the packing level of AMPAR is already likely close to its maximum at the basal state, making unlikely the hypothesis that an increase of AMPAR density inside nanodomains could underlie LTP.

Another hypothesis proposed to explain LTP is an improvement of the alignment of the presynaptic release site with AMPAR nanodomains. Modeling has demonstrated that such changes in preorganization–postorganization should improve both amplitude and reliability of synaptic transmission.[56,59,63] Tang et al. have investigated the effect of chemical-LTP on the transsynaptic alignment between RIM1/2 and PSD-95 clusters. They reported that nanocolumns are conserved after LTP induction, with an enrichment of PSD-95 clusters. Unfortunately they did not precisely quantify the potential nanoscale changes between glutamate release sites and AMPARs nanodomains alignment during LTP.[129]

The last hypothesis relates to the incorporation of new AMPAR during LTP. An increase in the total amount of surface AMPARs due to exocytosis as well as an immobilization at synaptic sites of surface receptors has been regularly observed after LTP induction.[30,96,151,152] The use of single-molecule tracking allowed to investigate the molecular mechanisms responsible for the activity-dependent trapping of AMPAR inside the synapse.[47,78,96] After N-méthyl-D-aspartic acid receptor (NMDAR) activation by a LTP protocol, the resulting calcium influx triggers CaMKII translocation from a dendritic position to the synapses, where it phosphorylates the C-Terminal domain of various AMPAR subunits and auxiliary proteins. In the case of the AMPAR auxiliary protein stargazin, phosphorylation of the stretch of serines upstream of the c-terminal PDZ-binding domain changes the positive charges of the C-tail to highly negative, inducing its repulsion from the negatively charged membrane lipids. This allows the unfolding of the C-tail and favors its interaction with the scaffolding proteins PSD95.[92,93,96] Such a mechanism triggers a net increase in the synaptic trapping of AMPARs. However, whether AMPARs become trapped on pre-existing nanodomains or if new ones are created remains to be determined.

Other auxiliary proteins than stargazin could be implicated in this process. For example, gamma-8 is required for LTP.[100] All of those results strongly support the hypothesis that new synaptic immobilization slots for AMPAR are created during LTP induction.[153] The discovery of the nanodomain organization of AMPAR inside synapses underlines the importance of the localization of such trapping events. Nanodomains have been identified as the place where AMPARs are immobilized. Thus, an increase in AMPAR trapping should be mediated by an increase either in the number of clusters, or in their sizes. Use of super-resolution microscopy should help to answer this question and provide further evidence of the highly dynamic reorganization of AMPARs at the nanoscale during LTP.

4 Conclusion

Application of super-resolution techniques in both live and fixed neurons has revealed a new and unexpected level of AMPAR organization inside synapses, allowing to tune our model of synaptic transmission. Indeed, single-particle tracking microscopy has demonstrated that lateral mobility of AMPAR impacts fast synaptic transmission by creating a constant turnover between desensitized and naïve receptors. Fixed and live super-resolution techniques led to the discovery of AMPAR nano-organization and led to the introduction of the notion of a postsynaptic quantum of response.

Even if the interplay between long-term plasticity and AMPAR nanoscale organization has not yet been determined, previous work tends to support the notion that an increase in molecular trapping into nanodomains during LTP is at least one cause of the increase in synaptic response.

One century after the first description of the synapse, our vision largely evolved, due to technical improvements. A modern synapse is not a homogenously organized organelle but a complex assembly of nanoscale compartments whose individual components exchange constantly. This level of organization seems adapted to optimize the efficiency of use of the presynaptically released glutamate. Indeed, if as it as been recently shown, presynaptic release sites are aligned with AMPAR nanoclusters, the various glutamate receptors will be organized at a distance from release site relative to their affinity for glutamate.[129] The higher their affinity (as for NMDAR or mGluR) the less stringent the location of receptors with respect to the release site.

Regulation of AMPAR localization and trafficking heavily relies on a complex interplay between the AMPAR complex composition and the level of phosphorylation of the various cytoplasmic tails of the complex—be it receptors or their auxiliary proteins. The next step will be the understanding of the role of each auxiliary protein on AMPAR nanoscale organization and the impact on synaptic transmission properties during the various state of the synapse, during development and plasticity events, and in the different brain regions.

Acknowledgments

We express our thanks to Corey Butler for discussions and corrections of the manuscript. This work was supported by the ANR NanoDom, Labex BRAIN, and ANR-10-INBS-04 FranceBioImaging, Centre National de la Recherche Scientifique, ERC Grant ADOS 339541 to D.C. and a fellowship from the MESR to B.C. The authors have no relevant financial interests in this paper and no other potential conflicts of interest to disclose.

References

1. S. R. Y. Cajal, "Estudios sobre el plan estructural y composición histológica de los centros nerviosos adicionados de consideraciones fisiológicas fundadas en los nuevos descubrimientos," in *Textura del Sistema Nervioso del Hombre y de los Vertebrados*, Imprenta y Librería de Nicolás Moya, Madrid (1904).
2. E. D. De Robertis and H. S. Bennett, "Some features of the submicroscopic morphology of synapses in frog and earthworm," *J. Biophys. Biochem. Cytol.* **1**(1), 47–58 (1955).
3. S. L. Palay and G. E. Palade, "The fine structure of neurons," *J. Biophys. Biochem. Cytol.* **1**(1), 69–88 (1955).
4. E. D. De Robertis and H. S. Bennett, "A submicroscopic vesicular component of Schwann cells and nerve satellite cells," *Exp. Cell Res.* **6**(2), 543–545 (1954).
5. S. L. Palay, "Synapses in the central nervous system," *J. Biophys. Biochem. Cytol.* **2**(4 Suppl), 193–202 (1956).
6. J. Del Castillo and B. Katz, "Quantal components of the end-plate potential," *J. Physiol.* **124**(3), 560–573 (1954).
7. P. Fatt and B. Katz, "An analysis of the end-plate potential recorded with an intracellular electrode," *J. Physiol.* **115**(3), 320–370 (1951).
8. O. P. Hamill et al., "Improved patch-clamp techniques for high-resolution current recording from cells and cell-free membrane patches," *Pflugers Arch. Eur. J. Physiol.* **391**(2), 85–100 (1981).
9. M. Hollmann and S. Heinemann, "Cloned glutamate receptors," *Annu. Rev. Neurosci.* **17**, 31–108 (1994).
10. K. O. Cho, C. A. Hunt, and M. B. Kennedy, "The rat brain postsynaptic density fraction contains a homolog of the Drosophila discs-large tumor suppressor protein," *Neuron* **9**(5), 929–942 (1992).
11. C. A. Hunt, L. J. Schenker, and M. B. Kennedy, "PSD-95 is associated with the postsynaptic density and not with the presynaptic membrane at forebrain synapses," *J. Neurosci.* **16**(4), 1380–1388 (1996).
12. H. C. Kornau et al., "Domain interaction between NMDA receptor subunits and the postsynaptic density protein PSD-95," *Science* **269**(5231), 1737–1740 (1995).
13. S. G. Grant, "SnapShot: organizational principles of the postsynaptic proteome," *Neuron* **80**(2), 534.e1 (2013).
14. H. Husi and S. G. Grant, "Proteomics of the nervous system," *Trends Neurosci.* **24**(5), 259–266 (2001).
15. K. W. Li et al., "Proteomics analysis of rat brain postsynaptic density. Implications of the diverse protein functional groups for the integration of synaptic physiology," *J. Biol. Chem.* **279**(2), 987–1002 (2004).
16. R. S. Walikonis et al., "Identification of proteins in the postsynaptic density fraction by mass spectrometry," *J. Neurosci.* **20**(11), 4069–4080 (2000).
17. T. V. Bliss and T. Lomo, "Long-lasting potentiation of synaptic transmission in the dentate area of the anaesthetized rabbit following stimulation of the perforant path," *J. Physiol.* **232**(2), 331–356 (1973).
18. S. M. Dudek and M. F. Bear, "Homosynaptic long-term depression in area CA1 of hippocampus and effects of N-methyl-D-aspartate receptor blockade," *Proc. Natl. Acad. Sci. U. S. A.* **89**(10), 4363–4367 (1992).
19. E. R. Kandel, "Genes, synapses, and long-term memory," *J. Cell. Physiol.* **173**(2), 124–125 (1997).
20. R. E. Nicholls et al., "Transgenic mice lacking NMDAR-dependent LTD exhibit deficits in behavioral flexibility," *Neuron* **58**(1), 104–117 (2008).
21. S. Brenowitz and L. O. Trussell, "Minimizing synaptic depression by control of release probability," *J. Neurosci.* **21**(6), 1857–1867 (2001).
22. J. M. Bekkers and C. F. Stevens, "Presynaptic mechanism for long-term potentiation in the hippocampus," *Nature* **346**(6286), 724–729 (1990).
23. H. Kamiya, S. Sawada, and C. Yamamoto, "Persistent enhancement of transmitter release accompanying long-term potentiation in the guinea pig hippocampus," *Neurosci. Lett.* **130**(2), 259–262 (1991).
24. R. Malinow and R. W. Tsien, "Presynaptic enhancement shown by whole-cell recordings of long-term potentiation in hippocampal slices," *Nature* **346**(6280), 177–180 (1990).
25. S. N. Davies et al., "Temporally distinct pre- and post-synaptic mechanisms maintain long-term potentiation," *Nature* **338**(6215), 500–503 (1989).
26. J. A. Kauer, R. C. Malenka, and R. A. Nicoll, "A persistent postsynaptic modification mediates long-term potentiation in the hippocampus," *Neuron* **1**(10), 911–917 (1988).
27. R. C. Malenka et al., "Postsynaptic calcium is sufficient for potentiation of hippocampal synaptic transmission," *Science* **242**(4875), 81–84 (1988).
28. D. J. Perkel et al., "The role of Ca^{2+} entry via synaptically activated NMDA receptors in the induction of long-term potentiation," *Neuron* **11**(5), 817–823 (1993).
29. S. Choi, J. Klingauf, and R. W. Tsien, "Postfusional regulation of cleft glutamate concentration during LTP at 'silent synapses'," *Nat. Neurosci.* **3**(4), 330–336 (2000).
30. J. T. Isaac, R. A. Nicoll, and R. C. Malenka, "Evidence for silent synapses: implications for the expression of LTP," *Neuron* **15**(2), 427–434 (1995).
31. D. Liao, N. A. Hessler, and R. Malinow, "Activation of postsynaptically silent synapses during pairing-induced LTP in CA1 region of hippocampal slice," *Nature* **375**(6530), 400–404 (1995).
32. G. Carlson, Y. Wang, and B. E. Alger, "Endocannabinoids facilitate the induction of LTP in the hippocampus," *Nat. Neurosci.* **5**(8), 723–724 (2002).
33. J. P. Terranova et al., "Inhibition of long-term potentiation in rat hippocampal slices by anandamide and WIN55212-2: reversal by SR141716 A, a selective antagonist of CB1 cannabinoid receptors," *Naunyn-Schmiedeberg's Arch. Pharmacol.* **352**(5), 576–579 (1995).
34. T. V. Bliss and A. R. Gardner-Medwin, "Long-lasting potentiation of synaptic transmission in the dentate area of the unanaestetized rabbit following stimulation of the perforant path," *J. Physiol.* **232**(2), 357–374 (1973).
35. G. Lynch and M. Baudry, "The biochemistry of memory: a new and specific hypothesis," *Science* **224**(4653), 1057–1063 (1984).
36. G. Lynch et al., "Intracellular injections of EGTA block induction of hippocampal long-term potentiation," *Nature* **305**(5936), 719–721 (1983).
37. T. V. Bliss and G. L. Collingridge, "A synaptic model of memory: long-term potentiation in the hippocampus," *Nature* **361**(6407), 31–39 (1993).
38. G. Lynch, S. Halpain, and M. Baudry, "Effects of high-frequency synaptic stimulation on glumate receptor binding studied with a modified in vitro hippocampal slice preparation," *Brain Res.* **244**(1), 101–111 (1982).
39. D. Muller and G. Lynch, "Long-term potentiation differentially affects two components of synaptic responses in hippocampus," *Proc. Natl. Acad. Sci. U. S. A.* **85**(23), 9346–9350 (1988).
40. E. C. Beattie et al., "Regulation of AMPA receptor endocytosis by a signaling mechanism shared with LTD," *Nat. Neurosci.* **3**(12), 1291–1300 (2000).
41. W. Lu et al., "Activation of synaptic NMDA receptors induces membrane insertion of new AMPA receptors and LTP in cultured hippocampal neurons," *Neuron* **29**(1), 243–254 (2001).
42. D. S. Bredt and R. A. Nicoll, "AMPA receptor trafficking at excitatory synapses," *Neuron* **40**(2), 361–379 (2003).
43. R. C. Carroll et al., "Dynamin-dependent endocytosis of ionotropic glutamate receptors," *Proc. Natl. Acad. Sci. U. S. A.* **96**(24), 14112–14117 (1999).
44. C. Luscher et al., "Role of AMPA receptor cycling in synaptic transmission and plasticity," *Neuron* **24**(3), 649–658 (1999).
45. S. H. Shi et al., "Rapid spine delivery and redistribution of AMPA receptors after synaptic NMDA receptor activation," *Science* **284**(5421), 1811–1816 (1999).
46. I. Song and R. L. Huganir, "Regulation of AMPA receptors during synaptic plasticity," *Trends Neurosci.* **25**(11), 578–588 (2002).
47. A. J. Borgdorff and D. Choquet, "Regulation of AMPA receptor lateral movements," *Nature* **417**(6889), 649–653 (2002).
48. D. Choquet and A. Triller, "The role of receptor diffusion in the organization of the postsynaptic membrane," *Nat. Rev.* **4**(4), 251–265 (2003).
49. C. Tardin et al., "Direct imaging of lateral movements of AMPA receptors inside synapses," *EMBO J.* **22**(18), 4656–4665 (2003).
50. A. Baude et al., "High–resolution immunogold localization of AMPA type glutamate receptor subunits at synaptic and non-synaptic sites in rat hippocampus," *Neuroscience* **69**(4), 1031–1055 (1995).
51. M. Antal et al., "Numbers, densities, and colocalization of AMPA- and NMDA-type glutamate receptors at individual synapses in the superficial spinal dorsal horn of rats," *J. Neurosci.* **28**(39), 9692–9701 (2008).

52. M. Masugi-Tokita et al., "Number and density of AMPA receptors in individual synapses in the rat cerebellum as revealed by SDS-digested freeze-fracture replica labeling," *J. Neurosci.* **27**(8), 2135–2144 (2007).
53. J. Tanaka et al., "Number and density of AMPA receptors in single synapses in immature cerebellum," *J. Neurosci.* **25**(4), 799–807 (2005).
54. G. Liu, S. Choi, and R. W. Tsien, "Variability of neurotransmitter concentration and nonsaturation of postsynaptic AMPA receptors at synapses in hippocampal cultures and slices," *Neuron* **22**(2), 395–409 (1999).
55. K. M. Franks, T. M. Bartol, and T. J. Sejnowski, "A Monte Carlo model reveals independent signaling at central glutamatergic synapses," *Biophys. J.* **83**(5), 2333–2348 (2002).
56. K. M. Franks, C. F. Stevens, and T. J. Sejnowski, "Independent sources of quantal variability at single glutamatergic synapses," *J. Neurosci.* **23**(8), 3186–3195 (2003).
57. T. A. Nielsen, D. A. DiGregorio, and R. A. Silver, "Modulation of glutamate mobility reveals the mechanism underlying slow-rising AMPAR EPSCs and the diffusion coefficient in the synaptic cleft," *Neuron* **42**(5), 757–771 (2004).
58. L. P. Savtchenko, S. Sylantyev, and D. A. Rusakov, "Central synapses release a resource-efficient amount of glutamate," *Nat. Neurosci.* **16**(1), 10–12 (2013).
59. E. Tarusawa et al., "Input-specific intrasynaptic arrangements of ionotropic glutamate receptors and their impact on postsynaptic responses," *J. Neurosci.* **29**(41), 12896–12908 (2009).
60. J. D. Clements, "Transmitter timecourse in the synaptic cleft: its role in central synaptic function," *Trends Neurosci.* **19**(5), 163–171 (1996).
61. J. D. Clements et al., "The time course of glutamate in the synaptic cleft," *Science* **258**(5087), 1498–1501 (1992).
62. J. E. Lisman, S. Raghavachari, and R. W. Tsien, "The sequence of events that underlie quantal transmission at central glutamatergic synapses," *Nat. Rev.* **8**(8), 597–609 (2007).
63. L. P. Savtchenko and D. A. Rusakov, "Moderate AMPA receptor clustering on the nanoscale can efficiently potentiate synaptic current," *Philos. Trans. R. Soc. London, Ser. B* **369**(1633), 20130167 (2014).
64. H. D. MacGillavry et al., "Nanoscale scaffolding domains within the postsynaptic density concentrate synaptic AMPA receptors," *Neuron* **78**(4), 615–622 (2013).
65. D. Nair et al., "Super-resolution imaging reveals that AMPA receptors inside synapses are dynamically organized in nanodomains regulated by PSD95," *J. Neurosci.* **33**(32), 13204–13224 (2013).
66. S. J. Singer and G. L. Nicolson, "The fluid mosaic model of the structure of cell membranes," *Science* **175**(4023), 720–731 (1972).
67. D. Axelrod et al., "Mobility measurement by analysis of fluorescence photobleaching recovery kinetics," *Biophys. J.* **16**(9), 1055–1069 (1976).
68. D. Axelrod et al., "Lateral motion of fluorescently labeled acetylcholine receptors in membranes of developing muscle fibers," *Proc. Natl. Acad. Sci. U. S. A.* **73**(12), 4594–4598 (1976).
69. N. M. Chao, S. H. Young, and M. M. Poo, "Localization of cell membrane components by surface diffusion into a "trap"," *Biophys. J.* **36**(1), 139–153 (1981).
70. S. H. Young and M. M. Poo, "Rapid lateral diffusion of extrajunctional acetylcholine receptors in the developing muscle membrane of Xenopus tadpole," *J. Neurosci.* **3**(1), 225–231 (1983).
71. J. Gelles, B. J. Schnapp, and M. P. Sheetz, "Tracking kinesin-driven movements with nanometre-scale precision," *Nature* **331**(6155), 450–453 (1988).
72. A. Kusumi, Y. Sako, and M. Yamamoto, "Confined lateral diffusion of membrane receptors as studied by single particle tracking (nanovid microscopy). Effects of calcium-induced differentiation in cultured epithelial cells," *Biophys. J.* **65**(5), 2021–2040 (1993).
73. K. Suzuki et al., "Rapid hop diffusion of a G-protein-coupled receptor in the plasma membrane as revealed by single-molecule techniques," *Biophys. J.* **88**(5), 3659–3680 (2005).
74. J. Meier et al., "Fast and reversible trapping of surface glycine receptors by gephyrin," *Nat. Neurosci.* **4**(3), 253–260 (2001).
75. A. Constals et al., "Glutamate-induced AMPA receptor desensitization increases their mobility and modulates short-term plasticity through unbinding from stargazin," *Neuron* **85**(4), 787–803 (2015).
76. M. D. Ehlers et al., "Diffusional trapping of GluR1 AMPA receptors by input-specific synaptic activity," *Neuron* **54**(3), 447–460 (2007).
77. M. Heine et al., "Surface mobility of postsynaptic AMPARs tunes synaptic transmission," *Science* **320**(5873), 201–205 (2008).
78. E. M. Petrini et al., "Endocytic trafficking and recycling maintain a pool of mobile surface AMPA receptors required for synaptic potentiation," *Neuron* **63**(1), 92–105 (2009).
79. P. Klemmer, A. B. Smit, and K. W. Li, "Proteomics analysis of immuno-precipitated synaptic protein complexes," *J. Proteomics* **72**(1), 82–90 (2009).
80. J. Schwenk et al., "High-resolution proteomics unravel architecture and molecular diversity of native AMPA receptor complexes," *Neuron* **74**(4), 621–633 (2012).
81. J. Schwenk et al., "Functional proteomics identify cornichon proteins as auxiliary subunits of AMPA receptors," *Science* **323**(5919), 1313–1319 (2009).
82. J. von Engelhardt et al., "CKAMP44: a brain-specific protein attenuating short-term synaptic plasticity in the dentate gyrus," *Science* **327**(5972), 1518–1522 (2010).
83. V. A. Letts et al., "The mouse stargazer gene encodes a neuronal Ca^{2+}-channel gamma subunit," *Nat. Genet.* **19**(4), 340–347 (1998).
84. L. Chen et al., "Stargazin regulates synaptic targeting of AMPA receptors by two distinct mechanisms," *Nature* **408**(6815), 936–943 (2000).
85. J. Choi et al., "Phosphorylation of stargazin by protein kinase A regulates its interaction with PSD-95," *J. Biol. Chem.* **277**(14), 12359–12363 (2002).
86. J. Schwenk et al., "Regional diversity and developmental dynamics of the AMPA-receptor proteome in the mammalian brain," *Neuron* **84**(1), 41–54 (2014).
87. A. I. Sobolevsky, M. P. Rosconi, and E. Gouaux, "X-ray structure, symmetry and mechanism of an AMPA-subtype glutamate receptor," *Nature* **462**(7274), 745–756 (2009).
88. S. Tomita et al., "Functional studies and distribution define a family of transmembrane AMPA receptor regulatory proteins," *J. Cell Biol.* **161**(4), 805–816 (2003).
89. M. B. Gill et al., "Cornichon-2 modulates AMPA receptor-transmembrane AMPA receptor regulatory protein assembly to dictate gating and pharmacology," *J. Neurosci.* **31**(18), 6928–6938 (2011).
90. A. R. Karataeva et al., "C-terminal interactors of the AMPA receptor auxiliary subunit Shisa9," *PLoS One* **9**(2), e87360 (2014).
91. R. V. Klaassen et al., "Shisa6 traps AMPA receptors at postsynaptic sites and prevents their desensitization during synaptic activity," *Nat. Commun.* **7**, 10682 (2016).
92. S. Tomita et al., "Bidirectional synaptic plasticity regulated by phosphorylation of stargazin-like TARPs," *Neuron* **45**(2), 269–277 (2005).
93. A. S. Hafner et al., "Lengthening of the stargazin cytoplasmic tail increases synaptic transmission by promoting interaction to deeper domains of PSD-95," *Neuron* **86**(2), 475–489 (2015).
94. A. Sumioka, D. Yan, and S. Tomita, "TARP phosphorylation regulates synaptic AMPA receptors through lipid bilayers," *Neuron* **66**(5), 755–767 (2010).
95. C. Bats, L. Groc, and D. Choquet, "The interaction between Stargazin and PSD-95 regulates AMPA receptor surface trafficking," *Neuron* **53**(5), 719–734 (2007).
96. P. Opazo et al., "CaMKII triggers the diffusional trapping of surface AMPARs through phosphorylation of stargazin," *Neuron* **67**(2), 239–252 (2010).
97. M. Sainlos et al., "Biomimetic divalent ligands for the acute disruption of synaptic AMPAR stabilization," *Nat. Chem. Biol.* **7**(2), 81–91 (2010).
98. C. Bats et al., "Channel properties reveal differential expression of TARPed and TARPless AMPARs in stargazer neurons," *Nat. Neurosci.* **15**(6), 853–861 (2012).
99. A. S. Kato et al., "New transmembrane AMPA receptor regulatory protein isoform, gamma-7, differentially regulates AMPA receptors," *J. Neurosci.* **27**(18), 4969–4977 (2007).
100. N. Rouach et al., "TARP gamma-8 controls hippocampal AMPA receptor number, distribution and synaptic plasticity," *Nat. Neurosci.* **8**(11), 1525–1533 (2005).
101. A. Sumioka et al., "PDZ binding of TARPgamma-8 controls synaptic transmission but not synaptic plasticity," *Nat. Neurosci.* **14**(11), 1410–1412 (2011).
102. A. S. Kato et al., "Hippocampal AMPA receptor gating controlled by both TARP and cornichon proteins," *Neuron* **68**(6), 1082–1096 (2010).

103. P. Farrow et al., "Auxiliary subunits of the CKAMP family differentially modulate AMPA receptor properties," *eLife* **4**, e09693 (2015).
104. M. J. Broadhead et al., "PSD95 nanoclusters are postsynaptic building blocks in hippocampus circuits," *Sci. Rep.* **6**, 24626 (2016).
105. Y. Fukata et al., "Local palmitoylation cycles define activity-regulated postsynaptic subdomains," *J. Cell Biol.* **202**(1), 145–161 (2013).
106. E. Hosy, C. Butler, and J. B. Sibarita, "Organization and dynamics of AMPA receptors inside synapses-nano-organization of AMPA receptors and main synaptic scaffolding proteins revealed by super-resolution imaging," *Curr. Opin. Chem. Biol.* **20**, 120–126 (2014).
107. B. Albrecht et al., "Spatially modulated illumination microscopy: online visualization of intensity distribution and prediction of nanometer precision of axial distance measurements by computer simulations," *J. Biomed. Opt.* **6**(3), 292–299 (2001).
108. E. Betzig, "Proposed method for molecular optical imaging," *Opt. Lett.* **20**(3), 237–239 (1995).
109. E. Betzig et al., "Imaging intracellular fluorescent proteins at nanometer resolution," *Science* **313**(5793), 1642–1645 (2006).
110. G. Giannone et al., "Dynamic superresolution imaging of endogenous proteins on living cells at ultra-high density," *Biophys. J.* **99**(4), 1303–1310 (2010).
111. M. G. Gustafsson, "Surpassing the lateral resolution limit by a factor of two using structured illumination microscopy," *J. Microsc.* **198**(Pt 2), 82–87 (2000).
112. M. Heilemann et al., "Subdiffraction-resolution fluorescence imaging with conventional fluorescent probes," *Angew. Chem. Int. Ed.* **47**(33), 6172–6176 (2008).
113. S. W. Hell and J. Wichmann, "Breaking the diffraction resolution limit by stimulated emission: stimulated-emission-depletion fluorescence microscopy," *Opt. Lett.* **19**(11), 780–782 (1994).
114. S. Manley et al., "High-density mapping of single-molecule trajectories with photoactivated localization microscopy," *Nat. Methods* **5**(2), 155–157 (2008).
115. M. J. Rust, M. Bates, and X. Zhuang, "Sub-diffraction-limit imaging by stochastic optical reconstruction microscopy (STORM)," *Nat. Methods* **3**(10), 793–796 (2006).
116. M. Bates et al., "Multicolor super-resolution imaging with photo-switchable fluorescent probes," *Science* **317**(5845), 1749–1753 (2007).
117. B. Huang et al., "Whole-cell 3D STORM reveals interactions between cellular structures with nanometer-scale resolution," *Nat. Methods* **5**(12), 1047–1052 (2008).
118. B. Huang et al., "Three-dimensional super-resolution imaging by stochastic optical reconstruction microscopy," *Science* **319**(5864), 810–813 (2008).
119. M. F. Juette et al., "Three-dimensional sub-100 nm resolution fluorescence microscopy of thick samples," *Nat. Methods* **5**(6), 527–529 (2008).
120. A. Vaziri et al., "Multilayer three-dimensional super resolution imaging of thick biological samples," *Proc. Natl. Acad. Sci. U. S. A.* **105**(51), 20221–20226 (2008).
121. P. Bethge et al., "Two-photon excitation STED microscopy in two colors in acute brain slices," *Biophys. J.* **104**(4), 778–785 (2013).
122. A. Dani et al., "Superresolution imaging of chemical synapses in the brain," *Neuron* **68**(5), 843–856 (2010).
123. J. Tonnesen et al., "Two-color STED microscopy of living synapses using a single laser-beam pair," *Biophys. J.* **101**(10), 2545–2552 (2011).
124. N. T. Urban et al., "STED nanoscopy of actin dynamics in synapses deep inside living brain slices," *Biophys. J.* **101**(5), 1277–1284 (2011).
125. S. Berning et al., "Nanoscopy in a living mouse brain," *Science* **335**(6068), 551–551 (2012).
126. B. C. Chen et al., "Lattice light-sheet microscopy: imaging molecules to embryos at high spatiotemporal resolution," *Science* **346**(6208), 1257998 (2014).
127. R. Galland et al., "3D high- and super-resolution imaging using single-objective SPIM," *Nat. Methods* **12**(7), 641–644 (2015).
128. L. Gao et al., "Noninvasive imaging beyond the diffraction limit of 3D dynamics in thickly fluorescent specimens," *Cell* **151**(6), 1370–1385 (2012).
129. A. H. Tang et al., "A trans-synaptic nanocolumn aligns neurotransmitter release to receptors," *Nature* **536**(7615), 210–214 (2016).
130. F. Levet et al., "SR-Tesseler: a method to segment and quantify localization-based super-resolution microscopy data," *Nat. Methods* **12**(11), 1065–1071 (2015).
131. L. Deng et al., "RIM proteins activate vesicle priming by reversing autoinhibitory homodimerization of Munc13," *Neuron* **69**(2), 317–331 (2011).
132. Y. Han et al., "RIM determines $Ca^{(2)+}$ channel density and vesicle docking at the presynaptic active zone," *Neuron* **69**(2), 304–316 (2011).
133. K. S. Liu et al., "RIM-binding protein, a central part of the active zone, is essential for neurotransmitter release," *Science* **334**(6062), 1565–1569 (2011).
134. I. Chamma et al., "Mapping the dynamics and nanoscale organization of synaptic adhesion proteins using monomeric streptavidin," *Nat. Commun.* **7**, 10773 (2016).
135. K. Perez de Arce et al., "Topographic mapping of the synaptic cleft into adhesive nanodomains," *Neuron* **88**(6), 1165–1172 (2015).
136. L. Saglietti et al., "Extracellular interactions between GluR2 and N-cadherin in spine regulation," *Neuron* **54**(3), 461–477 (2007).
137. P. Scheiffele et al., "Neuroligin expressed in nonneuronal cells triggers presynaptic development in contacting axons," *Cell* **101**(6), 657–669 (2000).
138. R. S. Zucker and W. G. Regehr, "Short-term synaptic plasticity," *Annu. Rev. Physiol.* **64**, 355–405 (2002).
139. D. A. DiGregorio et al., "Desensitization properties of AMPA receptors at the cerebellar mossy fiber granule cell synapse," *J. Neurosci.* **27**(31), 8344–8357 (2007).
140. M. Koike-Tani et al., "Involvement of AMPA receptor desensitization in short-term synaptic depression at the calyx of Held in developing rats," *J. Physiol.* **586**(9), 2263–2275 (2008).
141. A. Rozov and N. Burnashev, "Polyamine-dependent facilitation of postsynaptic AMPA receptors counteracts paired-pulse depression," *Nature* **401**(6753), 594–598 (1999).
142. G. O. Hjelmstad et al., "Lack of AMPA receptor desensitization during basal synaptic transmission in the hippocampal slice," *J. Neurophysiol.* **81**(6), 3096–3099 (1999).
143. C. Auger and A. Marty, "Quantal currents at single-site central synapses," *J. Physiol.* **526** (Pt 1), 3–11 (2000).
144. A. G. Petzoldt et al., "Gating characteristics control glutamate receptor distribution and trafficking in vivo," *Curr. Biol.* **24**(17), 2059–2065 (2014).
145. M. Morimoto-Tomita et al., "Autoinactivation of neuronal AMPA receptors via glutamate-regulated TARP interaction," *Neuron* **61**(1), 101–112 (2009).
146. S. Tomita et al., "Dynamic interaction of stargazin-like TARPs with cycling AMPA receptors at synapses," *Science* **303**(5663), 1508–1511 (2004).
147. B. Herguedas et al., "Structure and organization of heteromeric AMPA-type glutamate receptors," *Science* **352**(6285), aad3873 (2016).
148. N. Armstrong et al., "Measurement of conformational changes accompanying desensitization in an ionotropic glutamate receptor," *Cell* **127**(1), 85–97 (2006).
149. J. Krieger, I. Bahar, and I. H. Greger, "Structure, dynamics, and allosteric potential of ionotropic glutamate receptor N-terminal domains," *Biophys. J.* **109**(6), 1136–1148 (2015).
150. R. L. Graham et al., "Dense packings of congruent circles in a circle," *Discrete Math.* **181**, 139–154 (1998).
151. M. Park et al., "Recycling endosomes supply AMPA receptors for LTP," *Science* **305**(5692), 1972–1975 (2004).
152. Z. Szepesi et al., "Synaptically released matrix metalloproteinase activity in control of structural plasticity and the cell surface distribution of GluA1-AMPA receptors," *PLoS One* **9**(5), e98274 (2014).
153. P. Opazo and D. Choquet, "A three-step model for the synaptic recruitment of AMPA receptors," *Mol. Cell. Neurosci.* **46**(1), 1–8 (2011).

Benjamin Compans received his master's degree in neuroscience from the University of Bordeaux. He is a PhD student at the Interdisciplinary Institute for Neuroscience, Bordeaux, France, in Dr. Daniel Choquet's lab. During his PhD under the supervision of Dr. Eric Hosy, he aims to understand how the dynamic nano-organization of AMPA receptors contributes to the establishment of synaptic plasticity.

Daniel Choquet received his engineering degree from Ecole Centrale, Paris, France, and his PhD with Henri Korn from Pasteur Institute, Paris. He was a CNRS research officer in 1988 and a postdoc with Michael Sheetz at Duke University, North Carolina, USA. Currently, he is a director of the Institute for Interdisciplinary Neuroscience and the Bordeaux Imaging Center, Bordeaux, France, and a director of the BRAIN excellence cluster. He runs an interdisciplinary program on the use of high-resolution imaging to study the trafficking of neurotransmitter receptors in neurons.

Eric Hosy received his PhD in plant field in Montpellier, then studied channel structure function on KATP channel in Grenoble. He started working in neuroscience in 2006 in Rotterdam before moving to Daniel Choquet's Group, where he has been recruited at the CNRS in 2009. He is the coinventor of the U-PAINT technique and develops thematic centered around the coupling of live super-resolution technique and electrophysiology to determine the physiological role of AMPA receptor nano-organization.

Chapter 4

Regulation of synaptic inputs

1. Synaptic plasticity

Neurons communicate with their neighbors by sampling and integrating the thousands of synaptic inputs that they receive. Neurons display several mechanisms to specifically adjust the strength of a specific input among the entire bulk of synapses. This leads to an increase/ decrease of a particular stimulation input weight compare to all the other inputs received by the neuron. To this end, neuron can modulate independently or jointly the three parameters of the NPQ paradigm.

Indeed, as described in detail in the review (Compans et al., 2016), the post-synaptic organization of AMPARs play a key role to tune the quantum unit of synaptic transmission (Q value) (**Figure 9**). Due to the development of super-resolution microscopy and its recent application to Neuroscience, it has been possible to decipher the precise organization of the main actors of synaptic transmission. Mainly, AMPARs and its main scaffolding protein PSD-95 have been shown to be organized in nanodomains of less than 100 nm (Fukata et al., 2013; MacGillavry et al., 2013; Nair et al., 2013). Several studies have suggested that the control of the density rather than the global number of receptors at synapses plays a central role in controlling the weight of synaptic inputs (MacGillavry et al., 2013; Nair et al., 2013; Savtchenko and Rusakov, 2013). Thus, this nanodomain organization appears crucial in adjusting the synaptic gain. More recently, Blanpied's lab demonstrated that those AMPAR nanodomains are located in front of glutamate release sites (Tang et al., 2016). While the impact of this alignment accuracy has not been studied, Monte-Carlo based simulation suggested that it could have an important role in tuning synaptic transmission (Franks et al., 2003; MacGillavry et al., 2013; Nair et al., 2013; Tarusawa et al., 2009). However this last hypothesis remains to be investigated.

In addition to the direct control of the amplitude of unitary synaptic currents, synaptic connections may increase their contribution to the neuronal integrated input by being active at higher rates (variation of the Pr) or in synchrony with other inputs, or simply by modifying the number of active synapses on the postsynaptic neuron (modification of the N parameter). Through this chapter, I will do an overview of our knowledge on molecular mechanisms implicated in synaptic plasticity, with a particular focus on the role of AMPARs.

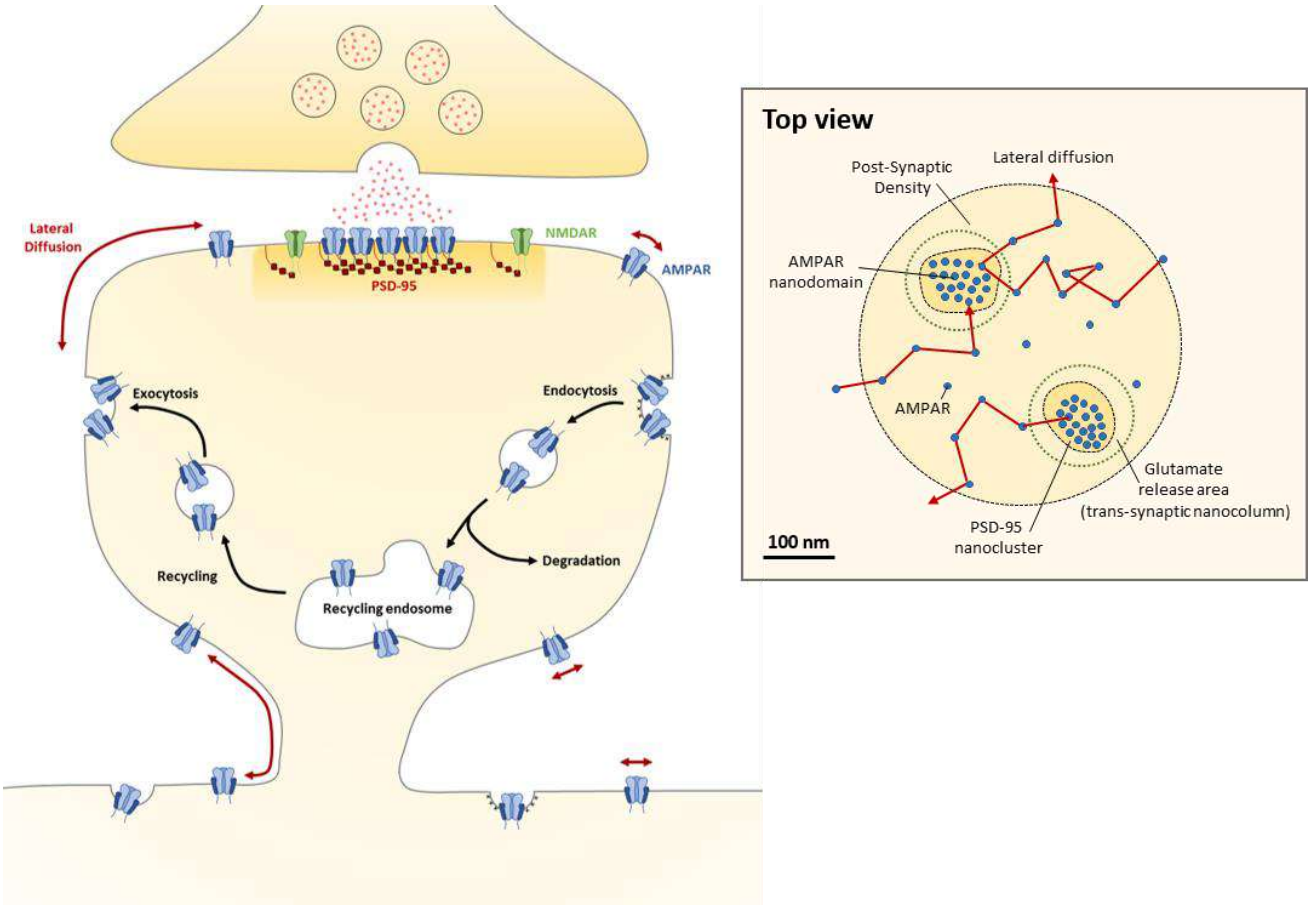

Figure 9. AMPAR dynamic organization at the synapse. AMPAR traffic between the plasma membrane and the intracellular compartment through endocytosis and exocytosis. Once at the cell surface, AMPARs reach the PSD through lateral diffusion and get trapped by interacting with PSD-95 via their associated stargazin. At synapses, AMPARs are organized in nanodomains located in front of glutamate release sites.

2. Short-term plasticity

Synapses display the ability to adapt their efficiency depending on the inputs they receive. This dynamic gain control occurs on short time scales (tens to thousands of milliseconds). This **S**hort-**T**erm **P**lasticity (STP) exists in two forms called **S**hort-**T**erm **F**acilitation and **S**hort-**T**erm **D**epression (STF and STD, respectively) which correspond to a short lasting strengthening or weakening of synaptic gain in response to high-frequency glutamate release (Zucker and Regehr, 2002). In contrast to long-term plasticity, STP-induced modifications of synaptic efficacy do not last and the synaptic efficacy returns quickly to its baseline level without continued pre-synaptic activity. The form of STP which is induced upon high-frequency stimulation depends on the neuronal cell type and can also vary within a same type of neuron. For instance, pyramidal neurons of the CA1 region in the hippocampus have both STD- and

STF-dominated synapses. In contrast, in the cerebellum, climbing fiber synapses express mainly STD while STF dominates in parallel fiber synapses (Dittman et al., 2000; Dobrunz and Stevens, 1997). Although the precise role of STP is not clearly understood, it is thought to have filtering functions that are used in information processing and could be simplified as a dynamic gain control of synaptic inputs (Abbott, 1997; Dittman et al., 2000; Fortune and Rose, 2000, 2001; Rotman et al., 2011).

a. Pre-synaptic origins of STP

STF and STD share an identical pre-synaptic origin. Facilitation of synaptic transmission on short time scale is caused by over-accumulation of Ca^{2+} at the AZ vicinity during high-frequency stimuli, leading to an increase of P_r. Substantial evidence has accumulated in support of this residual Ca^{2+} hypothesis: (i) pre-synaptic Ca^{2+} concentration correlates with STF of synaptic transmission, (ii) buffering pre-synaptic Ca^{2+} or reducing Ca^{2+} influx reduces STF (Salin et al., 1996; Schneggenburger and Neher, 2000; Scimemi and Diamond, 2012; Zucker and Regehr, 2002). Concerning STD, it is also attributed to a pre-synaptic mechanism but post-synaptic properties can contribute to it. The most widespread mechanism is attributed to a decrease of the glutamate release which is likely related to a depletion of the readily releasable pool of vesicles even if a decrease in pre-synaptic quantal size has been proposed (Burrone and Lagnado, 2000; Chen et al., 2002, 2004; Zucker and Regehr, 2002). From a general point of view, pre-synaptic short-term plasticities are based on transient Pr modifications.

b. Post-synaptic contribution to STD

Although it is well accepted that STPs originate from a pre-synaptic mechanism, desensitization of AMPARs has been implied at least partly in STD (Chen et al., 2002; Heine et al., 2008; Otis et al., 1996; Zucker and Regehr, 2002). Indeed, after the first stimulus, some AMPARs do not recover from desensitization before the following release, implying that less receptors can be activated during the second release. In the presence of AMPAR desensitization inhibitors, **P**aired-**P**ulse **D**epression (PPD) is impaired (Brenowitz and Trussell, 2001; Heine et al., 2008). In addition, the enhancement of residual glutamate in the synaptic cleft by blocking glutamate transporters increased PPD, while glutamate scavengers reduced it (Turecek and Trussell, 2000). Thus, most of studies explain STD as a combination of depression of pre-synaptic glutamate release and desensitization of AMPARs upon glutamate binding. Return

from depression is believed to arise from the replenishment of the readily releasable pool and from the recovery from desensitization (Trussell et al., 1993; Xu-Friedman and Regehr, 2004).

More recently, Heine *et al.* reported that AMPAR lateral diffusion was able to tune the recovery from post-synaptic depression induced at high-frequency glutamate release (**Figure 10**). They observed that blocking AMPAR lateral diffusion with an antibody crosslinking strategy increased the PPD. The explanation was that lateral diffusion is fast enough to allow an exchange of receptors in and out synapses between two consecutive releases of glutamate. Based on diffusion properties of AMPARs at synapses, the replacement of synaptic receptors after the first glutamate release by lateral diffusion occurs faster that the recovery of individual AMPAR from desensitization. Thus, short-term depression does not depend on two but three parameters: (i) depression of pre-synaptic glutamate release, (ii) AMPAR desensitization and (iii) AMPAR lateral diffusion (Heine et al., 2008). This study, confirmed by latter ones, showed the physiological importance of AMPAR surface mobility in controlling the synaptic gain during high-frequency inputs (Frischknecht et al., 2009; Heine et al., 2008; Opazo et al., 2010).

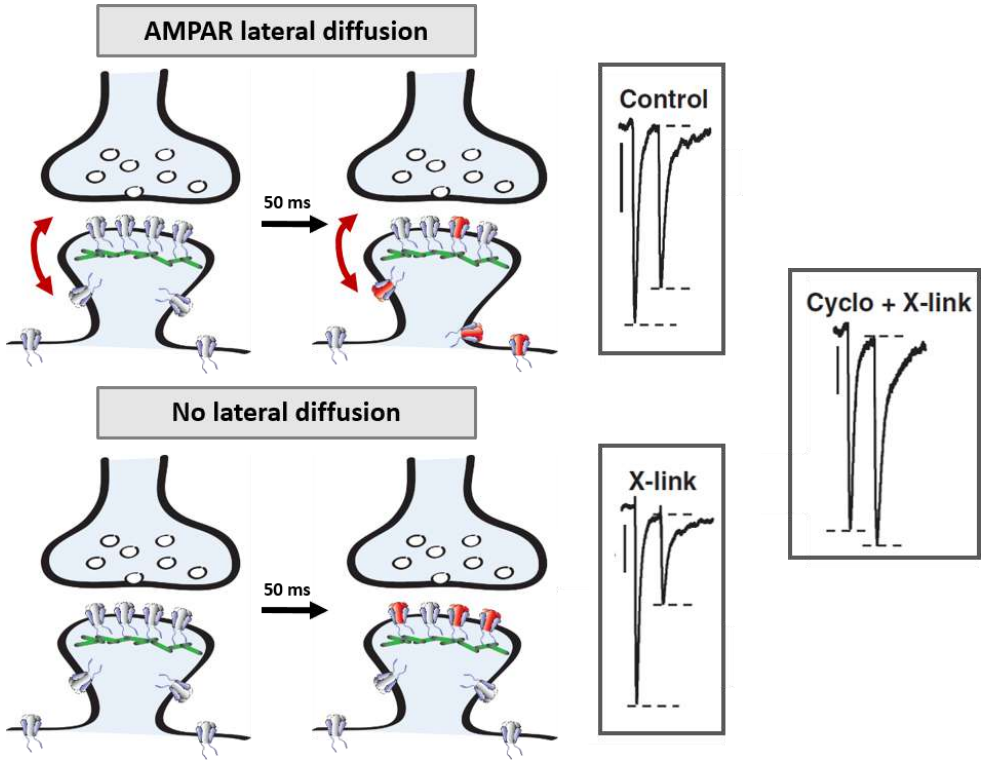

Figure 10. AMPAR lateral diffusion tunes Short-Term Plasticity. In control condition, in which AMPAR lateral diffusion occurs, paired-pulse stimulation at 20 Hz triggers a short-term depression. When lateral diffusion is blocked (X-link), similar paired-pulse stimulation triggers an exacerbated short-term depression which is prevented by the application of cyclothiazide (which prevent AMPAR desensitization). Electrophysiological traces from Heine et al 2008.

3. Long-term plasticity

It has been suggest by Ramon y Cajal and then by Hebb that learning and memory depend critically on long-lasting changes in synaptic strength (Hebb, 1949; Ramon y Cajal, 1909). Hebb postulated that "when an axon of cell A is near enough to excite a cell B and repeatedly or persistently takes part in firing it, some growth process or metabolic change takes place in one or both cells such that A's efficiency, as one of the cells firing B, is increased". In other words, the Hebbian postulate is that if a pre-synaptic neuron A is repeatedly taking part in activating the post-synaptic neuron B, along with a set of other pre-synaptic neurons, then the strength of the synaptic connection between A and B should be increased. This mechanism is believed to store memory traces. The first experimental evidences came from Bliss and Lomo in 1973. They demonstrated that EPSPs evoked in the hippocampus were increased by repeated high-frequency electrical stimulation, a phenomenon called **L**ong-**T**erm **P**otentiation (LTP) (Bliss and Lømo, 1973). Thus, repeated firing of a pre-synaptic neuron can induce a long-lasting increase of the activity of a post-synaptic neuron through synaptic strengthening. The fact that this mechanism was discovered in the hippocampus, a region involved in the process of learning and memory formation, has led to extensive studies on the role of LTP in learning paradigms (Bliss and Collingridge, 1993; Huganir and Nicoll, 2013). Several evidences suggested LTP to be the engram of memory formation, as interfering *in vivo* with its induction impaired some learning tasks (Holtmaat and Caroni, 2016; Nabavi et al., 2014; Takeuchi et al., 2014). However, the direct implication of LTP in learning and memory remains so far to be conclusively demonstrated.

Although Hebb's postulate appears exact, the inverse mechanism was not considered. At the time when LTP was discovered, it was suggested that an inverse of LTP could exist in the brain, termed **L**ong-**T**erm **D**epression (LTD). Based on monocular deprivation experiments in kittens (Hubel and Wiesel, 1965; Wiesel and Hubel, 1965), Stent postulated that "when the pre-synaptic axon of cell A repeatedly and persistently fails to excite the post-synaptic cell B while cell B is firing under the influence of other pre-synaptic axons, metabolic change takes place in one or both cells such that A's efficiency, as one of the cells firing B, is decreased" (Stent, 1973). As the depressing synapse is not active during this mechanism, this synaptic weakening was termed heterosynaptic LTD. It has been experimentally confirmed when LTD has been induced on an inactive pathway while inducing LTP in another (Abraham and Goddard, 1983; Lynch et al., 1977). More commonly, input-specific LTD (or homosynaptic LTD) can be observed in the cortex and hippocampus following low-frequency stimulation (Dudek and Bear,

1992; Mulkey and Malenka, 1992; Stanton and Sejnowski, 1989). LTD is thought to be a key mechanism to optimize information storage in a neuronal network, for behavioral flexibility and during sensory-experience adaptation, development and network refinement (Collingridge et al., 2010; Nabavi et al., 2014; Nicholls et al., 2008).

It is now clear that bidirectional long lasting changes in synaptic strength can be induced by frequency-dependent stimulations. However, those protocols do not reflect realistic firing patterns observed *in vivo*. On the contrary, some LTP paradigms are pathological as they reflect epileptic activity. Other paradigms, based on temporal order between pre-synaptic and post-synaptic firing, are accepted as more physiological and have been observed in several brain regions from different animal species. This plasticity mechanism termed **S**pike **T**iming-**D**ependent **P**lasticity (STDP) allows strengthening/weakening of synapses in a frequency- and timing-dependent manner. Typically, if the pre-synaptic neuron fires an AP a few milliseconds before or at the same time than the post-synaptic neuron, LTP is produced. The opposite temporal order triggers LTD (Levy and Steward, 1983; Magee, 1997; Markram, 1997; Sjostrom et al., 2008; Stanton and Sejnowski, 1989). STDP does not depend solely on the temporal order between pre- and post-synaptic firing but also on the input-frequency (Lisman and Spruston, 2005; Sjostrom et al., 2008; Sjöström et al., 2001). High-frequency (>20 Hz) burst of pre-before-post pairing produced LTP, while low-frequency (<10 Hz) burst of pre-before-post pairing failed to produced LTP. In contrast, low-frequency (<20 Hz) post-before-pre pairing produced LTD, while high-frequency (>40 Hz) post-before-pre pairing produced LTP (Sjöström et al., 2001).

The coincidence between pre- and post-synaptic activities is detected at synapses and is widely accepted to rely on NMDARs. As explained previously, NMDARs require post-synaptic depolarization to remove their Mg^{2+} block and allow Ca^{2+} influx. Thus they can detect coincidence between glutamate release due to pre-synaptic activity and depolarization due to post-synaptic spiking (back propagating AP or dendritic spike due to AMPAR activation in synaptic cluster area). Thus, the coincidence between pre- and post-synaptic activity (or pre-before-post) leads to the opening of NMDARs via depolarization-induced removal of Mg^{2+} block, resulting in a high level Ca^{2+} influx required to trigger LTP. In contrast, post-before-pre pairing leads to a low level of Ca^{2+} rise by the limited opening of NMDARs (Dan and Poo, 2004; Magee, 1997; Markram, 1997). Although both LTP and LTD are calcium-dependent phenomena, the signaling cascades involved are different and trigger distinct molecular modifications at the origin of the increase or decrease of synaptic strength, respectively.

4. Long-Term Potentiation

Originally thought to be a pre-synaptic mechanism, the discovery of silence synapses and their unsilencing during LTP changed the global vision of this process. The only evidence suggesting a pre-synaptic mechanism for LTP was a decrease of failure rate which in fact have been fully explained by synapse unsilencing (Isaac et al., 1995; Liao et al., 1999). Other experiments using glutamate-uncaging conclusively demonstrated the post-synaptic expression mechanism of LTP (Matsuzaki et al., 2004).

LTP is triggered through repetitive activations of NMDARs leading to a high Ca^{2+} influx into the spine. This influx results in the activation of a specific Ca^{2+}-dependent signaling cascade within the spine allowing two main processes (**Figure 11A-B**). The first one is the stabilization of the surface diffusive AMPARs at the PSD through their phosphorylation and through phosphorylation of their TARPs (Bats et al., 2007; Lee et al., 2000; Opazo et al., 2010; Penn et al., 2017; Sumioka et al., 2011; Tomita et al., 2005a). High increase of Ca^{2+} concentration within the post-synapse during LTP activates the Ca^{2+}/**Ca**l**m**odulin-dependent protein **k**inase **II** (CaMKII). This kinase is recruited at the PSD where it phosphorylates AMPARs and their TARPs to favor their interaction with PSD-95 and thus trigger their accumulation at the PSD, ultimately leading to the potentiation of AMPAR-mediated EPSCs in a long lasting manner (Huganir and Nicoll, 2013; Lee et al., 2010, 2000; Lisman et al., 2012; Lu et al., 2010; Murakoshi et al., 2017; Opazo et al., 2010). This fast initial recruitment of AMPARs is only possible thanks to the receptor lateral diffusion from extra-synaptic to synaptic sites (Bats et al., 2007; Borgdorff and Choquet, 2002; Makino and Malinow, 2009; Opazo et al., 2010; Penn et al., 2017). This increase in synaptic AMPAR content is accompanied by an increase of spine volume, a process known as structural LTP (sLTP) (Nägerl et al., 2004; Nishiyama and Yasuda, 2015) (**Figure 11C and 12A**). The second important process triggered by the influx of Ca^{2+} is the exocytosis of AMPARs from recycling and/or reserve vesicular pool. It has been suggested that the newly exocytosed receptors are enriched in GluA1 homomers, as they are calcium permeant. This could help synapses to maintain a higher cytoplasmic calcium level in order to stabilize the CAMKII activity (Granger et al., 2013; Lledo, 1998; Lu et al., 2001; Makino and Malinow, 2009; Park et al., 2004; Petrini et al., 2009; Wu et al., 2017). To conclude, LTP corresponds mainly to a post-synaptic event which tends to increase the number/efficiency of AMPARs under the glutamate release site.

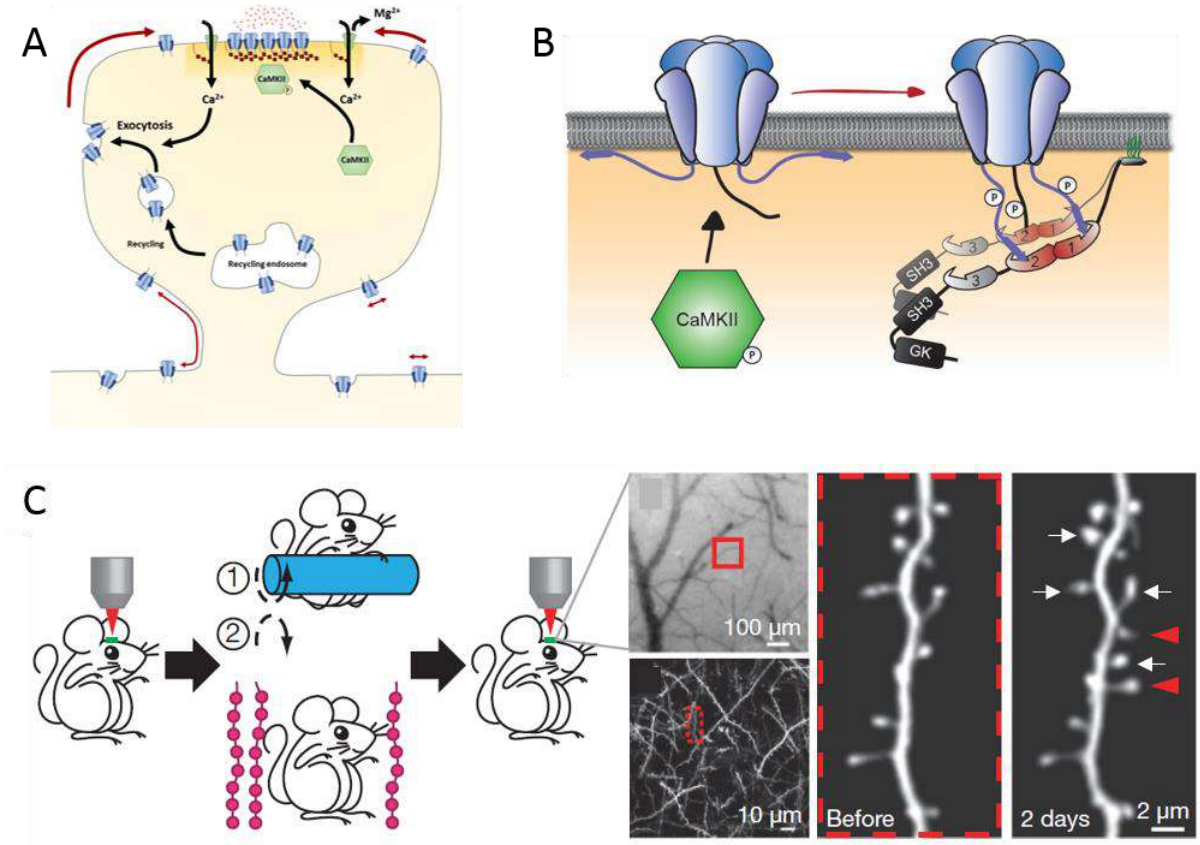

Figure 11. Long-Term Potentiation. (A) Molecular mechanism of LTP is dependent on both AMPAR immobilization at synapses and AMPAR exocytosis following Ca^{2+} influx and CaMKII activation. (B) AMPAR are immobilized at the PSD during LTP through CaMKII phosphorylation of both AMPAR and stargazin C-terminal domains. (C) Learning paradigms induce increase in spine volume (white arrows) and spine formation (red arrows) (adapted from Yang et al 2009)

5. Long-Term Depression

The LTD is a neuronal mechanism by which synaptic strength is decreased. Several forms of LTD have been characterized. It can be induced following LTP in a process called depotentiation and it can be either homosynaptic (input-specific) or heterosynaptic (not input-specific) (**Figure 12B-C**) (Collingridge et al., 2010). While these different forms of plasticity may seem similar as they all trigger weakening of synaptic strength, they use distinct molecular signaling pathways and probably have different functions. Here, we will use the term "LTD" to discuss about input-specific LTD only.

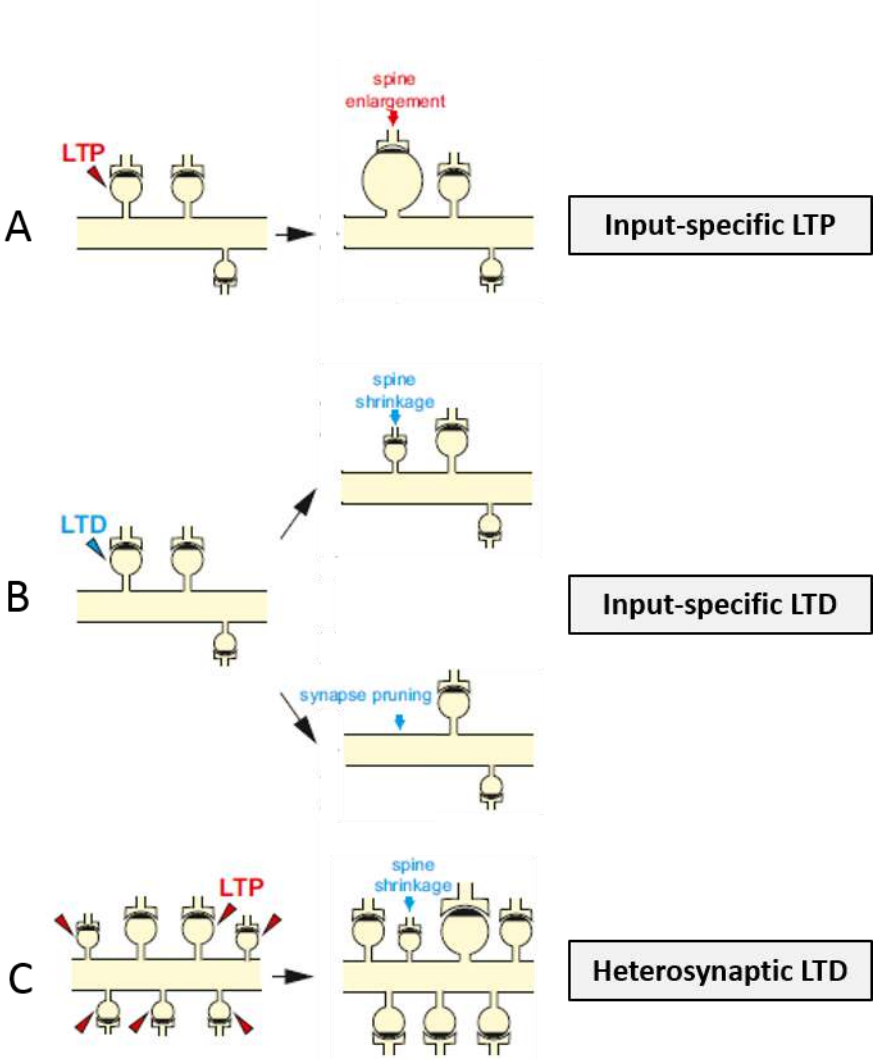

Figure 12. Long-term plasticity. (A) Input-specific LTP triggers increase in spine volume. (B) Input-specific LTD triggers either spine shrinkage or spine pruning. (C) Heterosynaptic LTD triggers spine shrinkage when surrounded spines undergo LTP. Figure adapted from Nishiyama and Yasuda 2015.

a. Input-specific LTD

LTD has been described in the hippocampus as a post-synaptic mechanism dependent on NMDAR activation (NMDAR-dependent LTD) (Dudek and Bear, 1992). Few studies investigated the role of the pre-synaptic element in the weakening of synaptic transmission. The existence of pre-synaptic mechanisms have been reported following a retrograde signaling (endocannabinoids, nitric oxide …) and are thought to modify the P_r or the readily releasable pool size. However this pre-synaptic mechanism is controversial, probably because the studies are performed in various brain regions and at different developmental stages (Collingridge et al., 2010; Goda and Stevens, 1998; Hjelmstad et al., 1997; Kreitzer and Malenka, 2007).

NMDAR-dependent LTD can be induced by low-frequency stimulation, STDP or chemically using specific agonist of NMDARs, which all result in a low or moderate increase of Ca^{2+} concentration into the post-synapse (Cummings et al., 1996; Dudek and Bear, 1992; Lee et al., 1998; Mulkey and Malenka, 1992; Sjöström et al., 2001). This low increase of calcium concentration in the spine triggers the activation of complex downstream signaling pathways which are not fully characterized yet. A simplified model presented in **Figure 13A** is that during NMDAR-dependent LTD, Ca^{2+} binds to calmodulin to activate the **P**rotein **P**hosphatase **2B (PP2B**, also named Calcineurin) which dephosphorylates Inhibitor-1 and thus release the **P**rotein **P**hosphatase **1 (PP1**) from inhibition (Mulkey et al., 1994, 1993). On the one hand, PP1 dephosphorylates S845 on the GluA1 C-terminal domain and stargazin (Lee et al., 2003, 1998; Sumioka et al., 2010; Tomita et al., 2005a). These dephosphorylations release AMPARs from synaptic trapping sites and thus decrease the amount of receptors at synapses, leading to synaptic depression (**Figure 13C**). But no direct evidence has been directly provided about the involvement of lateral diffusion following AMPAR and TARP dephosphorylations during LTD. In addition, PP1 has been described to rapidly dephosphorylate S295 on PSD-95, a phosphorylation site known to promote its synaptic accumulation (Kim et al., 2007). On the other hand PP1 dephosphorylates some kinases such as the **G**lycogen **S**ynthase **K**inase-**3** (GSK3) which in turn phosphorylates PSD-95 on T19. This phosphorylation on T19 requires S295 dephosphorylation and promotes PSD-95 removal from synapses (Nelson et al., 2013b). Recently, it has also been proposed that another important kinase could be involved in LTD. CaMKII, involved in the induction of LTP, could be activated during LTD and phosphorylate GluA1 subunit of AMPAR in its first intracellular loop at S567 (Coultrap et al., 2014; Goodell et al., 2017). This phosphorylation has been shown to decrease synaptic localization of AMPARs (Lu et al., 2010). Thus, CaMKII could sense and discriminate Ca^{2+} concentration, thus phosphorylate specific AMPAR sites and play a bidirectional role in long-term synaptic plasticities.

So far, the decrease of synaptic AMPAR number during LTD has been mainly attributed to an endocytosis process (Bhattacharyya et al., 2009; Carroll et al., 1999, 2001; Lüscher et al., 2000). The precise localization between extra-synaptic and peri-synaptic sites for AMPAR to get endocytosed is unclear. Also, the precise mechanism responsible for AMPAR endocytosis is poorly understood. The main evidence for AMPAR endocytosis is that the **N**-ethylmaleimide-**S**ensitive **F**actor (NSF), which stabilizes AMPARs at the membrane, is replaced by the **A**daptor **P**rotein **2** (AP2) that is involved in the recruitment of the machinery required for clathrin-dependent endocytosis (Man et al., 2000). AP2 also binds to dephosphorylated stargazin.

Disrupting the association between AP2 and stargazin blocks NMDAR-dependent LTD by preventing AMPAR internalization (Matsuda et al., 2013).

In parallel to molecular re-organization, LTD triggers morphological changes. In a similar manner than LTP triggers increase in spine volume and number, LTD triggers either spine shrinkage or pruning (Nägerl et al., 2004; Nishiyama and Yasuda, 2015; Oh et al., 2013; Woods et al., 2011). This network reorganization during LTD is thought to be at the origin of its physiological role (**Figure 13D**). During development, LTD is required to select the pertinent synapses when too many of them have been created. Later on, LTD plays an important role within circuits to trigger the selective elimination of weaker synapses (Wiegert and Oertner, 2013). This spine selection could be important for LTD function, meaning behavioral flexibility, experience-dependent adaptation, and memory erasing (Crozier et al., 2007; Nabavi et al., 2014; Nicholls et al., 2008).

A second major form of LTD requires the activation of group 1 mGluRs (mGluR-dependent LTD) (Bashir et al., 1993; Huber et al., 2001). Group 1 mGluRs are widely expressed in the CNS. Both NMDAR- and mGluR-dependent LTD exist in the hippocampus and the patterns of activation required to induce them are similar (Oliet et al., 1997). They also both depend on calcium signaling even if the origin of the calcium increase is different. Group 1 mGluR activation leads to the activation Ca^{2+} channels and of the phosphoinositide-specific **P**hospho**L**ipase **C** (PLC) which can trigger Ca^{2+} release from intracellular stores and activate the **P**rotein **K**inase **C** (PKC) (Collingridge et al., 2010; Gladding et al., 2009; Oliet et al., 1997). This increase in intracellular Ca^{2+} concentration results in the internalization of AMPARs through the possible recruitment of the **P**rotein **I**nteracting with **C** **K**inase **1 (**PICK1)-PKC complex at synapses in order to phosphorylate GluA2 subunit of AMPAR and dissociate GluA2-containing AMPAR from the **A**MPAR **B**inding **P**rotein (ABP) – **G**lutamate **R**eceptor **I**nteracting **P**rotein (GRIP) complex, leading to the receptor endocytosis (Casimiro et al., 2011; Collingridge et al., 2010; Gladding et al., 2009; Xiao et al., 2001).

b. Neuromodulator-induced LTD

Recently, Boué-Grabot's lab identified a new form of hippocampal LTD induced by the activation of post-synaptic purinergic receptor P2XR by noradrenalin-dependent astrocytic release of ATP (Pougnet et al., 2014; Yamazaki et al., 2002). This P2XR-dependent LTD, as the classical form of LTD, depends on Ca^{2+} to trigger AMPAR internalization and synaptic

depression (**Figure 13B**). However, in this form of LTD, Ca^{2+} enters in the post-synaptic element through P2XRs and activates both CaMKII and the phosphatases PP1 and PP2A. In contrary to NMDAR-dependent LTD, calcineurin is not involved. It was showed that both P2XR-dependent LTD and NMDAR-dependent LTD are independent from each other as the induction of one do not occlude the induction of the other one. P2XR stimulation through ATP application or noradrenergic stimulation of astrocytes (to trigger release of endogenous ATP) leads to a rapid removal of synaptic AMPARs and receptor internalization. This ATP-induced AMPAR internalization produces a long-lasting decrease of AMPAR-mediated EPSCs (Pougnet et al., 2014).

Astrocytes are known to regulate synaptic transmission. Release of gliotransmitters (ATP, glutamate and D-serine) has already been shown to be important for basal transmission and synaptic plasticity (Panatier et al., 2006, 2011; Pascual, 2005; Yang et al., 2003). Indeed, in addition to ATP, astrocytes can release D-serine, an endogenous co-agonist of NMDARs (Martineau et al., 2006; Mothet et al., 2000). By releasing D-serine, astrocytes can modulate the activity of synaptic NMDARs and control NMDAR-dependent long-term synaptic plasticity (Panatier et al., 2006; Yang et al., 2003).

In conclusion, neurons display two independent ways to decrease synaptic strength either via a synaptic input-specific response or through a more global neuromodulation by astrocytes. Although both lead to a decrease of AMPAR number at synapses, their distinct signaling pathways suggest a specific regulation of AMPAR organization and currents, as well as different physiological roles. It is thus important to decipher their specific impact on the regulation of the synaptic input.

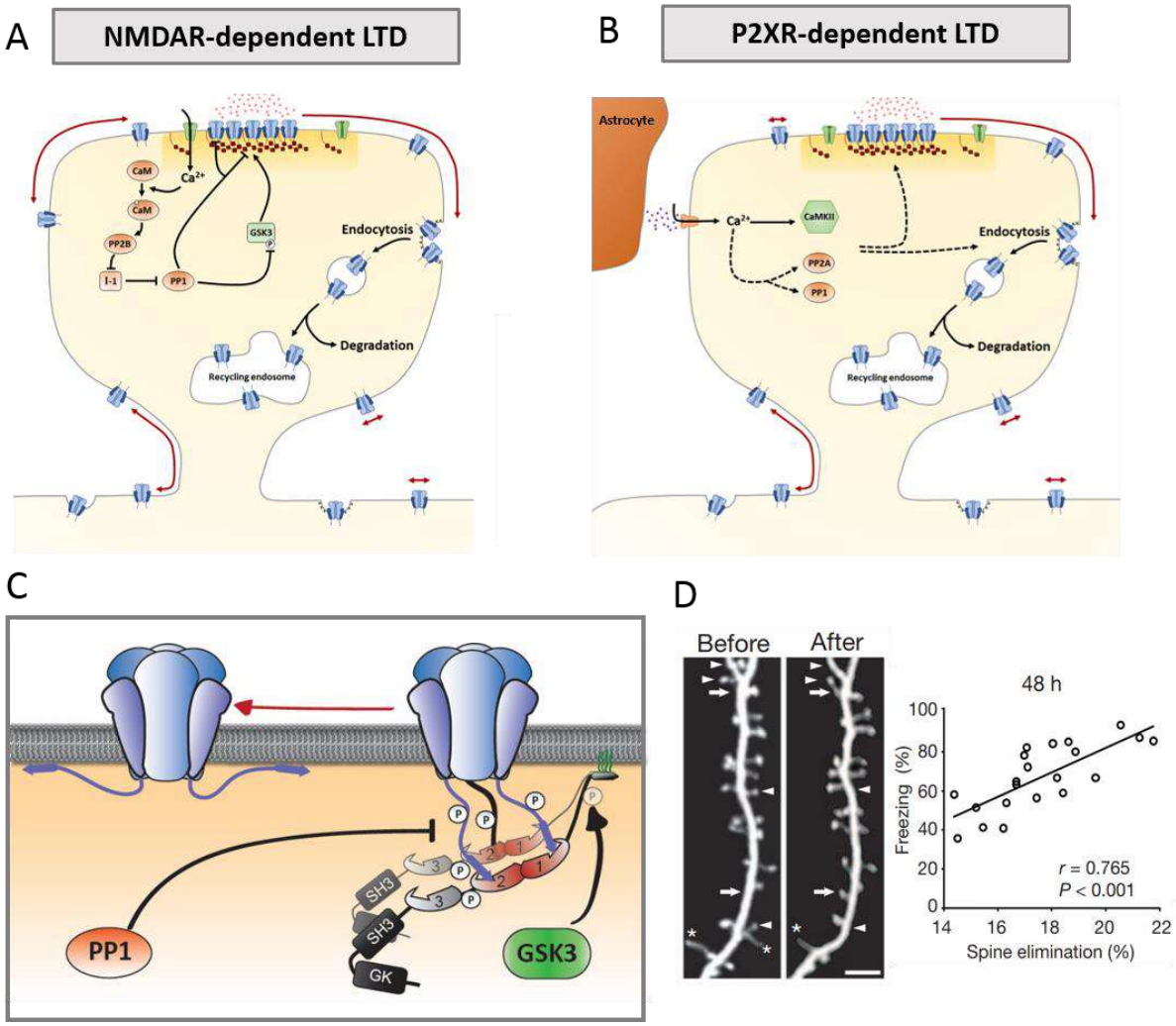

Figure 13. Long-Term Depression. (A) Molecular mechanism of NMDAR-dependent LTD. Calcium influx triggers the activation of a cascade of signalization base on the activation of various phosphatase and kinases to reorganize AMPARs through mobilization and endocytosis. (B) Molecular mechanism of P2XR-dependent LTD. (C) Dephosphorylation of AMPAR and stargazin by PP1 during NMDAR-dependent LTD reverse its immobilization at the PSD. (D) Learning paradigm triggers spine pruning (arrow head) often associated with LTD.

THESIS PROBLEMATIC

Neurons receive thousands of signals coming from other neurons in a spatial and temporal dependent manner and need to integrate them to transmit them in the form of an action potential. The first step occurs at synapses where chemical pre-synaptic signals have to be transformed as electrical signals. The emergence of super-resolution imaging techniques combined with modeling gave access to new understanding of synaptic function. As described in the introduction, AMPARs are densely organized in nanodomains which are molecularly aligned with glutamate release sites. Modeling reported that such pre-post co-organization with post-synaptic clustered AMPARs improves both the efficiency and the reproducibility of synaptic responses. However, the physiological impact of the trans-synaptic nanocolumn is difficult to estimate because it highly depends on both the number of glutamate per vesicle and the glutamate affinity of AMPARs (which is dependent on the complex composition). Unfortunately, these two parameters cannot technically be determine *in situ* for now.

Interestingly, the discovery of AMPAR clustering raised a paradox. Indeed, over-accumulation of AMPARs into nanodomains relies on their tight molecular trapping by scaffolding proteins, while multiple publications report the high rate of AMPAR exchange in the synaptic physiology. How can we reconcile the need to maintain AMPARs into nanodomains with the physiological observation of the mobility role? Such question necessitates to measure the individual receptor mobility at the ms scale.

Formulated with these words, it seems obvious that a deeper understanding of synaptic transmission is needed improvements of imaging techniques. For that reason, I spent a part of my PhD to develop/ improve our optical tools, to tackle these physiological questions. These developments are briefly evoked at the end of the material and methods part. Then, I applied them to study both the physiological role of the pre-post alignment and the mechanism of AMPAR mobility role during synaptic transmission.

In the first chapter of the results part, I will describe how dual-color super-resolution imaging combined with electrophysiology allowed us to identify neuroligin, a post-synaptic adhesion protein, as one of the main organizer of the trans-synaptic nanocolumns. In this first chapter, I will also describe how the expression of truncated form of neuroligin has been used to disrupt these nanocolumns and how it has affected synaptic transmission. In the second chapter, I will explain how the use of fast live single particle tracking revealed the transient decrease of AMPARs affinity for synaptic traps upon receptor desensitization.

All these works fully completed our new vision of the role of AMPAR organization and dynamic in the synaptic transmission at the basal state. As described in the introduction, synaptic plasticity go through deep refinements of the synaptic molecular organization. In the last part of my PhD, detailed in the third chapter of the results part, I used those super-resolution imaging techniques combined with electrophysiology to decipher the AMPAR re-organization induced during Long-Term Depression. To that, I compared two forms of LTD, the classical NMDAR-dependent LTD and the newly discovered P2XR-dependent LTD. Through this project, I demonstrated that compared to P2XR-dependent LTD, input-specific LTD cannot be restricted to an increase of AMPAR endocytosis, but corresponds to a precise new equilibrium between the main synaptic molecular components.

MATERIAL AND METHODS

In this part of the manuscript, I will describe the various techniques I have used during my PhD. The chapter on the super-resolution microscopy will be more detailed and will contained experiments/analysis that I implemented all along my PhD.

1. Neuronal culture and transfections

a. Primary hippocampal neurons culture

Cultures of dissociated hippocampal neurons were prepared from E18 Sprague-Dawley rats embryos of either sex, as described in (Kaech and Banker, 2006). Brains were extracted and hippocampi were isolated in HBSS containing **P**enicillin-**S**treptomycin (PS) and HEPES. For dissociation, all hippocampus were incubated in 5 mL of Trypsin-EDTA/PS/HEPES solution for 15 min at 37°C. After two washes with warm HBSS, a mechanical dissociation with Pasteur pipet pre-coated with horse serum was performed. The number of cells was counted in a Malassez grid in order to plate the appropriate number of cells according to the following requirement.

Glial cell feeder layers were prepared from dissociated hippocampi too, plated between 20 000 to 40 000 cells per 60 mm dish (according to the Horse Serum batch used), and cultured in MEM (Fisher Scientific) containing 4.5 g/L glucose, 2 mM L-glutamine and 10% horse serum (Invitrogen) for 14 days.

For cultured hippocampal neurons, cells were plated at a density of 200 000 cells per 60 mm dish containing four 18 mm coverslips (Mariefield). Cells were plated in supplemented Neurobasal medium containing 10% horse serum. After 2h, time required for neurons to adhere to coverslips, coverslips were transferred in 60 mm dish containing the 14 days old glial feeder layer, and MEM was replaced by supplemented Neurobasal medium. 5 µM Ara-C was added after 3 days in vitro (DIV) to stop glia's proliferation. Before experiments, cultured hippocampal neurons were maintained at 36.6°C with 5% CO_2 for 14-16 DIV.

b. Transfections

Depending on plasmids to express, three methods of transfection have been used:

- Neurons have been electroporated just before plating in the culture dishes with NucleofactorTM II (Lonza Cologne GmBH, Germany), following the instruction of the manufacturer.
- Neurons have been chemically transfected at 7-9 DIV using Effecten kit (Qiagen N.V, Venlo, Netherlands) following the protocol provided by the company.
- Neurons have been chemically transfected at 9-11 DIV using Calcium phosphate transfection method.

I most of the time tried to work on endogenous proteins, when it was not possible, neurons were transfected with constructs listed above:

- **Soluble EGFP** from Clontech Company was used as a cytosolic marker and as a transfection reporter.

- **EGFP-Homer1c** was used as post-synaptic marker for u-PAINT single particle tracking experiments. The coding DNA for Homer1c was subcloned in the eukaryotic vector pcDNA3 at EcoR1 sites. Then the "enhanced" GFP was inserted at the N-terminal part of Homer1c between HindIII/EcoRI sites.

- **HA-Neuroligin1 and HA-Neuroligin1ΔC** are generously provided by Dr Peter Scheiffele.

- **SEP-GluA2 conformational state mutants** were obtained as described in **Constals *et al.* 2015**.

- **Xph20-mEos3.2 CCR5TC** is a derived human fibronectin domain selected against the protein tandem of PSD-95 PDZ1 and PDZ2 and developed in the lab. Xph20 is a high affinity and specific monobody against endogenous PSD-95 (**Rimbault *et al.* in preparation**).

2. Electrophysiology

a. Whole-cell patch clamp on cultured neurons

Coverslips of transfected neurons were placed in a Ludin Chamber on an inverted motorized microscope (Nikon Eclipse Ti). Extracellular recording solution was composed of the following (in mM): 110 NaCl, 5.4 KCl, 1.8 $CaCl_2$, 0.8 $MgCl_2$, 10 HEPES, 10 D-Glucose, 0.001 Tetrodotoxin and 0.05 Picrotoxin (pH 7.4; ~245 mOsm/L). Patch pipettes were pulled using a horizontal puller (P-97, Sutter Instrument) from borosilicate capillaries (GB150F-8P, Science Products GmbH) to resistance of 4-6 MΩ and filled with intracellular solution composed of the following (in mM): 100 K-gluconate, 10 HEPES, 1.1 EGTA, 3 ATP, 0.3 GTP, 0.1 $CaCl_2$, 5 $MgCl_2$ (pH 7.2; 230 mOsm). Transfected neurons were identified under epifluorescence from the GFP signal. Recordings were performed using an EPC10 patch clamp amplifier operated with Patchmaster software (HEKA Elektronik). Whole-cell voltage clamp recordings were performed at room temperature and at a holding potential of -70 mV. Unless specified otherwise, all chemicals were purchased from Sigma-Aldrich except for drugs, which were from Tocris Bioscience.

Miniature EPSCs analysis were performed using a software developed by Andrew Penn, the matlab script is available on MATLAB File Exchange, ID: 61567;
http://uk.mathworks.com/matlabcentral/fileexchange/61567-peaker-analysis-toolbox.

b. Acute slice electrophysiology

i. Slice preparation

Acute slices were prepared from P16 Sprague-Dawley rats of both sexes. Rats were anesthetized with 5% isofluorane prior to decapitation. Brain were quickly extracted and the two hemispheres were separated and placed in ice-cold, oxygenated (95% O2/5% CO_2) sucrose-based artificial cerebrospinal fluid (ACSF) containing (in mM): 250 Sucrose, 2 KCl, 7 $MgCl_2$, 0.5 $CaCl_2$, 11 Glucose, 1.15 NaH_2PO_4 and 26 $NaHCO_3$ (pH 7.4; ~305 mOsm/L). Sagittal slices were cut (350 µm thick) and incubated for 30 minutes at 32°C in carbogenated (95% O2/5% CO_2) ACSF containing (in mM): 126 NaCl, 3.5 KCl, 2 $CaCl_2$, 1 $MgCl_2$, 1.2 NaH_2PO_4, 25 $NaHCO_3$ and 12.1 Glucose (pH 7.4; ~310 mOsm/L). Subsequently, slices were incubated for 30 minutes at room temperature and used until 5 hours after preparation. Experiments were performed in a submerged recording chamber at 30-32°C with continuous perfusion of carbogenated ACSF.

ii. Field EPSP recordings and analysis

Synaptic responses were measured extracellularly in the stratum radiatum of CA1 using glass pipettes (borosilicate, Science Products) filed with ACSF (1-2 MΩ). Responses were evoked by stimulating Schaffer collaterals with 0.2 ms pulses delivered using a stimulation electrode. Baseline responses were obtained by stimulating once every 20 seconds. After baseline stabilization, chemical LTD was induced by perfusion of ACSF containing NMDA (30 µM) for 3 minutes. Gabazine (2 µM, to block inhibitory currents) was present in ACSF all along experiments. Slopes of field EPSP were measured using NeuroMatic plug-in on Igor Pro (WaveMetrics, Lake Oswego, OR). Each data point corresponds to the average of 3 fEPSP slopes to have one data point per minute. Slopes were normalized to the intensity of the fiber volley, reflecting the number of stimulated fibers.

iii. Whole-cell patch clamp recording and analysis

Whole-cell voltage-clamp recordings (borosilicate pipettes, 4-6 MΩ) were made at 30-32°C from CA1 pyramidal neurons. Slices were perfused with the previously described carbogenated ACSF with added Gabazine (2 µM) and CGP52432 (2 µM). The intracellular solution was composed of (in mM): 130 Cs methane sulfonate, 10 HEPES, 10 EGTA, 2 $MgCl_2$, 1 $CaCl_2$, 4 Na_2-ATP, 0.4 Na-GTP and 5 QX314. Synaptic responses were obtained by 5 stimulations of Schaffer collateral with 0.2 ms pulses at 50 Hz. 20 series spaced by 20 seconds were performed and averaged. Each response was normalized to the first one. Paired-Pulse Ratios were measured using Stimfit software.

3. Immunolabeling

In order to investigate protein nano-organization with d-STORM technique, I first had to realize an immunolabeling on either surface or intracellular proteins. The following protocol describes the main steps realized for both types of immunolabeling.

For surface labeling, 14 DIV neurons were first incubated for 7 min at 37°C with the surface primary antibody diluted in culture medium. Then, cells were fixed by a solution of PFA/Sucrose at 4% for 10 minutes. After 3 PBS washes, neurons are incubated in 50 mM NH_4Cl (Sigma Aldrich) solution for 10 min to block PFA aldehyde groups and reduce background autofluorescence induced by these aldehyde groups.

For intracellular proteins, neurons were initially fixed with PFA/Sucrose at 4% for 10 minutes, then after 3 PBS washes, neurons were incubated in 50 mM NH_4Cl solution for 10 minutes. After 3 PBS washes, cells were treated for 5 minutes with triton at 0.1% to permeabilize cell membranes and following 3 PBS washes, they were incubated with 2% Bovine Serum Albumin (BSA) solution for 1 hour to saturate unspecific binding sites. Neurons were then incubated with primary antibody diluted in 2% BSA solution, and incubated for 1 hour at room temperature.

Then protocol is identical for both surface and intracellular labeling: following 3 BSA washes, another 2% BSA incubation was performed for 1 hour to precede the incubation with both secondary antibodies. A dye coupled secondary antibody at 1/500 in BSA was incubated for 1 hour at room temperature. Following 3 BSA and 3 PBS washes, a post-fixation in 2% PFA/Sucrose solution was performed. Finally, 3 PBS washes followed by 5 minutes in 50 mM NH_4Cl and 3 PBS washes, neurons were conserved in PBS in the dark and at fridge before to be imaged.

4. LTD induction

In order to investigate the organization or mobility of AMPAR during Long-Term Depression, 14 DIV transfected neurons were used. Neurons were maintained at 37°C before the fixation step. Six dishes containing 4 coverslips with neurons were used in parallel for 6 different conditions as described in the **table 1**. All conditions were made in presence of TTX to scale down the activity of cultured neurons. To induce LTD through P2XR stimulation, neurons were also incubated with the adrenergic receptor antagonist CGS15943 to avoid the activation of this other pathway by ATP treatment as referred in (Pougnet et al., 2016, 2014).

NMDAR-LTD				
Condition	**Treatment**	**Duration**	**Localization**	**Time**
30'	1µM TTX	10'	Dish	40' to 30'
	30µM NMDA + 1µM TTX	3'	12 well plate	30' to 27'
	1µM TTX	27'	Dish	27' to 0'
10'	1µM TTX	10'	Dish	20' to 10'
	30µM NMDA + 1µM TTX	3'	12 well plate	10' to 7'
	1µM TTX	7'	Dish	7' to 0'
Basal	1µM TTX	10'	Dish	10' to 0'

P2XR-LTD				
Condition	**Treatment**	**Duration**	**Localization**	**Time**
30'	1µM TTX + 3µM CGS15943	10'	Dish	40' to 30'
	100µM ATP + 1µM TTX + 3µM CGS15943	1'	12 well plate	30' to 29'
	1µM TTX + 3µM CGS15943	29'	Dish	29' to 0'
10'	1µM TTX + 3µM CGS15943	10'	Dish	20' to 10'
	100µM ATP + 1µM TTX + 3µM CGS15943	1'	12 well plate	10' to 9'
	1µM TTX + 3µM CGS15943	9'	Dish	9' to 0'
Basal	1µM TTX + 3µM CGS15943	10'	Dish	10' to 0'

Table 1. Long-Term Depression induction protocols.

5. Single Molecule Localization Microscopy

a. Principle of fluorescence microscopy

Fluorescence microscopy is the most widely used method to study protein organization on both fixed and living sample. The excitation of the fluorescent dye, resulting from the absorption of a photon, brings it from its electronic ground state (S_0) to an excited state (S_1). The energy of the photon must matches the energy difference between the ground (lower energy) and the excited state (higher energy) (**Figure 14**). Both S_0 and S_1 are singlet states, which means that all electrons of the dye are spin-paired. During the few nanoseconds in excited state, the fluorescent molecule undergoes into a vibrational relaxation or internal conversion, which corresponds to a loss of energy through vibration or heat. Dye is at this moment in the lowest excited state and can return to ground state by emission of a photon of lower energy that the absorbed one (because of the vibrational relaxation). This last notion is called the Stokes shift.

In addition to S_0 and S_1, other states can be reached following spin-unpairing of the dye (intersystem crossing) and bring the dye from the singlet excited state to an excited triplet state (T_n). This state is metastable which means that it can stay from nanosecond to second or even

minutes. The relaxation from T_n to S_0 is at the base of the phosphorescence. The exploitation of this excited triplet state is at the base of the d-STORM technique, a powerful method used in SMLM as it is described in the sub-chapter 6.

The photo-bleach corresponds to the disruption of the dye due to illumination. Its properties are specific from each type of dye and correspond to a loss of an electron, when they are either in S_1 or T_n, which interacts with oxygen to form reactive oxygen species. In function of time, local accumulation of ROS tends to break the dye by chemical reaction.

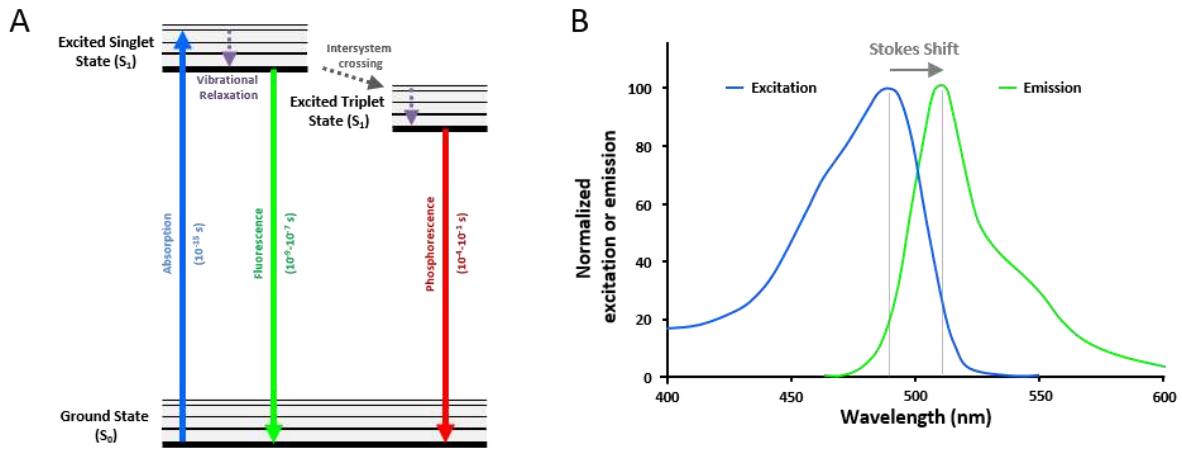

Figure 14. The principle of Flurorescence. (A) Jablonski diagram showing the timeline of fluorescence and the different energetic level in which the fluorescent dye can transit through. (B) Excitation and Emission spectrum of the Green Fluorescent Protein (GFP). The energy lost through vibrational relaxation is responsible for the increased wavelength of the emission spectrum. This displacement is named the Stokes shift.

b. Diffraction limit & resolution in fluorescent microscopy

A fluorescent molecule can be pictured as a point source emitting light waves. The fluorescent wavefronts emanating from the point source become diffracted at the edges of the objective aperture and lenses. This phenomenon of light diffraction, established by Huygens and Fresnel, is due to the waveform property of light (**Figure 15**). When light waves encounter an obstacle or an aperture, they tend to bend around it and spread at oblique angles. The spreading of the diffracted wavefronts produces an image composed by a central spot with a high intensity, and several interference rings of lower intensity. This diffracted point is called Airy disk and represents the idealized in focus 2D **P**oint **S**pread **F**unction (PSF) for a fluorescence microscope.

The Abbe theory says that the lateral resolution ($r_{x,y}$) correspond to the center of the Airy disk or $r_{x,y} = \lambda/2NA$ where λ corresponds to the wavelength and NA to the **N**umerical **A**perture of the objective. Technically, the resolution can be defined as the minimal separation distance between two point-like objects in which they can still be distinguished as individual emitters. This definition is provided by the Rayleigh criterion where the resolution corresponds to: $r_{x,y} = 0.61\lambda/NA$. In other terms, two points can be distinguished if the maximum intensity of one Airy pattern coincides with the first minimum of the other Airy pattern (**Figure 15C**).

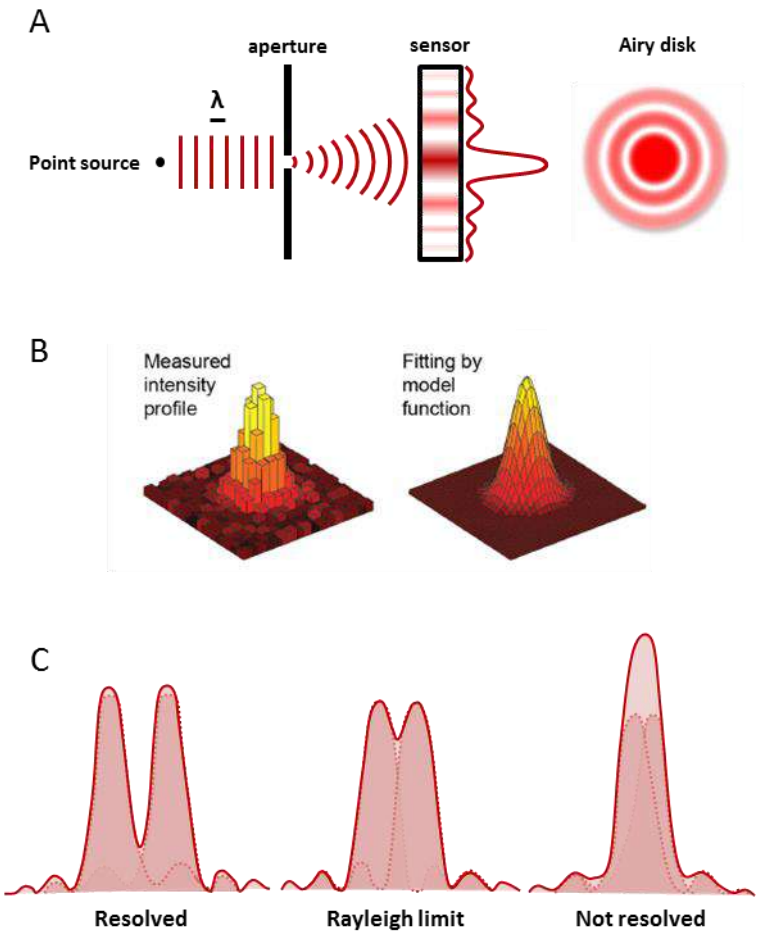

Figure 15. Diffraction and Resolution in fluorescence microscopy. (A) Principle of light diffraction. Due to this diffraction, a point source results in a diffracted point named Airy disk. (B) Representation of pattern of light formed on a camera by a single fluorescent molecule after diffraction (left) which can be fitted by a 2D Gaussian model (PSF) (right) (from Diezmann et al 2017). (C) Resolution in fluorescent microscopy is defined by the Rayleigh criterion.

c. Principle of SMLM

Over the last decade, new microscope techniques have been developed to bypass the diffraction limit and improve the resolution to observe the precise organization of proteins in biological samples. This part will only focus on **S**ingle **M**olecule **L**ocalization **M**icroscopy (SMLM), even if other techniques as **St**imulated **E**mission **D**epletion (STED) or **S**tructured **I**llumination **M**icroscopy (SIM) can be used to bypass the diffraction limit. It is important to note here that the development of this so-called super-resolution imaging techniques is closely linked to the discovery and creation of fluorescent dyes such as the **G**reen **F**luorescent **P**rotein (GFP), its derivatives and many organic fluorophores.

SMLM aims to decorrelate over the time the emission of fluorescence of single emitters. This allows to observe individual PSF and to fit mathematically this signal to determine the x,y coordinates of the source point (PSF centroid). In SMLM, the resolution obtained is not dependent anymore on our capacity to distinguish two close points, but relies on the precision to localize the object from its diffracted image. The resolution achieved in SMLM is in the range of 10-50 nm against ~250 nm with conventional fluorescence microscopy. For that, the first aim is to ensure that the emission of fluorescence of the biological sample is in a condition of single molecule detection. To achieve this goal, three approaches can be used: (i) the control of the labeling efficiency to maintain a fluorescent molecules concentration lower enough to be in single molecule condition, (ii) the use of fluorescent protein which require photo-activation to emit fluorescence (**P**hoto-**A**ctivated **L**ocalization **M**icroscopy, PALM), and (iii) to take advantage of the triplet state of some organic fluorophore to control the density of dyes which can produce fluorescence over the time (**d**irect-**STO**chastic **O**ptical **R**econstruction **M**icroscopy, d-STORM).

d. Resolution in SMLM

In SMLM, the resolution is linked to the precision in localizing the object from its airy pattern. However, it is important to know that the localization precision does not correspond to the resolution. The resolution can be approximated in SMLM to $r = 2.3p$, where p is the localization precision. Several factors can affect this precision: the number of photons emitted by the fluorophore, the background signal, the stability of the system during the acquisition, the labeling density and the labeling accuracy (**Figure 16B**).

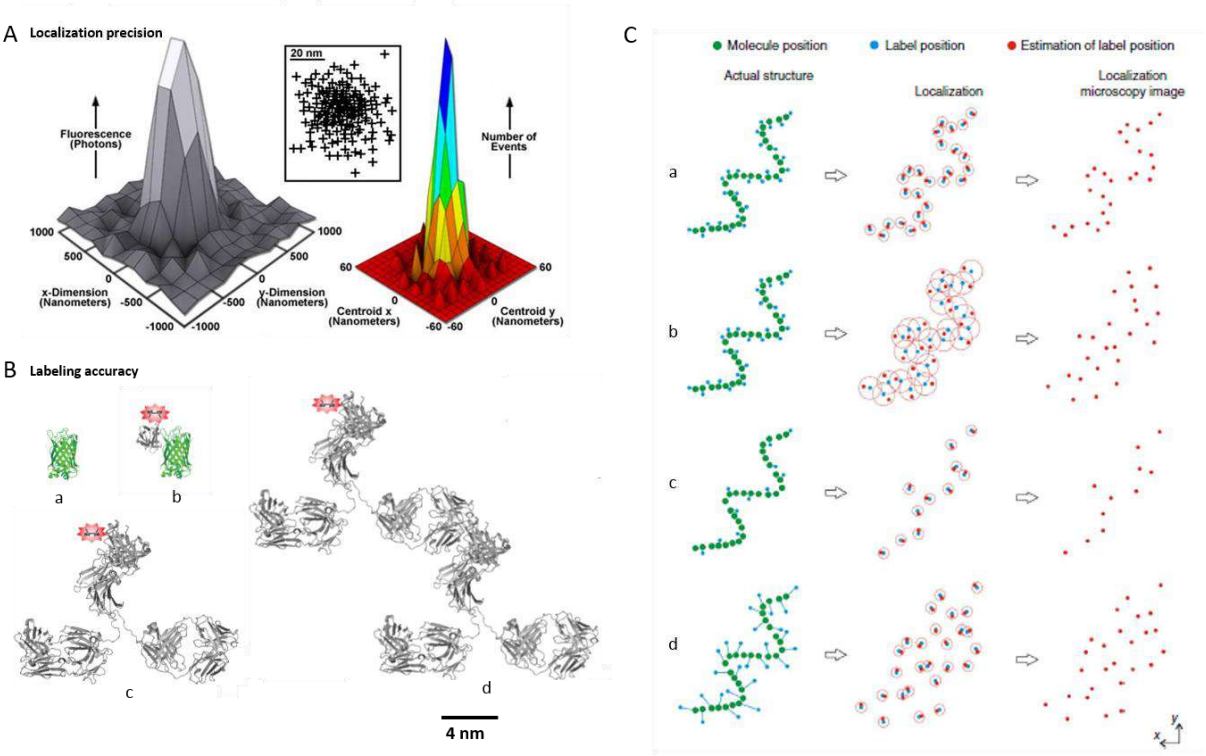

Figure 16. Resolution in SMLM. (A) The localization precision is dependent on both the number of detection per object and the number of photon per detection. (B) Various labeling strategies used in SMLM: (a) fusion of Fluorescent Protein, (b) fusion of fluorescent protein and labeling with a nanobody couple to an organic dye, (c) primary antibody coupled to an organic dye and (d) primary antibody and organic dye-coupled secondary antibody. The labeling strategy impacts the probe-protein proximity and thus the labeling accuracy (adapted from Platonova et al 2015). (C) Figure from Deschout et al 2014. Influence of localization precision, label density and label displacement on the resolution in a localization microscopy image. (a–d) The actual structure consisting of molecules is symbolized by the green dots. The apparent structure that is observed in the localization microscopy image consists of estimated positions (red dots) of the labels (blue dots). The open red circles represent the localization precision. (a) The localization microscopy image faithfully represents the actual structure only when the localization precision and label density are sufficiently high and the label displacement is sufficiently small. The resolution in the localization microscopy images is decreased by lower localization precision (b), lower label density (c) and higher label displacement (d).

Methods to determine the centroid coordinates are generally based on statistical curve-fitting algorithms to fit the measured photon distribution (the PSF) by a Gaussian function. The localization precision (σ) can be described by this complex relationship (Deschout et al., 2014):

$$\sigma^2 = \frac{s^2 + p^2/12}{N} + \frac{8\pi s^4 b^2}{p^2 N^2}$$

where *s* is the standard error of the Gaussian fit, *p* is the camera pixel size, *N* is the **number of photon**, *b* is the background photon count per pixel. To simplify, the localization precision can be resumed to:

$$\sigma = \frac{s}{\sqrt{N}}$$

Three other factors are critical to accurately reveal a structure with SMLM:

- As acquisitions are not instantaneous but can last couple of minutes to hours, it is crucial to be able to correct the lateral drift induced by the set-up properties. Better the xy drift correction is, better will be the precision of single molecule or biological object localization. To that, two methods can be used: either an image to image correction by the average of overall detections, or the use of fiducial markers such as fluorescent beads that we can track and then correct all images by the bead nanoscale position.

- The affinity of the labeling is a critical point. It has been reported that mEos only has 50 to 60% a well folded proteins, meaning that only half of the fused-proteins expressed will be detected. In parallel, antibody based labeling requires high quality antibody, with high specificity and affinity. The required density of fluorescent probes to label correctly a specific structure/protein of interest should satisfy the Shannon-Nyquist theorem which says that the distance between neighboring fluorescent probes (sampling interval) should be at least twice shorter than the desired resolution. In other terms, to resolve a structure of 50 nm of diameter, a fluorophore should be localized every 25 nm.

- Finally, antibody based SMLM presents an intrinsic bias due to the antibody size. The use of primary and secondary antibodies method of labeling implies that the fluorophore is positioned at ~20 nm from the target (when the pointing accuracy could be of 10 nm). Several ways to decrease the size of the labeling have been developed in the last few years as described in the following part. (**Figure 16**)

6. direct-Stochastic Optical Reconstruction Microscopy

a. d-STORM general principle

The technique takes advantage of biophysical properties of some organic fluorophores to reach triplet state as explained in **5.a**. Using high power laser and specific imaging solution containing thiols, dyes can be sent from ground state to triplet state. The stabilization of this triplet state thanks to oxygen scavengers (to avoid photo-bleaching), allows the stochastic relaxation to ground state of few fluorophores over the time and thus to have a sparse fraction of fluorophore emitting fluorescence at one time point. Each fluorophore is able to cycle several times between fluorescent (S_0-S_1-S_0) and non-fluorescent triplet state (T_n) before photobleaching. Several fluorophores can be used for d-STORM, however the best in term of resolution which can be achieved with, is unequivocally the Alexa647. Other fluorophores can be used to perform multicolor d-STORM experiments such as Alexa568 or Alexa532. Finally, it is important to note that d-STORM is not compatible with live imaging as it requires imaging solution containing thiols and oxygen scavengers. d-STORM has been extensively used to investigate the organization of endogenous and exogenous proteins into fixed biological sample with a resolution of ~10 nm (**Figure 17**).

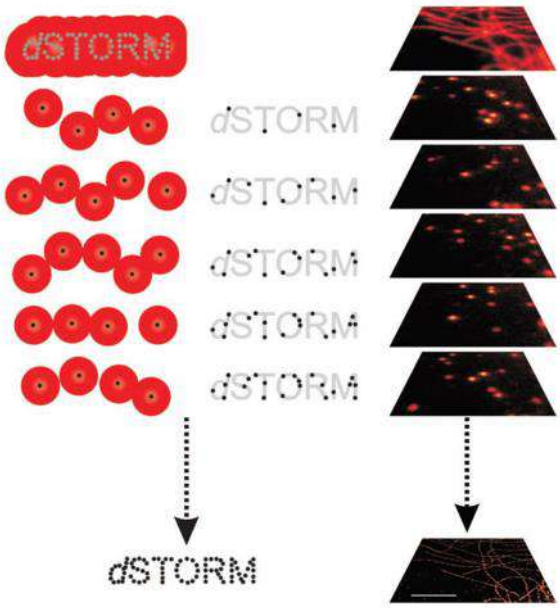

Figure 17. d-STORM principle. Figure from van de Linde et al 2011

b. d-STORM application

d-STORM experiments have been done on fixed neurons labeled as described in sub-chapter 3. d-STORM imaging was performed on a LEICA DMi8 mounted on an anti-vibrational table (TMC, USA) used to minimize drift, Leica HCX PL APO 160x 1.43 NA oil immersion TIRF objective and laser diodes with following wavelength: 405 nm, 488 nm, 532 nm, 561 nm and 642 nm (Roper Scientific, Evry, France). Fluorescent signal was detected with sensitive EMCCD camera (Evolve, Roper Scientific, Evry, France). Image acquisition and control of microscope were driven by Metamorph software (Molecular devices, USA). Image stack contained typically 50,000 frames. Selected ROI (region of interest) had dimension of 512x512 pixels (one pixel = 100 nm). Pixel size of reconstructed super-resolved image was set to 25 nm.

Power of a 405 nm laser controlled the level of single molecules per frame. Multi-color fluorescent microspheres (Tetraspeck, Invitrogen) were used as fiducial markers to register long-term acquisitions and correct for lateral drifts.

c. dual-colour d-STORM

Dual color d-STORM has been done on fixed neurons labeled for as previously described. d-STORM imaging was performed on same microscope as previously detailed.

The dyes were sequentially imaged (Alexa647 followed by Alexa532) to collect the desired single molecule frames and to avoid photobleaching. Before acquisition of Alexa532 signal, GFP signal coming from transfected cell was bleached using 488 nm laser, in order to decrease background observed with 532 nm laser. Multi-color fluorescent microspheres (Tetraspeck, Invitrogen) were used as fiducial markers to register long-term acquisitions and to correct for lateral drifts and chromatic shifts.

d. Imaging solution for d-STORM

18 mm coverslip covered by neurons was mounted in a Ludin chamber (Life Imaging Services, Switzerland) and 500 µL of imaging buffer are added. Another 18 mm coverslip was placed on top of the chamber to minimize oxygen exchanges during the acquisition.

The imaging buffer used for d-STORM experiments was the classical Glucose oxidase (Glox) buffer described in (van de Linde et al., 2011). The Glox buffer is composed of 1 mL G, 125 µL E and 125 µL M, and the final pH is adjusted to ~7.8 with NaOH.

Glucose base solution (G)		
50 mL		
45 mL	H_2O milliQ	
5 g	Glucose	Sigma G8270
5 mL	Glycerin	Sigma G2289

Enzyme solution (E)		
50 mL		
100 µL	catalase	Sigma C100
200 µL	TCEP	Sigma C4706
25 mL	Glycerin	Sigma G2289
22.5 mL	H_2O milliQ	
1.25 mL	KCl (1M)	Sigma P9541
1 mL	Tris-HCl (1M) pH 7.5	Euromedex EU0011
50 mg	Glucose oxidase	Sigma G2133

Thiol solution (M)		
10 mL		
1.136 g	MEA-HCl	Sigma M6500
10 mL	H_2O milliQ	
adjust pH to 8 with NaOH		

Table 2. d-STORM solution

e. Analysis and quantification

i. Localization processing

Single molecule detection recordings were processed using a Metamorph plug-in called PalmTracer and developed by the group of Jean-Baptiste Sibarita (Izeddin et al., 2012). The x,y coordinates were localized using image wavelets segmentation and centroid estimation methods. First, an intensity threshold was defined to detect single molecule signals. Once each single molecule has been localized in each frames of the recording, their centroid x,y coordinates were automatically written on a text file. An intensity map was created with a desire pixel size (25 nm) by positioning the several thousands of points localized during the first step.

ii. Cluster analysis

To analyze the clustering of proteins, we used two methods. The first one consist to detect cluster on the super-resolution image using PalmTracer Cluster Analysis. On the same manner that the localization detection, Cluster Analysis use wavelets segmentation to detect individual clusters based on set intensity threshold. Following clusters detection, a Gaussian fit was applied and their standard deviation σ was measured. This allowed to calculate the FWHM of clusters (FWHM = 2.3 σ) and to give clusters length and width. The intensity of these clusters was measured by the sum of all pixel values and the intensity of single emitters as well using Metamorph Integrated Morphometry Analysis. By dividing the intensity of each cluster by the median intensity of single emitters, we can approximate the number of proteins per cluster (**Figure 18A**). This method is commonly used in localization-based super resolution

microscopy. However, clusters quantification depend on the sampling chosen to reconstruct the super resolution image.

Recently, **Levet *et al.*, 2015** introduced a framework named SR-Tesseler, based on Voronoï diagrams, for a more precise automatic segmentation and quantification of protein organization at different scales from the same set of molecular coordinates, using a local density parameter (Levet et al., 2015). SR-Tesseler creates polygonal regions centered on localization centroid previously established with PalmTracer. These polygons are defined in an Euclidean space and provides information on the neighboring localization. The density is measured and can be a parameter used to identify clusters. After successive segmentation steps, SR-Tesseler allows to obtain the intensity of single emitters (isolated fluorophores on the coverslip and isolated proteins) and to quantify the protein cluster diameter and content (**Figure 18B-H**).

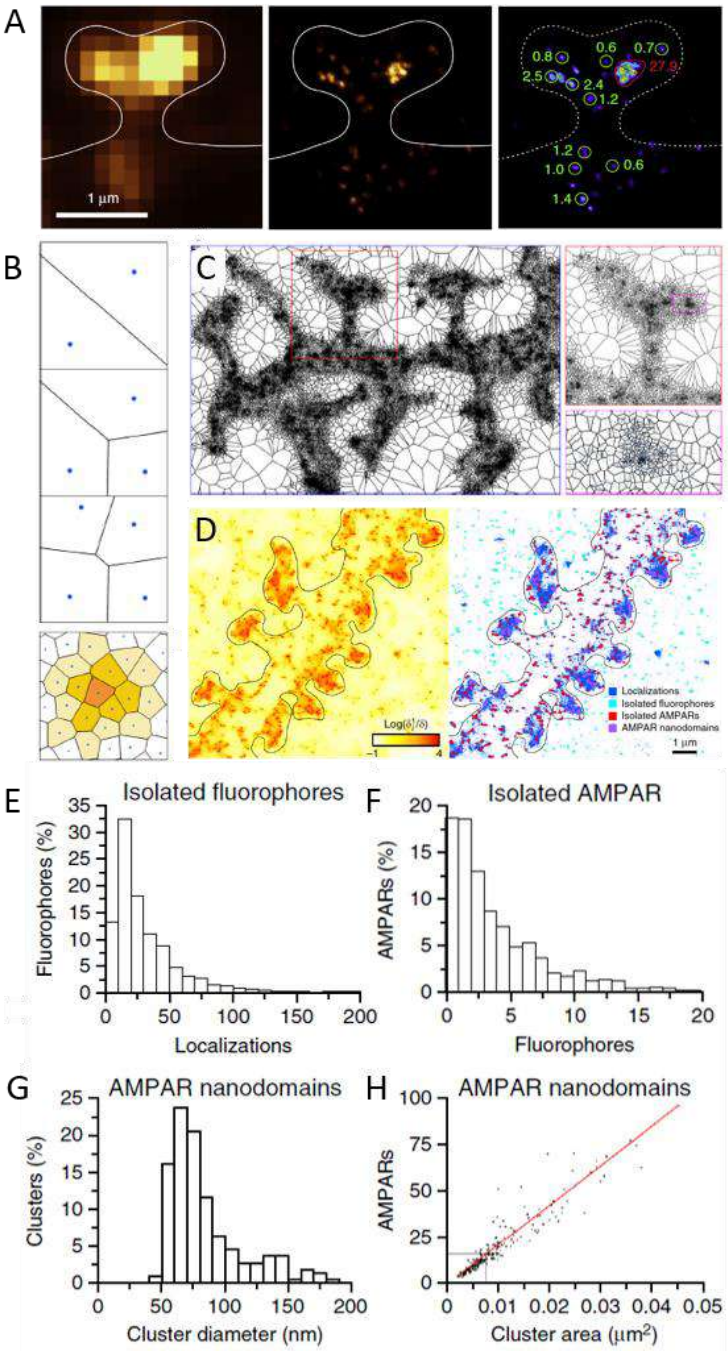

Figure 18. Quantification in SMLM. (A) AMPARs are organized in nanoclusters. Left: diffraction limited image of AMPARs (GluA2 subunit) labeled with primary antibody coupled to Alexa647 in a dendritic spine. Middle: Super-resolution image of GluA2-containing AMPARs inhomogeneously distributed at the surface of the post-synapse, showing both individual receptors and nanodomains concentrating a large number of receptors. Right: Quantitative estimation of the average number of receptors per individual objects. Values have been normalized based on the intensity distribution of single receptors. Green circles, with a ratio close to one, show single receptors, while the red surface shows a nanodomain composed of about 30 receptors. Counting through Metamorph Cluster Analysis and MIA (From Hosy et al 2014). (B-G) SR-Tesseler, a new method to quantify protein clustering. (B) Voronoï-based segmention principle. (C-D) Application to measure AMPAR organization with SMLM. (E-H) quantification of the number of localization/detection per isolated fluorophore, number of fluorophore per isolated AMPAR, AMPAR nanodomain diameter, and AMPAR number per nanodomain. (From Levet et al 2015)

iii. Cluster co-localization measurement

Co-localization analysis, when dual color d-STORM experiments are realized, was performed using homemade written program in Matlab script by a previous PhD student, Kalina Haas (Mathworks, UK). Manders' coefficients were chosen as co-localization measure because they do not depend on the relative intensity difference between two component images, therefore bypassing alteration in labeling efficiency of different cellular structures. Here we perform pairwise analysis between coincidental objects observed in two image components. Thus, our Manders' coefficients represent fraction of the intensity belonging to co-localizing super-resolution pixels of a given object.

In first step, two image components are threshold, segmented and reduced to sets of geometrical objects attributed with their weighted centroid location, pixel area, intensity and location. Objects in each component image were divided into two categories, according to their area. This distinction is based on the size of single emitter found both on the coverslip and on the dendrite. With this analysis, we can tell apart the single proteins from the clustered ones, and analyze them independently.

In subsequent step, first bivariate nearest neighbour distance distribution is calculated for one protein of interest to the nearest second protein of interest. Afterwards, the Manders' coefficients are evaluated between each first nearest neighbor pair of proteins. These coefficients were calculated only between pairs separated by the threshold distance, which reflects the maximum distance between two objects considered as related and was obtained from bivariate nearest neighbour distance distribution.

Co-localization significance was accounted for by image randomization. Objects in one image component were rearranged by random assignment of new position for their weighted centroids. This step was repeated up to 1000 times, each time appropriate measure of co-localization was evaluated. Bivariate first nearest neighbour distributions are compared to the mean of randomized samples and 95 % confidence intervals. If the experimental distribution lies above (below) randomized distribution, it indicates tendency towards association (dispersion) at given distances. However, if experimental distribution matches randomized one, it points to random or independent distribution between two classes of objects. Matlab scripts are available on request and will be deposited at http://uk.mathworks.com/matlabcentral/fileexchange.

7. Single-Particle Tracking

a. General principle of stochastic labelling methods

One of the first method imagined to visualize single protein behavior was based on a sparse labeling by pre-incubating the biological sample with a probe at really low density and to visualize/track this probe with a microscope. First techniques used latex beads coupled to antibody but this field of single particle tracking (SPT), quickly switch to fluorescent dyes like Quantum Dots (QD). Quantum dots are semiconductor nanocrystals with excellent optical properties and small in size compared to latex beads. They are highly bright, can be synthetized with various emission properties and are resistant to bleach despite their blinking behavior. These optical properties make it a really good candidate to SPT experiments, with long trajectories (few minutes) and high localization precision of the protein of interest (10-20 nm). However, two limitations can be highlighted: (i) QD coupled probe size (15-20 nm) may hinder the diffusion properties of the labeled protein, especially in narrow spaces (Groc et al., 2007), and (ii) the technique is based on sparse non-renewed labeling to pre-incubation with low probe concentration, providing only 10 to 100 trajectories which provide dynamic information of a small fraction of the proteins of interest and insufficient information regarding the spatial organization of proteins.

To overcome the limitations of QD, **u**niversal-**P**oint **A**ccumulation for **I**maging in **N**anoscale **T**opography (u-PAINT) has been developed. The idea come from the PAINT technique which consist in the precise lateral localization of individual fluorophore which transiently attach the membrane and become fluorescence only at the contact of the lipid layer (Sharonov and Hochstrasser, 2006). This principle of a stochastic labeling over the time during the imaging process raised the idea of u-PAINT (Giannone et al., 2010) (**Figure 19**). The method aims to retain the optical advantages of QD but using smaller dyes, coupled to the renewal of labeling with PAINT. Regarding the optical part, ATTO organic dyes have a very broad optical spectrum (UV to IR wavelength), are bright enough to be detected as single molecules with a localization precision of ~40-50 nm. However they are less resistant to bleach but allow to obtain medium range trajectories (1-60 seconds). The small size of organic fluorophore like ATTO compared to QD (1-2 nm vs 5-10 nm) allows a better tracking of the protein of interest in smaller spaced as the synaptic cleft. The PAINT aspect allows to renew the labeling of the protein population over the time. By adding a low concentration of fluorescent probes in the imaging chamber, this leads to a low density stochastic labeling. The

number of trajectories will increase in function of the duration of imaging, giving access to a high density dynamic information. An oblique illumination to decrease the background signal due to fluorescent probes floating in the solution is required. However, it is important to note that molecules freely moving in water have a diffusion coefficient (D) of ~100 $\mu m^2.s^{-1}$ rather than a membrane protein have a D comprised in a range between 0.0001 to 0.1 $\mu m^2.s^{-1}$. Thus, detection of freely moving molecule are filtered and most of floating dyes are not activated by the illumination.

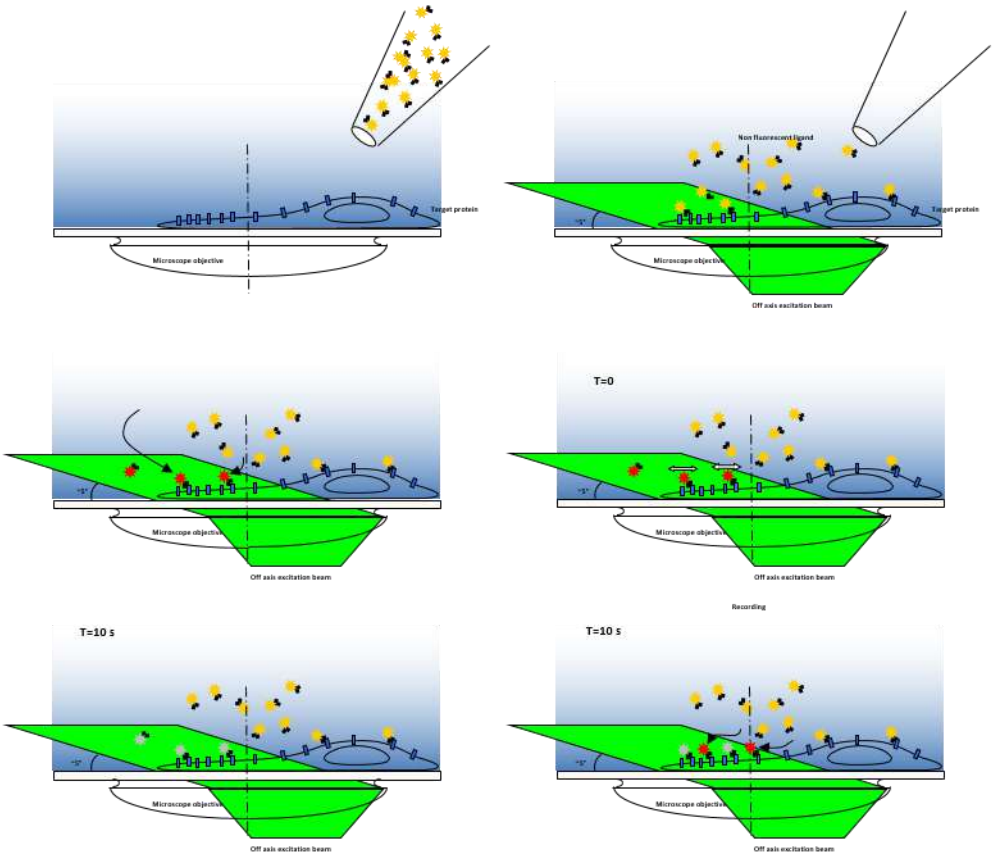

Figure 19. u-PAINT principle. Scheme adapted from Giannone et al 2010

b. u-PAINT application

u-PAINT experiments were performed on a Ludin chamber (Life Imaging Service, Switzerland). Cells were maintained in a Tyrode solution composed of the following (in mM): 15 D-Glucose, 100 NaCl, 5 KCl, 2 $MgCl_2$, 2 $CaCl_2$, 10 HEPES (pH7.4; 247mOsm). Imaging was performed on a Nikon Ti-Eclipse microscope equipped with an APO 100x 1.49 NA oil immersion TIRF objective and laser diodes with following wavelength: 405 nm, 488 nm, 561 nm and 642 nm (Roper Scientific, Evry, France). A TIRF device (Ilas, Roper Scientific, Evry, France) is placed on the laser path to modify the angle of illumination. Fluorescence signal was detected with sensitive EMCCD camera (Evolve, Roper Scientific, Evry, France). Image acquisition and control of microscope were driven by Metamorph software (Molecular devices, USA). The microscope is caged and heated in order to maintain the biological sample at 37°C.

The first step consisted to find an eGFP-Homer1c transfected neuron. This construct was used in order to visualize the neuron of interest and the synaptic area for more specific analysis as described later. After selection of the dendritic segment of interest, ATTO647N coupled-anti-GluA2 antibody (mouse antibody, provided by E. Gouaux, Portland, USA) at low concentration was added in the Ludin chamber to sparsely and stochastically label endogenous GluA2-containing AMPARs. The TIRF angle was adjusted in oblique configuration to detect ATTO647N signal at the cell surface and to decrease background noise due to freely moving ATTO647N coupled antibodies. 647nm laser was activated at a low power to avoid photo-toxicity but allowing a pointing accuracy of around 50 nm, and 4000 frames at 50Hz were acquired to record AMPAR lateral diffusion at basal state.

8. Photo-Activated Localization Microscopy

a. PALM general principle

The technique relies on the ability of certain fluorescent proteins (FP) to change their optical properties when exposed to light (photochromism) (Betzig et al., 2006). There are three types of photochromism: photo-activation and photo-conversion and photo-switching (**Figure 20**). The first observation of on/off blinking and switching behavior of the fluorescent protein GFP, and the development of its variants as the PA-GFP, are at the base of this method of SMLM (Patterson and Lippincott-Schwartz, 2002). Photo-activable fluorescent proteins are capable of being activated from a dark state to a bright fluorescent state upon UV illumination. This activation relies on the probability to change their conformation upon UV excitation and

so their emission spectrum. On the other side, photo-convertible proteins can be optically transformed from one fluorescence emission bandwidth to another, again upon UV illumination. Both type of photochromism are stochastic methods by which upon a certain power of UV excitation, the fluorophores have some probability to modify its spectrum properties. So far, the most used fluorophore is certainly mEos fluorescent protein. It is excited at 503 nm and upon 561 nm laser illumination, mEos does not emit fluorescence. However, upon low UV illumination, a part of the mEos is broken, changing its emission properties. Thus, the molecule becomes visible when excited with 561 nm laser. Thus, upon low level of photo-conversion or photo-activation, the single molecule detection situation is reached.

To apply this PALM technique, FPs need to be expressed and require a genetic fusion with the protein of interest. This fusion/over-expression necessity presents some limitations: (i) the level of over-expression which could modify the organization and dynamic properties of the protein, (ii) the function of the protein fused to the FP can be affected. New techniques of genetic replacement allow to control the first point such as Knock-in animals or Crispr-Cas9 approaches. FPs are less bright and less photo-resistant than organic fluorophore ATTO or QDs. However they also allow live imaging and SPT (spt-PALM) with a localization precision of ~40-50 nm. Trajectories are shorter than trajectories obtained with QD or u-PAINT (<3 seconds). It has the advantage to not require highly affine and specific antibody/probe to label the protein of interest and the signal obtained is highly specific as it does not rely on the interaction properties between a probe and its target. Moreover, PALM is the only method available for single particle tracking of intracellular proteins.

b. spt-PALM application

spt-PALM experiments were performed on a Ludin chamber (Life Imaging Service, Switzerland). Cells were maintained in a Tyrode solution composed of the following (in mM): 15 D-Glucose, 100 NaCl, 5 KCl, 2 $MgCl_2$, 2 $CaCl_2$, 10 HEPES (pH7.4; 247mOsm). Imaging was performed on a LEICA DMi8 mounted on an anti-vibrational table (TMC, USA) used to minimize drift, Leica HCX PL APO 160x 1.43 NA oil immersion TIRF objective and laser diodes with following wavelength: 405 nm, 488 nm, 532 nm, 561 nm and 642 nm (Roper Scientific, Evry, France). A TIRF device (Ilas2, Roper Scientific, Evry, France) is placed on the laser path to modify the angle of illumination. Fluorescent signal was detected with sensitive EMCCD camera (Evolve, Roper Scientific, Evry, France). Image acquisition and control of

microscope were driven by Metamorph software (Molecular devices, USA). The microscope is caged and heated in order to maintain the biological sample at 37°C.

The first step consisted to find a transfected neuron. After selection of the dendritic segment of interest, using mEos3.2 green signal (488 nm excitation laser), sptPALM was performed using low power 561 nm laser and photo-conversion of mEos3.2 molecule was induced by short and low pulse of 405 nm laser. 2000 frames at 50Hz were acquired to record protein dynamic and organization.

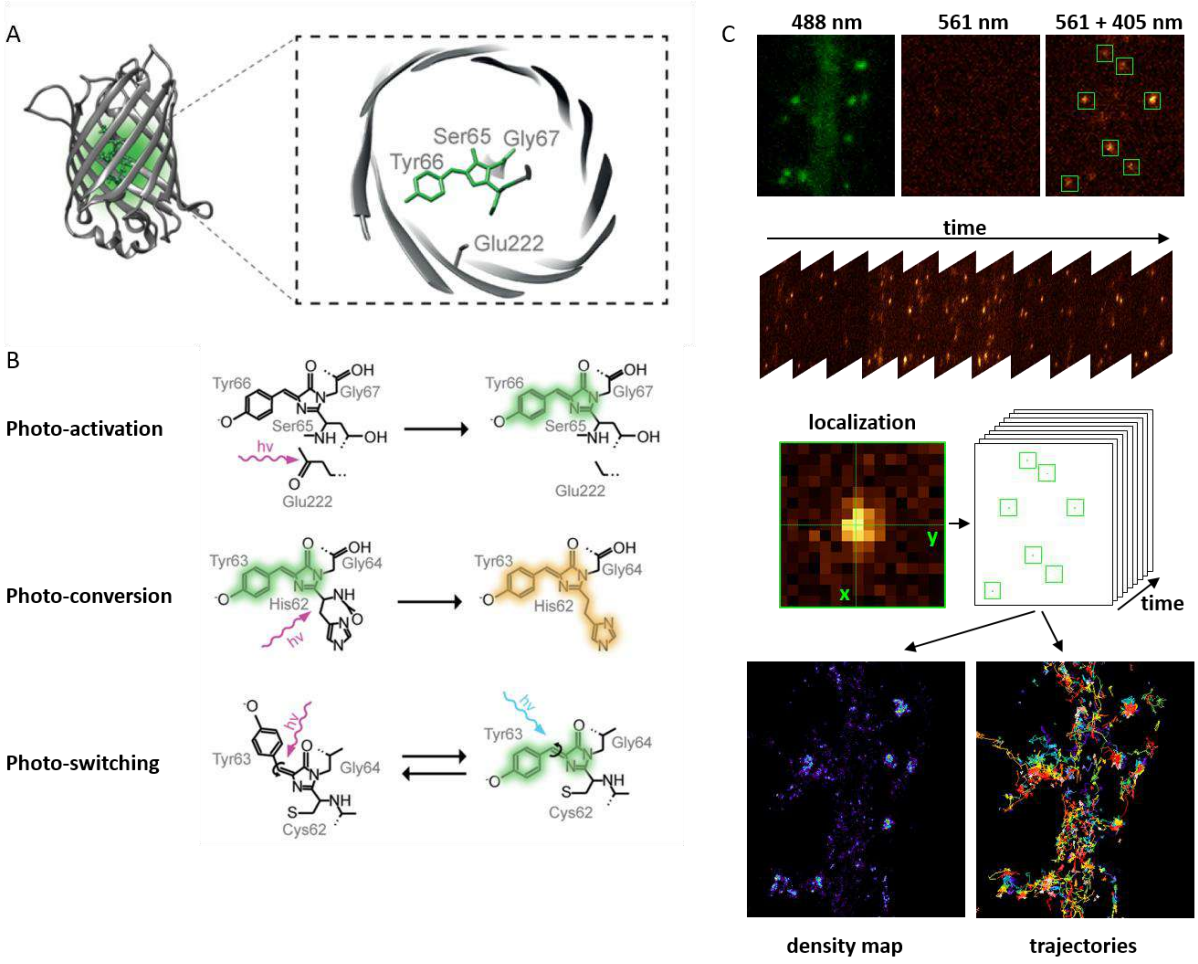

Figure 20. PALM principle. (A) Sturcture of Fluorescent Protein such as GFP. (B) Types of photochromism used in PALM. (C) General principle of PALM/spt-PALM imaging and analysis. (A and B adapted from Turkowyd et al 2016)

c. Analysis of single-particle tracking

As for d-STORM experiments, single particle tracking recordings (u-PAINT and spt-PALM) were analyzed using PalmTracer. The first step consisted in the localization of each detection recorded using image wavelet segmentation and centroid estimation (Izeddin et al., 2012). Only particles appearing in 8 consecutive frames were considered as trajectories. Two points were connected into a trajectory if their locations in two adjacent frames were lower than 3 low resolution pixels (3 x 160 nm). Once reconnections between single detections were done, the Mean Square Displacement (MSD) of each trajectories was calculated. It corresponds to the area that the molecule explores over time. The MSD is generally used to extract two parameters: (i) the diffusion coefficient (D) which is the global diffusion of the trajectory, and (ii) the instantaneous diffusion which is the molecule dynamic over time. Diffusion coefficient was calculated by a linear fit of the 4 first points of the MSD curve.

9. Improvement of SMLM

Despite the fact that current techniques of SMLM reach a localization precision of 10-20 nm, many labs try to push it further. Indeed many projects aim to understand molecular organization at the single nanometer scale. In collaboration with Corey Butler, from Jean-Baptiste Sibarita group (IINS, Bordeaux), we developed/ implemented various improvements to gain in localization precision. Our final aim was to obtain a sufficient precision to resolve the various subunits of the single receptor, corresponding to a resolution of around 7 to 10 nm.

The first step has been to improve the labeling strategy. As illustrated in **Figure 16B** depending on the chosen labeling method, the localization of the fluorescent dye regarding the target can be significantly far. To investigate the effect of labeling probe on the localization precision, we applied 3 labeling strategies on GFP patterns and on heterologous cells expressing p-display GluA1-SEP (which cannot form dimers) using: (i) primary anti-GFP and Alexa647-coupled secondary antibodies, (ii) primary anti-GFP primary directly coupled to Alexa647 and (iii) anti-GFP Alexa647-coupled nanobody. d-STORM was performed using conventional d-STORM buffer (**table 2**) and super-resolved objects were analyzed using Cluster Analysis (PalmTracer, Metamorph). Cluster size were significantly smaller with only primary (16 nm) or nanobody (17 nm) labeling strategy than with primary and secondary antibodies (23 nm). But the number of detections per object was higher when using primary and secondary labeling,

due to the labeling of primary antibody by a polyclonal secondary antibody (**Figure 21A**). This experience confirmed the importance of the labeling accuracy in SMLM. However, despite the decrease of the linker length using nanobody, the localization precision was still insufficient to decipher AMPAR subunit organization within a single receptor. We also noticed the absence of difference in localization precision between labeling with coupled-primary antibody and nanobody suggesting that our actual localization precision is of ~ 16 nm. Thus we couldn't observe improvement with the nanobody. However it is obvious that smaller probe improves the localization precision. For that reason, Matthieu Sainlos in Daniel Choquet group is developing nanobodies against endogenous proteins coupled to multiple dyes. This strategy will render it possible to, first, have a high number of detection, second, benefit of the small nanobodies size and, finally, to avoid artefact due to overexpression of GFP tagged proteins.

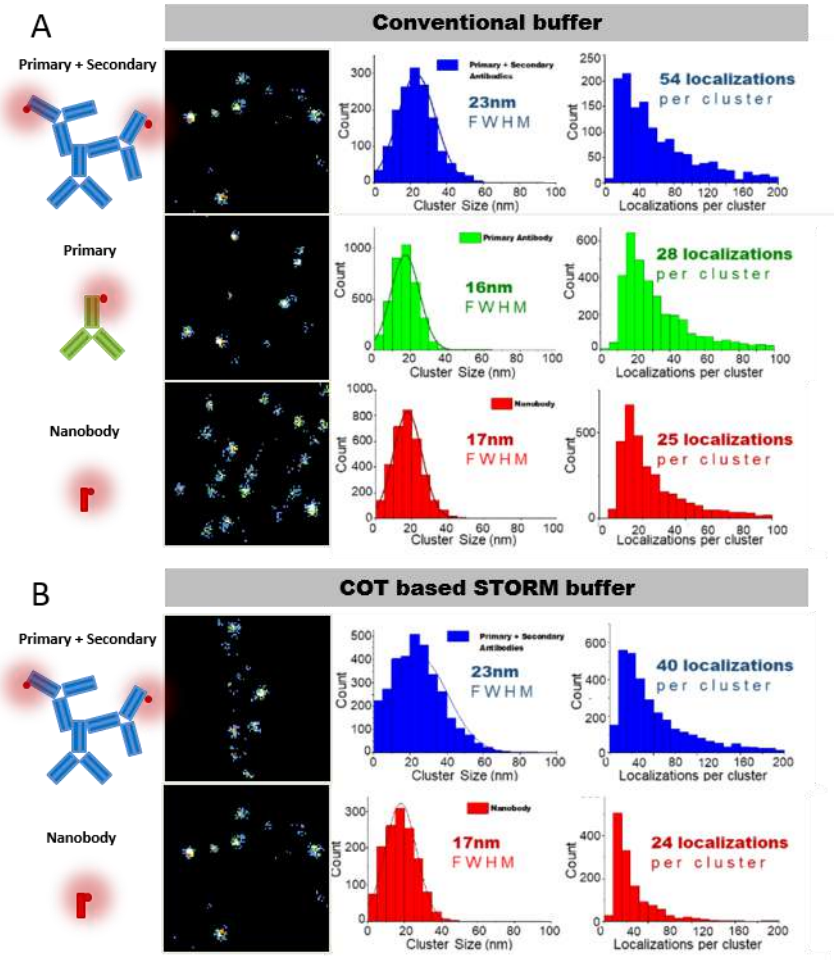

Figure 21. Resolution improvement in SMLM (with Corey Butler). (A) Impact of the labeling strategy in classical STORM buffer on localization precision and number of detection per molecule. (B) Impact of labeling strategy in COT-based STORM buffer on localization precision and number of detection per molecule.

The second improvement we worked on aimed to increase the number of photons per localization. Indeed, the localization precision increases linearly with the square root of the number of collected photons. As shown by simulations performed by Adel Kechkar in the group of Jean-Baptiste Sibarita, higher the number of photons per localization is, higher is the localization precision. Following this idea, we tried to increase the number of photon per localization during d-STORM recordings. For this purpose, we tested the effect of a different d-STORM buffer which has been reported to increase by four the number of photons emitted by single molecule, and so to approximatively double the resolution. We performed the previously described experiments using both conventional d-STORM buffer and COT (cyclooctatetraene) based d-STORM buffer as described in **Olivier *et al.*, 2013** (Olivier et al., 2013). Surprisingly, the number of photons was only increased by 25 %, far from the ~400 % obtained by Olivier and collaborators. We quantified cluster sizes and did not observe any difference with results obtained with conventional d-STORM buffer (**Figure 21B**).

Finally, another approach to improve the localization precision is to only keep high photon detections. Indeed, the localization precision of an object corresponds to the average of localization of each detection recorded for this object (from 20 to 100 per object). Each low intensity detection brings some noise around the object which tends to increase the uncertainty of localization. Unfortunately, the selection of only highly intense detections requires a high number of detections per molecule to suppress the lowest ones. As shown in **Figure 21**, the number of detections per object is not high enough with d-STORM to allow such selection.

To overcome this limitation, we recently took advantage of an emergent technique named DNA-PAINT. It consists in a classical immunolabeling of the biological sample, but antibodies are coupled to a single DNA strand. The complementary strand coupled with an organic fluorophore is added in the imaging buffer (Jungmann et al., 2014). This allows a stochastic transient (couple of hundred ms) labeling. In this condition, the number of detections per object is only dependent on the recording duration. However, as previously explained, long lasting acquisition requires the drift correction. Classical fiducial markers such as fluorescent beads have a limited life time because of photobleaching. We tested nanodiamonds as fiducial markers. These nanodiamonds emit with a broad spectral range of fluorescence, are small (100 nm) and fully stable over time. Their utilization improved localization precision and drift correction compared to fluorescent beads (Yi et al., 2016). Finally, we also implemented 3D cylindrical lenses in the imaging set-up. It creates a lateral (x,y) PSF deformation depending on the axial (z) position of the emitter. Preliminary results are are shown in **Figure 22**.

Through these developmental work we are now able to acquire for several hours and to correct for xy drift using nanodiamonds fiducial markers. This, combined to DNA-PAINT, should allow us to have an infinite number of detections per object and to filter those detections and keep only high number photon ones and thus to reach the desired localization precision. In addition, to complete this improvement, it is important to couple small probes as nanobody with DNA strand to perform DNA-PAINT with a better labeling accuracy and localization precision. Finally, just to mention it, Corey Butler developed a software to automatically correct Achromatism in dual-color SMLM. The ensemble of improvement has been used to complete the physiological project detailed in the following result chapters.

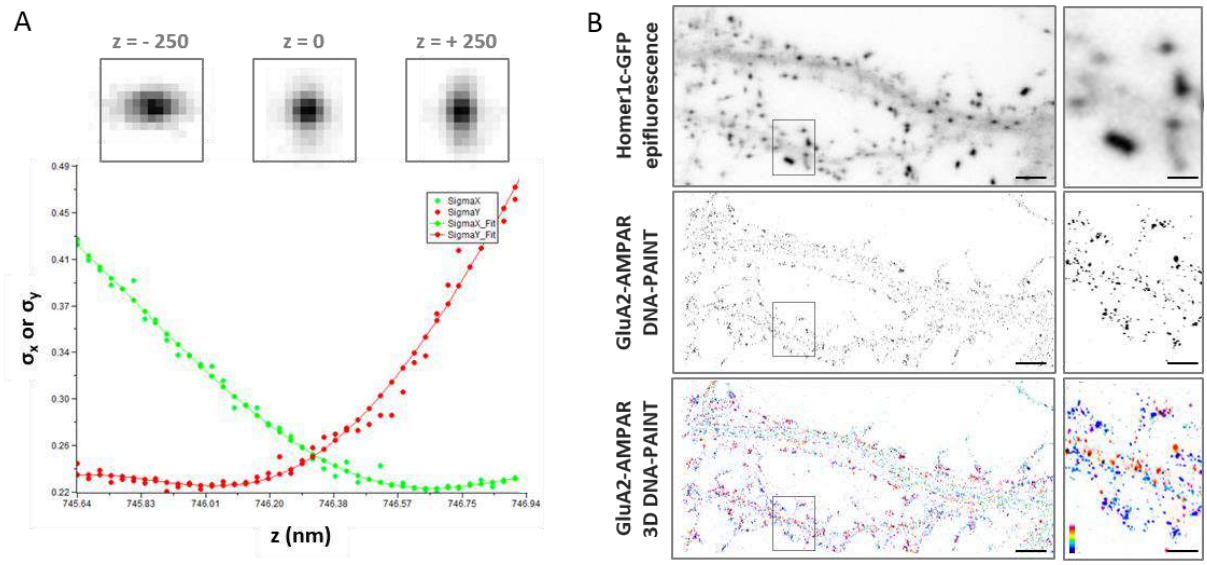

Figure 22. Resolution improvement in SMLM (with Corey Butler). (A) 3D astigmatism calibration on fiducial marker nanodiamonds. (B) DNA-PAINT on endogenous GluA2-containing AMPAR on neurons transfected with Homer1c-GFP in 2D and 3D.

RESULTS

Chapter 1

Alignment between AMPAR nanodomains and glutamate release sites tunes synaptic transmission

The molecular organization of synapses is the fundamental basis of neuronal communication. Previous studies trying to understand the NPQ theory are based on electrophysiology and diffracted limited imaging, and build an incorrect/incomplete vision of the input integration. The simple vision of glutamate being released in the synaptic cleft and saturating the randomly distributed post-synaptic receptors have been corrected by functional studies and by the emergence of super-resolution imaging techniques. Indeed, we know that AMPARs are organized in nanodomains and this organization impacts considerably the post-synaptic quantum of response. This key parameter associated to AMPAR lateral diffusion reveals a new level of complexity in the understanding of synaptic input optimization and regulation.

Throughout my PhD, efforts were made to understand how AMPAR dynamic and nanoscale organization could directly impact neuronal input integration. It is clear that information transfer relies on the "I=N.P.Q" rule but the molecular bases which regulate each feature still need to be precisely determined. The release probability (P_r) is obviously a pre-synaptic factor. The number of activated synapse N relies first of the number of existing synapses and the number of those synapses which will participate to the neuronal input. In theory it is mainly pre-synaptic but post-synaptic plasticities can affect this parameter as well. For example, it has been extensively described that during LTP and LTD, the number of synapses increases and decreases respectively.

The quantum of response (q) is probably the main adjustment parameter of this equation because it is dependent of pre-, post- and trans-synaptic properties. First, as initially described, the glutamate concentration inside vesicle is an important factor even if there is so far no solid evidences reported of physiological control of this parameter. Then, it has been shown that the density of AMPAR at synapses and their organization in nanodomain is a crucial feature which tunes the strength of synaptic transmission. For that, a precise molecular co-organization between PSD-95, TARPs and AMPARs is required. This co-organization is regulated by post-translational modifications of each partners of this tripartite complex. Finally, as glutamate gradient fades away rapidly in the synaptic cleft due to its diffusion properties and its active

recapture, the precise location of AMPAR nanodomains regarding glutamate release sites is a key parameter to control synaptic transmission efficiency. In 2016, a paper from Blanpied's laboratory revealed an alignment between post-synaptic proteins such as PSD-95 clusters and the pre-synaptic glutamate release site, introducing the concept of trans-synaptic nanocolumn. In parallel, they demonstrated that this column was dynamic and can be at least temporarily modulated by activity.

Some questions remain concerning this new vision of synaptic transmission, as the sensitivity of synaptic strength to pre-post alignment and the proteins responsible of such trans-synaptic nanocolumn. In the first result chapter of my PhD, we coupled electrophysiology approaches, modeling and super-resolution microscopy techniques to further address these questions. With these approaches, we were able to uncover the impact of AMPAR nano-organization regarding glutamate release site. We found that the alignment between glutamate release machinery and post-synaptic AMPA receptors appears to impact on a highly sensitive manner the intensity of neuronal input and that this alignment was driven by interaction between neurexin and neuroligin adhesion proteins.

Historically, this work has been initiated by Kalina Haas, PhD student in the group, who studied the role of various proteins on the AMPAR clustering. She discovered that transient expression of a C-truncated form of Neuroligin was able to separate the co-organization between neuroligin and AMPAR nanodomain, without affecting the overall AMPAR nanodomain structure. However, expression of Neuroligin ΔC-ter has been reported to decrease miniature current (Nam and Chen, 2005). Our working hypothesis was that this mutant was able to break the trans-synaptic column, and that current decrease could be due to the glutamate release far from AMPAR nanodomains.

This following paper, described the work realized to demonstrate this hypothesis.

Pre-post synaptic alignment through neuroligin tunes synaptic transmission efficiency

Kalina T. Haas[1,2,3]*, Benjamin Compans[1,2]*, Mathieu Letellier[1,2]*, Thomas M Bartol Jr[4], Dolors Grillo-Bosch[1,2], Terrence J Sejnowski[4], Matthieu Sainlos[1,2], Daniel Choquet[1,2,5], Olivier Thoumine[1,2] and Eric Hosy[1,2,$]

[1] Univ. Bordeaux, Interdisciplinary Institute for Neuroscience, UMR 5297, F-33000 Bordeaux, France
[2] CNRS, Interdisciplinary Institute for Neuroscience, UMR 5297, F-33000 Bordeaux, France
[3] Present address: Medical Research Council Cancer Unit, University of Cambridge, Hutchison/MRC Research Centre, Box 197 Biomedical Campus, CB20XZ, Cambridge, United Kingdom
[4] Howard Hughes Medical Institute, Salk Institute for Biological Studies, La Jolla, United States
[5] Bordeaux Imaging Center, UMS 3420 CNRS, Université de Bordeaux, US4 INSERM, F-33000 Bordeaux, France
[$] corresponding author
* Contributed equally to the work

Summary

The nanoscale organization of neurotransmitter receptors relative to pre-synaptic release sites is a fundamental determinant of both the amplitude and reliability of synaptic transmission. How modifications in the alignment between pre- and post-synaptic machineries affect synaptic current properties has only been addressed with computer modeling, and therefore remains hypothetical. Using dual-color single molecule based super-resolution microscopy, we found a strong spatial correlation between AMPA receptor (AMPAR) nanodomains and the post-synaptic adhesion protein neuroligin-1 (NLG1). Expression of a C-terminal truncated form of NLG1 disrupted this correlation without affecting the intrinsic organization of AMPAR nanodomains. Moreover, this NLG1 dominant-negative mutant significantly shifted the pre-synaptic release machinery from AMPAR synaptic clusters. Electrophysiology and computer modeling show that this physical shift is sufficient to induce a significant decrease in synaptic transmission. Thus, our results suggest the necessity for synapses to release glutamate in front of AMPAR nanodomains, to maintain a high efficiency of synaptic responses.

Introduction

AMPA-type glutamate receptors (AMPARs) mediate the vast majority of fast excitatory synaptic transmission in the mammalian brain. AMPARs are stabilized at the post-synaptic density (PSD) by interactions with PDZ domain containing proteins such as PSD-95. AMPARs were initially thought to be homogeneously distributed throughout the PSD, but recent work based on super-resolution optical imaging (SRI) and electron microscopy has demonstrated that AMPARs are concentrated in small nanodomains around 80 nm in size, and containing 20 receptors on average (Fukata et al., 2013; MacGillavry et al., 2013; Masugi-Tokita et al., 2007; Nair et al., 2013). This specific mode of organization might be critical for synaptic transmission, depending on the relative positioning of pre-synaptic release sites with respect to AMPAR nanodomains. Previous studies showed that the glutamate content of a single presynaptic vesicle is not sufficient to activate the entire pool of AMPARs inside the PSD (Liu et al., 1999; Raghavachari and Lisman, 2004), suggesting that synaptic currents might be stronger if AMPARs were concentrated in front of pre-synaptic release sites rather than dispersed throughout the PSD. Moreover, mathematical models predict that when AMPARs are clustered in front of glutamate release sites, both the amplitude and the reliability of synaptic responses are improved (Franks et al., 2002; Franks et al., 2003; Tarusawa et al., 2009). In contrast, when AMPAR clusters are not aligned with release sites, synaptic currents are predicted to be weaker and highly variable (Tarusawa et al., 2009). Therefore, it is critical to understand the spatial relationship between glutamate release sites and AMPAR domains at the nanoscale level.

Dual-color SRI offers a new way to analyze the alignment of pre- and post-synaptic elements underlying the intrinsic function of the synapse. Several studies have examined the nanoscale organization of various pre-synaptic proteins, including calcium channels, syntaxin, and neurexin (Chamma et al., 2016; Ribrault et al., 2011; Schneider et al., 2015), but these proteins did not display a clustered organization resembling that of AMPARs (Hosy et al., 2014; Nair et al., 2013). A recent study indicated that the pre-synaptic active zone protein RIM is concentrated in small domains (Tang et al., 2016). Furthermore, this study indicated that active glutamate release sites are co-localized with RIM and aligned with AMPAR nanodomains. This trans-synaptic "nanocolumn" organization is regulated by long-term synaptic plasticity, highlighting its importance for the control of synaptic transmission. However, the molecular mechanisms underlying this alignment are still unknown, and the sensitivity of synaptic currents to mis-alignment has not been experimentally investigated.

One way to test the importance of pre- to post-synaptic alignment would be to destabilize the trans-synaptic organization and study its effect on synaptic transmission. It has been abundantly described that the adhesion complex neurexin-neuroligin forms a trans-synaptic bridge (Sudhof, 2008). Pre-synaptic neurexin is implicated in active zone formation (Missler et al., 2003), while post-synaptic neuroligin recruits PSD-95, NMDA receptors and AMPARs to partly structure the PSD (Budreck et al., 2013; Graf et al., 2004; Heine et al., 2008; Mondin et al., 2011). In particular, a C-terminally truncated neuroligin-1 (NLG1) mutant, unable to bind PDZ domain containing PSD proteins (NLG1-ΔCter), was previously shown to prevent PSD-95 recruitment at newly formed synapses, and reduce AMPAR-mediated synaptic transmission (Chih et al., 2005; Mondin et al., 2011; Nam and Chen, 2005; Shipman et al., 2011). Here, using dual-color SRI, we report that the expression of the NLG1-ΔCter mutant suppresses the co-localization of NLG1 and AMPAR nanodomains without changing the overall AMPAR nanoscale organization. In parallel, we observed that NLG1-ΔCter induced a shift between pre-synaptic RIM clusters and post-synaptic AMPAR nanodomains, associated with a significant decrease in synaptic currents. We suggest that the neurexin-neuroligin mediated pre-post synaptic alignment tightly regulates synaptic efficacy.

Results

Expression of NLG1-ΔCter does not affect AMPAR nanoscale organization

To understand the role of NLG1 adhesion in AMPAR nano-organization, we performed direct STochastic Optical Reconstruction Microscopy (d-STORM) experiments on primary hippocampal neurons expressing either full length NLG1 (NLG1), or a NLG1 mutant with a truncation in the last 72 amino acid of the C-terminal domain (NLG1-ΔCter), both constructs carrying an N-terminal HA tag. The NLG1-ΔCter mutant has an intact extracellular domain allowing normal contacts with pre-synaptic partners such as neurexins (Chih et al., 2005; Mondin et al., 2011), but is unable to interact with cytoplasmic proteins within the PSD, and thus should behave as a dominant-negative mutant that uncouples trans-synaptic adhesion from the PSD. Given that AMPAR nanodomains are tightly associated with PSD-95 sites (MacGillavry et al., 2013; Nair et al., 2013), our rationale was that by disconnecting NLG1 from PSD-95, we would perturb the nanoscale positioning of AMPARs (n=13 cells per condition).

As previously described (Mondin et al., 2011; Nam and Chen, 2005), expression of both truncated and full length NLG1 **(Figure 1A and B)** increases spine density, revealing the synaptogenic role of neuroligin (n= 10; 12; 9 respectively; ANOVA p=0.0004). We then examined the effect of NLG1-ΔCter expression on AMPAR nano-organization. Surface AMPARs were detected by labeling live neurons with a primary antibody specific for the N-terminal domain of the AMPAR GluA2 subunit, followed by fixation and incubation with a secondary antibody conjugated to the Alexa 647 dye. Nanodomains are determined as clusters of AMPARs present inside the synapse and containing at least 5 receptors, based on single particle emission properties (see Nair et al, 2013). In control neurons expressing GFP alone, we detected typically between 1 to 2 AMPAR nanodomains per synapse, with an average size of 90 ± 3 nm **(Figure 1D and E)**, as reported previously (Nair et al., 2013). NLG1 overexpression increased the surface density of AMPAR nanodomains **(Figure 1C)**, in agreement with the previous finding that NLG1 potentiates the formation of excitatory synapses (Chih et al., 2005; Ko et al., 2009; Levinson et al., 2005; Mondin et al., 2011). Furthermore, NLG1 overexpression led to a re-organization of AMPAR nanodomains by increasing both their size and AMPAR content **(Figure 1D and E)**. Surprisingly, expression of NLG1-ΔCter for 3 days did not affect AMPAR nano-organization compared to the GFP control **(Figure 1C to E,** Anova post-test: p=0.72; 0.82 and 0.33 for figure C; D and E respectively**)**. To validate this observation, we analyzed d-STORM images of AMPARs acquired on neurons expressing either GFP alone or GFP + NLG1-ΔCter, using a cluster quantification method based on Tessellation (Levet et al., 2015) (**Figure S1A**). Through this analysis, we obtained an estimate of the number of endogenous GluA2-containing AMPARs per spine **(Figure S1B)**, per nanodomain **(Figure S1C)** and the size of the nanodomains **(Figure S1D)**. This analysis confirmed that NLG1-ΔCter expression does not affect the total amount of AMPARs per synapse, nor their organization in nanodomains.

Next, we measured the lateral mobility of endogenous GluA2-containing AMPARs at the dendritic surface in live neurons using the universal Point Accumulation in Nanoscale Topography (u-PAINT) technique (Giannone et al., 2010; Nair et al., 2013) **(Figure S2)**. The receptor lateral mobility is dependent on AMPAR complex composition, phosphorylation status and desensitization properties (Compans et al., 2016; Constals et al., 2015; Hafner et al., 2015; Tomita et al., 2007). Both the distribution of diffusion coefficients and the mobile fraction (i.e. proportion of AMPARs with diffusion coefficients above 0.01 $\mu m^2/s$) were not significantly affected by NLG1-ΔCter, as compared to GFP-expressing neurons **(Figure S2,** n=16 Ctrl and

21 NLG1-ΔCter, 2 sample t-test p=0.36), in agreement with previous findings using Quantum dots (Mondin et al., 2011).

Full-length NLG1 tightly co-localizes with AMPAR nanodomains

To examine the co-organization of AMPARs and NLG1 at the nanoscale level, we performed dual-color SRI experiments. Endogenous GluA2 were live-labelled with a primary mouse monoclonal antibody while NLG1 or NLG1-ΔCter were live-labelled with a primary monoclonal rat anti-HA antibody. Neurons were then fixed, incubated with a secondary anti-mouse antibody conjugated to Alexa 532 and an anti-rat antibody coupled to Alexa 647, and processed for d-STORM **(Figure 2A)**. Both AMPARs and NLG1 were detected as small synaptic and extra-synaptic clusters **(Figure 2B)**. Qualitatively, we observed that the majority of synaptic NLG1 spots (green) overlapped with AMPAR nanodomains (purple). To precisely quantify the degree of co-localization between AMPAR and NLG1 clusters, we developed a method based on Manders' coefficients and bivariate nearest neighbor distance (see Methods). Manders' coefficients have been widely used in diffraction-limited microscopy to quantify the co-localization between pairs of objects characterized by different fluorescent markers (Manders, 1993).

We first validated both the labeling efficiency and the co-localization by studying co-organization between HA-GluA1 (labelled with the same primary monoclonal rat anti-HA antibody, revealed with Alexa 647) and endogenous GluA2 (labelled with primary mouse monoclonal anti-GluA2 antibody, revealed with Alexa 532; **Figure S3**). These experiments have the advantage of using the same combination of antibodies as in **Fig. 2**. Since AMPARs form heterotetramers in neurons, the labelings for GluA1 and GluA2 are expected to exhibit a high level of co-localization **(Figure S3).** The comparison between the size of single fluorescence emitters and both Alexa 532 and Alexa 647 labelled objects clearly demonstrates the presence of GluA1 and GluA2 clusters **(Figure S3B)**. The distribution of bivariate nearest neighbor distances shows that 80% of HA-labelled GluA1 clusters have a GluA2 label within 80 nm **(Figure S3C).** The comparison of the experimental distribution of bivariate nearest neighbor distances to an *in silico* distribution obtained by randomization of cluster localization, clearly demonstrates that GluA1-HA and GluA2 clusters display a high degree of co-localization **(Figure S3C)**. Finally, the Manders' representation in (**Figure S3D)** reveals two points: first, only 5% of GluA1 and GluA2 object pairs have a null Manders' coefficient, reflecting that almost all Alexa 532-GluA2 labelled objects co-localize at least partly with

Alexa 647-GluA1 labelled objects. Second, even though we co-labelled proteins belonging to the same cluster, less than 20% of objects exhibit a Manders' coefficient higher than 0.8, but 60 % overlapped on an area larger than 50 %. This likely originates from the fact that high levels of co-localization are difficult to reach in 2-color super-resolved images due to achromatism and the antibody size.

We then applied the Manders' analysis to examine the co-localization between AMPAR nanodomains and NLG1 clusters inside synapses **(Figure 2C, D and E; green line)**. The similar area distribution between single fluorescence emitters and NLG1 clusters **(Figure 2C)** reveals that NLG1 does not form large domains inside synapses, but rather several small clusters, confirming previous findings with an alternative labeling strategy (Chamma et al., 2016). In contrast, the area distribution of AMPARs displays larger values, due to AMPAR clustering. For the remaining part of the analysis, we took into account all NLG1 objects, but only selected AMPAR objects larger than 0.005 µm² **(red dashed line Figure S3B)**, a threshold allowing the suppression of 80% of single emitters. The centroid to centroid bivariate nearest neighbor distance distribution between NLG1 and AMPAR nanodomains was significantly smaller than that expected from an independent distribution **(Figure 2D; green line,** n=512 pairs of co-localization), indicating a functional proximity between NLG1 and GluA2 clusters at the nanoscale. The difference between the two curves was already apparent in the first 100 nm, revealing a tight association between NLG1 and AMPAR nanodomains at a short length scale. Finally, Manders' coefficients were calculated between each pair of objects **(Figure 2E; green line,** n=512 pairs of co-localization). Only 20% of NLG1 clusters did not co-localize even partially with a GluA2 nanodomain, while almost 75% of NLG1 clusters co-localized to more than 80% with AMPAR nanodomains. These results demonstrate the tight nanoscale co-organization between AMPAR and NLG1 within a synapse.

NLG1-ΔC is delocalized from AMPAR nanodomains

Next, we analyzed the distribution of AMPAR nanodomains with respect to NLG1-ΔCter **(Figure 2D and E;** 316 pairs of co-localization). As NLG1, NLG1-ΔCter was organized in small clusters **(Figure 2C, red line)** with an average size of 0.005 µm², whereas AMPARs were distributed as both small and large objects. The bivariate nearest neighbor distances between NLG1-ΔCter and AMPAR clusters were significantly larger than for NLG1 and AMPAR nanodomains. Centroid to centroid bivariate nearest neighbor distance between all NLG1-ΔCter object and GluA2 clusters overlapped with a random distribution, at least for the first 250 nm

corresponding to the PSD size **(Figure 2F, red line)**. This led us to the conclusion that there is no preferential association of NLG1-ΔCter clusters with AMPAR nanodomains. This was confirmed by looking at the distribution of Manders' coefficients **(Figure 2G, red line)**. Only 38% of NLG1-ΔCter co-localized at least partially with AMPARs, compared with 80% for NLG1, revealing that the NLG1 C-terminal truncation strongly decreases the association between NLG1 and AMPAR nanodomains (comparison with NLG1: 2 sample t-test $p<0.0001$).

NLG1ΔC expression shifts the alignment between presynaptic RIM and post-synaptic AMPAR nanodomains

We then analyzed the effect of NLG1-ΔCter expression on the alignment between pre-synaptic RIM and post-synaptic AMPAR clusters. These two proteins are components of the trans-synaptic "nanocolumns", which organize pre-synaptic release sites in front of post-synaptic AMPAR clusters (Tang et al., 2016). Both RIM and AMPAR were endogenously labelled, while post-synaptic neurons expressed GFP, NLG1 or NLG1-ΔCter **(Figure 3A, B and C)**. The bivariate nearest neighbor distances between RIM and AMPAR clusters was not affected by NLG1 expression, but was significantly larger when NLG1-ΔCter was expressed **(Figure 3B, Anova p<0.001)**. The distribution of Manders' coefficients confirmed that NLG1-ΔCter expression decreased the RIM-AMPAR apposition **(Figure 3C, Anova p<0.001)**. These results demonstrate a physical misalignment between the presynaptic marker RIM and the postsynaptic AMPAR clusters upon NLG1-ΔCter expression, while NLG1 expression didn't display similar effect.

NLG1 C-terminus truncation impairs synaptic transmission

To estimate the effect of a decorrelation between AMPAR nanoclusters and pre-synaptic release sites on synaptic transmission, we first recorded miniature AMPAR currents on dissociated hippocampal cultures by electrophysiology, upon expression of NLG1-ΔCter + GFP, GFP alone as a control, or full length NLG1 + GFP **(Figure 4A to C)**. Chronic NLG1-ΔCter expression (3 days) reduced the amplitude of AMPAR mEPSCs by 24% as compared to GFP expressing control **(Figures 4C, Anova p=0.0002)**. In contrast, NLG1 expression did not affect the miniature amplitude, even if as expected by the high increase in synapse number observed in **Figure 1A**, we observed a significant increase in miniature frequency **(Figure S4A)**. These results show that synaptic elementary transmission is not altered by NLG1

overexpression but when the linkage between NLG1-based adhesion and AMPAR clusters is perturbed.

To confirm these conclusions in a model system having preserved synaptic connectivity, we used mouse organotypic hippocampal cultures, in which single CA1 neurons were electroporated with GFP-tagged either NLG1 or NLG1-ΔCter. One week later, evoked whole-cell currents were recorded from electroporated neurons and from neighboring non-electroporated counterparts, upon stimulation of Schaffer collaterals **(Figure 4D to I)**. Calcium was replaced by strontium in the extracellular solution to induce the asynchronous release of pre-synaptic vesicles following stimulation, thereby evoking a train of miniature AMPA currents post-synaptically (Goda and Stevens, 1994). Both NLG1 and NLG1-ΔCter expression increased the number of evoked miniature currents compared to non-electroporated neurons, again likely reflecting the synaptogenic effect of NLG1 **(Figure S4B)**. As observed in cell cultures, the current amplitude was reduced by 26% in neurons expressing NLG1-ΔCter but not in neurons expressing NLG1, when compared to control non-electroporated neurons **(Figure 4H and I, paired t-test p=0.99 and 0.018)**. Similar results were obtained on the NLG1 KO background **(Figure S5)**, with a 32 % decrease of aEPSC amplitude on NLG1-ΔCter expressing neurons relatively to unelectroporated counterparts. The similarity of the current decrease, both in the WT or NLG1 KO background, emphasizes the dominant negative role of the NLG1-ΔCter expression (see discussion). Finally, in order to investigate whether expression of NLG1 or NLG1-ΔCter could affect presynaptic function, we measured the paired-pulse ratio (PPR) in an extracellular solution containing calcium. There was no significant change in PPR upon expression of either NLG1 or NLG1-ΔCter **(Figure S6)**, indicating no specific modification of the pre-synaptic release probability.

Cell permeant neuroligin biomimetic divalent ligand disrupt pre-post alignment and decrease AMPAR-mediated synaptic transmission

To confirm the role of NLG1 C-terminal interactions in aligning AMPARs in front of pre-synaptic release sites, without overexpressing NLG1-ΔCter mutants which might also affect pre-synaptic development, we used an alternative strategy. Based on our previous expertise to perturb interactions between stargazin and PSD-95 (Sainlos et al.), we developed divalent biomimetic ligands comprising the 15 C-terminal amino acids of NLG1, conjugated to a TAT sequence to favor cell penetration. In contrast to the NLG1-ΔCter mutant, those ligands directly compete with endogenous neuroligins to bind PDZ domain containing scaffolding proteins at

the post-synapse, without altering the binding of neuroligins to pre-synaptic proteins such as neurexins. Control non-sense ligands had the same structure but mutations in the sequence prevent interaction with PDZ-domain. Incubation of 14 DIV hippocampal neurons for 1-2 days with NLG1 competing ligands caused a misalignment between RIM and GluA2 containing AMPARs observed by dual-color STORM **(Figure 5A-C)**, and a 30% decrease in AMPAR-mediated mEPSC amplitudes **(Figure 5E)**. In both assays, non-sense peptides had no effect compared to untreated neurons, demonstrating the absence of effect of TAT peptide treatment. Interestingly, NLG1 peptides did not alter AMPAR-mediated mEPSC frequency **(Figure 5F)**, suggesting an exclusive post-synaptic effect. Overall, NLG1 competing peptides and NLG1-ΔCter expression had very similar effects on AMPAR positioning and synaptic responses, suggesting a common mechanism of action.

Synaptic efficiency critically depends on the AMPAR nanodomains to glutamate release sites distance

To examine theoretically the effects of delocalizing AMPAR nanodomains from pre-synaptic glutamate release sites, we performed Monte-Carlo based simulation using the MCell software **(Figure 6)**. The synaptic shape and perisynaptic environment was obtained from 3D electron microscopy images reconstructing the neuropil of a hippocampal CA1 stratum radiatum area, previously developed to model synaptic transmission (Bartol et al., 2015a; Bartol et al., 2015b; Kinney et al., 2013) (See Methods). AMPAR chemical kinetic properties were obtained from a well-established model (Jonas et al., 1993) **(Figure 6B)** and the kinetic parameters were adjusted to fit both the recorded mEPSCs, and the AMPAR organization map extracted from the d-STORM data (**Figure 1** and (Nair et al., 2013) see Methods). In the simulations, the number of released glutamate molecules was fixed to 1500, 2000, 3000 or 4500, to be in the range of the estimated amount per pre-synaptic vesicle (Savtchenko et al., 2013). Simulations computed the number of open AMPARs, when vesicles containing the various glutamate quantities were released in front of a single AMPAR cluster, or up to 200 nm away from the cluster center, varied with a 50 nm increment **(Figure 6B)**. As expected, simulated curves demonstrated that the glutamate content per pre-synaptic vesicle was positively correlated to the synaptic response **(Figure 6C)**. Strikingly, the simulation further showed that the current amplitude was inversely correlated to the distance between the release site and AMPAR nanodomains **(Figure 6D)**. A release of 3000 glutamate molecules, which is in the upper range of glutamate content per vesicle, at 150 nm from an AMPAR nanodomain,

lead to a decrease of almost 40% of the synaptic response. In this model, the release distance is measured from the center of the nanodomain, which has a 90 nm diameter size. Even at 50 nm from the centroid (i.e., at the close periphery of the nanodomain), a significant decrease of current amplitude was already observed for low glutamate content **(Figure 6D)**. The expected decrease in synaptic current amplitude was also sensitive to the glutamate content **(Figure 6E)**. Specifically, the 26% decrease of AMPAR current observed experimentally corresponds to a glutamate content of around 2000 molecules when the release site is localized 90 nm away from the nanodomain centroid **(Figure 6E)**.

Discussion

Our study advocates two main conclusions. First, NLG1 is one of the main organizers of trans-synaptic "nano-columns", positioning AMPAR nanodomains in close proximity to pre-synaptic release sites. Second, the amplitude of AMPAR-mediated currents is highly sensitive to pre-post synaptic nanoscale alignment **(Figure 6F)**. At the synapse, NLG1 executes two distinct functions. One is to regulate synapse number, the other is to organize the post-synaptic compartment (Ko et al., 2009; Levinson et al., 2005; Sara et al., 2005; Scheiffele et al., 2000). NLG1 binds pre-synaptic neurexins via its extracellular domain, while its cytoplasmic tail exhibits various binding sites including a C-terminal PDZ domain binding motif, a central gephyrin binding motif, and an upstream non-canonical motif without identified interactor but also important for neuroligin function (Dean et al., 2003; Giannone et al., 2013; Irie et al., 1997; Shipman et al., 2011). Here, we used a NLG1 construct lacking both the PSD-95 and gephyrin binding domains. When expressed during the normal period of synaptogenesis, this NLG1 mutant is able to strongly increase synapse number, but does not recruit enough PSD-95 and AMPARs to sustain normal synaptic transmission (Budreck et al., 2013; Mondin et al., 2011; Nam and Chen, 2005).

We found that expressing NLG1-ΔCter later in development (synapse maturation stage) caused a modest increase in spine density, accompanied by a decrease in quantal transmission. Interestingly, the AMPAR content per synapse was not affected, nor their organization in nanodomains. Rather, the NLG1-ΔCter displaced their spatial alignment with pre-synaptic release sites visualized by RIM clusters. Our interpretation is that NLG1-ΔCter outcompeted with endogenous NLG1 for the binding to neurexins (or other pre-synaptic partners), allowing unanchored PSD-95 scaffolds and AMPAR nanodomains to flow away from the release site (MacGillavry et al., 2013; Nair et al., 2013). As previously published, heterodimerization might

occur between recombinant NLG1-ΔCter and endogenous NLG1(Shipman et al., 2011), but on average we observed a clear shift between NLG1-ΔCter labeling and AMPAR nanodomains, suggesting a dominant negative effect. Interestingly, a similar reduction in AMPAR currents induced by NLG1-ΔCter was observed in organotypic slices from both NLG1 WT and KO genetic backgrounds, revealing a potential heterodimerization of NLG1-ΔCter with other NLGs, specifically NLG3 (Shipman et al., 2011). Acute application of cell-permeant NLG1 ligand confirmed these conclusions. The obtained results demonstrate that C-terminal interactions between NLG1 and PDZ domain containing scaffold proteins such as PSD-95, are important to align AMPAR nanodomains in front of pre-synaptic release sites.

The functional effect of such a molecular disorganization caused either by NLG1-ΔCter expression or NLG1 peptide incubation was found to be unexpectedly important, i.e. less than 100 nm displacement triggers decreases mEPSC amplitude by about 30%. Modeling confirmed the high sensitivity of the AMPAR synaptic currents to the position of the pre-synaptic release with respect to AMPAR nanodomains. Considering that quantal synaptic transmission results from the release of glutamate from one vesicle in front of an AMPAR nanodomain, three obvious parameters determine the number of activated AMPARs: 1/ the amount of glutamate per vesicle; 2/ the number of AMPARs per nanodomain; and 3/ the degree of apposition between release sites and nanodomains. Our simulations predict that an equivalent 25% decrease of current could be explained by either a 3-fold decrease in glutamate content (from 4500 to 1500 molecules per vesicle), a 32% loss in the number of AMPARs per nanodomain, or a 100 nm shift between pre- and post-organization (for a glutamate content of 2000 molecules per vesicle).

Our observations support a new model of synaptic function, where the quantum of synaptic transmission is more sensitive to AMPAR nanoscale organization and alignment with respect to release sites, than to the glutamate content per vesicle and even AMPAR content per nanodomain. These specific properties are due in part to the relatively low affinity of AMPAR for glutamate (mM range) and the fact that released glutamate rapidly fades away laterally as it crosses the synaptic cleft (Lisman et al., 2007; Liu et al., 1999; Tarusawa et al., 2009). These results suggest two changes in our conception of the efficacy of synaptic function. First, synapses exhibit a relative tolerance to variability both in the glutamate content per vesicle and in the number of AMPAR per nanodomains. Indeed, 10 to 20% variation in these parameters will not drastically affect synaptic transmission efficacy. We show that the combination of pre-post alignment and nanodomain organization is sufficient to bring some stability to synaptic transmission. Second, fast and large modifications in synaptic amplitude can be better achieved

by molecular pre-post misalignment than by changes in AMPAR number. This prediction is in line with the transient physiological misalignment previously described upon induction of chemical Long Term Depression (LTD) (Tang et al., 2016).

In conclusion, this study suggests that synapses, via trans-synaptic adhesion, optimize the use of glutamate, by controlling an alignment between pre-synaptic release sites and AMPAR nanodomains. Previous modeling experiments suggested that high efficiency of synaptic transmission, high amplitude response and low variability, requires a tight clustering of AMPA receptors, and an alignment of these clusters with the pre-synaptic release site (Nair et al., 2013; Tarusawa et al., 2009). Based on super-resolution imaging techniques and the use of the NLG1 C-terminal truncation mutant, our study reveals the surprisingly high sensitivity of the system to this trans-synaptic molecular organization.

Material and methods

Cell and brain slice culture and transfection

Preparation of cultured neurons was performed as previously described (Nair et al., 2013). Hippocampal neurons from 18-day-old rat embryos of either sex were cultured on glass coverslips following the Banker protocol. Neurons were transfected using Effectene (Qiagen) at 10-11 days in vitro (DIV) with either HA::SEP::GluA1, HA::NLG1ΔC, where the last 72 amino acid are truncated, HA::NLG1 WT or GFP alone and the cells were used for immunocytochemistry at 13-15 DIV. All experiments are done on at least 3 independent dissections.

Organotypic hippocampal slice cultures were prepared from wild type mice (C57Bl6/J strain). Briefly, hippocampi were dissected out from animals at postnatal day 5-7 and slices (350 µm) were cut using a tissue chopper (McIlwain) and incubated with serum-containing medium on Millicell culture inserts (CM, Millipore). The medium was replaced every 2–3 days. After 3–4 days in culture, CA1 pyramidal cells were processed for single-cell electroporation with plasmids encoding enhanced GFP (EGFP) along with wild type or -ΔCter AP-NLG1 (Chamma et al., 2016). The pipette containing 33 $ng.\mu l^{-1}$ total DNA was placed close to the soma of individual CA1 pyramidal neurons. Electroporation was performed by applying three square pulses of negative voltage (10 V, 20 ms duration) at 1 Hz, and then the pipette was gently removed. Three to five neurons were electroporated per slice, and the slice was placed back in the incubator for 7 days before experiments.

Immunocytochemistry

For the GluA2, HA-tagged proteins and RIM, primary neuronal cultures were co-incubated with monoclonal mouse anti-GluA2 antibody (Nair et al., 2013), monoclonal rat anti-HA antibody (Roche, France), RIM 1/2 antibody (synaptic systems, Gottingen, Germany) or for 5-7 minutes at 37° C and then fixed with 4% PFA. A preliminary permeabilization step with triton is used for the RIM labelling.

Then cells were washed 3 times for 5 min in 1x PBS. PFA was quenched with NH4Cl 50 mM for 30 minutes. Unspecific staining was blocked by incubating coverslips in 1% BSA for 1h at room temperature. Primary antibodies were revealed with Alexa 532 coupled anti-mouse IgG secondary antibodies and Alexa 647 coupled anti-rat secondary antibodies (Jackson ImmunoResearch Laboratories, USA).

Direct Stochastic Optical Reconstruction Microscopy (d-STORM)

d-STORM imaging was performed on a commercial LEICA SR GSD, model DMI6000B TIRF (Leica, Germany). LEICA SR GSD was equipped with anti-vibrational table used to minimize drift, Leica HCX PL APO 160x 1.43 NA oil immersion TIRF objective and laser diodes with following wavelength: 405 nm, 488 nm, 532 nm, 642 nm (Coherent, USA). Fluorescence signal was detected with sensitive iXon3 EMCCD camera (Andor, UK). Image acquisition and control of microscope was driven by Leica software. Images were streamed at 94 fps (frames per second); image stack contained typically 30,000 frames. Selected ROI (region of interest) had dimension of 200 x 200 pixels (one pixel = 100 nm). Pixel size of reconstructed super-resolved image was set to 20 nm.

Power of a 405 nm laser controlled the level of single molecules per frame. The dyes were sequentially imaged (Alexa 647 first, followed by Alexa 532) to collect the desired single molecule frames and to avoid photo bleaching. Multi-color fluorescent microspheres (Tetraspeck, Invitrogen) were used as fiducial markers to register long-term acquisitions and correct for lateral drifts and chromatic shifts. A spatial resolution of 14 nm was measured using centroid determination on 100 nm Tetraspeck beads acquired with similar signal to noise ratio than d-STORM single molecule images. Details of experimental procedure and data analysis was followed as described before (Nair et al., 2013).

Tesselation analysis of d-STORM experiments are done as described in the original paper (Levet et al., 2015).

uPAINT

13-14 Days in Vitro (DIV) dissociated neurons were imaged at 37°C in an open Ludin Chamber (Ludin Chamber, Life Imaging Services, Switzerland) filled with 1 ml of Tyrode's. Dendritic ROIs were selected based on fluorescence from GFP. ATTO-647 coupled to antibody against AMPAR subunit GluA2 was added to the chamber after appropriate cell was identified and region selected. Adding a suitable amount of probes controlled density of labelling. The fluorescence signal was collected using a sensitive EMCCD (Evolve, Photometric, USA). Acquisition was driven with MetaMorph software (Molecular Devices, USA) and acquisition time was set to 20 ms. Around 20 000 frames were acquired in typical experiment, collecting up to few thousands of trajectories. Sample was illuminated in oblique illumination mode. Angle of refracted beam varied smoothly and was adjust manually to maximize signal to noise ratio. The main parameters determined from the experiments was the diffusion coefficient (D) based on the fit of the mean square displacement curve (MSD). Multi-colour fluorescence microspheres were used for image registration and drift compensation. uPAINT data analysis was reported before (Giannone et al., 2010; Nair et al., 2013).

Electrophysiology recordings on cell culture

Coverslips of transfected neurons were placed in a Ludin Chamber on an inverted motorized microscope (Nikon Eclipse Ti). Extracellular recording solution was composed of the following (in mM): 110 NaCl, 5.4 KCl, 1.8 $CaCl_2$, 0.8 $MgCl_2$, 10 HEPES, 10 D-Glucose, 0.001 Tetrodotoxin and 0.05 Picrotoxin (pH 7.4; 245 mOsm). Patch pipettes were pulled using a horizontal puller (P-97, Sutter Instrument) from borosilicate capillaries (GB150F-8P, Science Products GmbH) to resistance of 4-6 MΩ and filled with intracellular solution composed of the following (in mM): 100 K-gluconate, 10 HEPES, 1.1 EGTA, 3 ATP, 0.3 GTP, 0.1 $CaCl_2$, 5 $MgCl_2$ (pH 7.2; 230 mOsm). Transfected neurons were identified under epifluorescence from the GFP signal. Recordings were performed using an EPC10 patch clamp amplifier operated with Patchmaster software (HEKA Elektronik). Whole-cell voltage clamp recordings were performed at room temperature and at a holding potential of -70 mV. Unless specified otherwise, all chemicals were purchased from Sigma-Aldrich except for drugs, which were from Tocris Bioscience.

Data were collected and analysis of miniature EPSCs were performed using a software developed by Andrew Penn, the matlab script is available on MATLAB File Exchange, ID: 61567; http://uk.mathworks.com/matlabcentral/fileexchange/61567-peaker-analysis-toolbox).

Electrophysiology recordings on organotypic brain slices

Dual whole-cell patch-clamp recordings were carried out in the CA1 region from organotypic hippocampal slices placed on the stage of a Nikon Eclipse FN1 upright microscope at room temperature and using Multiclamp 700B amplifier (Axon Instruments). The recording chamber was continuously perfused with aCSF bubbled with 95% O_2/ 5% CO_2 and containing (in mM): 125 NaCl, 2.5 KCl, 26 $NaHCO_3$, 1.25 $NaH2PO_4$, 2 $CaCl_2$, 1 $MgCl_2$, and 25 glucose. Resistance of patch-pipettes was 4-6 mΩ when filled with a solution containing (in mM) : 135 $CesMeSO_4$, 8 CsCl, 10 HEPES, 0.3 EGTA, 4 MgATP, 0.3 NaGTP, 5 QX-314, pH 7.28, 302 mOsm. EPSCs were elicited in CA1 pyramidal neurons by stimulating Schaffer collaterals in the stratum radiatum with a bipolar stimulation electrode in borosilicate theta glass filled with aCSF. Bicuculline (20 µM) was added to the aCSF to block inhibitory currents and DNQX (100 nM) was added to control epileptic activity. Series resistance was always lower than 20 mΩ. Paired-pulse ratio was determined by delivering two stimuli 50 ms apart and dividing the peak response to the second stimulus by the peak response of the first one. For recordings aEPSCs, extracellular $CaCl_2$ was substituted to equimolar $SrCl_2$. aEPSCs evoked within 500 ms after the stimulation, were analyzed off-line with Mini Analysis software (Synaptosoft). In all cases, at least 20 sweeps per recording were analysed.with a detection threshold set at 5 pA.

Co-localization analysis

Co-localization analysis was performed using custom written program in Matlab (Mathworks, UK). Manders' coefficients were chosen as co-localization measure because they do not depend on the relative intensity difference between two component images, therefore bypassing alteration in labeling efficiency of different cellular structures. Here we perform pairwise analysis between coincidental objects observed in two image components. Thus, our Manders' coefficients represent fraction of the intensity belonging to co-localizing super-resolution pixels of a given object. Manders' coefficients are calculated using following equations:

$$M_1 = \frac{\sum_i^n I_{1i,coloc}}{\sum_i^n I_{1i}}$$

$$M_2 = \frac{\sum_i^n I_{2i,coloc}}{\sum_i^n I_{2i}}$$

Where *i* is a pixel index, 1 and 2 stands for two image components and *n* is the number of pixels in an object for which coefficient is evaluated. $I_{1i} \geq 0$ ($I_{2i} \geq 0$) are intensity values at the i^{th} pixel of an object in the first (second) component of the dual-color image.

In first step, two image components are threshold, segmented and reduced to sets of geometrical objects attributed with their weighted centroid location, pixel area, intensity and location. Objects in each component image were divided into two categories, according to their area. This distinction is based on the size of single emitter found both on the coverslip and on the dendrite. With this analysis, we can tell apart the single proteins from the clustered ones, and analyze them independently.

In subsequent step, first bivariate nearest neighbor distance distribution is calculated for each neuroligin to the nearest AMPAR cluster. Afterwards, the Manders' coefficients are evaluated between each first nearest neighbor pair of AMPAR cluster and neuroligin. These coefficients were calculated only between pairs of AMPAR and neuroligin separated by the threshold distance, which reflects the maximum distance between two objects considered as related and was obtained from bivariate nearest neighbor distance distribution.

Co-localization significance was accounted for by image randomization. Objects in one image component were rearranged by random assignment of new position for their weighted centroids. This step was repeated up to 1000 times, each time appropriate measure of co-localization was evaluated. Bivariate first nearest neighbour distributions are compared to the mean of randomized samples and 95 % confidence intervals. If the experimental distribution lies above (below) randomized distribution, it indicates tendency towards association (dispersion) at given distances. However, if experimental distribution matches randomized one, it points to random or independent distribution between two classes of objects. Matlab scripts are available on request and will be deposited at http://uk.mathworks.com/matlabcentral/fileexchange.

Biomimetic ligands

Synthesis of the divalent TAT-non-sense ligands was previously described in sainlos et al 2011 (Sainlos et al.). The neuroligin divalent ligands was produced similarly using the last 15 amino acids of NLG1 as PDZ domain binding motifs.

Modeling

Computer modeling were performed using the MCell/CellBlender simulation environment (http://mcell.org) with MCell version 3.3, CellBlender version 1.1, and Blender version 2.77a (http://blender.org). The realistic model of glutamatergic synaptic transmission (Fig 5A) was constructed from 3DEM of hippocampal area CA1 neuropil as described in (Bartol et al., 2015a; Bartol et al., 2015b; Kinney et al., 2013). The 3DEM reconstruction is highly accurate and detailed and contains all plasma membrane bounded components including dendrites, axons, astrocytic glia and the extracellular space itself, in a 6x6x5 um^3 volume of hippocampal area CA1 stratum radiatum from adult rat. As fully described in Kinney et al. (2013) special methods were developed and applied to the 3DEM to correct for shrinkage and fixation artifacts to accurately recover the dimensions and topology of the extracellular space. The model contains glutamate transporters, 10000 per square micron, on the astrocytic glia processes, as described in Bartol et al., 2015. The images in Fig 5A were generated from the 3DEM reconstruction using Blender (blender.org) and the CellBlender addon (mcell.org). For the dendritic spine synapse shown in Fig 5A, the cleft height is 20 nm and the lateral size of the PSD area is 350x250 nm.

The AMPAR rate constants in the model were adjusted using simplex optimization with minimum least-squares to best fit the shape of the AMPAR current (20-80% rise time, peak amplitude, 10-90% fall time of the AMPAR current) reported in Nair et al., 2013. The initial parameter values are as reported in Jonas et al, 1993 with release of glutamate directly over the cluster while holding fixed values of n_Glu = 3000, n_AMPAR = 25 in cluster. The best fit parameter values are reported in the caption for Fig 5B. We averaged the AMPAR activation time courses of 100 simulation trials at each release location and number of glutamate released.

Statistics

Summary statistics are presented as mean ± SEM (Standard Error of the Mean). Statistical significance tests were performed using GraphPad Prism software (San Diego, CA). Test for normality was performed with D'Agostino and Pearson omnibus tests. For non-normally distributed data, we applied Mann-Whitney test or Wilcoxon matched-pairs signed rank test for paired observations. When the data followed normal distribution, we used paired or unpaired t-test for paired observations unless stated otherwise. ANOVA test was used to compare means of several groups of normally distributed variables. Indications of significance correspond to p values <0.05(*), $p < 0.005$(**), and $p<0.0005$(***).

Ethical Approval

All experiments were approved by the Regional Ethical Committee on Animal Experiments of Bordeaux.

ACKNOWLEDGEMENTS

We acknowledge E. Gouaux for the anti-GluA2 antibody; J-B Sibarita and Corey Butler for providing single particle analysis software, M. Sainlos and I. Gauthereau for anti-GFP nanobody production; C. Breillat and E. Verdier for cell culture and plasmid production; M. Goillandeau and Andrew Penn for mEPSC analysis software (Detection Mini). This work was supported by funding from the Ministère de l'Enseignement Supérieur et de la Recherche (ANR NanoDom), Centre National de la Recherche Scientifique, FRM to BC, ERC Grant nano-dyn-syn to DC. SyMBaD – ITN Marie Curie, Grant Agreement n° 238608 – 7th Framework Program of the EU.

AUTHOR CONTRIBUTION

E.H. conceived the study and formulated the models.
K.T.H. developed the co-localization program.
K.T.H., B.C. and E.H. performed single molecule experiments, analyzed the data and prepared the corresponding figures.
B.C., M.L. and E.H. designed and performed the electrophysiology experiments and corresponding data analysis.
T.B. T.S. developed simulation program and performed simulations.
D.G-B and M.S. developed the NLG peptide
O.T. and DC helped to the conception of experiments.
E.H., O.T. and D.C. wrote the manuscript with help of other authors

References

Bartol, T.M., Bromer, C., Kinney, J., Chirillo, M.A., Bourne, J.N., Harris, K.M., and Sejnowski, T.J. (2015a). Nanoconnectomic upper bound on the variability of synaptic plasticity. eLife 4, e10778.

Bartol, T.M., Keller, D.X., Kinney, J.P., Bajaj, C.L., Harris, K.M., Sejnowski, T.J., and Kennedy, M.B. (2015b). Computational reconstitution of spine calcium transients from individual proteins. Frontiers in synaptic neuroscience 7, 17.

Budreck, E.C., Kwon, O.B., Jung, J.H., Baudouin, S., Thommen, A., Kim, H.S., Fukazawa, Y., Harada, H., Tabuchi, K., Shigemoto, R., *et al.* (2013). Neuroligin-1 controls synaptic abundance of NMDA-type glutamate receptors through extracellular coupling. Proceedings of the National Academy of Sciences of the United States of America 110, 725-730.

Chamma, I., Letellier, M., Butler, C., Tessier, B., Lim, K.H., Gauthereau, I., Choquet, D., Sibarita, J.B., Park, S., Sainlos, M., and Thoumine, O. (2016). Mapping the dynamics and nanoscale organization of synaptic adhesion proteins using monomeric streptavidin. Nature communications 7, 10773.

Chih, B., Engelman, H., and Scheiffele, P. (2005). Control of excitatory and inhibitory synapse formation by neuroligins. Science 307, 1324-1328.

Compans, B., Choquet, D., and Hosy, E. (2016). Review on the role of AMPA receptor nano-organization and dynamic in the properties of synaptic transmission. Neurophotonics 3, 041811.

Constals, A., Penn, A.C., Compans, B., Toulme, E., Phillipat, A., Marais, S., Retailleau, N., Hafner, A.S., Coussen, F., Hosy, E., and Choquet, D. (2015). Glutamate-induced AMPA receptor desensitization increases their mobility and modulates short-term plasticity through unbinding from Stargazin. Neuron 85, 787-803.

Dean, C., Scholl, F.G., Choih, J., DeMaria, S., Berger, J., Isacoff, E., and Scheiffele, P. (2003). Neurexin mediates the assembly of presynaptic terminals. Nature neuroscience 6, 708-716.

Franks, K.M., Bartol, T.M., Jr., and Sejnowski, T.J. (2002). A Monte Carlo model reveals independent signaling at central glutamatergic synapses. Biophysical journal 83, 2333-2348.

Franks, K.M., Stevens, C.F., and Sejnowski, T.J. (2003). Independent sources of quantal variability at single glutamatergic synapses. J Neurosci 23, 3186-3195.

Fukata, Y., Dimitrov, A., Boncompain, G., Vielemeyer, O., Perez, F., and Fukata, M. (2013). Local palmitoylation cycles define activity-regulated postsynaptic subdomains. The Journal of cell biology 202, 145-161.

Giannone, G., Hosy, E., Levet, F., Constals, A., Schulze, K., Sobolevsky, A.I., Rosconi, M.P., Gouaux, E., Tampe, R., Choquet, D., and Cognet, L. (2010). Dynamic superresolution imaging of endogenous proteins on living cells at ultra-high density. Biophysical journal 99, 1303-1310.

Giannone, G., Mondin, M., Grillo-Bosch, D., Tessier, B., Saint-Michel, E., Czondor, K., Sainlos, M., Choquet, D., and Thoumine, O. (2013). Neurexin-1beta binding to neuroligin-1 triggers the preferential recruitment of PSD-95 versus gephyrin through tyrosine phosphorylation of neuroligin-1. Cell reports 3, 1996-2007.

Goda, Y., and Stevens, C.F. (1994). Two components of transmitter release at a central synapse. Proceedings of the National Academy of Sciences of the United States of America 91, 12942-12946.

Graf, E.R., Zhang, X., Jin, S.X., Linhoff, M.W., and Craig, A.M. (2004). Neurexins induce differentiation of GABA and glutamate postsynaptic specializations via neuroligins. Cell 119, 1013-1026.

Hafner, A.S., Penn, A.C., Grillo-Bosch, D., Retailleau, N., Poujol, C., Philippat, A., Coussen, F., Sainlos, M., Opazo, P., and Choquet, D. (2015). Lengthening of the Stargazin Cytoplasmic Tail Increases Synaptic Transmission by Promoting Interaction to Deeper Domains of PSD-95. Neuron 86, 475-489.

Heine, M., Groc, L., Frischknecht, R., Beique, J.C., Lounis, B., Rumbaugh, G., Huganir, R.L., Cognet, L., and Choquet, D. (2008). Surface mobility of postsynaptic AMPARs tunes synaptic transmission. Science 320, 201-205.
Hosy, E., Butler, C., and Sibarita, J.B. (2014). Organization and dynamics of AMPA receptors inside synapses-nano-organization of AMPA receptors and main synaptic scaffolding proteins revealed by super-resolution imaging. Current opinion in chemical biology 20, 120-126.
Irie, M., Hata, Y., Takeuchi, M., Ichtchenko, K., Toyoda, A., Hirao, K., Takai, Y., Rosahl, T.W., and Sudhof, T.C. (1997). Binding of neuroligins to PSD-95. Science 277, 1511-1515.
Jonas, P., Major, G., and Sakmann, B. (1993). Quantal components of unitary EPSCs at the mossy fibre synapse on CA3 pyramidal cells of rat hippocampus. The Journal of physiology 472, 615-663.
Kinney, J.P., Spacek, J., Bartol, T.M., Bajaj, C.L., Harris, K.M., and Sejnowski, T.J. (2013). Extracellular sheets and tunnels modulate glutamate diffusion in hippocampal neuropil. J Comp Neurol 521, 448-464.
Ko, J., Zhang, C., Arac, D., Boucard, A.A., Brunger, A.T., and Sudhof, T.C. (2009). Neuroligin-1 performs neurexin-dependent and neurexin-independent functions in synapse validation. The EMBO journal 28, 3244-3255.
Levet, F., Hosy, E., Kechkar, A., Butler, C., Beghin, A., Choquet, D., and Sibarita, J.B. (2015). SR-Tesseler: a method to segment and quantify localization-based super-resolution microscopy data. Nature methods 12, 1065-1071.
Levinson, J.N., Chery, N., Huang, K., Wong, T.P., Gerrow, K., Kang, R., Prange, O., Wang, Y.T., and El-Husseini, A. (2005). Neuroligins mediate excitatory and inhibitory synapse formation: involvement of PSD-95 and neurexin-1beta in neuroligin-induced synaptic specificity. The Journal of biological chemistry 280, 17312-17319.
Lisman, J.E., Raghavachari, S., and Tsien, R.W. (2007). The sequence of events that underlie quantal transmission at central glutamatergic synapses. Nature reviews 8, 597-609.
Liu, G., Choi, S., and Tsien, R.W. (1999). Variability of neurotransmitter concentration and nonsaturation of postsynaptic AMPA receptors at synapses in hippocampal cultures and slices. Neuron 22, 395-409.
MacGillavry, H.D., Song, Y., Raghavachari, S., and Blanpied, T.A. (2013). Nanoscale scaffolding domains within the postsynaptic density concentrate synaptic AMPA receptors. Neuron 78, 615-622.
Manders, E., Verbeek, FJ. and Aten JA. (1993). Measurement of co-localization of objects in dual-colour confocal images. J Microscopy 169, 375-382.
Masugi-Tokita, M., Tarusawa, E., Watanabe, M., Molnar, E., Fujimoto, K., and Shigemoto, R. (2007). Number and density of AMPA receptors in individual synapses in the rat cerebellum as revealed by SDS-digested freeze-fracture replica labeling. J Neurosci 27, 2135-2144.
Missler, M., Zhang, W., Rohlmann, A., Kattenstroth, G., Hammer, R.E., Gottmann, K., and Sudhof, T.C. (2003). Alpha-neurexins couple Ca2+ channels to synaptic vesicle exocytosis. Nature 423, 939-948.
Mondin, M., Labrousse, V., Hosy, E., Heine, M., Tessier, B., Levet, F., Poujol, C., Blanchet, C., Choquet, D., and Thoumine, O. (2011). Neurexin-neuroligin adhesions capture surface-diffusing AMPA receptors through PSD-95 scaffolds. J Neurosci 31, 13500-13515.
Nair, D., Hosy, E., Petersen, J.D., Constals, A., Giannone, G., Choquet, D., and Sibarita, J.B. (2013). Super-resolution imaging reveals that AMPA receptors inside synapses are dynamically organized in nanodomains regulated by PSD95. J Neurosci 33, 13204-13224.
Nam, C.I., and Chen, L. (2005). Postsynaptic assembly induced by neurexin-neuroligin interaction and neurotransmitter. Proceedings of the National Academy of Sciences of the United States of America 102, 6137-6142.

Raghavachari, S., and Lisman, J.E. (2004). Properties of quantal transmission at CA1 synapses. Journal of neurophysiology 92, 2456-2467.
Ribrault, C., Reingruber, J., Petkovic, M., Galli, T., Ziv, N.E., Holcman, D., and Triller, A. (2011). Syntaxin1A lateral diffusion reveals transient and local SNARE interactions. J Neurosci 31, 17590-17602.
Sainlos, M., Tigaret, C., Poujol, C., Olivier, N.B., Bard, L., Breillat, C., Thiolon, K., Choquet, D., and Imperiali, B. (2011). Biomimetic divalent ligands for the acute disruption of synaptic AMPAR stabilization. Nature chemical biology 7, 81-91.
Sara, Y., Biederer, T., Atasoy, D., Chubykin, A., Mozhayeva, M.G., Sudhof, T.C., and Kavalali, E.T. (2005). Selective capability of SynCAM and neuroligin for functional synapse assembly. J Neurosci 25, 260-270.
Savtchenko, L.P., Sylantyev, S., and Rusakov, D.A. (2013). Central synapses release a resource-efficient amount of glutamate. Nature neuroscience 16, 10-12.
Scheiffele, P., Fan, J., Choih, J., Fetter, R., and Serafini, T. (2000). Neuroligin expressed in nonneuronal cells triggers presynaptic development in contacting axons. Cell 101, 657-669.
Schneider, R., Hosy, E., Kohl, J., Klueva, J., Choquet, D., Thomas, U., Voigt, A., and Heine, M. (2015). Mobility of calcium channels in the presynaptic membrane. Neuron 86, 672-679.
Shipman, S.L., Schnell, E., Hirai, T., Chen, B.S., Roche, K.W., and Nicoll, R.A. (2011). Functional dependence of neuroligin on a new non-PDZ intracellular domain. Nature neuroscience 14, 718-726.
Sudhof, T.C. (2008). Neuroligins and neurexins link synaptic function to cognitive disease. Nature 455, 903-911.
Tang, A.H., Chen, H., Li, T.P., Metzbower, S.R., MacGillavry, H.D., and Blanpied, T.A. (2016). A trans-synaptic nanocolumn aligns neurotransmitter release to receptors. Nature 536, 210-214.
Tarusawa, E., Matsui, K., Budisantoso, T., Molnar, E., Watanabe, M., Matsui, M., Fukazawa, Y., and Shigemoto, R. (2009). Input-specific intrasynaptic arrangements of ionotropic glutamate receptors and their impact on postsynaptic responses. J Neurosci 29, 12896-12908.
Tomita, S., Shenoy, A., Fukata, Y., Nicoll, R.A., and Bredt, D.S. (2007). Stargazin interacts functionally with the AMPA receptor glutamate-binding module. Neuropharmacology 52, 87-91.

Figures legends

Figure 1. Expression of WT neuroligin but not NLG1-ΔCter affects AMPAR synaptic nano-organization. A. Example of neurons transfected either with GFP, NLG1 + GFP or NLG1-ΔCter + GFP (from the left to the right), and two examples of AMPAR organization visualized with d-STORM technique. Intensity is color coded, scale go from 1 (purple) to 100 (white) detection per pixel. Average of spine density **(B)**, AMPAR nanodomain density **(C)**, nanodomains intensity expressed as number of receptors per nanodomain **(D)** and nanodomain length **(E)**, on neuron expressing GFP, GFP + NLG1 and NLG1-ΔCter + GFP (n=10; 9; 12 cells respectively; and between 200 to 500 individual domains).

Figure 2. Delta C neuroligin does not co-localize with AMPAR nanoclusters. (A) Example of dual-color d-STORM super-resolution image of GluA2 containing AMPAR labelled with Alexa 532 nm and HA-tagged NLG1 labelled with Alexa 647 nm. **(B)** Examples of GluA2 and NLG1 (left) or GluA2 and NLG1-ΔCter (right) co-labeling of two synapses. Dark spots on the overlay image represent co-localizing pixels; NLG1 (in green) strongly co-localizes with AMPAR nanodomains (in purple). NLG1-ΔCter (in green) does not co-localize with AMPAR nanodomains (in purple). **C, D and E** presents the quantification of this co-localization. **(C)** The size distribution of NLG1 (green), NLG1-ΔCter (red) and GluA2 (black) super-resolved objects. The expression of NLG1-ΔCter does not affect the size of neuroligin 1 and GluA2 nanodomain objects. **(D)** Cumulative distribution of the measured (red) and randomized (dark) bivariate nearest neighbor distance between large object of GluA2 and NLG1-ΔCter. Green line represents the nearest neighbor distance between large object of GluA2 and neuroligin 1, demonstrating clustering as compared to random distribution. Insert represents a zoom on the 250 nm, approximate size of a PSD; NLG1-ΔCter and GluA2 nanodomain distance overlaps with the random distribution distance. **(E)** Manders' coefficients calculated between GluA2 nanodomains and NLG1-ΔCter (red) and between GluA2 nanodomains and NLG1 (green). More than 60% of AMPAR nanodomains are not co-localized with NLG1-ΔCter (n= 18 and 12 NLG1 and NLG1-ΔCter cells respectively, corresponding to 516 and 312 independent pairs of co-localization).

Figure 3. Delta C neuroligin expression decorrelates pre-synaptic RIM from AMPAR nanoclusters. (A) Example of dual-color d-STORM super-resolution image of GluA2 containing AMPAR labelled with Alexa 532 nm and RIM labelled with Alexa 647 nm. Right panels, examples of GluA2 and RIM co-labeling when post-synaptic neurons are transfected

with GFP, NLG1 or NLG1-ΔCter respectively (from the left to the right). **B** and **C** presents the quantification of this co-localization. **(B)** Cumulative distribution of the bivariate nearest neighbor distance between GluA2 and RIM clusters when post-synaptic neuron expressed GFP (dark), NLG1 (green) or NLG1-ΔCter (red). These data demonstrate a loss of the pre-post synaptic alignment when NLG1-ΔCter is expressed. **(C)** Manders' coefficients calculated between GluA2 nanodomains and RIM clusters in function of the neuroligin wt or truncated form expression. NLG1-ΔCter expression significantly alters the co-localization (n= 9; 9 and 8 Control, NLG1-ΔCter and NLG1 cells respectively, corresponding to 354; 573 and 562 independent pairs of co-localization).

Figure 4. NLG1-ΔCter expression strongly impaired synaptic transmission efficacy. (A) Example of mEPSC traces recorded in cultured neurons expressing either GFP, GFP + NLG1-ΔCter or GFP + NLG1. **(B)** Cumulative distribution and **(C)** average of the mEPSC amplitude recorded on neurons expressing GFP (dark), GFP + NLG1-ΔCter (red) or GFP + NLG1 (green) (n=14; 14 and 13 respectively). mEPSCs amplitude is decreased by 25 % in neurons expressing NLG1-ΔCter. **(D)** Scheme of the patch clamp protocol used to record asynchronous EPSC on organotypic hippocampus slices. Two neighboring neurons are simultaneously patched, one transfected and one non transfected, Schaffer collateral connecting both neuron are then stimulated. **(E and F)** Representative traces of asynchronous EPSCs recorded in the presence of strontium, of either a control and a NLG1-ΔCter expressing neuron **(E)** or a control and a NLG1 **(F).** To avoid multi synaptic responses, 50 ms following the stimulation are excluded from the analysis. **(G)** Cumulative distribution of aEPSCs amplitude recorded from control (dark),or neurons expressing GFP + NLG1-ΔCter (red) or GFP + NLG1 (green) (n=8 and 6 paired of cells, respectively). Average of aEPSCs amplitude, with connection between the transfected cell and their respective neighboring non transfected control, when either GFP + NLG1 **(H)** or GFP + NLG1-ΔCter **(I)** are expressed. NLG1-ΔCter expression decreased by 25 % the average aEPSCs amplitude.

Figure 5. Acute disruption of PSD95-NLG interaction impaired both pre-post alignment and synaptic transmission. (A) Example of dual-color d-STORM image of GluA2 containing AMPAR labelled with Alexa 532 nm and RIM labelled with Alexa 647 nm. Right panels, examples of GluA2 and RIM co-labeling without ligand or after 1 days treatment with Nlg biomimetic ligand or non-sense ligand (from the left to the right). **(B) and (C)** presents the quantification of this co-localization. **(B)** Cumulative distribution of the bivariate nearest

neighbor distance between GluA2 and RIM clusters without ligand (dark), with NLG ligand NLG1 (green) or non-sense ligand (blue). These data demonstrate a loss of the pre-post synaptic alignment in the presence of NLG ligand. **(C)** Manders' coefficients calculated between GluA2 nanodomains and RIM clusters in function of ligand treatment (n= 4; 5 and 4 Control, NLG ligand and non-sense ligand respectively, corresponding to 451; 1311 and 640 independent pairs of co-localization). **(D)** Example of mEPSC traces recorded in cultured neurons without ligand, with NLG ligand or with non-sense ligand. **(E) and (F)** average of the mEPSC amplitude and amplitude recorded when neurons in culture are incubated without ligand (dark) or with either NLG ligand (red) or with non-sense ligand (blue) (n=9; 15 and 13 respectively). mEPSCs amplitude is decreased by 30 % in neurons incubated with NLG ligand.

Figure 6. Simulation of AMPAR activation. (A) View of dendritic spine with synaptic contact area (red patch) containing 25 AMPARs anchored in nanocluster (blue particles) and 70 freely diffusible AMPAR (red particles). The simulated glutamate release locations are shown by white dots spaced 50 nm apart. **(B)** Kinetic scheme for activation of AMPAR by glutamate (Jonas et al. 1993). Kinetic rate constants values (after fitting as described in Methods): k1 = 9.18 $\mu M^{-1}s^{-1}$; k1r = 4260 s^{-1}; k2 = 56.8 $\mu M^{-1}s^{-1}$; k2r = 3260 s^{-1}; alpha = 2650 s^{-1}; beta = 200 s^{-1}; alpha1 = 2890 s^{-1}; beta1 = 20 s^{-1}; alpha2 = 120 s^{-1}; beta2 = 0.727 s^{-1}; alpha3 = 200 s^{-1}; beta3 = 4 s^{-1}; alpha4 = 16.8 s^{-1}; beta4 = 190.4 s^{-1}; k3 = 1.27 $\mu M^{-1}s^{-1}$; k3r = 45.7 s^{-1}; AMPAR diffusion constant = 0.1 $\mu m^2 s^{-1}$; and glutamate diffusion constant = 100 $\mu m^2 s^{-1}$. **(C)** Time course of simulated AMPAR activation resulting from release of 1500, 3000, and 4500 glutamate molecules at each release location are shown. Each time course is the average of 100 simulations. **(D)** Normalized peak number of open AMPARs activated by release of 1500, 2000, 3000, and 4500 glutamate molecules at each release location is shown. Dashed line at 90 nm indicates data displayed in E. **(E)** Percent decrease in peak number of open AMPAR as a function of number of glutamate molecules released, at 90 nm release distance. Dashed lines indicate that when ~2000 glutamate molecules are released the peak number of open AMPARs will be decreased by 25% at a release distance of 90 nm.

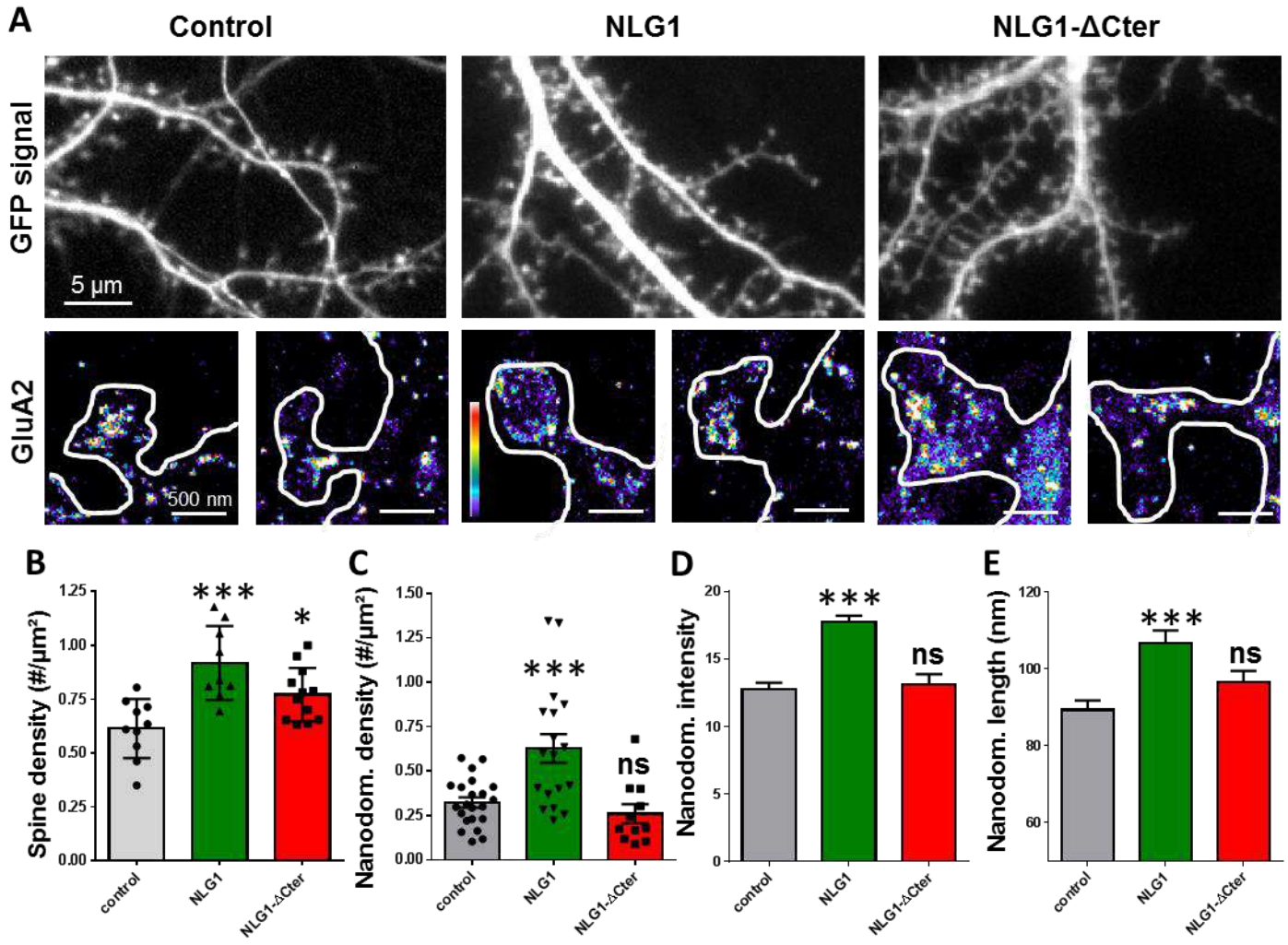
A
Control
NLG1
NLG1-ΔCter
GFP signal
5 µm
GluA2
500 nm
B
Spine density (#/µm²)
C
Nanodom. density (#/µm²)
D
Nanodom. intensity
E
Nanodom. length (nm)
control
NLG1
NLG1-ΔCter
***
*
ns

Figure 1

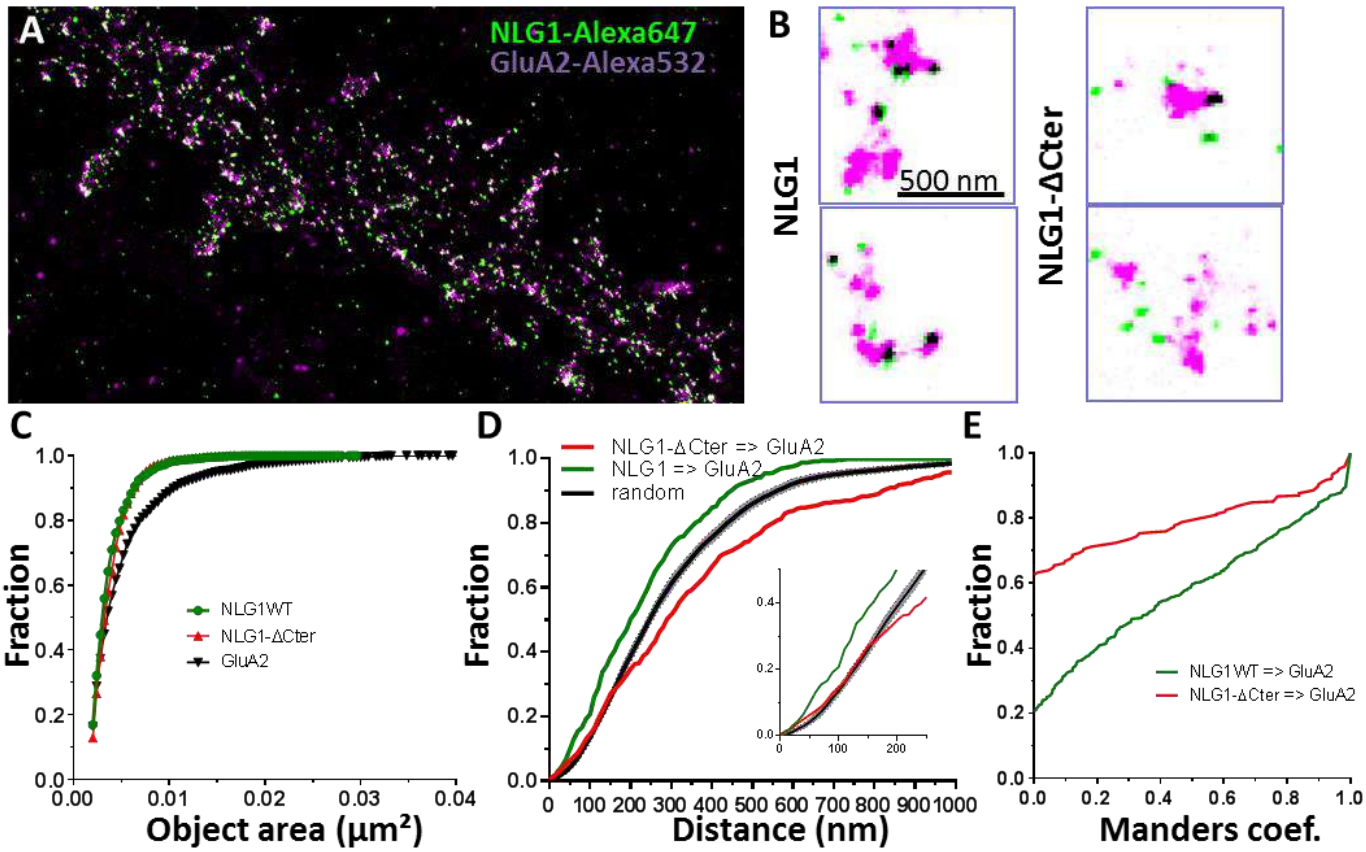
A
NLG1-Alexa647
GluA2-Alexa532
B
NLG1
NLG1-ΔCter
500 nm
C
Fraction
Object area (µm²)
NLG1WT
NLG1-ΔCter
GluA2
D
Fraction
Distance (nm)
NLG1-ΔCter => GluA2
NLG1 => GluA2
random
E
Fraction
Manders coef.
NLG1WT => GluA2
NLG1-ΔCter => GluA2

Figure 2

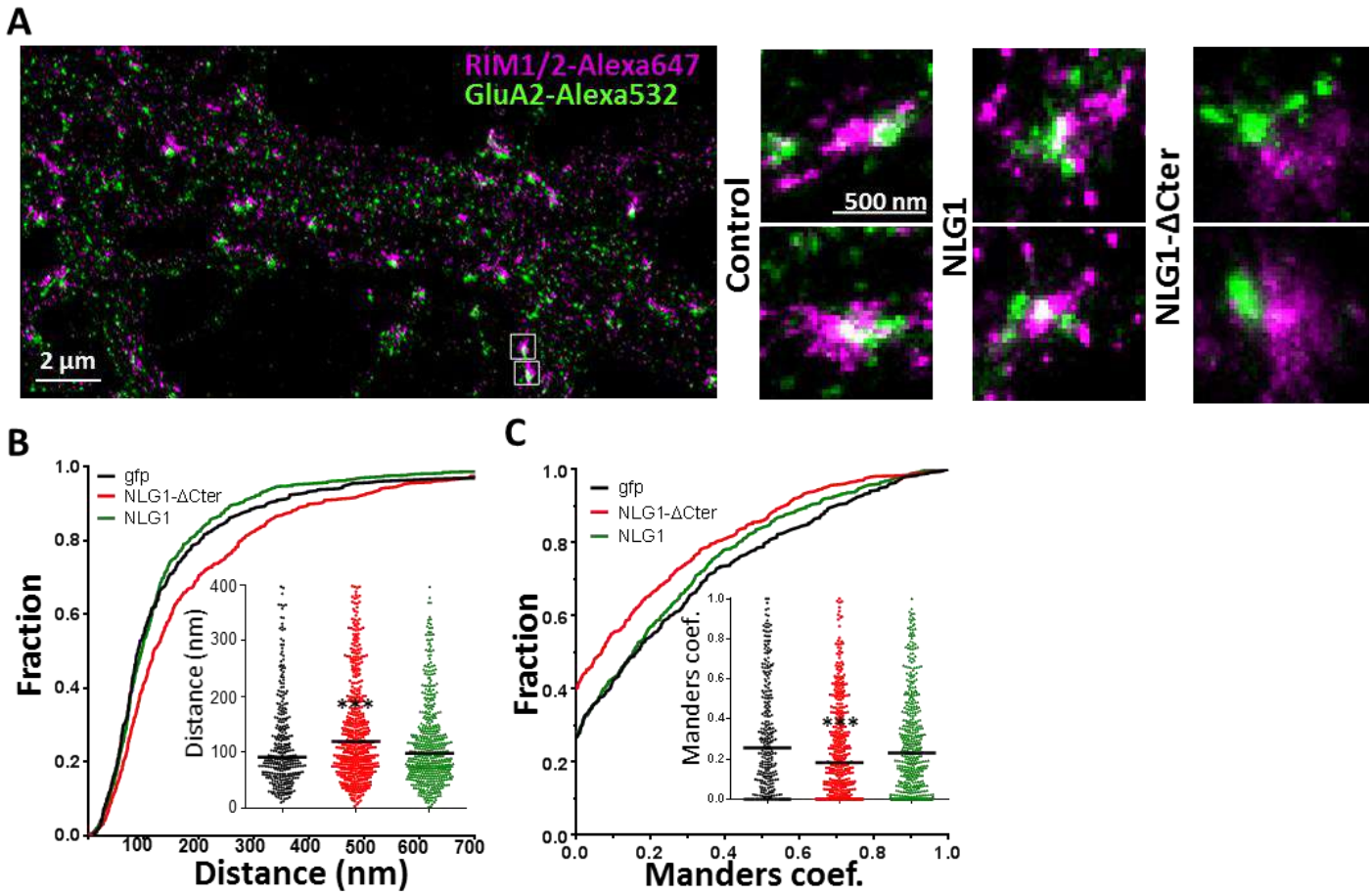
A
RIM1/2-Alexa647
GluA2-Alexa532
2 µm
Control
500 nm
NLG1
NLG1-ΔCter
B
gfp
NLG1-ΔCter
NLG1
Fraction
Distance (nm)
***
C
gfp
NLG1-ΔCter
NLG1
Fraction
Manders coef.
***

Figure 3

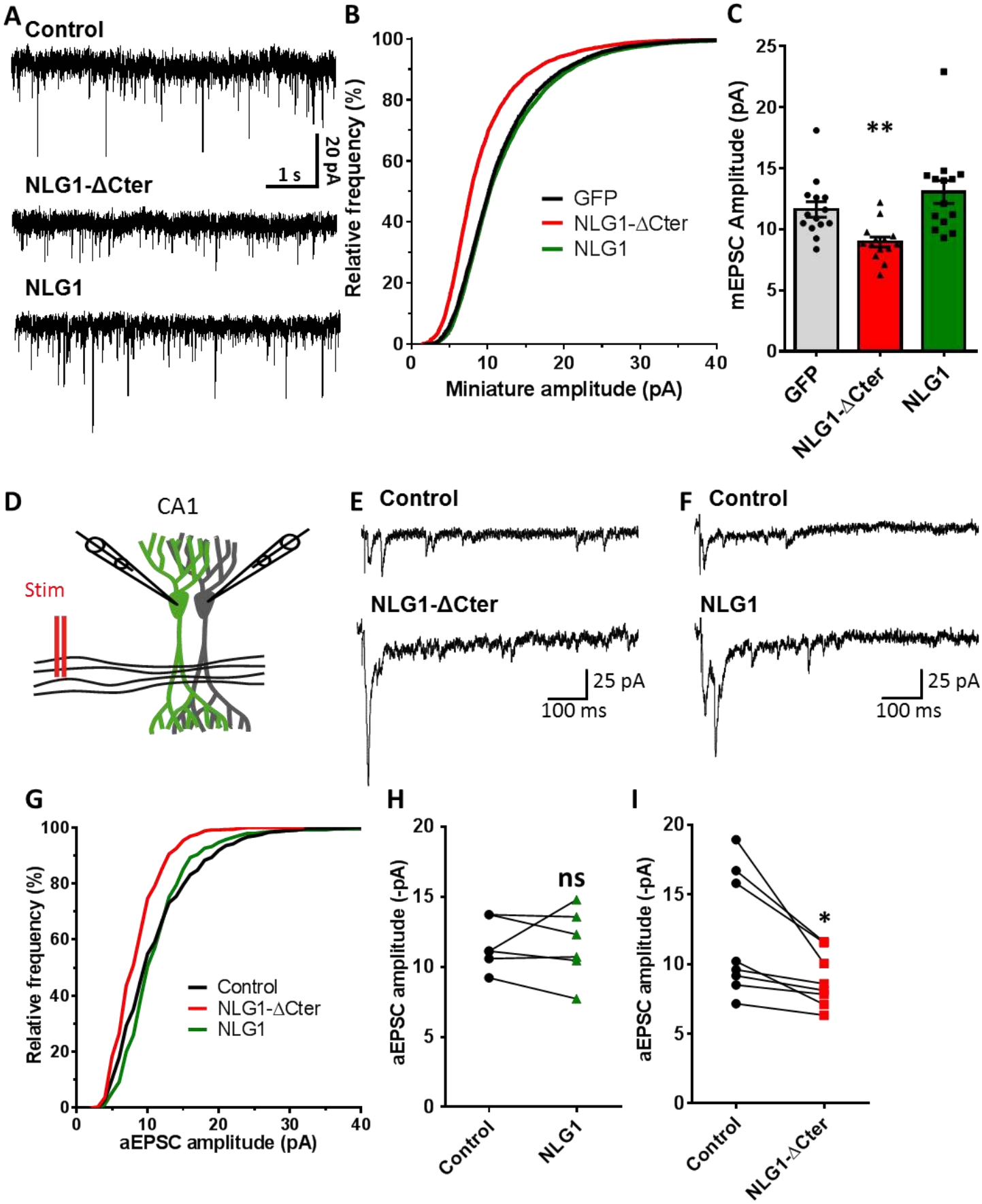
A
Control
1 s
20 pA
NLG1-ΔCter
NLG1
B
Relative frequency (%)
Miniature amplitude (pA)
GFP
NLG1-ΔCter
NLG1
C
mEPSC Amplitude (pA)
**
GFP
NLG1-ΔCter
NLG1
D
CA1
Stim
E
Control
NLG1-ΔCter
25 pA
100 ms
F
Control
NLG1
25 pA
100 ms
G
Relative frequency (%)
aEPSC amplitude (pA)
Control
NLG1-ΔCter
NLG1
H
aEPSC amplitude (-pA)
ns
Control
NLG1
I
aEPSC amplitude (-pA)
*
Control
NLG1-ΔCter

Figure 4

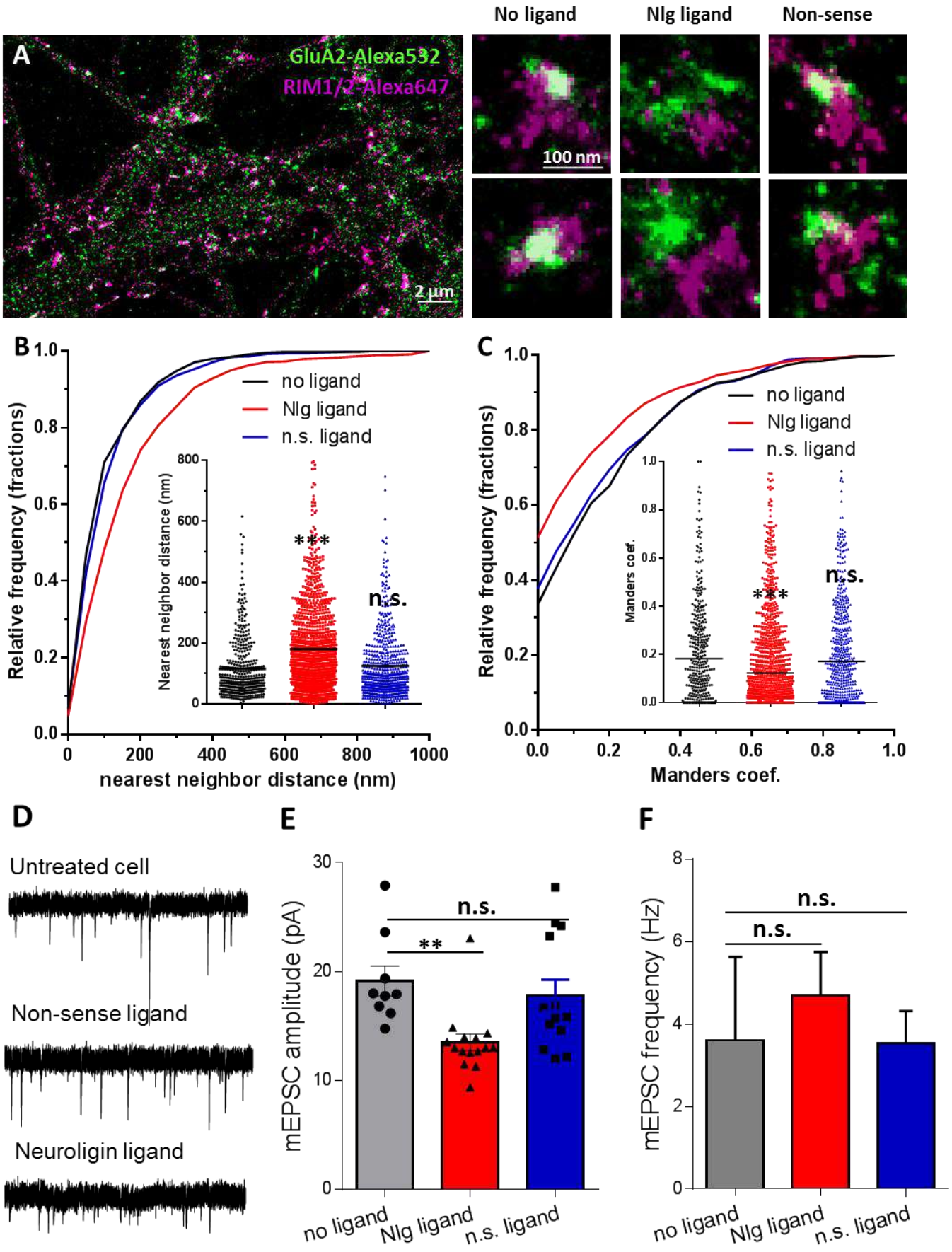
No ligand
Nlg ligand
Non-sense
A
GluA2-Alexa532
RIM1/2-Alexa647
2 µm
100 nm
B
Relative frequency (fractions)
nearest neighbor distance (nm)
no ligand
Nlg ligand
n.s. ligand
Nearest neighbor distance (nm)
***
n.s.
C
Relative frequency (fractions)
Manders coef.
Manders coef.
***
n.s.
D
Untreated cell
Non-sense ligand
Neuroligin ligand
E
mEPSC amplitude (pA)
n.s.
**
no ligand
Nlg ligand
n.s. ligand
F
mEPSC frequency (Hz)
n.s.
n.s.
no ligand
Nlg ligand
n.s. ligand

Figure 5

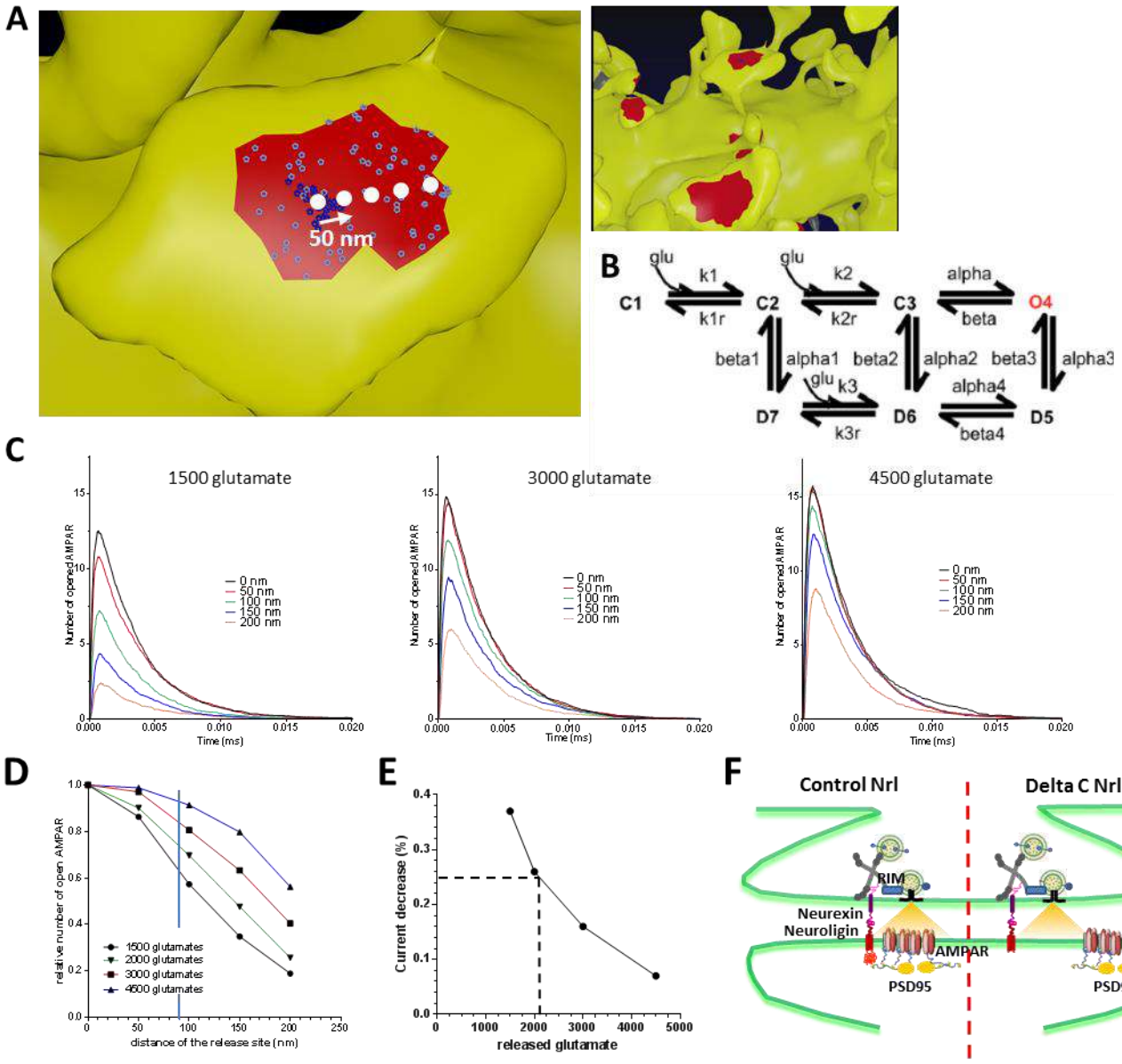
A
50 nm
B
glu
k1
k1r
C1
C2
k2
k2r
C3
alpha
beta
O4
beta1
alpha1
beta2
alpha2
beta3
alpha3
glu
k3
k3r
D7
D6
alpha4
beta4
D5
C
1500 glutamate
3000 glutamate
4500 glutamate
Number of opened AMPAR
Time (ms)
0 nm
50 nm
100 nm
150 nm
200 nm
D
relative number of open AMPAR
distance of the release site (nm)
1500 glutamates
2000 glutamates
3000 glutamates
4500 glutamates
E
Current decrease (%)
released glutamate
F
Control Nrl
Delta C Nrl
RIM
Neurexin
Neuroligin
AMPAR
PSD95
PSD95

Figure 6

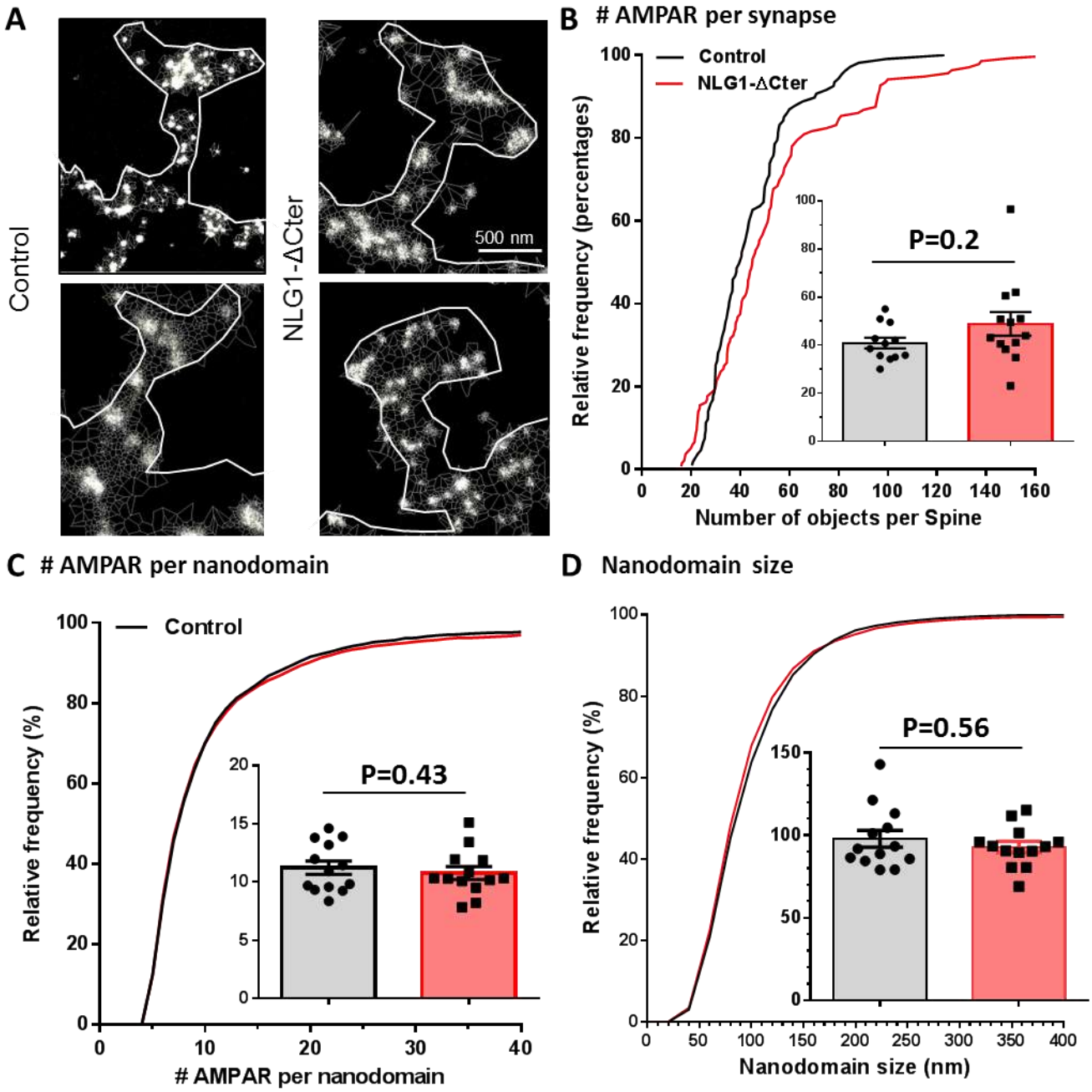

Suppl Figure 1

Tessellation based analysis reveals that synaptic AMPA receptor nanoscale organization is not affected by the expression of NLG1-ΔCter. (A) Example of endogenous GluA2 organization inside synapse obtained with d-STORM technique on GFP (left panels) and GFP + NLG1-ΔCter (right panels) expressing cells. (B) Cumulative distribution of the estimated number of endogenous AMPAR per synapse. The insert represents the cell to cell variability of the synaptic AMPAR content. (C) Cumulative distribution and cell to cell variability (insert) of the number of endogenous AMPAR per nanodomain. (D) Cumulative distribution and cell to cell variability of the nanodomain diameter. (B-D) reveals no changes in synaptic AMPAR organization when NLG1-ΔCter is expressed (n= 12 and 13 cells, corresponding to 107 and 136 individual domains for control and NLG1-ΔCter respectively).

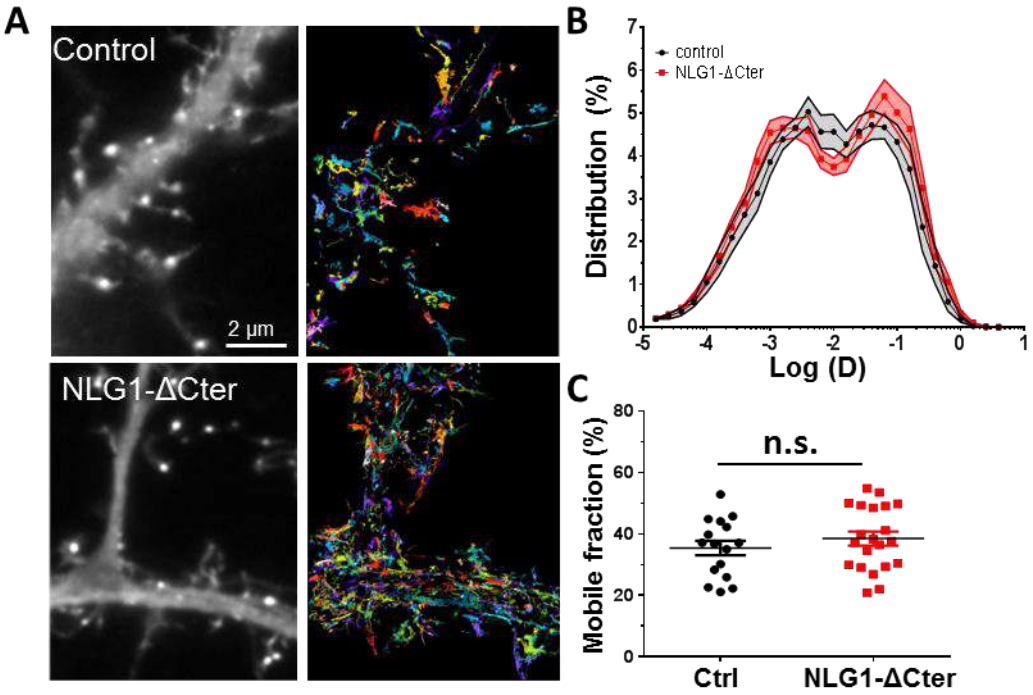

Suppl. Figure 2

NLG1-ΔCter expression does not affect AMPAR lateral mobility. (A) Example of endogenous GluA2 containing AMPAR mobility recorded with uPAINT technique on GFP (upper panel) and GFP + NLG1-ΔCter expressing cells. Each individual trajectory is color coded. (B) Average distribution of the logarithm of the diffusion coefficient and (C) mobile fraction reveal no modification of AMPAR mobility induced by the NLG1-ΔCter expression (n=16 and 21 cells for control and NLG1-ΔCter respectively).

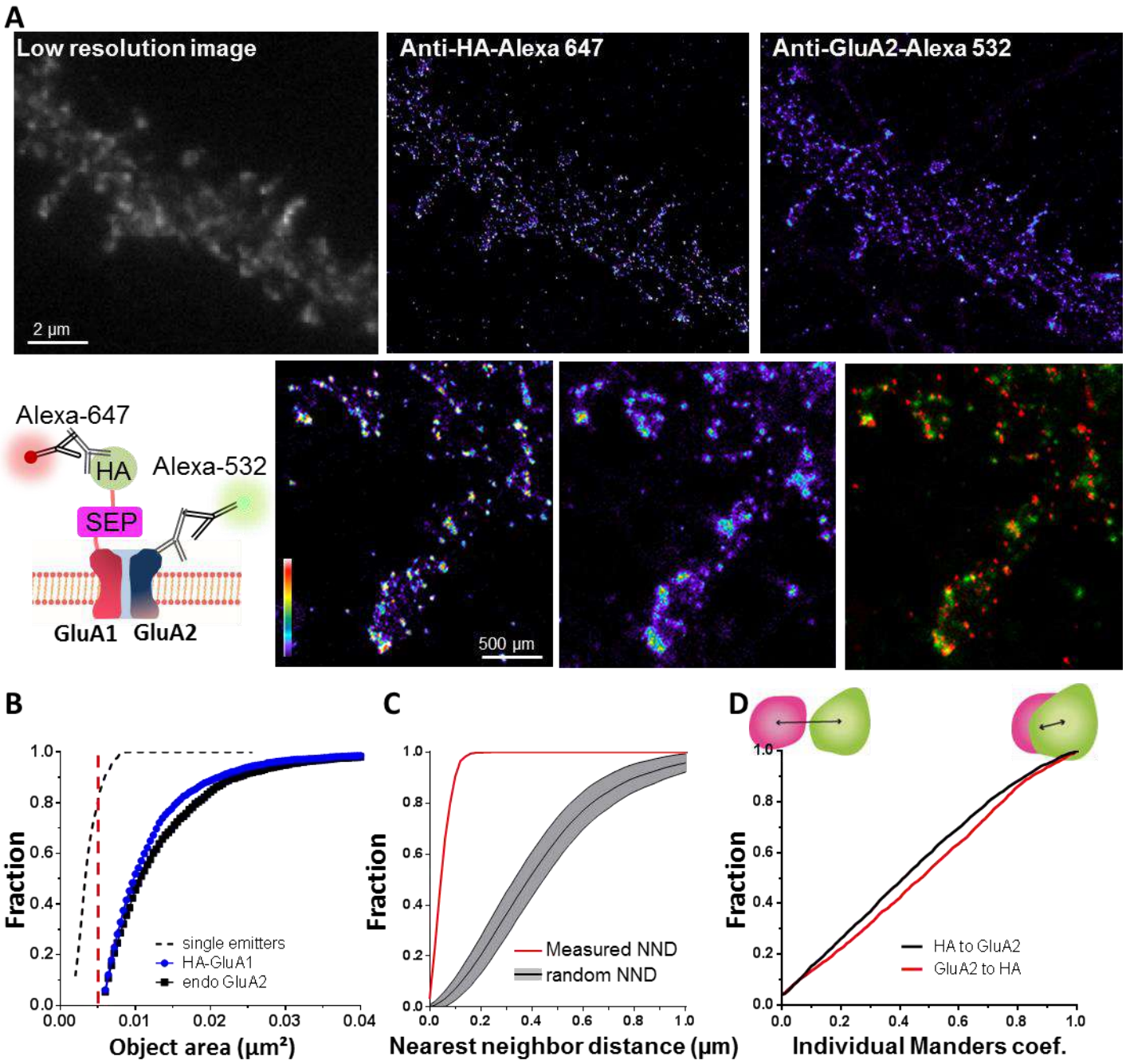

Suppl. Figure 3

Validation of the method to analyze super-resolved object co-localization with a dual labeling of AMPAR. (A) Example of dual color image obtained by a GluA1 and GluA2 dual labeling (epifluorescence image on the left) and the super-resolved image acquired with d-STORM technique, both at 647 and 532 (middle and right image). GluA1 presents a HA tag, as shown on the scheme, HA tag is labelled with Alexa 647 and endogenous GluA2 with Alexa 532. An example of colocalizationof two super-resolved clusters is reported down to the right. (B), (C) and (D) represent the three steps necessary to determine super-resolved object co-localization (n=6 cells, and 151 individual clusters). In (B), the size of an object is determined to discriminate potential clusters from the single particle, both having a different physiological meaning. In (C), the bivariate nearest neighbor distance is calculated to determine the average distance between two objects. Control distributions are obtained with the calculation of the distance when the same number of objects is randomly redistributed within the cell border. Finally, (D) is the distribution of Manders' coefficients. No co-localization gives a null value, 100% co-localization a value of one. The dual labeling of GluA1/A2 reports the presence of small and large objects (B), distance between cluster of GluA1 labelled with anti-HA is closer to GluA2 cluster than randomly distributed (C) 95% of clusters co-localized at least partly (D).

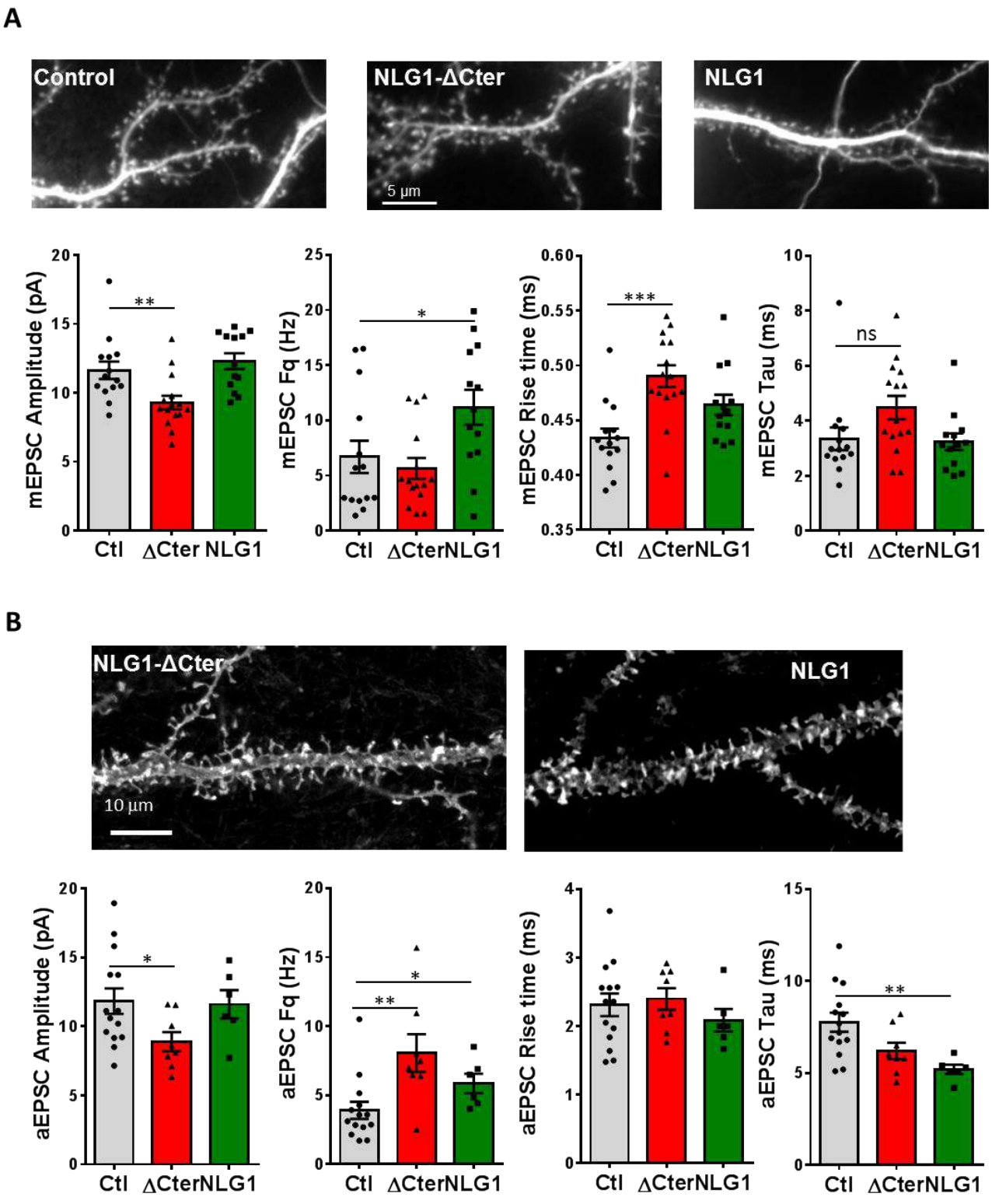

Suppl. Figure 4

Neuroligin 1 and NLG1-ΔCter expression have various effect on synaptic transmission properties both on neuronal cell culture and organotypic slices. (A) Representative images from control and NLG1 and NLG1-ΔCter expressing neurons in culture. (B) Analysis of miniature EPSC, from left to right are represented the amplitude, the frequency, the rise time and the decay time. (C) Representative images from NLG1 and NLG1-ΔCter expressing neurons in organotypic hippocampal culture. (D) Analysis of asynchronous EPSC, from left to right are represented the amplitude, the frequency, the rise time and the decay time. For all figures, the control is represented in dark, the NLG1-ΔCter in red and the NLG1 in green. Each dot represent the mean value for an individual cell.

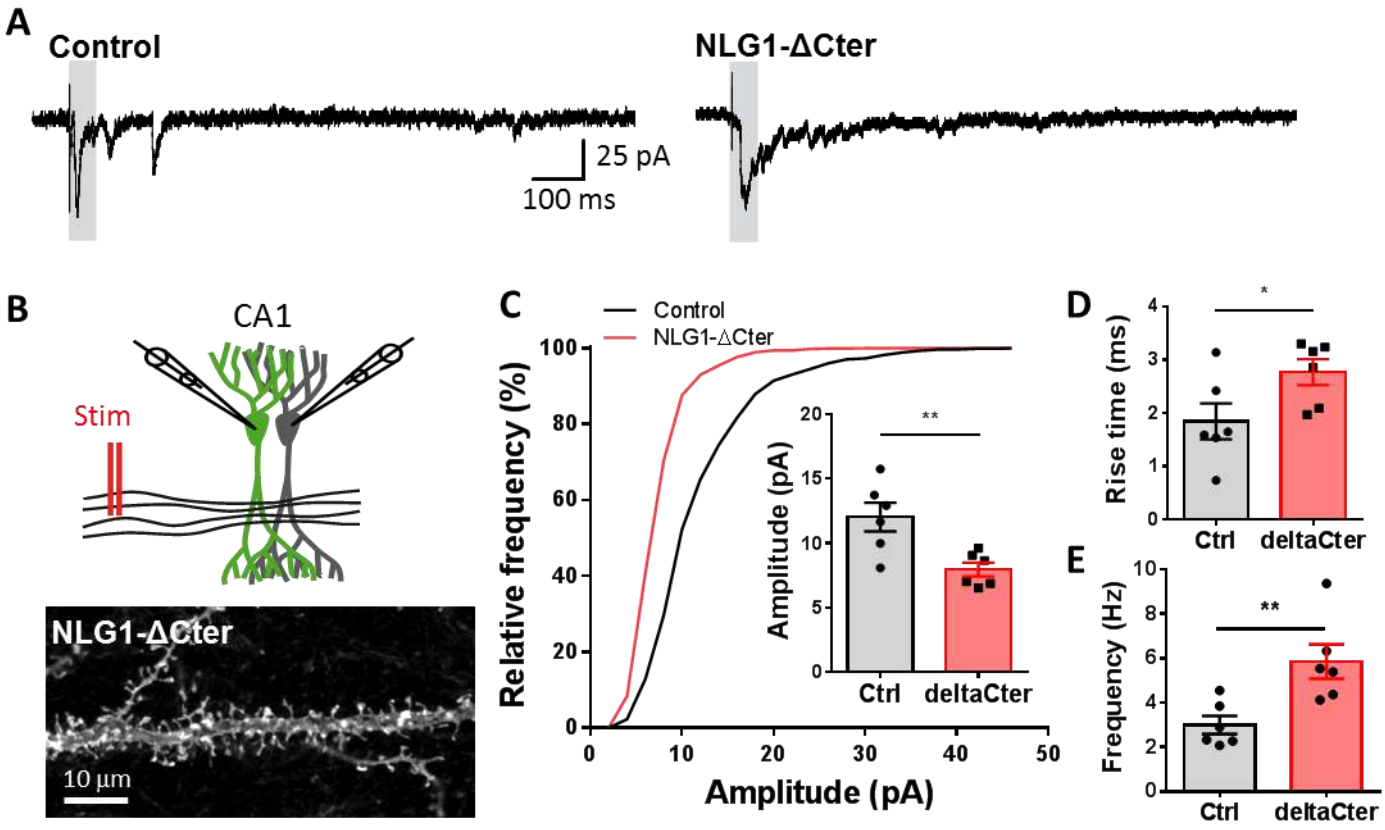

Suppl. Figure 5

aEPSCs are decreased when NLG1-ΔCter is expressed in NLG1 KO background. (A) Representative traces of asynchronous EPSCs recorded in the presence of strontium, of either a control or a NLG1-ΔCter expressing neuron in a Nlg1 KO background. (B) Scheme of the patch clamp protocol used to record asynchronous EPSC on organotypic hippocampus slices. Two neighboring neurons are simultaneously patched, one transfected and one non transfected, Schaffer collateral connecting both neuron are then stimulated. To avoid multisynaptic responses, 50 ms following the stimulation are excluded from the analysis. Bottom, example of a transfected cell. (C) Cumulative distribution of aEPSCs amplitude recorded from control (dark),or neurons expressing GFP + NLG1-ΔCter (red). Average of aEPSCs amplitude, with connection between the transfected cell and their respective neighboring non transfected control. (D and E) Rise time and frequency of aEPSC of non-transfected cell and when NLG1-ΔCter is expressed (n=6 pairs of neurons, 20 sweeps per cell).

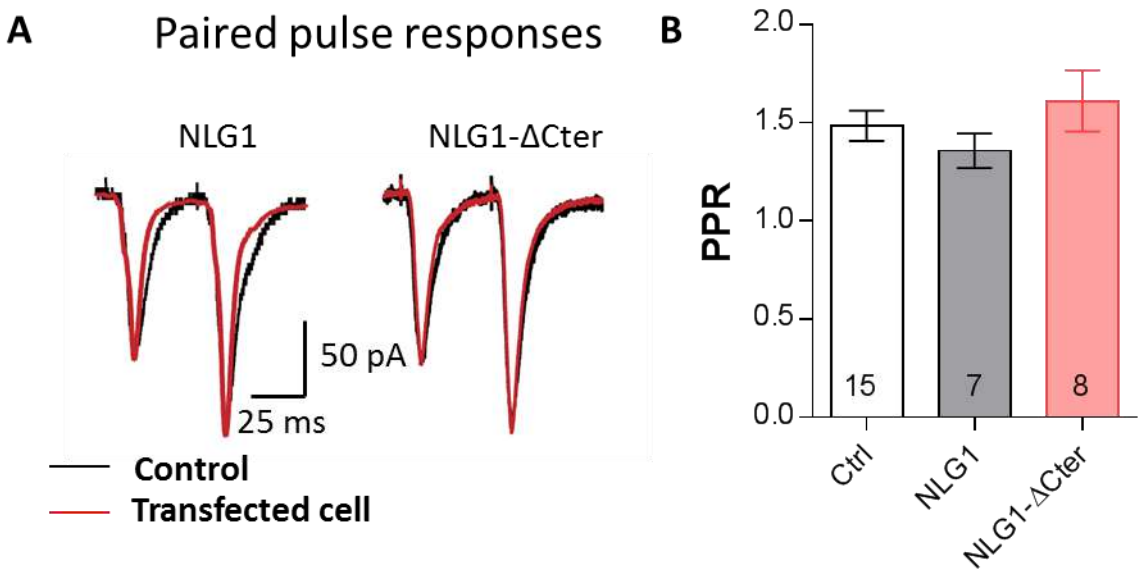

Suppl. Figure 6

Expression of NLG1-ΔCter does not affect paired-pulse ratio. (A) Example of paired-pulse currents recorded from CA1 neurons in organotypic hippocampal slices, expressing either NLG1 or NLG1-ΔCter (in red) and from their respective untransfected neighbors (in black). (B) Average paired pulse ratio for the same conditions as in (A) (n= 7 and 8 pairs of cells for NLG1 and NLG1-ΔCter respectively).

Chapter 2

Glutamate-induced AMPAR desensitization increases their mobility and modulates short-term plasticity through unbinding from stargazin

The characterization of synapse molecular organization at the nanoscale change our vision of how synaptic inputs are generated. The release of glutamate on a restricted area of the synapse, where AMPAR are packed in nanodomains, tunes the efficiency of information transfer. However, it is well defined that information coding occurs on a spatial and temporal manner. Indeed, a single synapse can be proned to release glutamate at high frequency. The limitation in this case is linked to the biophysical properties of AMPAR to get desensitized after activation for tens to hundreds of milliseconds. Thus the synapse has to provide a way to, in one hand maintain a stable number of AMPARs to answer efficiently to glutamate release, and in the other hand to compensate the desensitization of those receptors after the first glutamate release to insure the fidelity of high frequency inputs.

In 2008, Martin Heine shown using paired-pulse stimulations and AMPAR cross-linking approach that lateral diffusion was responsible for a fast exchange of synaptic AMPARs at the milliseconds scale. This mechanism allows synapses to maintain a stable pool of naïve receptors at synapse and thus to maintain the fidelity of high frequency synaptic transmission (Heine et al., 2008). Several evidences support the idea that AMPAR diffusion allows synapses to sustain higher frequencies than the rate of AMPAR recovery from desensitization would normally allow. However, the precise molecular mechanism describing how synapses can deal between the necessity to maintain a pool of immobilized receptors under release site and the observation that AMPAR receptor mobility has a role in synaptic transmission, has not been solved. The understanding of this mechanism was the aim of Audrey Constals' PhD project under the supervision of Eric Hosy. I began my PhD during the paper revision process and I had the opportunity to realize almost the entire experiments necessary to the paper acceptance. The main conclusions of the paper are described just after, and the paper has been added in annex 1.

1. Glutamate increases mobility of endogenous GluA2-containing AMPAR

The first observation of Audrey was that 100 µM glutamate application increases surface lateral diffusion of AMPAR. Using u-PAINT to track GluA2-containing AMPAR labeled with ATTO647N-coupled antibody targeting the extracellular domain of GluA2 on hippocampal neuron cultures (13-16 DIV), AMPAR can be sorted in two groups based on their diffusion properties. The first group is composed of AMPAR with a D value inferior to 0.008 $\mu m^2.s^{-1}$ and referred as "immobile" as they explore an area inferior to the one defined by the image spatial resolution (0.08 µm) within one frame. The second group is defined as the mobile part composed of receptors with a diffusion coefficient superior to 0.008 $\mu m^2.s^{-1}$. The same neurons were record before and after application of 100 µM glutamate. The mobile fraction increases by 30.7 ± 9.4 % upon glutamate treatment (**Figure 1**). All experiments have been performed in minimal intracellular signaling condition. Blockers of NMDAR, mGluR1 and 2, L-type Ca^{2+} channels, voltage-dependent Na^{+} channels and GluA2-lacking AMPAR were used. In their absence, an increase of Ca^{2+} signaling can be observed, and as it has been reported several times by our group that Ca^{2+} do influence AMPAR lateral mobility, the strategy has been to block this signaling to study the specific effect of glutamate-binding on AMPAR. These datas show that glutamate modifies AMPAR mobility at synaptic membrane independently of downstream signaling, and possibly directly through changes in receptor conformation.

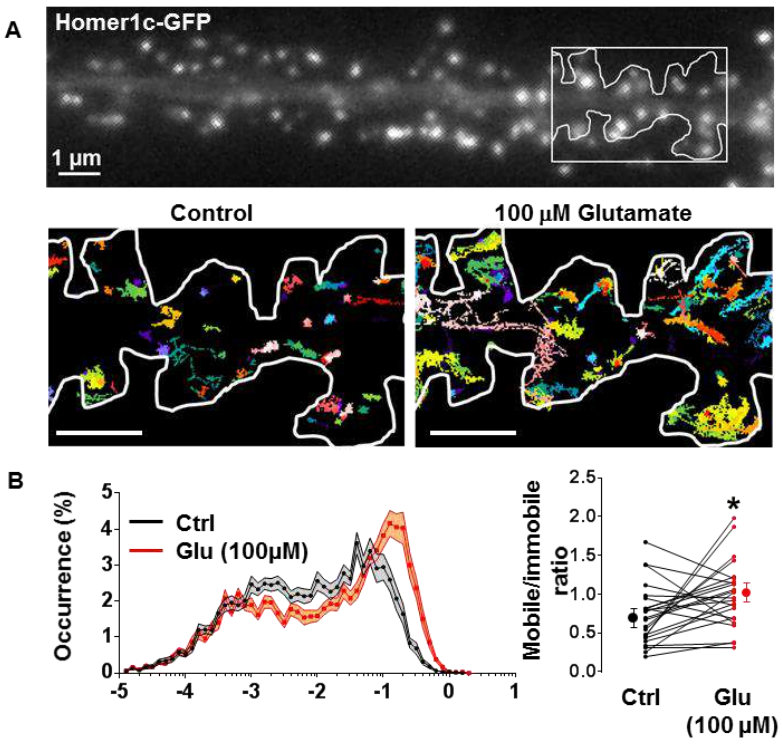

Figure 1. Glutamate Increases Endogenous GluA2-Containing AMPAR Diffusion in Synapse. (A) Epifluorescence image of a dendritic segment expressing eGFP-Homer1c as a synaptic marker (top) and corresponding synaptic trajectories of endogenous GluA2-containing AMPAR before and after application of 100 mMglutamate (bottom) recorded in the boxed region on the top Homer image. Each trajectory map is obtained by overaccumulation of 2,000 images acquired with uPAINT technique. (B) Modulation of endogenous GluA2-containing AMPAR synaptic mobility by application of glutamate 100 mM. From left to right are represented the average distribution of the logarithm of the diffusion coefficient and the paired ratios of the mobile over the immobile fraction (n = 24 cells, paired t-test, p = 0.023 and n = 10 cells, paired t test, p < 0.01),

2. AMPAR conformation impacts its mobility

To confirm the hypothesis that glutamate-induced AMPARs conformational changes modifies their mobility, Audrey measured the mobility of AMPAR mutants stabilized in distinct conformational states. Three mutated GluA2 have been expressed in neurons separately to block receptor in a closed, opened or desensitized state, and those mutated GluA2 are fused to SEP at their N-terminal domain to specifically track them with ATTO647N-coupled anti-GFP nanobodies. T686A mutation on GluA2 blocks AMPAR in a closed-resting state and displays an increase in their immobile fraction compared to WT over-expressed GluA2. 100 µm glutamate failed to increase GluA2 T686A mobility. The second mutant, GluA2 L483Y, stabilized AMPAR in an open state. It displays similar diffusion properties than WT GluA2. Finally, GluA2 S729C mutant was expressed in neurons. This AMPAR stabilized in a desensitized state displayed an increase of diffusion coefficient compared to WT and closed AMPAR (**Figure 2**). Altogether, the increase of mobility of endogenous GluA2-containing AMPAR and the increase of mobility of AMPAR locked in a desensitized conformation indicate that desensitization of AMPARs increases their mobility and suggest that glutamate-induced conformation changes may trigger release of receptors from synapses.

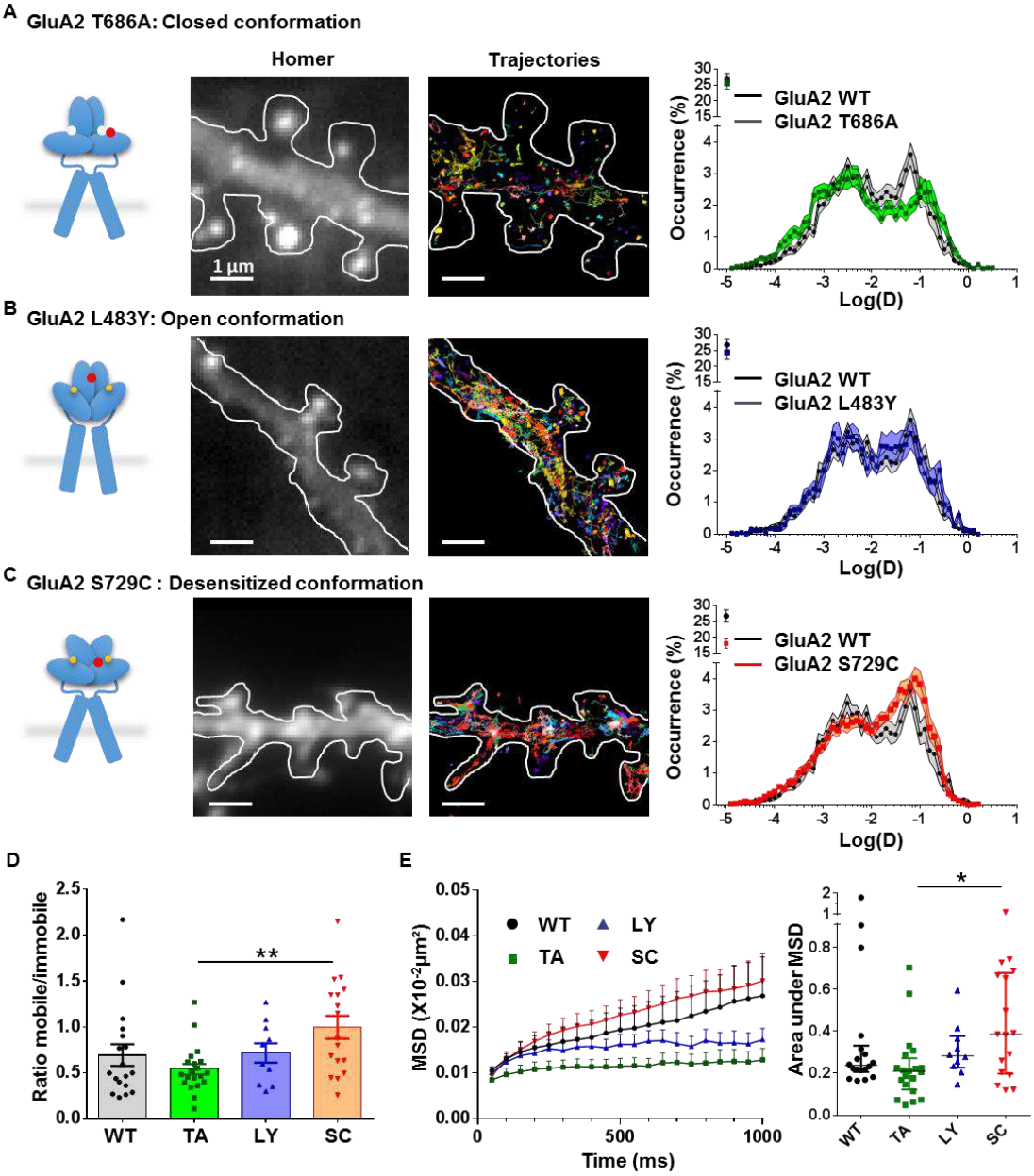

Figure 2. Mutated GluA2 Stabilized in a Desensitized State Are More Mobile than GluA2 Locked in a Closed or Open Conformation. (A–C) The left panels depict schemes representing the tracked AMPAR stabilized in specific conformations using point mutations (red dots). Image panels from left to right show the epifluorescence image of DsRed-Homer1c in a sample neuron, a map of the recorded trajectories using the u-PAINT technique in the corresponding stretch of dendrite, and the total distribution of the logarithm of the synaptic diffusion coefficient. On each distribution, the dark line represents the control distribution of WT GluA2. (A) Comparison between GluA2 WT and T686A, a mutant stabilized in the closed state. (B) Comparison between GluA2 WT and L483Y, a mutant stabilized in the open state and so cannot desensitize. (C) Comparison between GluA2 WT and S729C, a mutant stabilized in a desensitized state. (D) Mean ratio of the mobile over the immobile fractions (±SEM) for synaptic overexpressed SEP-GluA2 and conformational mutants of GluA2 (WT, n = 17 cells; T686A, n = 20 cells; L483Y, n = 10 cells; S729C, n = 17 cells; one-way ANOVA, p = 0.0161, and Sidak's post test p = 0.009, between T686A and S729C). (E) Plot of the synaptic MSD versus time for overexpressed SEP-GluA2 and the conformational mutants of GluA2 (left panel) (mean ± SEM, one-way ANOVA, p = 0.03, Sidak's post test show that TA/SC is significantly different p = 0.02). Median (±IQR) of the area under MSD are also represented (right panel) to illustrate cell to cell variability.

3. Glutamate-induced AMPAR increased mobility is specific of AMPAR conformational change

In order to confirm that desensitization increases AMPAR mobility is related to the presence of glutamate, I performed u-PAINT experiments with various pharmacological controls. AMPARs affinity for glutamate has been measured at around 1 mM, which corresponds to the concentration range reached under the release site. Thus, I investigated with u-PAINT technique, the sensitivity of the increase of AMPAR mobility to various glutamate concentrations. In the presence of only the vehicle or of a low glutamate concentration (1 µM and 20 µM), no modification in the mobile/immobile ratio has been observed (**Figure 3A**). In contrast, application of high glutamate concentration (100 µM, 300 µM and 1 mM) increased the mobile/immobile ratio in a dose-dependent manner. These results demonstrate that (i) the glutamate induced increase of mobility could be compatible with the glutamate concentration reached during a vesicle release. (ii) The dose response effect observed when measuring AMPAR mobility follows the same magnitude order than the AMPAR glutamate affinity. These two correlations could suggest a direct regulation of glutamate on AMPAR mobility.

To confirm that the effect of glutamate on AMPAR mobility was mediated directly by their activation, we applied NBQX, a specific competitive antagonist. NBQX alone at 20 µM significantly decreased AMPAR mobile fraction. This demonstrated that ambient glutamate was enough to affect AMPAR mobility. In parallel, addition of glutamate at 100 µM to the medium was able to compete out NBQX and to trigger an increase of AMPAR lateral diffusion (**Figure 3B**).

Finally, we applied cyclothiazide (CTZ, 20 µM) which prevents entry in desensitized state, to confirm that glutamate-induced increase mobility of AMPAR was specifically induced by desensitization and not by the activation. CTZ alone was sufficient to trigger decrease of AMPAR mobility in absence of glutamate treatment, confirming the previous NBQX results on ambient glutamate. In addition, CTZ prevents the increase of endogenous GluA2-containing AMPAR diffusion upon glutamate treatment (100 µM) (**Figure 3C**). Altogether, those results reinforced the following conclusions: (i) glutamate binding to AMPARs increases their mobility on a dose-dependent manner, and (ii) AMPAR increased mobility is due to AMPAR desensitization.

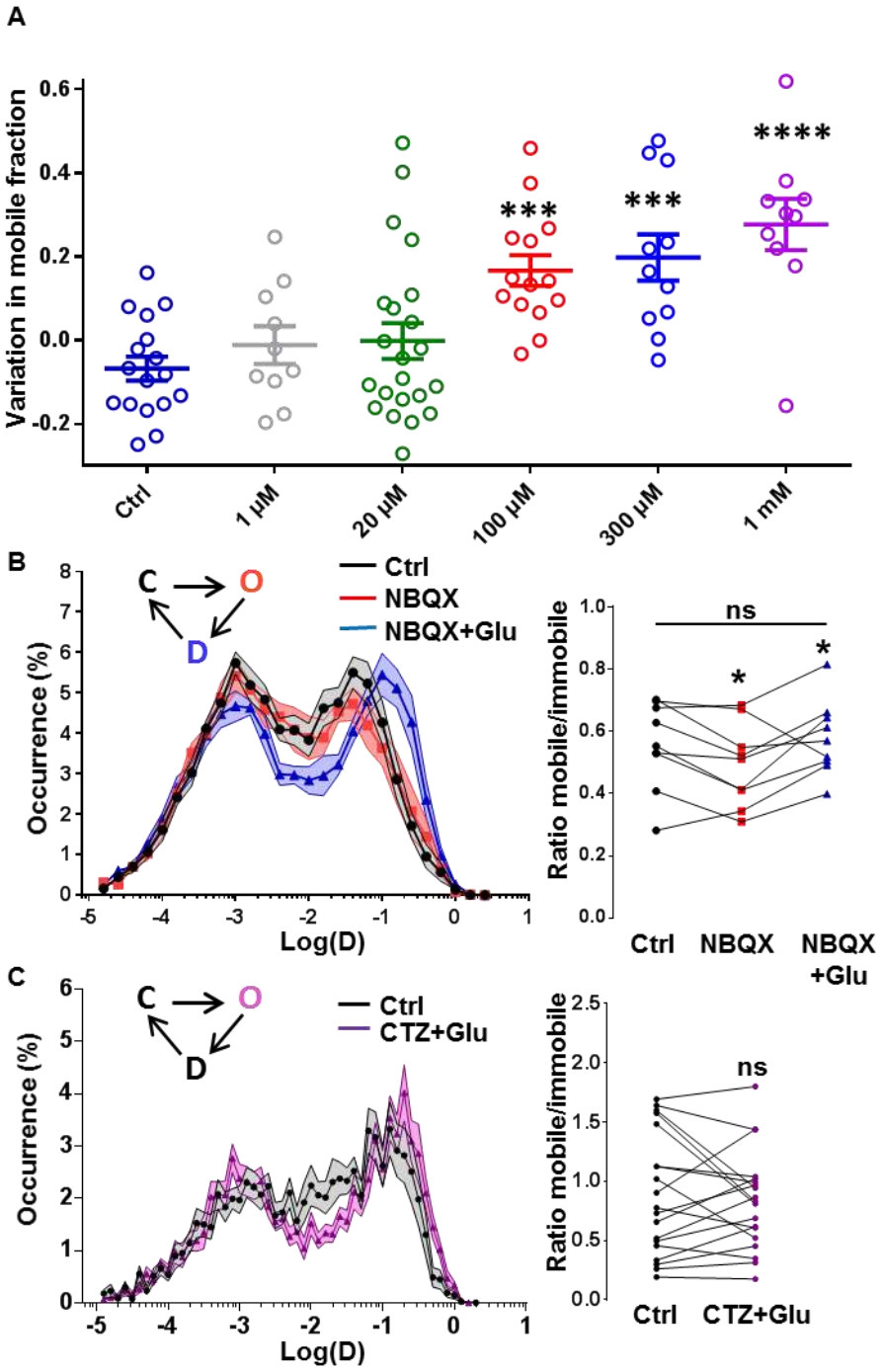

Figure 3. Glutamate-induced AMPAR increased mobility is specific of AMPAR conformational change (A) Dose-response curve for changes in the paired ratio of mobile over the immobile fraction following addition of varying glutamate concentrations (or vehicle for control). Five glutamate concentrations are tested from 1 mM to 1 mM. (mean ± SEM are plotted, statistical test is one-way ANOVA with Dunnet's post test). (B) Modulation of endogenous GluA2 containing AMPAR synaptic mobility by sequential application of NBQX (20 mM) (competitor antagonist), then additionally glutamate (100 mM). From left to right are represented the average distribution of the logarithm of the diffusion coefficient and the paired ratios of the mobile over the immobile fraction (n = 9 cells, $p < 0.05$). (C) Absence of modulation of endogenous GluA2-containing AMPAR synaptic mobility by coapplication of 100 mM glutamate and 20 mM cyclothiazide. From left to right are represented the average distribution of the logarithm of the diffusion coefficient, the paired ratios of the mobile over the immobile fraction (n = 19 cells, paired t test, $p = 0.539$).

4. Glutamate-induced increase in desensitized AMPAR mobility tunes short-term plasticity through unbinding from stargazin

The molecular explanation of this mobility increase has been investigated. We used co-immunoprecipitation between AMPAR and stargazin to demonstrate that desensitized state presents a lower affinity for stargazin than close or open receptors. In parallel, a genetic fusion between stargazin and GluA1 abolishes the glutamate induced mobility increase. We hypothesized that AMPAR conformational changes occurring during desensitization trigger an important decrease of AMPAR affinity for stargazin, leading to a remobilization of previously trapped receptors.

Finally, we tried to determine the effect of glutamate-induced AMPAR mobility on synaptic transmission properties. Previous works from the lab shown that AMPAR fast diffusion tunes frequency-dependent synaptic transmission in paired-pulse experiments. Andrew Penn in the group recorded synaptic currents induced by train of stimulations in neuron expressing SEP-GluA1 alone or co-expressing SEP-GluA1-stargazin tandem. The impact of mobility on short-term plasticity was investigated using antibody cross-linking (**Figure 4**). In neurons expressing SEP-GluA1 alone, a short term facilitation was observed in absence of antibody cross-link. When AMPAR lateral diffusion was blocked with antibody, short-term facilitation was turned into a short-term depression, as previously described in **Heine et al., 2008** (Heine et al., 2008). In neurons expressing SEP-GluA1 fused to stargazin, paired-pulse stimulation induced a short-term depression, and occluded the effect of antibody cross-linking. This suggests that the fusion of AMPAR to stargazin has direct consequence on AMPAR mobility as it produces similar effect on short-term plasticity than blocking mobility with antibodies. Altogether, these experiments establish that preventing AMPAR dissociation from stargazin prevents the positive impact of AMPAR diffusion to compensate the desensitization of receptors and insure the fidelity of high-frequency inputs.

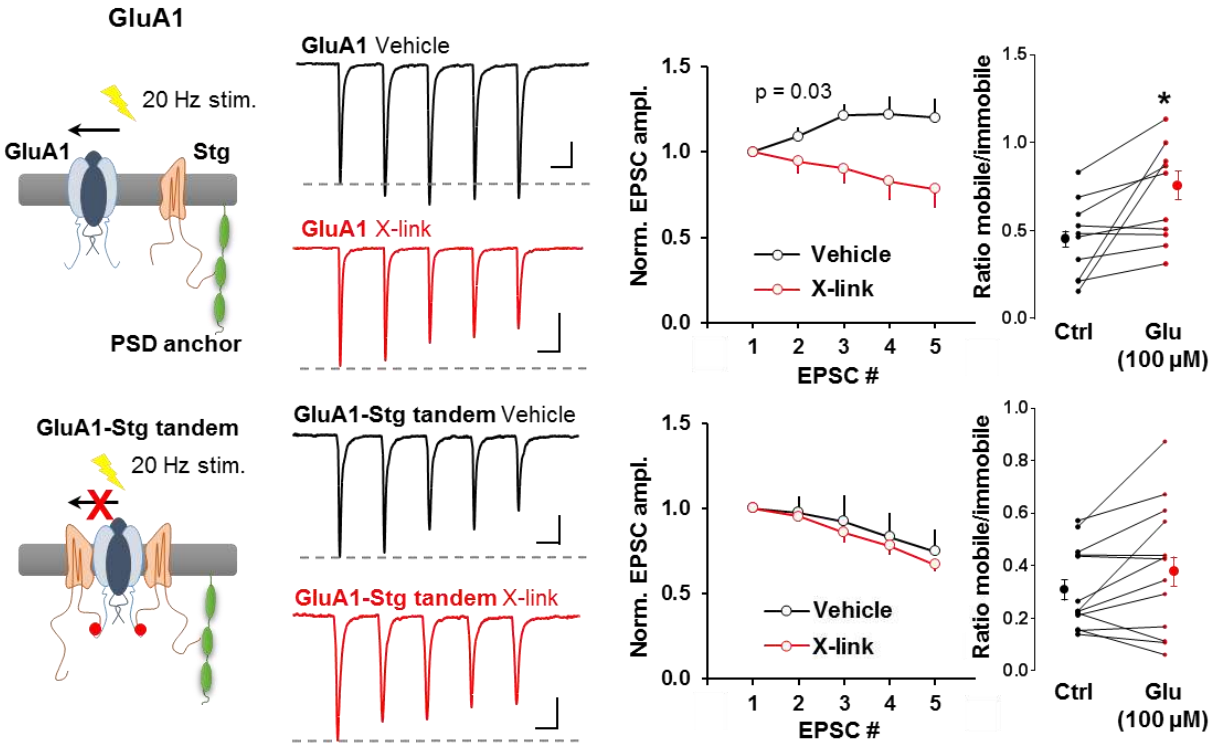

Figure 4. Glutamate-induced increase in desensitized AMPAR mobility tunes short-term plasticity through unbinding from stargazin. (A) The diagrams on the left represent the experimental paradigm: SEP-GluA1 and endogenous stargazin are expressed separately or linked in a SEP-GluA1-stargazin tandem. GluA1 interact with stargazin (maroon, either endogenous or covalently linked) that traps AMPARs at synapses via PDZ interactions. To test the role of AMPAR mobility during a train of stimulation, lateral diffusion was blocked by crosslinking the receptors with an anti-GFP antibody (X-Link). The middle left panels represent the average EPSC trains (five pulses at 20 Hz), for example cells in conditions with and without crosslinking. (Middle Right) Plots of the EPSC amplitude normalized to the initial EPSC for stimulations with (n = 5 cells) and without (n = 6 cells) crosslinking. When GluA1 cannot dissociate from stargazin, EPSCs elicited by a train of stimulation already have depressed short-term plasticity, which occludes crosslinking (n = 7 cells, both with and without crosslinking). Right panels, paired ratio of the mobile over the immobile fraction before and after treatment with 100 mM glutamate (for GluA1: n = 10 cells, paired t test, p = 0.024; for GluA1-stargazin chimera: n = 13 cells, paired t test, p > 0.05)

5. Working model

Using single particle tracking, biochemistry and electrophysiology, as well as other approaches detailed in the full article in annex 1, we investigated the impact of changes of AMPAR conformational states on their surface diffusion at synapses and its impact on high frequency synaptic transmission. Our results on both endogenous, conformational state mutants and chimera receptors (either GluA1 or GluA2 AMPAR subunit) show that glutamate binding to AMPAR induces a ~20-30 % increase of their mobility in the presence of glutamate.

Glutamate binding triggers major changes in receptor conformation that lead to opening of the ion pore and ultimately entry into the desensitized state. Desensitization is characterized by a drastic rearrangements of AMPAR extracellular N-terminal domain. This conformational change decreases the interaction between desensitized receptors and auxiliary proteins (stargazin) allowing them to diffuse out of synaptic traps, probably nanodomains. The fact that only ~20-30 % of desensitized receptors display an increased mobility is compatible with the existence of various desensitized conformation. This is supported by the dose-dependent effect of glutamate and biochemical experiments showing that AMPARs locked in desensitized conformation display a lower but not abolished binding to stargazin. Moreover, AMPARs are stabilized in 80 nm diameter nanodomains at synapses (Nair et al., 2013). Our d-STORM experiments (cf paper) indicate that upon glutamate application, nanodomains organization is maintained, but presents a ~20% reduction of their receptors content. This percentage is similar to the fraction of receptors which displays an increase of diffusion. We thus postulate that the increased mobility of a fraction of desensitized AMPARs is important to accelerate their exit from trapping sites such as nanodomains to help synapses recover faster from desensitization-dependent depression.

In conclusion, previous work from the lab established that AMPAR nanodomains represent a post-synaptic quantum of response by being positioned in front of glutamate release sites (**Nair et al., 2013, Haas et al., submitted**). As AMPARs are stable in nanodomains and highly diffusive in between them, freeing desensitized ones from their anchor allows them to quickly diffuse away from the glutamate release area between two consecutive releases. Thus, naive receptors can enter and stabilize into nanodomains and participate to the synaptic response. This fast exchange could be responsible of the maintenance of the fidelity of synaptic inputs during high frequency stimulations.

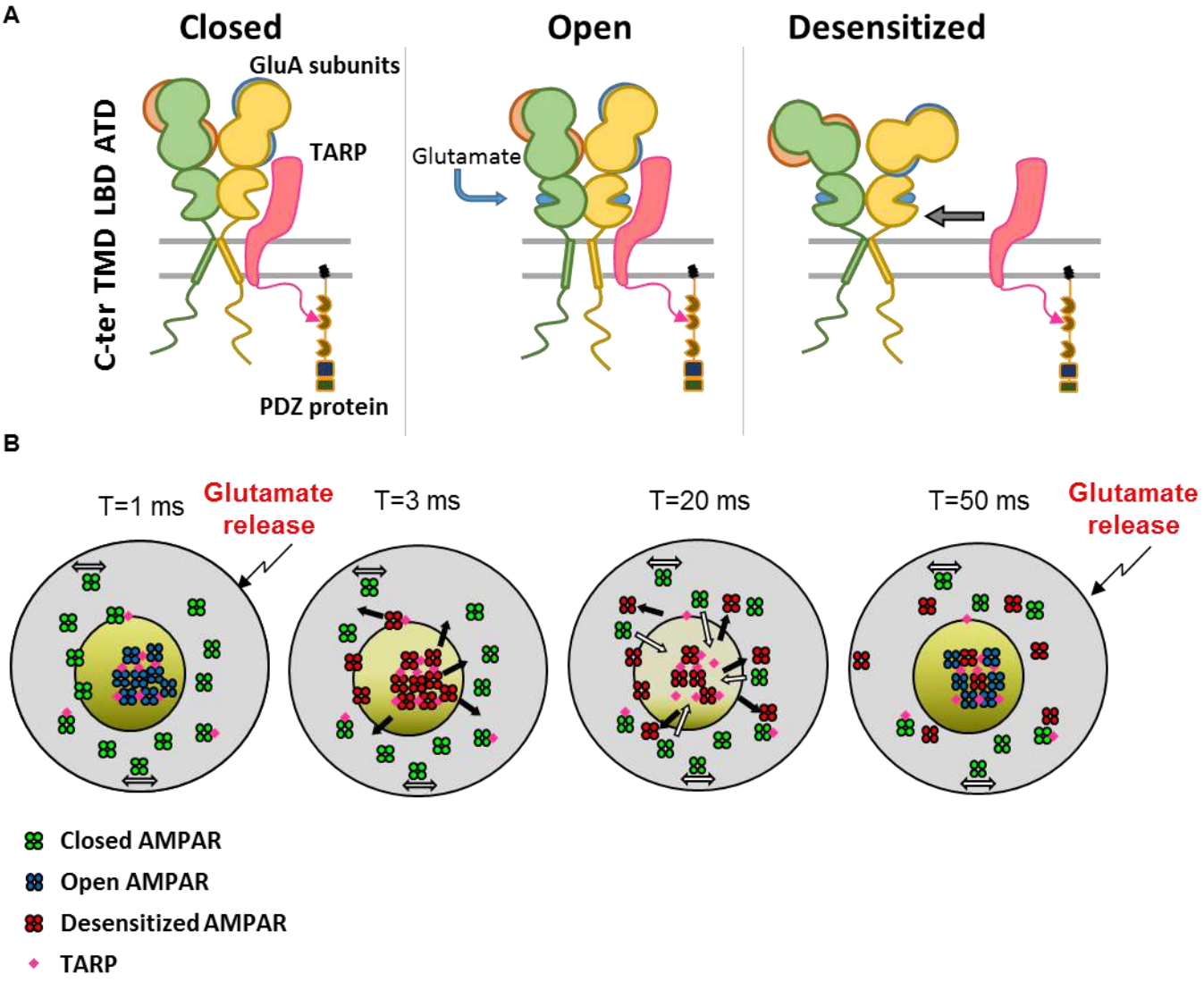

Figure 5. Hypothetical Model of Glutamate-Induced AMPAR Mobility and Effect on Synaptic Organization. (A) AMPAR are tightly coassembled with TARP at least via its transmembrane (TMD) and ligand-binding domain (LBD); the drastic changes operating at the LBD and ATD in the presence of glutamate lead to the desensitization of the AMPAR and to a decrease of its avidity for TARP. This effect could trigger a detrapping of AMPAR and an increase of its mobility.
(B) The schemes represent a top view of a synapse where naive (closed-green) AMPAR are regrouped partly in a nanocluster. The first glutamate release activates AMPAR during the first ms (T = 1 ms, blue, synaptic area covered by glutamate represented by yellow circle), then they quickly desensitize (T = 3 ms, red). This conformational change triggers an increase of AMPAR mobility, freeing TARP immobilization site. Free diffusive closed receptor can be specifically trapped at this free site (T = 20 ms), allowing a renewing of AMPAR in the nanocluster (T = 50 ms). Desensitized receptors are now out of the release site, and closed receptors replace them inside the nanocluster. This specific glutamate-induced mobility of desensitized AMPAR can be at the base of the constant receptor turnover essential for fidelity of fast synaptic transmission.

Chapter 3

Study of the role of AMPAR dynamic nano-organization during Long-Term Depression

We and others have demonstrated how AMPAR nanoscale organization and trafficking, both through endocytosis/exocytosis and lateral diffusion, determine synaptic transmission properties at basal state. Parameters such as AMPAR molecular organization with respect to release site and exchange rate at synapses tune both the amplitude of synapses responses and their ability to follow frequency stimulations. However, the fundamental properties of this transmission are not fixed but rather changed by ongoing neuronal communication. Indeed, synapses constantly undergo morphological and functional changes. They can strengthen and weaken on a long-lasting manner through long-term potentiation and long-term depression respectively. Those forms of synaptic plasticity are thought to be the cellular mechanism that underlies learning and memory storage in the CNS. During the last 45 years, hippocampal studies have provided decisive insights to the understanding of the molecular mechanisms of LTP and LTD. But most of these canonical studies have been mostly focused on LTP thought to be the principal memory engram. However, LTP would be of limited use if there was no mechanism to counterbalance its effects. During development or during learning, synapses are created and suppressed, both being important to refine the neuronal network and to allow cognitive function and behavioral flexibility. We forget and learn, both are important.

What are the molecular mechanisms underlying changes induced by LTD? Literature reported that specific activation pattern of either NMDARs and/or mGluRs triggers a decrease in synaptic transmission due to a rapid and massive endocytosis of AMPARs. This initial phase corresponds to the establishment of synaptic depression during the first minutes. After few tens of minutes, a second phase less characterized takes place to maintain the depression and corresponds to a new depressed equilibrium state of the synapse. This long lasting synaptic modification can remain stable for hours to days and involves in this case new protein synthesis and translation. Strong of our experience on the characterization of AMPAR nanoscale organization role on synaptic transmission at basal state, I decided to determine the intimate modifications of AMPAR dynamic organization induced during early and sustained LTD.

In parallel of input-specific LTD, some laboratories reported that neuromodulators as insulin could also trigger a loss of synaptic AMPARs and thus decrease synaptic transmission in a long-lasting manner, even if the physiological relevance of this phenomenon has not been

established yet (Beattie et al., 2000). Recently, the group of Eric Boué-Grabot discovered another LTD-like mechanism which relies on the activation of post-synaptic purinergic receptors (P2XRs) through astrocyte-released ATP, and inducing AMPAR internalization (Pougnet et al., 2014). In a recently published paper and in collaboration with Eric Boué-Grabot lab, we demonstrated by using electrophysiology and super-resolution microscopy that P2XR-dependent LTD triggers AMPAR internalization through modulation of AMPAR phosphorylation state on a distinct manner compared to the classical NMDAR-dependent LTD. This work being not in the core of my research, the paper has been added in annex 2 and will not be detailed in my PhD manuscript.

In this chapter, I will describe the main work of my PhD which aimed to understand the AMPAR and scaffolding proteins re-organization induced by classical NMDAR- or P2XR-dependent Long-Term Depression and the role of such re-organization on synaptic transmission properties. To that, I have used various live and fixed super-resolution microscopy techniques coupled to electrophysiological recordings on hippocampal cell cultures and brain slices.

1. NMDA and ATP treatments trigger a long-term depression of miniature synaptic currents

Miniature currents correspond to the q value abundantly discussed all along this manuscript. It is dependent on the number of AMPARs at the synapse, their nanoscale organization, their position regarding release site and their subunit composition. Long-term depression corresponds to an initial decrease of synaptic strength (Q) which has been extensively described to lead to a decrease of the N value. Changes in the P_r have also been reported while it is still not clear. We first investigated if both chemical treatment to induce NMDAR- and P2XR-dependent LTD (NMDA 30 µM for 3 min and ATP 100 µM for 1 min respectively) were able to decrease AMPAR-mediated currents as currently described in the literature (Lee et al., 1998; Pougnet et al., 2014). We measured the evolution of miniature synaptic currents (corresponding to individual synapse response) in function of time after LTD induction. NMDA treatment triggered a rapid (less than 10 minutes) and stable (more than 30 minutes) decrease of synaptic currents (t0: 11.04±0.44, t10: 7.60±0.49, t30: 7.99±0.65; figure 1A). In parallel, we observed a significant but transient decrease of miniature frequency probably due to some decrease of synaptic input (**Figure 1A**).

On a similar way, ATP treatment triggered a decrease of synaptic current (t0: 10.57±0.56, t10: 8.22±0.48, t30: 8.22±0.65; **figure 1B**) as previously described in Pougnet *et al.*.

Surprisingly, no decrease of mEPSC frequency was induced by ATP. Those results confirm our ability to induce long-term decrease of synaptic transmission with both NMDA and ATP treatments.

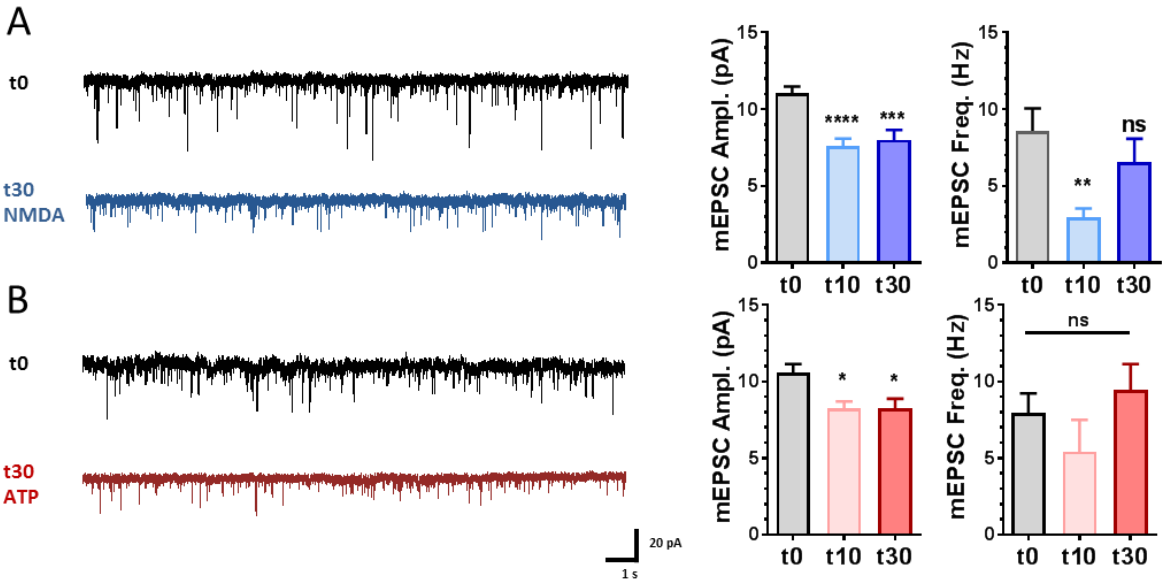

Figure 1. NMDA (A) and ATP (B) treatment trigger a long lasting decrease of synaptic transmission. Left panels represent electrophysiological recordings of mEPSCs in basal state (black traces) or 30 minutes after NMDA or ATP treatment (blue or red respectively). Middle panels correspond to mEPSC amplitudes at basal state, 10 or 30 minutes after LTD induction. Right panels show mEPSC frequencies at basal state, 10 or 30 minutes after LTD induction. NMDAR-dependent LTD (t0, t10, t30) n = 12, 13, 10 cells respectively. P2XR-dependent LTD (0, t10, t30) n = 12, 9, 8 respectively. One-way ANOVA tests with Tukey post test.

2. NMDAR- and P2XR-dependent LTD are associated to a reorganization of AMPARs at the nanoscale

In previous papers, we have demonstrated a strong correlation between the number of AMPARs per nanodomain and the amplitude of synaptic currents (Hafner et al., 2015; Nair et al., 2013). To test this correlation after LTD protocol, we applied d-STORM technique to characterize the endogenous AMPAR nanoscale modification induced by the two forms of LTD.

Both NMDA and ATP treatments decrease AMPARs number per nanodomain after 10 minutes (**Figure 2**; average values during NMDAR-dependent LTD: t0 = 19.77 ± 1.19, t10 = 12.82 ± 1.05, t30 = 12.59 ± 0.82, and during P2XR-dependent LTD: t0 = 19.28 ± 1.76, t10 = 13.21 ± 0.46, t30 = 15.38 ± 0.53). Interestingly, nanodomains size were unchanged despite the 30% decrease of their content. This observation reveals either a limitation of our technical

accuracy or a reduction in the packaging of AMPARs within the ~80 nm nanodomains (**Figure 2 - middle panels**). We previously observed that nanodomain organization was not necessarily dependent of AMPAR content (Constals et al., 2015; Nair et al., 2013). To investigate how nanodomain content could decrease without affecting its size, we planned to realize high resolution experiments as detailed in the methods chapter and decipher the deep organization of AMPARs within nanodomains.

Finally, NMDA treatment triggered a specific decrease of the number of nanodomains per spine, as well as an increase of the number of spines without AMPAR nanodomains. This could potentially be one explanation for the decreased in mEPSC frequency (**Figure 2A - right panel**).

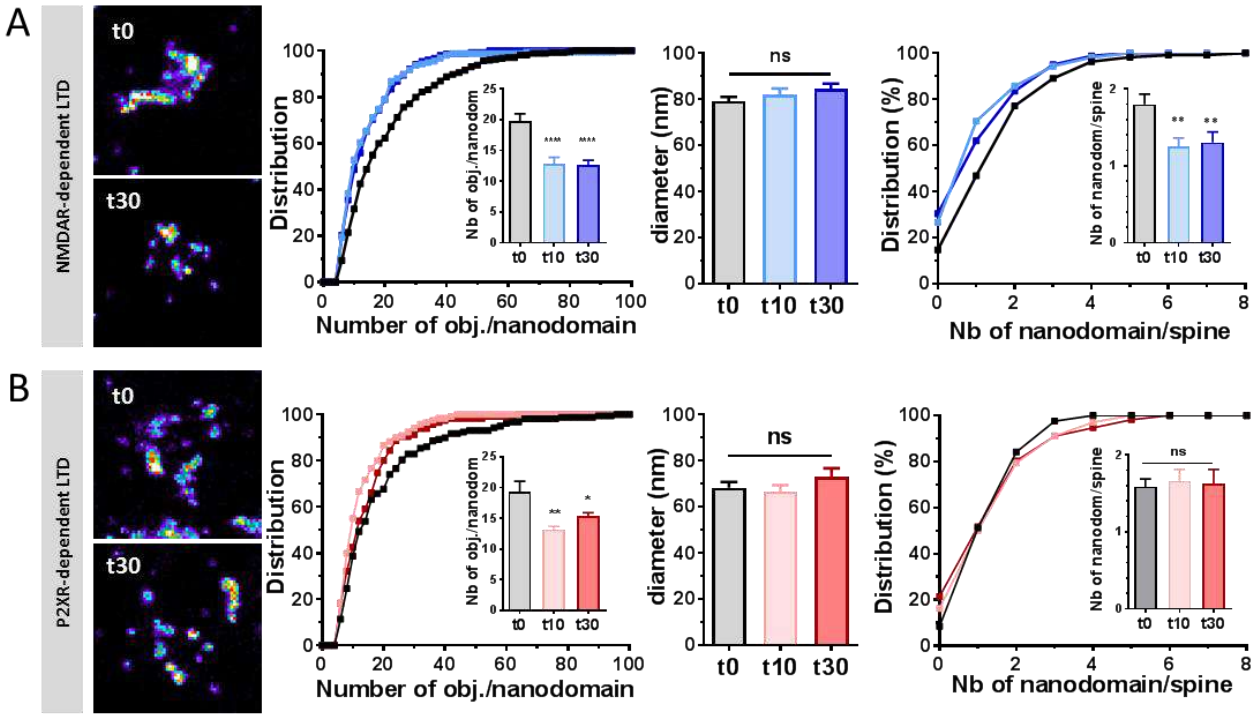

Figure 2. NMDAR- (A) and P2XR-dependent LTD (B) trigger a long lasting depletion of AMPAR nanodomain content without affecting the overall nanodomain organization. Left panels are representative images of dendritic spine labeled for endogenous GluA2 and recorded with d-STORM technique at basal state or 30 min after LTD induction. Middle left panels represent the cumulative distribution of object number per nanodomain. Inserts represent the mean value object/nanodomain for N number of cells (N for NMDAR-dependent LTD: t0 = 17, t10 = 14, t30 = 14; for P2XR-dependent LTD: t0 = 8, t10 = 6, t30 = 7). Middle left panels represent average values of nanodomain diameter. Left panels represent the cumulative distribution of the number of nanodomain per dendritic spine. Inserts correspond to the average value for N number of cells. NMDAR-dependent LTD (t0, t10, t30) n = 17, 14, 14 cells respectively. P2XR-dependent LTD (0, t10, t30) n = 8, 6, 7 respectively. One-way ANOVA tests with Tukey post test.

Altogether, these results show that LTD induction triggers a rapid decrease of AMPARs at the cell surface but also inside nanodomains at synapses, leading to a rapid decrease of synaptic strength. This first change in synaptic organization and function occurs in less than 10 minutes following both ATP and NMDA-induced LTD.

3. NMDAR-dependent LTD triggers a long-lasting increase of AMPAR mobility during a late phase

Surface lateral mobility makes the link between endo/exocytosis area and PSD. The proportion of mobile AMPARs is dependent of complex equilibrium of protein-protein interactions regulated by kinases and phosphatases activity. This modulation of the phosphorylation balance on AMPARs, associated proteins and scaffolding proteins is a key feature known to regulate the immobilization of AMPARs at synapses. To characterize the potential modification of AMPAR lateral mobility during NMDAR-dependent LTD, we tracked endogenous GluA2-containing AMPARs with u-PAINT imaging technique. Receptors mobility has been measured in basal condition and every 5 minutes for 30 minutes following LTD induction (**Figure 3A-D**). No change of AMPAR lateral diffusion was observed on the early phase of NMDAR-dependent LTD. However, surprisingly, we observed a robust and significant increase of AMPAR mobility 25 minutes after LTD induction (**Figure 3D**). To test the stability of this AMPAR mobility increase, we compared mobility with u-PAINT on neurons in basal states or 3 hours after NMDA treatment. The increase in AMPAR mobility during NMDAR-LTD was still present after 3 hours suggesting that a new equilibrium of AMPAR diffusion has been reached (**Figure 3F-G**).

In order to decipher the molecular mechanism at the origin of AMPAR increased mobility during NMDAR-dependent LTD, we analyzed individual synaptic trajectories. For each time frame, an instantaneous diffusion coefficient has been calculated. This gave access to the time that each individual tracked receptors spend immobilized at synapses, probably into nanodomains. We extracted two parameters: the percentage of fully immobile trajectories (100% with a $\log(D) < -1.6$) and the percentage of time that each receptor spends immobile (% immobility for trajectories with < 95% of time spent immobile). We used u-PAINT recording of GluA2-containing AMPARs upon NMDAR-dependent LTD at 3 time points: t0, t10 and t30. The fraction of fully immobile receptors was unchanged between conditions. However, AMPARs were less immobilized at synapses during NMDAR-dependent LTD, already after 10 min, but even more after 30 min (**Figure 3E**). The change of immobility time during NMDAR-

dependent LTD shows that AMPARs are less retained at synaptic trapping sites, suggesting a change in protein to protein interaction which affects AMPAR affinity for synaptic traps.

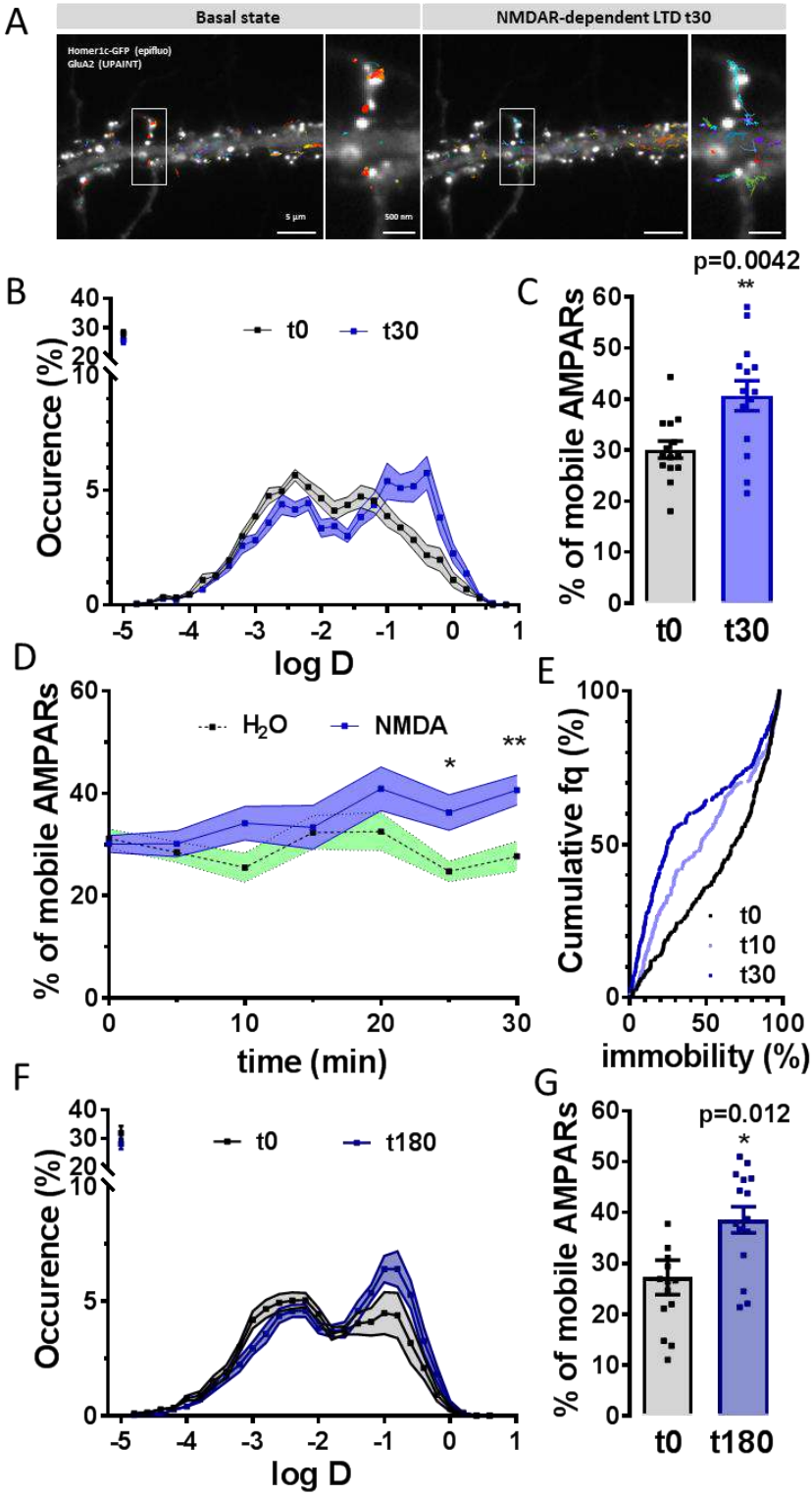

Figure 3. NMDAR-dependent LTD induces a late but robust increase in AMPAR mobility. (A) Epifluorescence image of a dendritic segment expressing eGFP-Homer1c as a synaptic marker and the corresponding u-PAINT image overlapped showing the individual trajectories of GluA2-containing AMPARs on the same dendritic segment at basal state or 30 minutes after NMDA treatment. ➔

➔ (B) Average distribution of the logarithmic diffusion coefficient of GluA2-containing AMPAR at basal state (grey) and 30 minutes after NMDA treatment (blue). (C) Mean value of the mobile fraction at basal state and 30 minutes after NMDA treatment. (D) Average value of AMPAR mobile fraction over the time (0 - 30minutes) after NMDA or H_2O treatment. (E) Cumulative distribution of the immobility time of individual synaptic trajectories of GluA2-containing AMPARs. (F) Average distribution of the logarithmic diffusion coefficient of GluA2-containing AMPAR at basal state (grey) and 180 minutes after NMDA treatment (dark blue). (G) Mean value of the mobile fraction at basal state and 30 minutes after NMDA treatment. (B-C) N=14 cells, (D) N=14, 10 (NMDA and H_2O respectively), (E) N=252, 235, 280 (t0, t10 and t30 respectively), (F-G) N= 14, 15 (t0 and t180 respectively). (C) paired t-test, (G) unpaired t-test, (D) Two-way ANOVA tests with Dunnett post test.

These results showed that AMPAR lateral diffusion is increased during NMDAR-dependent LTD. Interestingly, this increase occurred only between 20 to 25 minutes after the induction (late phase), while decrease of nanodomain content and AMPAR-mediated currents was observed already after 10 minutes (early phase). Based on literature which reported a rapid and transient (around 0 to 10 minutes) increase of endocytosis rate immediately after NMDA treatment (Ashby et al., 2004; Carroll et al., 1999; Rosendale et al., 2017), we hypothesize that LTD initial phase is due to a massive endocytosis of dendritic and synaptic AMPARs. In parallel, progressive decrease of AMPAR affinity for trapping site occurs leading to a long-lasting displacement of the equilibrium from immobile to mobile AMPARs at synapses.

We repeated the same experiment to investigate changes in AMPAR surface diffusion when LTD was induced by ATP. No modification of AMPAR mobility has been observed neither during the early phase nor during the late phase (30 minutes and 3 hours). Similarly, we did not detect any modification of AMPAR immobilization duration. These experiments (**Figure 4**) reported that only input-specific LTD triggers an increase of AMPAR mobility and so probably a long lasting new equilibrium of AMPAR organization.

To confirm this conclusion, we realized the same experiments by inducing LTD with a protocol activating mGluR. This well characterized protocol (DHPG 100 µM for 10 min), has been shown to share many features with NMDAR-dependent LTD. On a similar manner than NMDA-induced LTD, mGluR-dependent LTD increased AMPAR diffusion 25 minutes after DHPG application (**Figure 5A**). Finally, to assess the specificity of NMDA-induced LTD on NMDAR activation, we repeated these experiments in presence of AP5, a NMDAR specific antagonist. As expected, no AMPAR mobility increase was observed after NMDA treatment in the presence of AP5 (**Figure 5B**).

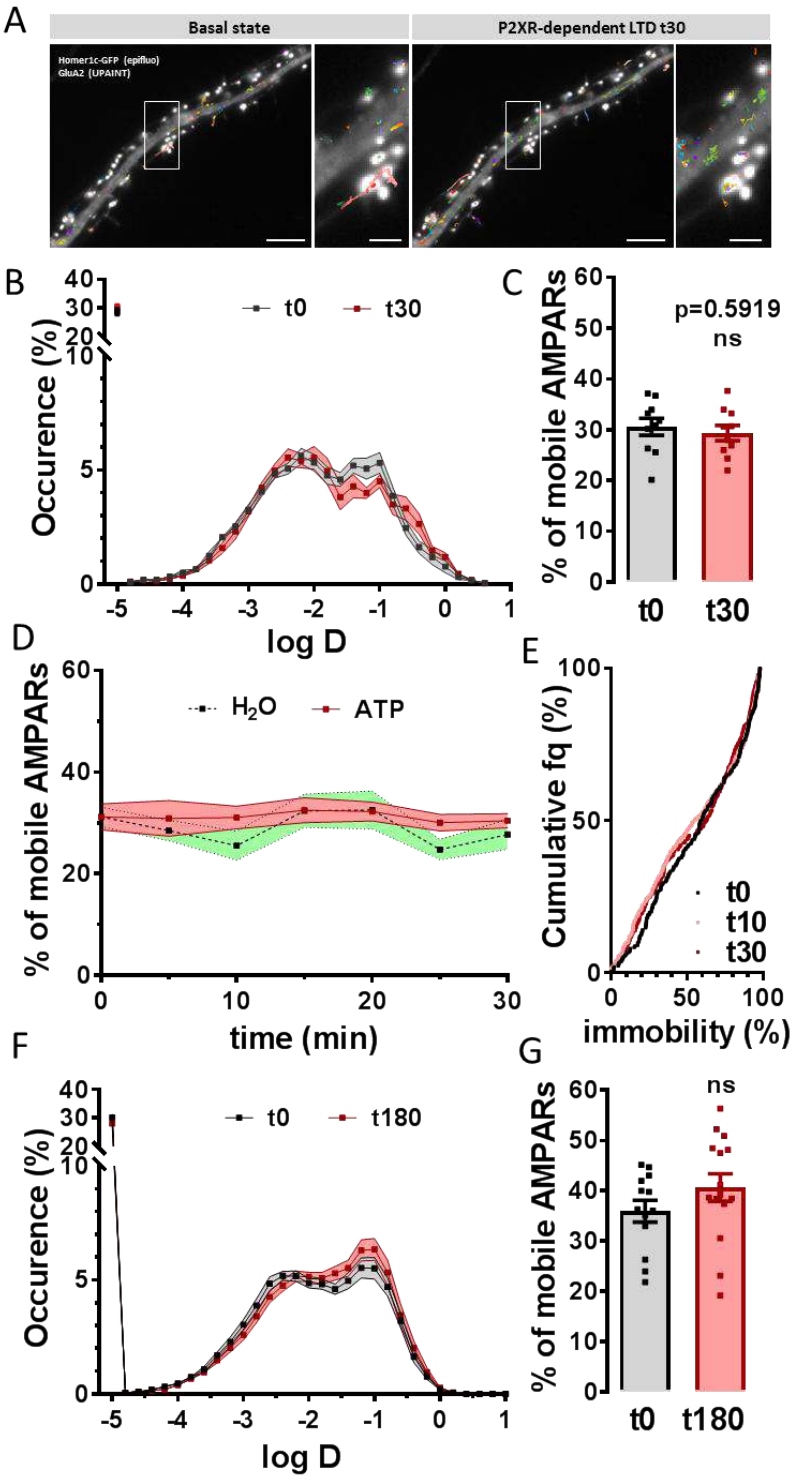

Figure 4. P2XR-dependent LTD does not change AMPAR lateral diffusion properties.

Altogether, these results proposed for the first time that homosynaptic LTD leads to a new equilibrium of AMPAR dynamic at synapses, while LTD induced by neuromodulator triggers AMPAR endocytosis without affecting the dynamic equilibrium at synapses.

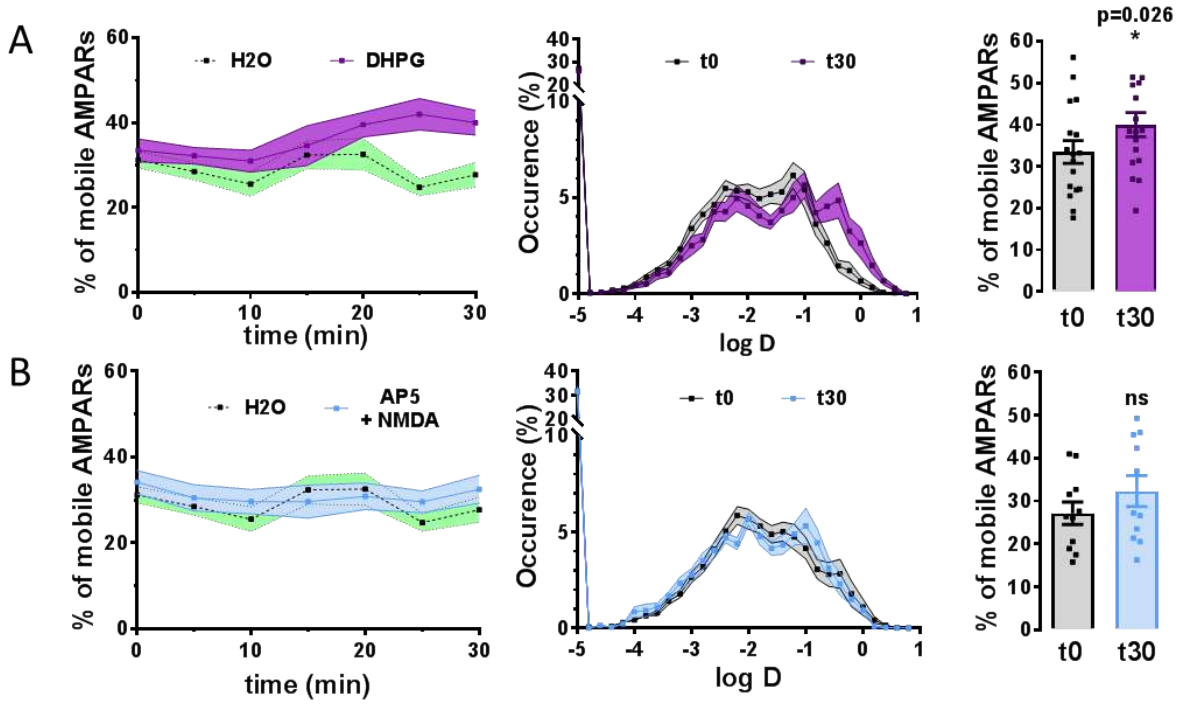

Figure 5. AMPAR increased mobility is specific of input-specific LTD. (A) mGluR-dependent LTD also triggers a late increase in AMPAR mobility. Left panel corresponds to the average value of AMPAR mobile fraction over the time (0 – 30 minutes) after DHPG (purple) or H_2O treatment (green) (N = 17 and 10 respectively). Middle panel corresponds to the average distribution of the logarithmic diffusion coefficient of GluA2-containing AMPAR at basal state (grey) and 30 minutes after DHPG treatment (purple). Right panel represents the mean value of the mobile fraction at basal state and 30 minutes after DHPG treatment (N = 17 cells, paired t-test).
(B) The increase in AMPAR mobility following NMDA treatment is prevented by AP5 application. Left panel corresponds to the average value of AMPAR mobile fraction over the time (0 - 30minutes) after AP5+NMDA (cyan) or H_2O treatment (green) (N = 11 and 10 respectively). Middle panel corresponds to the average distribution of the logarithmic diffusion coefficient of GluA2-containing AMPAR at basal state (grey) and 30 minutes after AP5+NMDA treatment (cyan). Right panel represents the mean value of the mobile fraction at basal state and 30 minutes after AP5+NMDA treatment (N = 11 cells, paired t-test)

4. Molecular modifications responsible for AMPAR increase mobility during NMDAR-dependent LTD

The molecular basis of AMPAR mobility increase during LTD has been then explored. Literature reported that AMPAR trapping at synapse is mainly due to a tripartite interaction between AMPARs, auxiliary proteins such as stargazin and PSD-95, as schematized in **Figure 6**. Thus, an increase of AMPAR mobility can be explained by three potential events: (i) as

reported the result chapter 2, AMPARs can decrease their affinity for stargazin, and thus favor the escape of AMPARs from nanodomains. (ii) Modification of the phosphorylation state of stargazin, as expected during LTD, can decrease the interaction between stargazin and PSD-95. (iii) LTD can induce post-translational modification of PSD-95, leading to a decrease of PSD-95 slots at synapses and thus decreasing AMPAR complex trapping into nanodomains.

Literature confirmed the validity of each hypothesis. A physical dissociation between AMPARs and stargazin has already been observed upon AMPAR conformational changes (Constals et al., 2015). However, AMPAR-stargazin interactions are mainly stabilized through trans-membrane and extracellular segments. It is difficult to conceive how LTD could impact such interactions. The two other hypothesis are more probable. Concerning the separation between PSD-95 and stargazin, it has been abundantly described that post-translational modifications of the cytosolic tail of stargazin can regulate its interaction with PSD-95 and so the AMPAR complex mobility (Hafner et al., 2015; Matsuda et al., 2013; Opazo et al., 2010; Tomita et al., 2005a). Activation of phosphatases and kinases during LTD have been shown to be responsible of such type of modifications. Concerning the decrease of PSD-95 slots, Tang *et al.* reports a clear decrease of PSD-95 after NMDA treatment. Moreover, LTD triggers removal of PSD-95 and is thought to be a requirement for AMPAR suppression at synapses (Nelson et al., 2013b). In addition, LTD has been shown to trigger synaptic shrinkage and even pruning which has been correlated to a decrease of PSD-95 inside PSD (Woods et al., 2011).

We realized a series of experiments to discriminate between these three possibilities. We first expressed a genetic fusion between GluA2-subunit of AMPAR and stargazin and we measured the mobility of overexpressed GluA2-stargazin tandem after NMDAR-dependent LTD. As shown in **Figure 6**, preliminary results indicate an increase of AMPAR-Stg tandem mobility 20 minutes after LTD induction through NMDARs activation. This experiments need to be completed but they indicate that a fusion between AMPAR and stargazin does not occlude LTD-induced AMPAR increase of mobility. Then we realized the same experiments but using a tandem in which stargazin cytosolic tail has been mutated to mimic phosphorylation on nine residues (9 serine residues to 9 aspartate residues, S9D). This S9D mutant presents a higher level of interaction with PSD-95 (Hafner et al., 2015; Tomita et al., 2005a). Induction of LTD on neurons expressing AMPAR-stargazin S9D tandem does not trigger an increase of AMPAR mobility. These experiments suggest that AMPAR increase of mobility induced during the late phase of NMDAR-dependent LTD could be due to a modification of stargazin phosphorylation, decreasing the duration of interaction of AMPAR complex with PSD-95. This

dephosphorylation is impaired when the S9D mutant is expressed, suppressing the mobility increase.

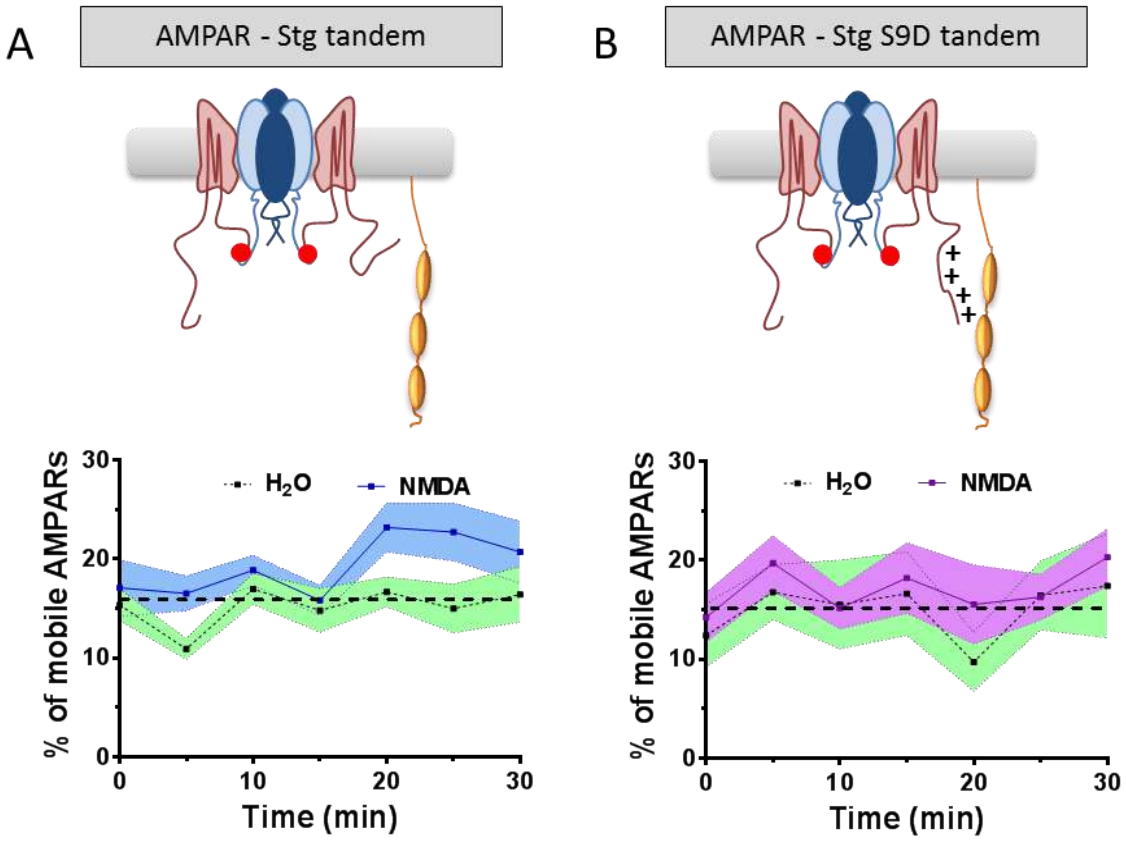

Figure 6. AMPAR mobility triggered by NMDAR-dependent LTD is blocked by the expression of phosphomimetic mutant of stargazin. (A) The upper panel is a schematic representation of the GluA2-stargazin tandem tracked using u-PAINT. The lower panel represents the average value of AMPAR mobile fraction over the time (0 – 30 minutes) after NMDA (blue) or H_2O treatment (green) (N = 9 and 6 respectively). (B) The upper panel is a schematic representation of the GluA2-stargazin S9D tandem tracked using u-PAINT. The lower panel represents the average value of AMPAR mobile fraction over the time (0 – 30 minutes) after NMDA (blue) or H_2O treatment (green) (N = 8 and 5 respectively).

The last experiment realized to understand the molecular determinant of AMPAR increase mobility, induced by NMDAR-dependent LTD, consists to characterize PSD-95 nanoscale organization before and after both NMDA- and ATP-induced LTD. As previously discussed, PSD-95 is the main scaffolding protein of excitatory synapses responsible for AMPAR immobilization. It has been shown that PSD-95 is organized in clusters of ~100nm, at least partly co-localized with AMPAR nanodomains (Fukata et al., 2013; MacGillavry et al., 2013; Nair et al., 2013). Tang *et al.* even reported that NMDA treatment induced a decrease of PSD-95 cluster intensity as well as a suppression of some clusters. Such decrease could be responsible of the observed increase of AMPAR mobility following NMDA treatment. To

confirm these results, we performed d-STORM experiments on hippocampal neurons labeled for endogenous PSD-95 in basal condition and 10 or 30 minutes after LTD induction via NMDA or ATP treatment. We measured both the number of PSD-95 per cluster and their diameter. We observed a 25% decrease of the PSD-95 content per cluster specifically during NMDAR-dependent LTD, without modification of PSD-95 cluster size (**Figure 7A-C**). This decrease of PSD-95 number per nanoclusters induced by NMDAR-dependent LTD protocol was not observed during P2XR-dependent LTD suggesting that this could be a reason why AMPAR lateral diffusion is increased during NMDAR- but not P2XR-dependent LTD.

To confirm the importance of PSD-95 reorganization in the increase of AMPAR mobility, we expressed PSD-95 mutated on T19. This threonine residue has been described as important for the decrease of synaptic PSD95 density during NMDAR-dependent LTD (Nelson et al., 2013b). Preliminary results shown in **Figure 7**D, reported a clear increase of AMPAR mobility in neurons transfected with the PSD-95 T19A mutant. Even if important, this result needs to be carefully interpreted because we did not test yet the effect of this mutation on the PSD-95 depletion during LTD with d-STORM techniques. In addition, electrophysiology recordings should as well been performed to measure the impact of PSD-95 over-expression on LTD induction. These experiments are in progress.

Altogether, these experiments seem to indicate that NMDAR-dependent LTD specifically induced a mobilization of AMPARs either through dephosphorylation of the stargazin, or through the partial suppression of PSD-95 at synapses. As this increase of mobility is not observed during ATP-induced LTD, this dynamic change should correspond to a specific modification of interaction within the AMPAR complex, and thus have a physiological meaning. To understand this physiological role, we then tested the effect of AMPAR mobility on synaptic transmission properties.

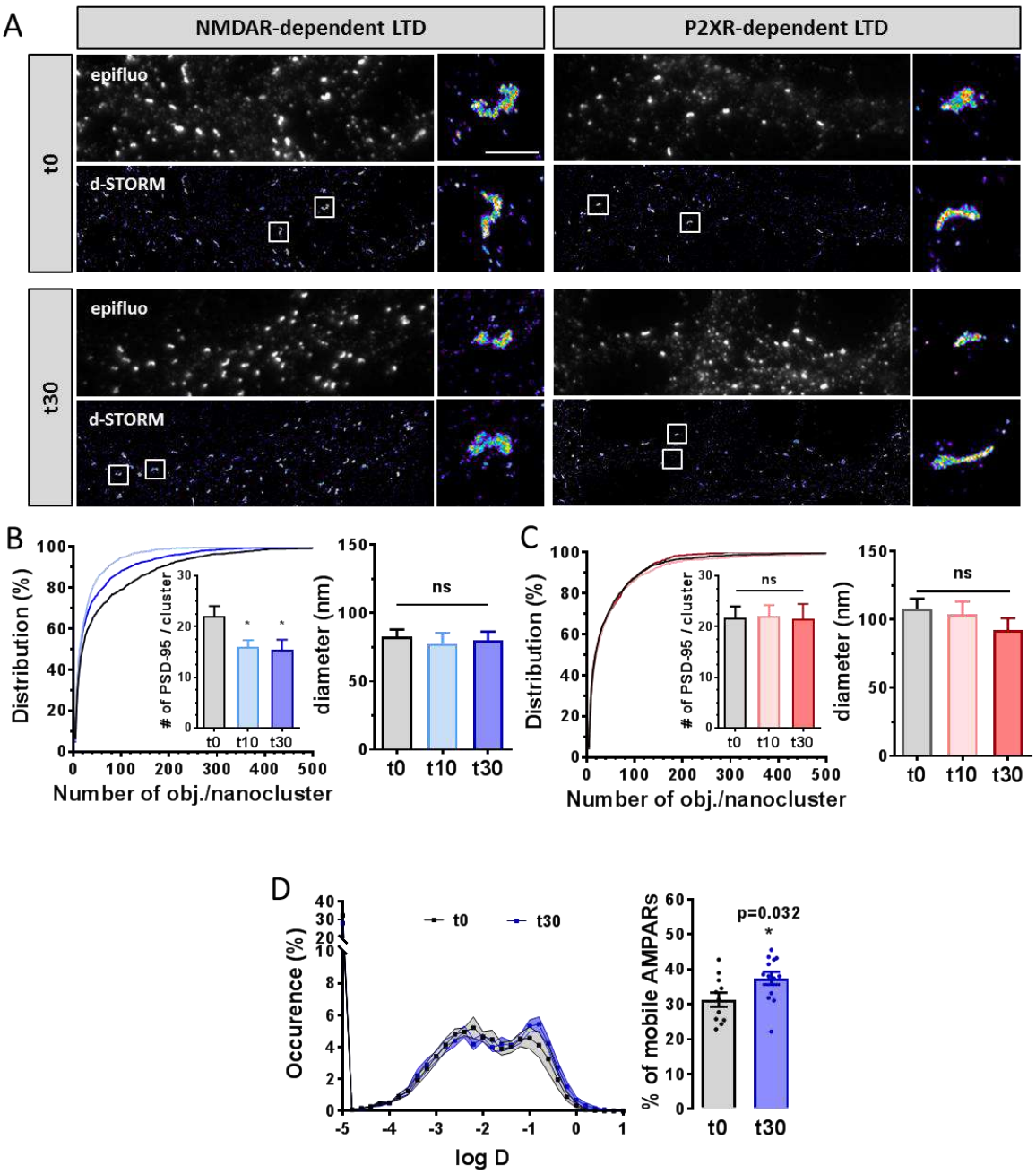

Figure 7. PSD-95 nano-clusters are reorganized specifically during NMDAR-dependent LTD. (A) Representative images of endogenous PSD-95 imaged with d-STORM technique (and the corresponding epifluorescence image) at basal state (upper images) and 30 minutes (lower images) after NMDA (left) or ATP (right) treatments. (B-C) The left panel represents the cumulative distribution of object number per nanocluster. Inserts represent the median value object/nanocluster for N number of cells. Right panel represents the median values of nanodomain diameter. (B) NMDAR-dependent LTD (t0, t10, t30) n = 11, 12, 12 cells respectively. (C) P2XR-dependent LTD (0, t10, t30) n = 11, 11, 10 respectively. One-way ANOVA tests with Tukey post test. (D) Tracking of endogenous GluA2-containing AMPAR in neurons expressing PSD-95 T19A. Left panel corresponds to the average distribution of the logarithmic diffusion coefficient of GluA2-containing AMPAR at basal state (grey) and 30 minutes after NMDA treatment (blue). Right panel represents the mean value of the mobile fraction at basal state and 30 minutes after NMDA treatment (N = 11, 13 cells respectively, unpaired t-test)

5. Increase in AMPAR mobility tunes short-term plasticity during NMDAR-dependent LTD

Our laboratory have previously shown that AMPAR mobility tunes frequency-dependent synaptic transmission in paired-pulse experiments in both culture neurons and hippocampal slices. We thus investigated if AMPAR increased mobility during NMDAR-dependent LTD was correlated with a change in short-term plasticity in hippocampal slices. To conserve the specific signaling pathway to trigger LTD, we applied NMDA in acute slices and examined if this protocol triggered LTD in this more physiological model. We measured field EPSP and quantified the slope of field potentials and normalized it to the fiber volley (**Figure 8A**). We observed a long lasting decrease of fEPSPs after NMDA treatment, confirming the validity of this cLTD protocol in hippocampal slices.

Next, we performed whole-cell patch clamp measurements of short-term synaptic plasticity. We applied 20 Hz stimulus trains to stimulate pre-synaptic axons and evoke a series of 5 EPSCs. In basal condition and consistent with what we demonstrated previously for paired-pulse protocols, we observed a short-term facilitation of the EPSCs. An increase of this short-term facilitation was observed 30 minutes after cLTD induction through NMDAR activation (**Figure 8B**).

Altogether, these results suggest that during NMDAR-dependent LTD, depressed synapses are capable to facilitate their responses to high-frequency inputs probably through an increase of AMPAR mobility.

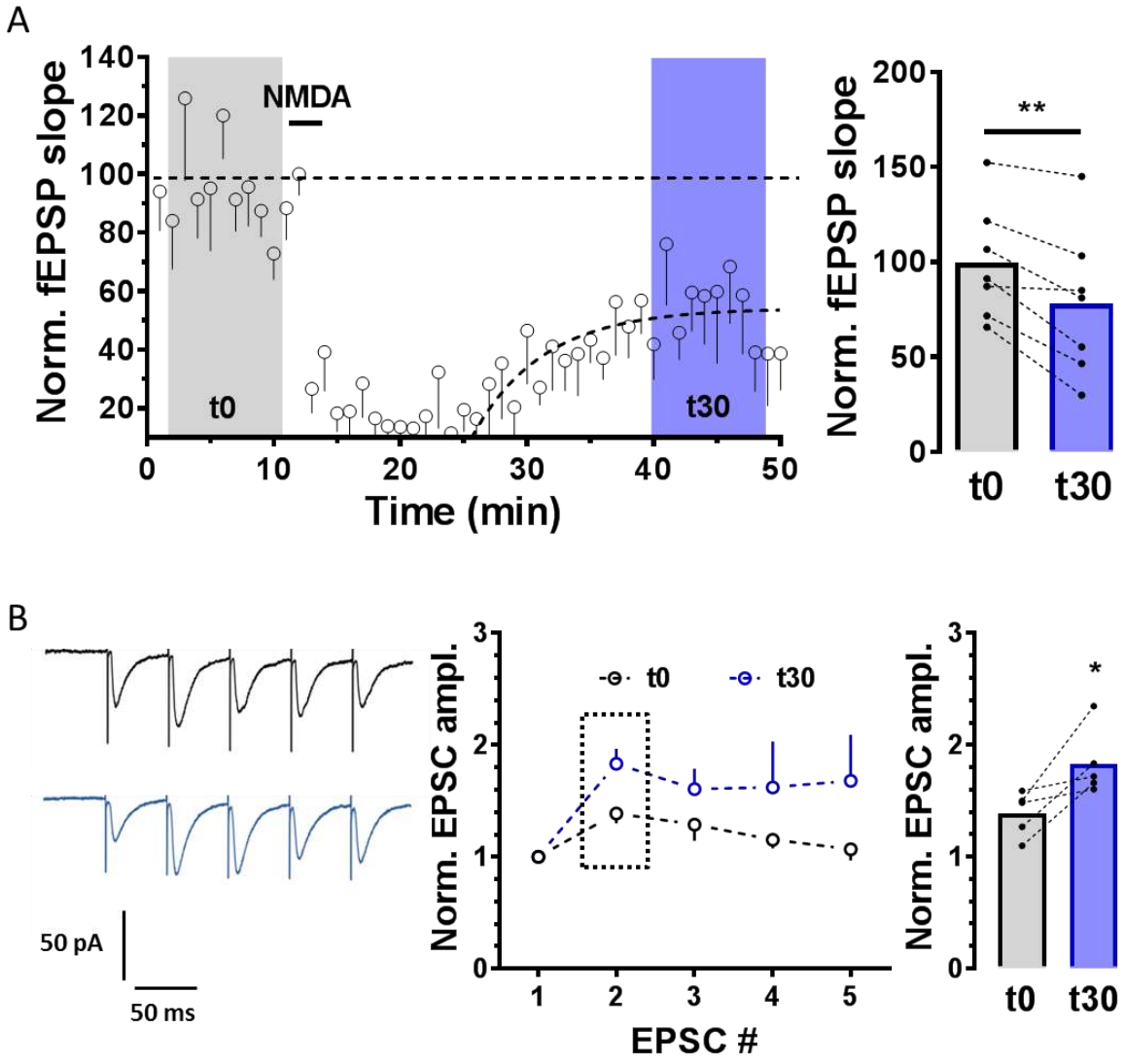

Figure 8. Increased in AMPAR mobility is correlated with an increase of paired-pulse response during NMDAR-dependent LTD. (A) field EPSP recording in acute hippocampal slices. Left panel corresponds to the normalized fEPSP slopes in function of time before and after NMDA perfusion (30 µM, 3 min). Right panel shows the mean value per slice of normalized fEPSP slope at basal state (grey zone and grey bar) and ~ 30 minutes after LTD induction (blue zone and blue bar). N = 7 slices, paired t-test. (B) Paired-Pulse stimulation recorded in whole-cell patch clamp in acute hippocampal slices before and 30 minutes after NMDAR-dependent LTD induction. Left panel shows representative eEPSC recorded following 5 stimulations at 20 Hz. Middle panel corresponds to the plot of the EPSC amplitude normalized to the initial EPSC for stimulations before and 30 minutes after NMDA perfusion. The right panel corresponds to the quantification of the Paired-Pulse Ratio between the 2nd EPSC and the 1st EPSC. N=5 slices, paired t-test.

6. Discussion and perspectives

Using super-resolution microscopy in fixed and live neurons, coupled to electrophysiological recording in culture and hippocampal slices, we have investigated the AMPAR organization changes induced by two forms of Long-Term Depression. We investigated the modification triggered either by the classical input-specific NMDAR-dependent LTD or by the newly described P2XR-dependent LTD. Our results suggest a dichotomy in the definition of LTD. Common to both NMDAR-dependent LTD and P2XR-dependent LTD is the reorganization of AMPARs at synapses involved in the depression of the synaptic input transfer. However, in a latter phase, a more deep reorganization of AMPAR complex at synapses lead to stable long-lasting new equilibrium between immobile receptors trapped into synaptic nanodomains and diffusive extra-nanodomain receptors. This latter phase allows synapses to maintain their capacity to respond to high-frequency stimulation, probably a key mechanism in spine selection and network refinement.

a. Depression of synaptic transmission is correlated to AMPAR nanodomain reorganization

Long-Term Depression has been extensively described to rely on either NMDARs or mGluRs activation. However, it has been recently shown that a similar long-lasting decrease of synaptic transmission through AMPAR internalization could be induced through the activation of post-synaptic purinergic receptors by astrocytic ATP. Based on the discovery of AMPAR nanodomains and their role in determining the Q value, we decided to investigate whether synaptic depression induced by both NMDAR- and P2XR-dependent LTD relied simply on AMPAR decreases at synapses or in a more precise reorganization of AMPAR nanodomains.

We first confirmed that both NMDA and ATP treatment, as described in the literature, triggered a long-lasting decrease of mEPSC amplitude (Lee et al., 1998; Pougnet et al., 2014). This decrease in synaptic strength was highly correlated to a depletion of synaptic AMPAR nanodomains for both forms of LTD. This result confirms once again that nanodomain content represents the post-synaptic quantum of response (Constals et al., 2015; Nair et al., 2013; Savtchenko and Rusakov, 2013).

However, as described previously, the synaptic quantum could relies on other parameters. While it is unlikely that the vesicular content in glutamate vary, the composition of AMPAR

complexes could vary. This will impact the conductance of receptors located at synapses and so change the quantum of response. It has been proposed that in the early phase of LTD, transient incorporation of AMPAR complexes during synaptic plasticity occurs. However, the modification of AMPAR complexes should lead to modifications of current kinetic, which has not been observed on our data. The more probable hypothesis regarding changes in AMPAR complexes during synaptic plasticity would be a change in the composition of auxiliary subunits surrounding AMPARs. This could affect both gating properties and location of AMPARs and thus modulate on a long-lasting manner synaptic transmission efficiency. However, this last point remains so far unstudied. Finally, another key feature able to regulate the efficiency of synaptic transmission is the location of AMPAR nanodomains with respect to glutamate release sites. It has been suggested that these alignments, as well as the density of AMPAR under release sites, would be the more optimal way to trigger an efficient and long-lasting change of synaptic strength (MacGillavry et al., 2013; Nair et al., 2013; Savtchenko and Rusakov, 2013).

Recently, Tang *et al.* have shown that pre-synaptic glutamate release sites and AMPAR nanodomains/PSD-95 clusters are aligned forming trans-synaptic nanocolumns. They reported that NMDA treatment suppressed some nano-columns by suppressing some PSD-95 clusters (Tang et al., 2016). However, we have no clues for now that pre-post alignment could be a physiological way to regulate synaptic strength.

Here we observed a clear decrease in the number of AMPAR nanodomain per spines after LTD induction. Changes in the number of either AMPAR nanodomains reported in this work or number of trans-synaptic nanocolumn reported in Tang *et al.* could provide an additional mechanism by which LTD could decrease the N number and thus the mEPSC frequency, other than the suppression of existing synapse (pruning). Experiments are currently on going to investigate if trans-synaptic nanocolumns represent a feature used during LTD to impact synaptic inputs. To that, we are performing dual-color d-STORM imaging to measure the accuracy of the alignment between AMPAR nanodomains and the glutamate release machinery in basal state and during various time point after both forms of LTD induction.

b. NMDAR-dependent LTD induces a specific increase in AMPAR lateral diffusion corresponding to a new dynamic equilibrium of synapses

We investigated AMPAR lateral diffusion during LTD. NMDAR-dependent LTD but not P2XR-dependent LTD triggered an increase of AMPAR mobility 20 minutes after induction. This increase of mobility corresponds to a new dynamic equilibrium of AMPAR at the cell

surface as indicated by its stability over hours (until at least 3 hours after induction). This increase of mobility happened relatively late after the LTD induction which takes place in the first 5 minutes after induction. This clearly indicates that the early reorganization of synaptic receptors inducing synaptic depression does not rely on this mobility changes. Literature always attributed LTD induction to endocytosis. Recently, Rosendale *et al.* directly measured endocytic events after NMDAR-dependent LTD and reported a rapid but transient increase of AMPAR endocytosis rate which comes back to its original level after only 10 minutes (Rosendale et al., 2017).

Altogether, these experiments allow us to suggest a new model of LTD, where the initial depression is linked to a massive endocytosis of AMPARs, depleting both dendritic and synaptic receptors. This first phase is triggered by a smooth displacement of AMPAR equilibrium between "dendritic mobile", "synaptic mobile" and "synaptic immobile" receptors. After 10 to 20 minutes, endocytosis rate drops down, and molecular modifications of AMPAR complexes decrease their affinity for synaptic traps, limiting their capacity to over-accumulate inside the nanodomains. This modification of AMPAR trapping stability maintains the depression for at least 3 hours.

As ATP treatment is not able to induce similar modification of AMPAR dynamic, we propose two distinct models of Long-Term Depression. The first model follows the activation of glutamatergic NMDA-type or mGluR-type receptors (input-specific LTD) and is composed of two phases as described above. A first phase based on AMPAR internalization and nanoscale reorganization at synapses, at the origin of the long-lasting decrease of AMPAR-mediated synaptic currents. After few minutes, a specific and precise molecular rearrangement of synapses leads to a change in AMPAR lateral diffusion.

The second model could be described as a neuromodulatory effect. On a similar manner than reported for insulin (Beattie et al., 2000), ATP released by astrocyte induces a global decrease of AMPAR surface expression, which depresses synaptic transmission. However, P2XR-dependent LTD triggers changes in AMPAR organization and synaptic transmission is not followed by a second phase. Indeed, ATP treatment did induce modifications neither of AMPAR lateral diffusion, nor of PSD-95 synaptic organization. This can be explained by the distinct signaling pathway implicated in P2XR-dependent LTD compare to input-specific LTD, as we demonstrated in collaboration with Boué-Grabot lab, see paper in Annex 2 (Pougnet et al., 2016, 2014). In the first paper in 2014, it clearly appears that ATP-induced LTD is not stable over time but return to initial synaptic strength after 40 to 50 minutes. It is possible that this form of LTD could be involved in regulation of synaptic transmission in specific cases

involving astrocytic control, while more classical forms of LTD (NMDAR- or mGluR-dependent LTD) are thought to be involved in cognitive functions and behavioral tasks.

c. Molecular mechanism of NMDAR-dependent LTD-induced increase of AMPAR lateral diffusion

The specific molecular modifications responsible of NMDAR-dependent LTD mobility increase has been investigated. Three main mechanisms could be involved, (i) the separation between AMPARs and its associated proteins, (ii) the modification of the interaction between associated proteins and traps formed by PSD-95, (iii) the decrease of PSD-95 synaptic slots. The first one, described recently in Constals *et al.* which requires conformational change of AMPARs can be abolished by stargazin-AMPAR tandem expression. However, in our conditions, the increase of mobility following NMDA treatment has been observed in neurons expressing this tandem.

Concerning the second possibility, post-translational modifications as phosphorylation of associated proteins is the main reason of AMPAR immobilization at synapse at basal state and during LTP (Hafner et al., 2015; Opazo et al., 2010; Sumioka et al., 2010; Tomita et al., 2005a). Moreover, modification of the phosphorylation level of AMPAR complex during LTD has been abundantly described (Matsuda et al., 2013; Tomita et al., 2005a). Using genetic manipulations and single particle tracking experiments, we started to investigate the possibility that change in stargazin phosphorylation state could be responsible for NMDAR-dependent LTD-mediated increase in AMPAR mobility. Preliminary results suggest that GluA2 subunit of AMPAR fused to S9D mutant of stargazin (mimicking constitutive phosphorylation) does not display increase in mobility while GluA2 subunit fused to wild-type stargazin seems to diffuse more during NMDAR-dependent LTD. However, stargazin dephosphorylation has been shown to play a role earlier and to be also involved in AMPAR internalization (Matsuda et al., 2013; Tomita et al., 2005a). Thus, this result need to be carefully interpreted and experiments need to be repeated before to conclude on the role of stargazin dephosphorylation in LTD-mediated increase in AMPAR mobility. It could also be interesting to investigate if AMPAR endocytosis is a pre-requisite for the increase in receptor mobility.

Finally, the last mechanism which has also been observed to regulate AMPAR mobility is based on the "slot theory". Indeed, lateral diffusion has been shown to be affected by the number of PSD-95 slots available at synapse (Arendt et al., 2010; Ehrlich and Malinow, 2004; Opazo et al., 2012; Stein et al., 2003). To test this possibility, we first investigated PSD-95 nano-

organization during both form of LTD. Using d-STORM, we have shown that PSD-95 is reorganized at the nanoscale at synapse during NMDAR-dependent LTD but remains unchanged during P2XR-dependent LTD. Similarly to AMPAR mobility increase, PSD-95 depletion occurs only following NMDA treatment, suggesting that these two effects could be correlated. To test this correlation, we investigated the effect of PSD-95 T19A mutant on AMPAR mobility following NMDA treatment. This mutant has been shown to block PSD-95 depletion during LTD. Preliminary results indicated that neurons overexpressing PSD-95 T19A still display an increase of AMPAR mobility during NMDAR-dependent LTD, suggesting that both effects could be distinct, while this result has to be confirmed and adequate controls have to be performed. Altogether, our results, even if preliminary for some of them, support the idea that LTD-induced AMPAR mobility is due to modification of associate proteins (stargazin in our case) phosphorylation level. Interestingly, we and other demonstrated that initial phase of LTD due to endocytosis, is triggered by changes in the AMPAR phosphorylation status. Such results suggest that various kinases/phosphatases which target AMPAR complexes are timely activated during LTD. In a first step, they will favor endocytosis by dephosphorylating AMPAR C-term domain, and in a second state they will affect AMPAR complexes mobility through modifications of the phosphorylation state of stargazin.

d. Increase in AMPAR mobility during input-specific LTD correlates with short-term facilitation

Our lab previously reported the role of AMPAR mobility in the capacity of synapses to respond to high frequency stimulation (Constals et al., 2015; Heine et al., 2008; Opazo et al., 2010). Here, we showed that change in AMPAR mobility during NMDAR-dependent LTD is associated with an increase in short-term plasticity. Such electrical effect could have important consequence first on the integration of synaptic inputs and network activity, even if the exact role of short term plasticity into synaptic integration is not well understood. Moreover, it could directly impact the synaptic fate.

Indeed, Wiegert and Oertner reported that inactive synapses are more susceptible to elimination when they are weakened by LTD (Wiegert and Oertner, 2013). They observed that following LTD, active synapses are maintained, and re-potentiate after couple of days while inactive one are pruned. We can hypothesized that the increase of AMPAR mobility during NMDAR-dependent LTD could be a molecular mechanism to select active synapses. The resulting short term facilitation, will maintain a relatively high level of calcium, avoiding the

pruning. Several experiments have been planned to investigate this hypothesis based on spine turnover measurement during NMDAR-dependent LTD to verify first that LTD triggers spine selection as previously reported (Oh et al., 2013; Wiegert and Oertner, 2013; Woods et al., 2011). In addition, if u-PAINT experiments in neurons expressing GluA2-stargazin S9D confirm that NMDAR-dependent LTD induces an increase of AMPAR mobility through stargazin dephosphorylation, it could be interesting to see if spine selection during LTD is still possible when the late increase of AMPAR mobility is blocked.

Through this work, we demonstrated that specific molecular modifications of AMPAR complex are implicated in the expression of a late phase during input-specific LTD. Such modifications are not similar when LTD is induced by a neuromodulatory path. We still have to understand the physiological role of such modifications, which trigger a new synaptic equilibrium and change its ability to integrate the temporal stimulation.

CONCLUSION AND PERSPECTIVES

Through my PhD, I learned the importance to decipher the precise molecular organization of synaptic proteins to understand the synaptic physiology. Although the synaptic input is only the first actor in the input/output relationship, and that several studies still need to be done to fully understand the functioning of synapses, I think that my PhD work helps to improve our current vision of synaptic transmission both in basal state and during synaptic plasticity.

Thus it is logical to start this conclusion by talking about our ability to observe this "infinitely small" with super-resolution microscopy and how this powerful method helped us to revisit synaptic transmission. Finally, I will discuss the importance of protein nanoscale organization and dynamic during synaptic plasticity though to store memories following learning processes.

1. Super-resolution microscopy, a powerful tool in neuroscience

It is fair to say that super-resolution microscopy has been my favourite technique all along my PhD. I discovered and learned this technique because of the scientific environment in the lab. I rapidly acquired the fundamental bases of various techniques of single-molecule localization microscopy (PALM/spt-PALM, u-PAINT and d-STORM). In addition, thanks to a close collaboration with Jean-Baptiste Sibarita's group which enriched my knowledge in the field, I participated to the improvement of techniques available at laboratory. Indeed, as reported in the Material & Methods chapter, work realized with Corey Butler allowed us to set up several tools which already improve the resolution obtained during acquisition, to perform multi-colours and/ or 3D imaging and to take into account achromatic aberrations. In parallel, these developments will be meaningless without the development of new analysis software. For that, and again in a close collaboration with Jean-Baptiste Sibarita's team, we provided imaging raw datas with specific concerns for them to improve their home made analysis software such as SR-Tesseler or PalmTracer.

The overall goal of this SMLM resolution improvement in the lab is to understand better how synaptic proteins within AMPAR complexes are organized and potentially to identify a new level of complexity of protein regulation which could be important at basal state or during synaptic plasticity as evoked in the previous chapter. While this has not been yet achieved, we are confident in the capacity to reach the required resolution in a close future.

Although SMLM is fully relevant for studying protein organization, I have repeatedly referred to structural changes which could occur probably in parallel to molecular

reorganization, particularly during synaptic plasticity and network connectivity refinement. However, to look at those structural changes, SMLM is not adapted and techniques such as electron microscopy or STED are more suitable. Even though I did not mentioned it in the manuscript as it was not important for the results described, it is interesting to indicate that a collaborative work between Sibarita-Nagerl-Choquet-Giannone groups, in which I am involved, has allowed to couple both STED and SMLM in live samples. This highly complex optical development has allowed us to measure in the same neuron the nanoscale organization of PSD-95 (spt-PALM), the AMPAR mobility (u-PAINT) and the spine morphology (STED) (**Inavalli *et al.*, submitted**). This technique could allow us in the future to directly correlate structural plasticity known to be involved in learning processes and synaptic plasticity at the molecular level.

2. New vision of synaptic transmission

Since the discoveries that AMPARs diffuse at the cell surface and get trapped into nanodomains at synapses, the vision of the functioning of synaptic transmission has changed considerably (Borgdorff and Choquet, 2002; Choquet and Triller, 2013; Nair et al., 2013). Indeed, the simple vision in which glutamatergic transmission simply depends on the number of glutamate released and on the number AMPARs located at synapses appeared more complex and more regulated. Especially by revisiting the concept of synaptic quantum, super-resolution and single-particle tracking microscopy help the scientific community to understand the importance of the precise dynamic organization of synaptic proteins at synapses.

It is now well accepted, since the observations in 2013 by three laboratories, that the PSD is sub-organized with PSD-95 nano-clusters and AMPAR nanodomains (Fukata et al., 2013; MacGillavry et al., 2013; Nair et al., 2013). As proposed by several mathematical models taking into account the properties of glutamate into the synaptic cleft (diffusion, affinity and transport), the discovery of AMPAR nanodomains confirmed the hypothesis that more important than the global number is the density of receptors present at synapses (Franks et al., 2002; Fukata et al., 2013; MacGillavry et al., 2013; Nair et al., 2013; Savtchenko and Rusakov, 2013). Thus, it was proposed by our lab that AMPAR nanodomain could represent the post-synaptic quantum of response as its content was shown to impact the intensity of the synaptic input.

However, the post-synaptic site cannot be considered as an independent structure and has to be always observed in association with the pre-synaptic site. Indeed, this nanodomain

organization influence the efficiency of synaptic transmission only in a dependent manner of the location of glutamate release site. Two possibilities were proposed following the observation of AMPAR clustering at synapses: (i) glutamate release can occurr randomly within the AZ, increasing the variability in the efficiency to activate AMPARs or (ii) release sites can be aligned with AMPAR nanodomains improving both efficiency and reliability of synaptic transmission (MacGillavry et al., 2013; Nair et al., 2013; Tarusawa et al., 2009). The recent observation of trans-synaptic nanocolumns, supported by our work based on the identification of neuroligin-neurexin as organizers of this alignment, improved our understanding on the importance of such precise organization of synaptic proteins (Tang et al., 2016, Haas et al submitted)

. During this work, we have also shown that synaptic efficiency was highly sensitive to the accuracy of the location of AMPAR nanodomain regarding glutamate release sites. This alignment, in addition to AMPAR clustering, is an important feature to take into account when investigating the synaptic quantum and the weight of synapses for neuronal integration.

During my PhD, I have been interested also to the mechanism by which synapses were capable to maintain a stable pool of receptors into nanodomains to ensure an efficient Q value. It has been demonstrated by our lab that lateral diffusion is a key parameter to compensate short-term depression due to receptor desensitization (Heine et al., 2008). However, it was difficult to reconcile the observed fast exchange of synaptic AMPARs and the need of the synapse to maintain a stable pool inside nanodomains.

Lateral diffusion has been shown to rely on the tripartite interaction between the receptor itself, auxiliary proteins such as stargazin and PSD-95, and regulation of either stargazin or PSD-95 can affect AMPAR lateral diffusion. In the Constals *et al.*, we reported that conformational state of AMPARs is a way to control receptors dynamic. Indeed, upon glutamate binding, receptors change their conformation to get desensitized, changing at the same time their affinity for their auxiliary protein and thus releasing them from synaptic trapping sites. This new mechanism, explain how synapses can maintain a pool of naïve receptors at synapses through exchange between desensitized receptors being untrapped and naïve diffusive receptors getting trapped during high-frequency stimulations (Constals et al., 2015).

Although this study has provided significant insights in the time scale during which AMPARs could change affinity with proteins of its interactome, it has also raised several questions such as the specificity of this mechanism between AMPAR and stargazin. Indeed,

AMPARs can interact with several different auxiliary proteins, sometimes few at the same time. How AMPAR conformational changes affect its affinity with others proteins within the complex? Could it be a way to modify AMPAR macromolecular complex composition on a rapid manner during activity? Those questions are interesting when taking into account the spectrum of effects that various auxiliary proteins can have on AMPAR trafficking and/or gating properties. These open questions would probably require super-resolution microscopy with improved resolution to decipher AMPAR complex in function of synaptic activity.

Through this work concerning the nanoscale organization and dynamic of AMPA receptors, we succeed to draft a more accurate vision of the synaptic transmission properties. Less than 20 years ago, the classical vision presented a synapse in which receptors were immobile inside the entire PSD for hours and days, exchanging sometimes per endocytosis/exocytosis. We know now that AMPARs are grouped in small domains located in front of glutamate release site to optimize synaptic transmission efficiency. The sensitivity of synaptic transmission to this alignment, reported in chapter 1 of the results, confirmed initial experiments and modelling from Richard Tsien's lab describing a sharp area where glutamate can activate AMPARs (Lisman et al., 2007b; Liu et al., 1999). Synaptic transmission was mainly based on pre-synaptic number of glutamate per vesicle but we now have a more cooperative view, based on four main parameters: (i) the number of glutamate per vesicle, (ii) the AMPAR density inside domains, (iii) the co-organization between AMPAR nanodomains and pre-synaptic release sites, and (iv) the AMPAR macromolecular complex composition.

3. Importance of the dynamic nanoscale organization for neuronal plasticity

Synapses are plastic compartments of neurons. They can be strengthen or weaken through specific input patterns. These changes have been extensively shown to be dependent on a regulation of the number of AMPARs at synapses through exocytosis and endocytosis. However, the new level of complexity regarding the molecular surface dynamic organization has driven us to go deeper in the understanding of the precise rearrangement of protein in the control of synaptic strength. The final aimed of my PhD has been to investigate the role of the previously described parameters (nanoscale organization and lateral diffusion) during LTD.

Comparing two forms of synaptic depression, I have demonstrated that the classical definition of LTD, meaning a decrease of synaptic strength through an internalization of AMPARs is not sufficient to describe this phenomenon. Although it is true that the initial phase

at the origin of synaptic weakening is correlated to AMPAR endocytosis, it is also linked to a precise reorganization of AMPARs at synapses. This initial phase is followed, specifically during input-specific LTD, by a full molecular reorganization of synapses, increasing AMPAR diffusion as well as synaptic capacity to respond to high-frequency inputs. This last point is important knowing that one major feature of LTD is a structural plasticity. Indeed, LTD induction has been shown to lead to spine elimination and thus to refine the network connectivity (N value). The physiological impact of this structural modification appears to be of prime importance as demonstrated by *in vivo* experiments which have shown that learning, sensory-experience, and behavioural flexibility induce changes in synapse turnover (spine formation, maintenance and elimination). We hypothesize that initial molecular reorganization of synapses could be the first step for structural plasticity. Regarding LTD, the link between AMPAR depletion at synapses to weaken synaptic transmission, change in mobility to favour synaptic responsiveness and synaptic pruning is not clear. Our hypothesis is that synaptic depression allows, by specific modifications of AMPAR dynamic organization, to suppress weakly integrated synapses and to maintain important synapses based on their input patterns. In this way, the Q and N values, important for neuronal signal integration, appears to be regulated by nanoscale organization of synaptic proteins. In addition, even if we didn't investigate this parameter, it is important to keep in mind that the P_r value also probably relies on nanoscale regulation of the presynaptic release machinery and could as well be modified during long-term plasticity. Although several regulation of this synaptic inputs occur between the synaptic inputs and the output generation, as well as parallel mechanisms such as change in neuronal excitability or change in the inhibitory inputs, it suggests a key role of the organization at this nanoscale in the input/output balance which should be further investigated.

BIBLIOGRAPHY

Abbott, L.F. (1997). Synaptic Depression and Cortical Gain Control. Science (80-.). *275*, 221–224.

Abraham, W.C., and Goddard, G. V (1983). Asymmetric relationships between homosynaptic long-term potentiation and heterosynaptic long-term depression. Nature *305*, 717–719.

Acuna, C., Guo, Q., Burré, J., Sharma, M., Sun, J., and Südhof, T.C. (2014). Microsecond dissection of neurotransmitter release: SNARE-complex assembly dictates speed and Ca2+ sensitivity. Neuron *82*, 1088–1100.

Acuna, C., Liu, X., Gonzalez, A., and Südhof, T.C. (2015). RIM-BPs Mediate Tight Coupling of Action Potentials to Ca^{2+}-Triggered Neurotransmitter Release. Neuron *87*, 1234–1247.

Acuna, C., Liu, X., and Südhof, T.C. (2016). How to Make an Active Zone: Unexpected Universal Functional Redundancy between RIMs and RIM-BPs. Neuron *91*, 792–807.

Arendt, K.L., Royo, M., Fernández-Monreal, M., Knafo, S., Petrok, C.N., Martens, J.R., and Esteban, J. a (2010). PIP3 controls synaptic function by maintaining AMPA receptor clustering at the postsynaptic membrane. Nat. Neurosci. *13*, 36–44.

Armstrong, N., Jasti, J., Beich-Frandsen, M., and Gouaux, E. (2006). Measurement of Conformational Changes accompanying Desensitization in an Ionotropic Glutamate Receptor. Cell *127*, 85–97.

Ashby, M.C., De La Rue, S. a, Ralph, G.S., Uney, J., Collingridge, G.L., and Henley, J.M. (2004). Removal of AMPA receptors (AMPARs) from synapses is preceded by transient endocytosis of extrasynaptic AMPARs. J. Neurosci. *24*, 5172–5176.

Auger, C., and Marty, A. (2000). Quantal currents at single-site central synapses. J. Physiol. *526*, 3–11.

Bashir, Z.I., Jane, D.E., Sunter, D.C., Watkins, J.C., and Collingridge, G.L. (1993). Metabotropic glutamate receptors contribute to the induction of long-term depression in the CA1 region of the hippocampus. Eur. J. Pharmacol. *239*, 265–266.

Bats, C., Groc, L., and Choquet, D. (2007). The Interaction between Stargazin and PSD-95 Regulates AMPA Receptor Surface Trafficking. Neuron *53*, 719–734.

Bats, C., Soto, D., Studniarczyk, D., Farrant, M., and Cull-Candy, S. (2012). Channel properties reveal differential expression of TARPed and TARPless AMPARs in stargazer neurons. Nat. Neurosci. *15*.

Beattie, E.C., Carroll, R.C., Yu, X., Morishita, W., Yasuda, H., von Zastrow, M., and Malenka, R.C. (2000). Regulation of AMPA receptor endocytosis by a signaling mechanism shared with LTD. Nat. Neurosci. *3*, 1291–1300.

Betzig, E., Patterson, G.H., Sougrat, R., Lindwasser, O.W., Olenych, S., Bonifacino, J.S., Davidson, M.W., Lippincott-Schwartz, J., and Hess, H.F. (2006). Imaging Intracellular Fluorescent Proteins at Nanometer Resolution. Science (80-.). *313*, 1642–1645.

Bhattacharyya, S., Biou, V., Xu, W., Schlüter, O., and Malenka, R.C. (2009). A critical role for PSD-95/AKAP interactions in endocytosis of synaptic AMPA receptors. Nat. Neurosci. *12*, 172–181.

Bliss, T. V, and Collingridge, G.L. (1993). A synaptic model of memory: long-term potentiation in the hippocampus. Nature *361*, 31–39.

Bliss, T.V.P., and Lømo, T. (1973). Long-Lasting Potentiation of Synaptic Transmission in the Dentate Area of the Anaesthetized Rabbit Following Stimulation of the Perforant Path. J.

Physiol. *232*, 331–356.

Borgdorff, A.J., and Choquet, D. (2002). Regulation of AMPA receptor lateral movements. Nature *417*, 649–653.

Branco, T., and Staras, K. (2009). The probability of neurotransmitter release: variability and feedback control at single synapses. Nat. Rev. Neurosci. *10*, 373–383.

Brenowitz, S., and Trussell, L.O. (2001). Minimizing synaptic depression by control of release probability. J. Neurosci. *21*, 1857–1867.

Burrone, J., and Lagnado, L. (2000). Synaptic depression and the kinetics of exocytosis in retinal bipolar cells. J. Neurosci. *20*, 568–578.

Carroll, R.C., Lissin, D. V, von Zastrow, M., Nicoll, R. a, and Malenka, R.C. (1999). Rapid redistribution of glutamate receptors contributes to long-term depression in hippocampal cultures. Nat. Neurosci. *2*, 454–460.

Carroll, R.C., Beattie, E.C., von Zastrow, M., and Malenka, R.C. (2001). Role of AMPA receptor endocytosis in synaptic plasticity. Nat Rev Neurosci *2*, 315–324.

Casimiro, T., Sossa, K.G., Uzunova, G., Beattie, J.B., Kurt, C., and Carroll, R.C. (2011). mGluR and NMDAR activation internalize distinct populations of Mol Cell Neurosci . 2011 October ; 48(2): 161–170. doi:10.1016/j.mcn.2011.07.007. AMPARs. Mol. Cell Neurosci. *48*, 161–170.

Del Castillo, J., and Katz, B. (1954). Quantal Components of the End-Plate Potential. J. Physiol *124*, 560–573.

Chen, C., Blitz, D.M., and Regehr, W.G. (2002). Contributions of receptor desensitization and saturation to plasticity at the retinogeniculate synapse. Neuron *33*, 779–788.

Chen, G., Harata, N.C., and Tsien, R.W. (2004). Paired-pulse depression of unitary quantal amplitude at single hippocampal synapses. Proc. Natl. Acad. Sci. U. S. A. *101*, 1063–1068.

Chen, L., Chetkovich, D.M., Petralia, R.S., Sweeney, N.T., Kawasaki, Y., Wenthold, R.J., Bredt, D.S., and Nicoll, R. a (2000). Stargazin regulates synaptic targeting of AMPA receptors by two distinct mechanisms. Nature *408*, 936–943.

Chen, X., Nelson, C.D., Li, X., Winters, C.A., Azzam, R., Sousa, A.A., Leapman, R.D., Gainer, H., Sheng, M., and Reese, T.S. (2011). PSD-95 Is Required to Sustain the Molecular Organization of the Postsynaptic Density. J. Neurosci. *31*, 6329–6338.

Chen, Shanshuang; Yan Zhao, Yuhang (Steven) Wang, Mrinal Shekhar, Emad Tajkhorshid, and E.G. (2017). Activation and desensitization mechanism of AMPA receptor - TARP complex by cryo-EM. Cell Press 1–13.

Choquet, D., and Triller, A. (2013). The dynamic synapse. Neuron *80*, 691–703.

Cole, A.A., Chen, X., and Reese, T.S. (2016). A Network of Three Types of Filaments Organizes Synaptic Vesicles for Storage, Mobilization, and Docking. J. Neurosci. *36*, 3222–3230.

Collingridge, G.L., Peineau, S., Howland, J.G., and Wang, Y.T. (2010). Long-term depression in the CNS. Nat. Rev. Neurosci. *11*, 459–473.

Colquhoun, B.Y.D., Jonas, P., and Sakmann, B. (1992). Zellphysiologie, 6900. 261–287.

Compans, B., Choquet, D., and Hosy, E. (2016). Review on the role of AMPA receptor nano-organization and dynamic in the properties of synaptic transmission. Neurophotonics *3*, 41811.

Constals, A., Penn, A.C., Compans, B., Toulmé, E., Phillipat, A., Marais, S., Retailleau, N., Hafner, A.S., Coussen, F., Hosy, E., et al. (2015). Glutamate-Induced AMPA Receptor Desensitization Increases Their Mobility and Modulates Short-Term Plasticity through Unbinding from Stargazin. Neuron *85*, 787–803.

Coultrap, S.J., Freund, R.K., O'Leary, H., Sanderson, J.L., Roche, K.W., Dell'Acqua, M.L., and Bayer, K.U. (2014). Autonomous CaMKII mediates both LTP and LTD using a mechanism for differential substrate site selection. Cell Rep. *6*, 431–437.

Crozier, R. a, Wang, Y., Liu, C.-H., and Bear, M.F. (2007). Deprivation-induced synaptic depression by distinct mechanisms in different layers of mouse visual cortex. Proc. Natl. Acad. Sci. U. S. A. *104*, 1383–1388.

Cummings, J. a., Mulkey, R.M., Nicoll, R. a., and Malenka, R.C. (1996). Ca2+ signaling requirements for long-term depression in the hippocampus. Neuron *16*, 825–833.

Dan, Y., and Poo, M.M. (2004). Spike timing-dependent plasticity of neural circuits. Neuron *44*, 23–30.

Dani, A., Huang, B., Bergan, J., Dulac, C., and Zhuang, X. (2010). Superresolution Imaging of Chemical Synapses in the Brain. Neuron *68*, 843–856.

Denker, A., and Rizzoli, S.O. (2010). Synaptic vesicle pools: An update. Front. Synaptic Neurosci. *2*, 1–12.

Derkach, V.A., Oh, M.C., Guire, E.S., and Soderling, T.R. (2007). Regulatory mechanisms of AMPA receptors in synaptic plasticity. Nat. Rev. Neurosci. *8*, 101–113.

Deschout, H., Cella Zanacchi, F., Mlodzianoski, M., Diaspro, A., Bewersdorf, J., Hess, S.T., and Braeckmans, K. (2014). Precisely and accurately localizing single emitters in fluorescence microscopy. Nat. Methods *11*, 253–266.

Dittman, J.S., Kreitzer, A.C., and Regehr, W.G. (2000). Interplay between facilitation, depression, and residual calcium at three presynaptic terminals. J. Neurosci. *20*, 1374–1385.

Dobrunz, L.E., and Stevens, C.F. (1997). Heterogeneity of release probability, facilitation, and depletion at central synapses. Neuron *18*, 995–1008.

Doussau, F., and Augustine, G.J. (2000). The actin cytoskeleton and neurotransmitter release: An overview. Biochimie *82*, 353–363.

Dudek, S.M., and Bear, M.F. (1992). Homosynaptic long-term depression in area CA1 of hippocampus and effects of N-methyl-D-aspartate receptor blockade. Proc. Natl. Acad. Sci. U. S. A. *89*, 4363–4367.

Dürr, K.L., Chen, L., Stein, R.A., De Zorzi, R., Folea, I.M., Walz, T., McHaourab, H.S., and Gouaux, E. (2014). Structure and dynamics of AMPA receptor GluA2 in resting, pre-open, and desensitized states. Cell *158*, 778–792.

Ehrlich, I., and Malinow, R. (2004). Postsynaptic Density 95 controls AMPA Receptor Incorporation during Long-Term Potentiation and Experience-Driven Synaptic Plasticity. J. Neurosci. *24*, 916–927.

El-Husseini, A.E.D., Schnell, E., Dakoji, S., Sweeney, N., Zhou, Q., Prange, O., Gauthier-Campbell, C., Aguilera-Moreno, A., Nicoll, R. a., and Bredt, D.S. (2002). Synaptic strength regulated by palmitate cycling on PSD-95. Cell *108*, 849–863.

El-Husseini, a E., Schnell, E., Chetkovich, D.M., Nicoll, R. a, and Bredt, D.S. (2000). PSD-95 involvement in maturation of excitatory synapses. Science *290*, 1364–1368.

Elias, G.M., Funke, L., Stein, V., Grant, S.G., Bredt, D.S., and Nicoll, R.A. (2006). Synapse-Specific and Developmentally Regulated Targeting of AMPA Receptors by a Family of MAGUK Scaffolding Proteins. Neuron *52*, 307–320.

Engelhardt, J. Von, Mack, V., Sprengel, R., Kavenstock, N., Li, K.W., Stern-bach, Y., Smit, A.B., Seeburg, P.H., and Monyer, H. (2010). Plasticity in the Dentate Gyrus. Situ *60*, 1518–1522.

Ermolyuk, Y.S., Alder, F.G., Surges, R., Pavlov, I.Y., Timofeeva, Y., Kullmann, D.M., and Volynski, K.E. (2013). Differential triggering of spontaneous glutamate release by P/Q-, N- and R-type Ca2+ channels. Nat. Neurosci. *16*, 1754–1763.

Fatt, P., and Katz, B. (1951). An analysis of the end-plate potential recorded with an intra-cellular electrode. J. Physiol. *115*, 320–370.

Ferraguti, F., and Shigemoto, R. (2006). Metabotropic glutamate receptors. Cell Tissue Res. *326*, 483–504.

Forster, and Sherrington (1897). A text book of physiology.

Fortune, E.S., and Rose, G.J. (2000). Short-term synaptic plasticity contributes to the temporal filtering of electrosensory information. J. Neurosci. *20*, 7122–7130.

Fortune, E.S., and Rose, G.J. (2001). MARCM Erratum Short-term synaptic plasticity as a temporal filter. Trends Neurosci. *24*, 381–385.

Franks, K.M., Bartol, T.M., and Sejnowski, T.J. (2002). A Monte Carlo model reveals independent signaling at central glutamatergic synapses. Biophys. J. *83*, 2333–2348.

Franks, K.M., Stevens, C.F., and Sejnowski, T.J. (2003). Independent sources of quantal variability at single glutamatergic synapses. J. Neurosci. *23*, 3186–3195.

Frischknecht, R., Heine, M., Perrais, D., Seidenbecher, C.I., Choquet, D., and Gundelfinger, E.D. (2009). Brain extracellular matrix affects AMPA receptor lateral mobility and short-term synaptic plasticity. Neuroforum *15*, 94–95.

Fukata, Y., Dimitrov, A., Boncompain, G., Vielemeyer, O., Perez, F., and Fukata, M. (2013). Local palmitoylation cycles define activity-regulated postsynaptic subdomains. J. Cell Biol. *202*, 145–161.

Geppert, M., Goda, Y., Stevens, C.F., and Sudhof, T.C. (1997). The small GTP-binding protein Rab3A regulates a late step in synaptic vesicle fusion. Nature *387*, 810–814.

Giannone, G., Hosy, E., Levet, F., Constals, A., Schulze, K., Sobolevsky, A.I., Rosconi, M.P., Gouaux, E., Tampe, R., Choquet, D., et al. (2010). Dynamic superresolution imaging of endogenous proteins on living cells at ultra-high density. Biophys. J. *99*, 1303–1310.

Gill, M.B., Kato, A.S., Roberts, M.F., Yu, H., Wang, H., Tomita, S., and Bredt, D.S. (2011). Cornichon-2 modulates AMPA receptor-transmembrane AMPA receptor regulatory protein assembly to dictate gating and pharmacology. J. Neurosci. *31*, 6928–6938.

Gladding, C.M., Fitzjohn, S.M., and Molnar, E. (2009). Metabotropic Glutamate Receptor-Mediated Long- Term Depression : Molecular Mechanisms. Pharmacol. Rev. *61*, 395–412.

Glebov, O.O., Jackson, R.E., Winterflood, C.M., Owen, D.M., Barker, E.A., Doherty, P., Ewers, H., and Burrone, J. (2017). Nanoscale Structural Plasticity of the Active Zone Matrix Modulates Presynaptic Function. Cell Rep. *18*, 2715–2728.

Goda, Y., and Davis, G.W. (2003). Mechanisms of synapse assembly and disassembly. Neuron *40*, 243–264.

Goda, Y., and Stevens, C.F. (1998). Readily releasable pool size changes associated with long term depression. Proc. Natl. Acad. Sci. U. S. A. *95*, 1283–1288.

Goodell, D.J., Zaegel, V., Coultrap, S.J., Hell, J.W., and Bayer, K.U. (2017). DAPK1 Mediates LTD by Making CaMKII/GluN2B Binding LTP Specific. Cell Rep. *19*, 2231–2243.

Granger, A.J., Shi, Y., Lu, W., Cerpas, M., and Nicoll, R. a (2013). LTP requires a reserve pool of glutamate receptors independent of subunit type. Nature *493*, 495–500.

Grauel, M.K., Maglione, M., Reddy-Alla, S., Willmes, C.G., Brockmann, M.M., Trimbuch, T., Rosenmund, T., Pangalos, M., Vardar, G., Stumpf, A., et al. (2016). RIM-binding protein 2 regulates release probability by fine-tuning calcium channel localization at murine hippocampal synapses. Proc. Natl. Acad. Sci. *113*, 11615–11620.

Gray, E.G. (1959). Electron Microscopy of Synaptic Contacts on Dendrite Spines of the Cerebral Cortex. Nature *183*, 1592–1593.

Greger, I.H., and Esteban, J.A. (2007). AMPA receptor biogenesis and trafficking. Curr. Opin. Neurobiol. *17*, 289–297.

Greger, I.H., Watson, J.F., and Cull-Candy, S.G. (2017). Structural and Functional Architecture of AMPA-Type Glutamate Receptors and Their Auxiliary Proteins. Neuron *94*, 713–730.

Groc, L., Heine, M., Cognet, L., Brickley, K., Stephenson, F.A., Lounis, B., and Choquet, D. (2004). Differential activity-dependent regulation of the lateral mobilities of AMPA and NMDA receptors. Nat. Neurosci. *7*, 695–696.

Groc, L., Heine, M., Cousins, S.L., Stephenson, F.A., Lounis, B., Cognet, L., and Choquet, D. (2006). NMDA receptor surface mobility depends on NR2A-2B subunits. Proc. Natl. Acad. Sci. U. S. A. *103*, 18769–18774.

Groc, L., Lafourcade, M., Heine, M., Renner, M., Racine, V., Sibarita, J.-B., Lounis, B., Choquet, D., and Cognet, L. (2007). Surface trafficking of neurotransmitter receptor: comparison between single-molecule/quantum dot strategies. J. Neurosci. *27*, 12433–12437.

Grubb, M.S., and Burrone, J. (2010). Activity-dependent relocation of the axon initial segment fine-tunes neuronal excitability. Nature *465*, 1070–1074.

Hafner, A.S., Penn, A.C., Grillo-Bosch, D., Retailleau, N., Poujol, C., Philippat, A., Coussen, F., Sainlos, M., Opazo, P., and Choquet, D. (2015). Lengthening of the stargazin cytoplasmic tail increases synaptic transmission by promoting interaction to deeper domains of PSD-95. Neuron *86*, 475–489.

Harris, K.M., Weinberg, R.J., Long-term, N.R., Lüscher, C., Malenka, R.C., Harris, K.M., Weinberg, R.J., Smart, T.G., Paoletti, P., and Südhof, C. (2013). Ultrastructure of Synapses in the Mammalian Brain Ultrastructure of Synapses in the.

Häusser, M. (2001). Synaptic function: Dendritic democracy. Curr. Biol. *11*, 10–12.

Häusser, M., Stuart, G., Racca, C., and Sakmann, B. (1995). Axonal initiation and active dendritic propagation of action potentials in substantia nigra neurons. Neuron *15*, 637–647.

Hebb, D.O. (1949). The Organization of Behavior; A Neuropsychological Theory. Am. J. Psychol. *63*, 633.

Heine, M., Groc, L., Frischknecht, R., Bei que, J.-C., Lounis, B., Rumbaugh, G., Huganir, R.L., Cognet, L., and Choquet, D. (2008). Surface Mobility of Postsynaptic AMPARs Tunes Synaptic Transmission. Science (80-.). *320*, 201–205.

Herguedas, B., Garcia-Nafria, J., Cais, O., Fernandez-Leiro, R., Krieger, J., Ho, H., and Greger,

I.H. (2016). Structure and organization of heteromeric AMPA-type glutamate receptors. Science (80-.). *352*, aad3873-aad3873.

Heuser, J.E., Reese, T.S., Dennis, M.J., Jan, Y., Jan, L., and Evans, L. (1979). Synaptic vesicle exocytosis captured by quick freezing and correlated with quantal transmitter release. J. Cell Biol. *81*, 275–300.

Hjelmstad, G.O., Nicoll, R.A., and Malenka, R.C. (1997). Synaptic refractory period provides a measure of probability of release in the hippocampus. Neuron *19*, 1309–1318.

Hollmann, M., and Heinemann, S. (1994). Cloned Glutamate. Annu Rev Neurosci 31–108.

Holtmaat, A., and Caroni, P. (2016). Functional and structural underpinnings of neuronal assembly formation in learning. Nat. Neurosci. *19*, 1553–1562.

Holtmaat, A., and Svoboda, K. (2009). Experience-dependent structural synaptic plasticity in the mammalian brain. Nat. Rev. Neurosci. *10*, 647–658.

Hubel, D.H., and Wiesel, T.N. (1965). Binocular interaction reared in striate artificial cortex squint. J. Neurophysiol. *28*, 1041–1059.

Huber, K.M., Roder, J.C., Bear, M.F., Choi, C.H., Schoenfeld, B.P., Weisz, E.D., Bell, A.J., Chambers, D.B., Hinchey, J., Choi, R.J., et al. (2001). Chemical Induction of mGluR5- and Protein Synthesis − Dependent Long-Term Depression in Hippocampal Area CA1 Chemical Induction of mGluR5- and Protein Synthesis – Dependent Long-Term Depression in Hippocampal Area CA1. J Neurophysiol. *86*, 321–325.

Huganir, R.L., and Nicoll, R.A. (2013). AMPARs and synaptic plasticity: The last 25 years. Neuron *80*, 704–717.

Huxley, A.F. (2002). Classical perspectives. J. Physiol. *538*, 1–2.

Isaac, J.T.R., Nicoll, R. a., and Malenka, R.C. (1995). Evidence for silent synapses: Implications for the expression of LTP. Neuron *15*, 427–434.

Izeddin, I., Boulanger, J., Racine, V., Specht, C.G., Kechkar, a, Nair, D., Triller, a, Choquet, D., Dahan, M., and Sibarita, J.B. (2012). Wavelet analysis for single molecule localization microscopy. Opt. Express *20*, 2081–2095.

Jackson, A.C., and Nicoll, R.A. (2011). The Expanding Social Network of Ionotropic Glutamate Receptors: TARPs and Other Transmembrane Auxiliary Subunits. Neuron *70*, 178–199.

Jahn, R., and Fasshauer, D. (2012). Molecular machines governing exocytosis of synaptic vesicles. Nature *490*, 201–207.

Jin, R., Singh, S.K., Gu, S., Furukawa, H., Sobolevsky, A.I., Zhou, J., Jin, Y., and Gouaux, E. (2009). Crystal structure and association behaviour of the GluR2 amino-terminal domain. EMBO J. *28*, 1812–1823.

Jungmann, R., Avendaño, M.S., Woehrstein, J.B., Dai, M., Shih, W.M., and Yin, P. (2014). Multiplexed 3D cellular super-resolution imaging with DNA-PAINT and Exchange-PAINT. Nat. Methods *11*, 313–318.

Kaech, S., and Banker, G. (2006). Culturing hippocampal neurons. Nat. Protoc. *1*, 2406–2415.

Kaeser, P.S., Deng, L., Wang, Y., Dulubova, I., Liu, X., Rizo, J., and Südhof, T.C. (2011). RIM proteins tether Ca2+ channels to presynaptic active zones via a direct PDZ-domain interaction. Cell *144*, 282–295.

Karataeva, A.R., Klaassen, R. V., Stroder, J., Ruiperez-Alonso, M., Hjorth, J.J.J., Van Nierop, P., Spijker, S., Mansvelder, H.D., and Smit, A.B. (2014). C-terminal interactors of the AMPA receptor auxiliary subunit Shisa9. PLoS One *9*.

Kato, A.S., Gill, M.B., Ho, M.T., Yu, H., Tu, Y., Siuda, E.R., Wang, H., Qian, Y.W., Nisenbaum, E.S., Tomita, S., et al. (2010). Hippocampal AMPA Receptor Gating Controlled by Both TARP and Cornichon Proteins. Neuron *68*, 1082–1096.

Kim, M.J., Futai, K., Jo, J., Hayashi, Y., Cho, K., and Sheng, M. (2007). Synaptic Accumulation of PSD-95 and Synaptic Function Regulated by Phosphorylation of Serine-295 of PSD-95. Neuron *56*, 488–502.

Klaassen, R. V, Stroeder, J., Coussen, F., Petersen, J.D., Renancio, C., Lodder, J.C., Diana, C., Schmitz, L.J.M., Rao-ruiz, P., Spijker, S., et al. Shisa6 traps AMPARs at postsynaptic sites and prevents their desensitization during high frequency synaptic stimulation.

Koike-Tani, M., Kanda, T., Saitoh, N., Yamashita, T., and Takahashi, T. (2008). Involvement of AMPA receptor desensitization in short-term synaptic depression at the calyx of Held in developing rats. J. Physiol. *586*, 2263–2275.

Kreitzer, A.C., and Malenka, R.C. (2007). Endocannabinoid-mediated rescue of striatal LTD and motor deficits in Parkinson's disease models. Nature *445*, 643–647.

Kuriu, T., Inoue, A., Bito, H., Sobue, K., and Okabe, S. (2006). Differential control of postsynaptic density scaffolds via actin-dependent and -independent mechanisms. J Neurosci *26*, 7693–7706.

Lee, H.-K., Takamiya, K., Han, J.-S., Man, H., Kim, C.-H., Rumbaugh, G., Yu, S., Ding, L., He, C., Petralia, R.S., et al. (2003). Phosphorylation of the AMPA Receptor GluR1 Subunit Is Required for Synaptic Plasticity and Retention of Spatial Memory. Cell *112*, 631–643.

Lee, H.-K., Takamiya, K., He, K., Song, L., and Huganir, R.L. (2010). Specific roles of AMPA receptor subunit GluR1 (GluA1) phosphorylation sites in regulating synaptic plasticity in the CA1 region of hippocampus. J. Neurophysiol. *103*, 479–489.

Lee, H.K., Kameyama, K., Huganir, R.L., and Bear, M.F. (1998). NMDA induces long-term synaptic depression and dephosphorylation of the GluR1 subunit of AMPA receptors in hippocampus. Neuron *21*, 1151–1162.

Lee, H.K., Barbarosie, M., Kameyama, K., Bear, M.F., and Huganir, R.L. (2000). Regulation of distinct AMPA receptor phosphorylation sites during bidirectional synaptic plasticity. Nature *405*, 955–959.

Levet, F., Hosy, E., Kechkar, A., Butler, C., Beghin, A., Choquet, D., and Sibarita, J.-B. (2015). SR-Tesseler: a method to segment and quantify localization-based super-resolution microscopy data. Nat. Methods *12*, 1065–1071.

Levy, W.B., and Steward, O. (1983). temporal contiguity requirements for long-term associative potentiation/depression in the hippocampus. *8*.

Levy, J.M., Chen, X., Reese, T.S., and Nicoll, R. a (2015). Synaptic Consolidation Normalizes AMPAR Quantal Size following MAGUK Loss. Neuron *87*, 534–548.

Liao, D., Zhang, X., O'Brien, R., Ehlers, M.D., and Huganir, R.L. (1999). Regulation of morphological postsynaptic silent synapses in developing hippocampal neurons. Nat. Neurosci. *2*, 37–43.

van de Linde, S., Löschberger, A., Klein, T., Heidbreder, M., Wolter, S., Heilemann, M., and Sauer, M. (2011). Direct stochastic optical reconstruction microscopy with standard fluorescent

probes. Nat. Protoc. *6*, 991–1009.

Lisman, J., and Spruston, N. (2005). Postsynaptic depolarization requirements for LTP and LTD: a critique of spike timing-dependent plasticity. Nat. Neurosci. *8*, 839–841.

Lisman, J., Yasuda, R., and Raghavachari, S. (2012). Mechanisms of CaMKII action in long-term potentiation. Nat. Rev. Neurosci. *13*, 169–182.

Lisman, J.E., Raghavachari, S., and Tsien, R.W. (2007). The sequence of events that underlie quantal transmission at central glutamatergic synapses. Nat. Rev. Neurosci. *8*, 597–609.

Liu, G., Choi, S., and Tsien, R.W. (1999). Variability of neurotransmitter concentration and nonsaturation of postsynaptic AMPA receptors at synapses in hippocampal cultures and slices. Neuron *22*, 395–409.

Lledo, P. (1998). Postsynaptic Membrane Fusion and Long-Term Potentiation. Science (80-.). *279*, 399–403.

Lodge, D. (2009). The history of the pharmacology and cloning of ionotropic glutamate receptors and the development of idiosyncratic nomenclature. Neuropharmacology *56*, 6–21.

Lu, W., Shi, Y., Jackson, A.C., Bjorgan, K., During, M.J., Sprengel, R., Seeburg, P.H., and Nicoll, R.A. (2009). Subunit Composition of Synaptic AMPA Receptors Revealed by a Single-Cell Genetic Approach. Neuron *62*, 254–268.

Lu, W., Isozaki, K., Roche, K.W., and Nicoll, R. a (2010). Synaptic targeting of AMPA receptors is regulated by a CaMKII site in the first intracellular loop of GluA1. Proc. Natl. Acad. Sci. U. S. A. *107*, 22266–22271.

Lu, W.Y., Man, H.Y., Ju, W., Trimble, W.S., MacDonald, J.F., and Wang, Y.T. (2001). Activation of synaptic NMDA receptors induces membrane insertion of new AMPA receptors and LTP in cultured hippocampal neurons. Neuron *29*, 243–254.

Lüscher, C., Nicoll, R. a, Malenka, R.C., and Muller, D. (2000). Synaptic plasticity and dynamic modulation of the postsynaptic membrane. Nat. Neurosci. *3*, 545–550.

Lynch, G.S., Dunwiddie, T., and Gribkoff, V. (1977). Heterosynaptic depression: a postsynaptic correlate of long-term potentiation. Nature *266*, 737–739.

MacGillavry, H.D., Song, Y., Raghavachari, S., and Blanpied, T.A. (2013). Nanoscale scaffolding domains within the postsynaptic density concentrate synaptic ampa receptors. Neuron *78*, 615–622.

Magee, J.C. (1997). A Synaptically Controlled, Associative Signal for Hebbian Plasticity in Hippocampal Neurons. Science (80-.). *275*, 209–213.

Magee, J.C. (2000). Dendritic integration of excitatory synaptic input. Nat. Rev. Neurosci. *1*, 181–190.

Magee, J.C., and Cook, E.P. (2000). Somatic EPSP amplitude is independent of synapse location in hippocampal pyramidal neurons. Nat. Neurosci. *3*, 895–903.

Makino, H., and Malinow, R. (2009). AMPA Receptor Incorporation into Synapses during LTP: The Role of Lateral Movement and Exocytosis. Neuron *64*, 381–390.

Man, H.-Y., Lin, J.W., Ju, W.H., Ahmadian, G., Liu, L., Becker, L.E., Sheng, M., and Wang, Y.T. (2000). Regulation of AMPA Receptor–Mediated Synaptic Transmission by Clathrin-Dependent Receptor Internalization. Neuron *25*, 649–662.

Markram, H. (1997). Regulation of Synaptic Efficacy by Coincidence of Postsynaptic APs and

EPSPs. Science (80-.). *275*, 213–215.

Martineau, M., Baux, G., and Mothet, J.P. (2006). d-Serine signalling in the brain: friend and foe. Trends Neurosci. *29*, 481–491.

Matsuda, S., Kakegawa, W., Budisantoso, T., Nomura, T., Kohda, K., and Yuzaki, M. (2013). Stargazin regulates AMPA receptor trafficking through adaptor protein complexes during long-term depression. Nat. Commun. *4*, 1–15.

Matsuzaki, M., Honkura, N., Ellis-Davies, G.C.R., and Kasai, H. (2004). Structural basis of long-trm potentiation in single dendritic spines. Nature *429*, 761–766.

Mayer, M.L. (2006). Glutamate receptors at atomic resolution. Nature *440*, 456–462.

McLachlan, E.M. (1978). The statistics of transmitter release at chemical synapses. Int. Rev. Physiol. *17*, 49–117.

Menon, V., Musial, T.F., Liu, A., Katz, Y., Kath, W.L., Spruston, N., and Nicholson, D.A. (2013). Balanced synaptic impact via distance-dependent synapse distribution and complementary expression of AMPARs and NMDARs in hippocampal dendrites. Neuron *80*, 1451–1463.

Meyerson, J.R., Kumar, J., Chittori, S., Rao, P., Pierson, J., Bartesaghi, A., Mayer, M.L., and Subramaniam, S. (2014). Structural mechanism of glutamate receptor activation and desensitization. Nature *advance on*.

Miki, T., Malagon, G., Pulido, C., Llano, I., Neher, E., and Marty, A. (2016). Actin- and Myosin-Dependent Vesicle Loading of Presynaptic Docking Sites Prior to Exocytosis. Neuron *91*, 808–823.

Moser, M.B., Trommald, M., and Andersen, P. (1994). An increase in dendritic spine density on hippocampal CA1 pyramidal cells following spatial learning in adult rats suggests the formation of new synapses. Proc. Natl. Acad. Sci. U. S. A. *91*, 12673–12675.

Mothet, J.-P., Parent, A.T., Wolosker, H., Brady, R.O., Linden, D.J., Ferris, C.D., Rogawski, M.A., and Snyder, S.H. (2000). D-Serine is an endogenous ligand for the glycine site of the N-methyl-D-aspartate receptor. Proc. Natl. Acad. Sci. *97*, 4926–4931.

Mukherjee, K., Yang, X., Gerber, S.H., Kwon, H.-B., Ho, A., Castillo, P.E., Liu, X., and Sudhof, T.C. (2010). Piccolo and bassoon maintain synaptic vesicle clustering without directly participating in vesicle exocytosis. Proc. Natl. Acad. Sci. *107*, 6504–6509.

Mulkey, R.M., and Malenka, R.C. (1992). Mechanisms underlying induction of homosynaptic long-term depression in area CA1 of the hippocampus. Neuron *9*, 967–975.

Mulkey, R., Endo, S., Shinolikar, S., and Malenka, R. (1994). Involvement of a calcineurin/ inhibitor-1 phosphatase cascade in hippocampal long-term depression. Nature *369*, 486–488.

Mulkey, R.M., Herron, C.E., and Malenka, R.C. (1993). An essential role for protein phosphatases in Hippocampal long term depression. Science (80-.). *261*, 1051–1055.

Murakoshi, H., Shin, M.E., Parra-Bueno, P., Szatmari, E.M., Shibata, A.C.E., and Yasuda, R. (2017). Kinetics of Endogenous CaMKII Required for Synaptic Plasticity Revealed by Optogenetic Kinase Inhibitor (Neuron (2017) 94(1) (37–47.e5) (S0896627317301447) (10.1016/j.neuron.2017.02.036)). Neuron *94*, 690.

Nabavi, S., Fox, R., Proulx, C.D., Lin, J.Y., Tsien, R.Y., and Malinow, R. (2014). Engineering a memory with LTD and LTP. Nature *511*, 348–352.

Nägerl, U.V., Eberhorn, N., Cambridge, S.B., and Bonhoeffer, T. (2004). Bidirectional activity-

dependent morphological plasticity in hippocampal neurons. Neuron *44*, 759–767.

Nair, D., Hosy, E., Petersen, J.D., Constals, a., Giannone, G., Choquet, D., and Sibarita, J.-B. (2013). Super-Resolution Imaging Reveals That AMPA Receptors Inside Synapses Are Dynamically Organized in Nanodomains Regulated by PSD95. J. Neurosci. *33*, 13204–13224.

Nakagawa, T., Futai, K., Lashuel, H.A., Lo, I., Okamoto, K., Walz, T., Hayashi, Y., and Sheng, M. (2004). Quaternary structure, protein dynamics, and synaptic function of SAP97 controlled by L27 domain interactions. Neuron *44*, 453–467.

Nam, C.I., and Chen, L. (2005). Postsynaptic assembly induced by neurexin-neuroligin interaction and neurotransmitter. Proc. Natl. Acad. Sci. U. S. A. *102*, 6137–6142.

Nelson, C.D., Kim, M.J., Hsin, H., Chen, Y., and Sheng, M. (2013). Phosphorylation of Threonine-19 of PSD-95 by GSK-3 is Required for PSD-95 Mobilization and Long-Term Depression. J. Neurosci. *33*, 12122–12135.

Nicholls, R.E., Alarcon, J.M., Malleret, G., Carroll, R.C., Grody, M., Vronskaya, S., and Kandel, E.R. (2008). Transgenic Mice Lacking NMDAR-Dependent LTD Exhibit Deficits in Behavioral Flexibility. Neuron *58*, 104–117.

Nicoll, R. a. (2006). Auxiliary Subunits Assist AMPA-Type Glutamate Receptors. Science (80-.). *311*, 1253–1256.

Nishiyama, J., and Yasuda, R. (2015). Biochemical Computation for Spine Structural Plasticity. Neuron *87*, 63–75.

Oh, W.C., Hill, T.C., and Zito, K. (2013). Synapse-specific and size-dependent mechanisms of spine structural plasticity accompanying synaptic weakening. Proc. Natl. Acad. Sci. *110*, E305–E312.

Okabe, S. (2007). Molecular anatomy of the postsynaptic density. Mol. Cell. Neurosci. *34*, 503–518.

Oliet, S.H., Malenka, R.C., and Nicoll, R. a (1997). Two distinct forms of long-term depression coexist in CA1 hippocampal pyramidal cells. Neuron *18*, 969–982.

Olivier, N., Keller, D., Gönczy, P., and Manley, S. (2013). Resolution Doubling in 3D-STORM Imaging through Improved Buffers. PLoS One *8*, 1–9.

Opazo, P., Labrecque, S., Tigaret, C.M., Frouin, A., Wiseman, P.W., De Koninck, P., and Choquet, D. (2010). CaMKII triggers the diffusional trapping of surface AMPARs through phosphorylation of stargazin. Neuron *67*, 239–252.

Opazo, P., Sainlos, M., and Choquet, D. (2012). Regulation of AMPA receptor surface diffusion by PSD-95 slots. Curr. Opin. Neurobiol. *22*, 453–460.

Otis, T., Zhang, S., and Trussell, L.O. (1996). Direct measurement of AMPA receptor desensitization induced by glutamatergic synaptic transmission. J. Neurosci. *16*, 7496–7504.

Palay, S.S.L. (1956). Synapses in the central nervous system. J. Biophys. Iochemical Cytol. *2*, 193–202.

Palay, B.Y.S.L., and Palade, G.E. (1955). (From the Laboratories of The Rockefdler Inai~ute for M e d ~ Research). Public Health *1*.

Panatier, A., Theodosis, D.T., Mothet, J.P., Touquet, B., Pollegioni, L., Poulain, D.A., and Oliet, S.H.R. (2006). Glia-Derived d-Serine Controls NMDA Receptor Activity and Synaptic Memory. Cell *125*, 775–784.

Panatier, A., Vallée, J., Haber, M., Murai, K.K., Lacaille, J.C., and Robitaille, R. (2011). Astrocytes are endogenous regulators of basal transmission at central synapses. Cell *146*, 785–798.

Park, M., Penick, E.C., Edwards, J.G., Kauer, J. a, and Ehlers, M.D. (2004). Recycling endosomes supply AMPA receptors for LTP. Science *305*, 1972–1975.

Pascual, O. (2005). Astrocytic Purinergic Signaling Coordinates Synaptic Networks. Science (80-.). *310*, 113–116.

Patterson, G.H., and Lippincott-Schwartz, J. (2002). A Photoactivatable GFP for Selective Photolabeling of Proteins and Cells. Science (80-.). *297*, 1873–1877.

Penn, A.C., Balik, A., Wozny, C., Cais, O., and Greger, I.H. (2012). Activity-Mediated AMPA Receptor Remodeling, Driven by Alternative Splicing in the Ligand-Binding Domain. Neuron *76*, 503–510.

Penn, A.C., Zhang, C.L., Georges, F., Royer, L., Breillat, C., Hosy, E., Petersen, J.D., Humeau, Y., and Choquet, D. (2017). Hippocampal LTP and contextual learning require surface diffusion of AMPA receptors. Nature.

Petrini, E.M., Lu, J., Cognet, L., Lounis, B., Ehlers, M.D., and Choquet, D. (2009). Endocytic Trafficking and Recycling Maintain a Pool of Mobile Surface AMPA Receptors Required for Synaptic Potentiation. Neuron *63*, 92–105.

Pettit, D.L., and Augustine, G.J. (2009). Distribution of Functional Glutamate and GABA Receptors on Hippocampal Pyramidal Cells and Interneurons. J. Neurophysiol. *84*, 28–38.

Pougnet, J.-T., Compans, B., Martinez, A., Choquet, D., Hosy, E., and Boué-Grabot, E. (2016). P2X-mediated AMPA receptor internalization and synaptic depression is controlled by two CaMKII phosphorylation sites on GluA1 in hippocampal neurons. Sci. Rep. *6*, 31836.

Pougnet, J.T., Toulme, E., Martinez, A., Choquet, D., Hosy, E., and Boué-Grabot, E. (2014). ATP P2X receptors downregulate AMPA receptor trafficking and postsynaptic efficacy in hippocampal neurons. Neuron *83*, 417–430.

Pulido, C., and Marty, A. (2017). Quantal fluctuations in central mammalian synapses: Functional role of vesicular docking sites. Physiol. Rev. *97*, 1403–1430.

Raghavachari, S., and Lisman, J.E. (2004). Properties of Quantal Transmission at CA1 Synapses. J. Neurophysiol. *92*, 2456–2467.

Rall, W. (1962). Theory of Physiological Properties of Dendrites. Ann. N. Y. Acad. Sci. *96*, 1071–1092.

Ramon y Cajal, S. (1909). Histologia del sistema nervioso del hombre y de los animales.

Rizzoli, S.O., and Betz, W.J. (2005). Synaptic vesicle pools. Nat. Rev. Neurosci. *6*, 57–69.

Robert, A., and Howe, J.R. (2003). How AMPA receptor desensitization depends on receptor occupancy. J Neurosci *23*, 847–58.

De Robertis, E.D., and Bennett, H.S. (1955). Some features of the submicroscopic morphology of synapses in frog and earthworm. J. Biophys. Biochem. Cytol. *1*, 47–58.

Rosendale, M., Julli??, D., Choquet, D., and Perrais, D. (2017). Spatial and Temporal Regulation of Receptor Endocytosis in Neuronal Dendrites Revealed by Imaging of Single Vesicle Formation. Cell Rep. *18*, 1840–1847.

Rosenmund, C. (1998). The Tetrameric Structure of a Glutamate Receptor Channel. Science

(80-.). *280*, 1596–1599.

Rotman, Z., Deng, P.-Y.P.-Y., and Klyachko, V. a. (2011). Short-Term Plasticity Optimizes Synaptic Information Transmission. J. Neurosci. *31*, 14800–14809.

Sainlos, M., Tigaret, C., Poujol, C., Olivier, N.B., Bard, L., Breillat, C., Thiolon, K., Choquet, D., and Imperiali, B. (2011). Biomimetic divalent ligands for the acute disruption of synaptic AMPAR stabilization. Nat. Chem. Biol. *7*, 81–91.

Salin, P.A., Scanziani, M., Malenka, R.C., and Nicoll, R.A. (1996). Distinct short-term plasticity at two excitatory synapses in the hippocampus. Proc. Natl. Acad. Sci. U. S. A. *93*, 13304–13309.

Sanderson, J.L., Gorski, J. a., and Dell'Acqua, M.L. (2016). NMDA Receptor-Dependent LTD Requires Transient Synaptic Incorporation of Ca2+-Permeable AMPARs Mediated by AKAP150-Anchored PKA and Calcineurin. Neuron *89*, 1000–1015.

Sankaranarayanan, S., Atluri, P.P., and Ryan, T.A. (2003). Actin has a molecular scaffolding, not propulsive, role in presynaptic function. Nat. Neurosci. *6*, 127–135.

Savtchenko, L.P., and Rusakov, D. a (2013). Moderate AMPA receptor clustering on the nanoscale can efficiently potentiate synaptic current. Philos. Trans. R. Soc. Lond. B. Biol. Sci. *369*, 20130167.

Schikorski, T., and Stevens, C.F. (1997). Quantitative ultrastructural analysis of hippocampal excitatory synapses. J. Neurosci. *17*, 5858–5867.

Schneggenburger, R., and Neher, E. (2000). Intracellular calcium dependence of transmitter release rates at a fast central synapse. Nature *406*, 889–893.

Schneider, R., Hosy, E., Kohl, J., Klueva, J., Choquet, D., Thomas, U., Voigt, A., and Heine, M. (2015). Mobility of Calcium Channels in the Presynaptic Membrane. Neuron *86*, 672–679.

Schnell, E., Sizemore, M., Karimzadegan, S., Chen, L., Bredt, D.S., and Nicoll, R.A. (2002). Direct interactions between PSD-95 and stargazin control synaptic AMPA receptor number. Proc. Natl. Acad. Sci. *99*, 13902–13907.

Schoch, S., Castillo, P.E., Jo, T., Mukherjee, K., Geppert, M., Wang, Y., Schmitz, F., Malenka, R.C., and Südhof, T.C. (2002). RIM1α forms a protein scaffold for regulating neurotransmitter release at the active zone. Nature *415*, 321–326.

Schwenk, J., Harmel, N., Zolles, G., Bildl, W., Kulik, A., Heimrich, B., Chisaka, O., Jonas, P., Schulte, U., Fakler, B., et al. (2009). Functional proteomics identify cornichon proteins as auxiliary subunits of AMPA receptors. Neuroforum *15*, 62–63.

Schwenk, J., Harmel, N., Brechet, A., Zolles, G., Berkefeld, H., Müller, C.S., Bildl, W., Baehrens, D., Hüber, B., Kulik, A., et al. (2012). High-Resolution Proteomics Unravel Architecture and Molecular Diversity of Native AMPA Receptor Complexes. Neuron *74*, 621–633.

Schwenk, J., Baehrens, D., Haupt, A., Bildl, W., Boudkkazi, S., and Roeper, J. (2014). Regional Diversity and Developmental Dynamics of the AMPA-Receptor Proteome in the Mammalian Brain. Neuron 1–14.

Scimemi, A., and Diamond, J.S. (2012). The Number and Organization of Ca2+ Channels in the Active Zone Shapes Neurotransmitter Release from Schaffer Collateral Synapses. J. Neurosci. *32*, 18157–18176.

Sharma, K., Fong, D.K., and Craig, A.M. (2006). Postsynaptic protein mobility in dendritic

spines: Long-term regulation by synaptic NMDA receptor activation. Mol. Cell. Neurosci. *31*, 702–712.

Sharonov, A., and Hochstrasser, R.M. (2006). Wide-field subdiffraction imaging by accumulated binding of diffusing probes. Proc. Natl. Acad. Sci. *103*, 18911–18916.

Sheng, M., and Kim, E. (2011). The postsynaptic organization od synapses. Cold Spring Harb. Perspect. Biol. *3*, a005678.

Sjostrom, P.J., Rancz, E.A., Roth, A., and Hausser, M. (2008). Dendritic Excitability and Synaptic Plasticity. Physiol. Rev. *88*, 769–840.

Sjöström, P.J., Turrigiano, G.G., Nelson, S.B., Jesper Sjostrom, Turrigiano, G.G., and Nelson, S.B. (2001). Rate , Timing , and Cooperativity Jointly Determine Cortical Synaptic Plasticity. Neuron *32*, 1149–1164.

Smith, M.A., Ellis-Davies, G.C.R., and Magee, J.C. (2003). Mechanism of the distance-dependent scaling of Schaffer collateral synapses in rat CA1 pyramidal neurons. J. Physiol. *548*, 245–258.

Stanton, P.K., and Sejnowski, T.J. (1989). associative long-term depression in the hippocampus induced by hebbian covariance. Nature *342*, 189–192.

Stein, V., House, D.R.C., Bredt, D.S., and Nicoll, R.A. (2003). Postsynaptic density-95 mimics and occludes hippocampal long-term potentiation and enhances long-term depression. J. Neurosci. *23*, 5503–5506.

Stent, G.S. (1973). A physiological mechanism for Hebb's postulate of learning. Proc. Natl. Acad. Sci. U. S. A. *70*, 997–1001.

Stuart, G.J., and Sakmann, B. (1994). Active propagation of somatic action potentials into neocortical pyramidal cell dendrites. Nature *367*, 69–72.

Stuart, G., Schiller, J., and Sakmann, B. (1997). Action potential initiation and propagation in rat neocortical pyramidal neurons. J. Physiol. *505*, 617–632.

Südhof, T.C. (2012). The presynaptic active zone. Neuron *75*, 11–25.

Sumioka, A., Yan, D., and Tomita, S. (2010). TARP phosphorylation regulates synaptic AMPAR through lipid bilayers. Neuron *86*, 3279–3288.

Sumioka, A., Brown, T.E., Kato, A.S., Bredt, D.S., Kauer, J. a, and Tomita, S. (2011). PDZ binding of TARPγ-8 controls synaptic transmission but not synaptic plasticity. Nat. Neurosci. *14*, 1410–1412.

Sun, Y., Olson, R., Horning, M., Armstrong, N., Mayer, M., and Gouaux, E. (2002). Mechanism of glutamate receptor desensitization. Nature *417*, 245–253.

Swanson, G.T., Kamboj, S.K., and Cull-Candy, S.G. (1997). Single-channel properties of recombinant AMPA receptors depend on RNA editing, splice variation, and subunit composition. J. Neurosci. *17*, 58–69.

Takeuchi, T., Duszkiewicz, A.J., and Morris, R.G.M. (2014). The synaptic plasticity and memory hypothesis: encoding, storage and persistence. Philos. Trans. R. Soc. Lond. B. Biol. Sci. *369*, 20130288.

Tang, A.-H., Chen, H., Li, T.P., Metzbower, S.R., MacGillavry, H.D., and Blanpied, T.A. (2016). A trans-synaptic nanocolumn aligns neurotransmitter release to receptors. Nature *536*, 210–214.

Tarusawa, E., Matsui, K., Budisantoso, T., Molnar, E., Watanabe, M., Matsui, M., Fukazawa, Y., and Shigemoto, R. (2009). Input-Specific Intrasynaptic Arrangements of Ionotropic Glutamate Receptors and Their Impact on Postsynaptic Responses. J. Neurosci. *29*, 12896–12908.

Tom Dieck, S., Sanmartí-Vila, L., Langnaese, K., Richter, K., Kindler, S., Soyke, A., Wex, H., Smalla, K.H., Kämpf, U., Fränzer, J.T., et al. (1998). Bassoon, a novel zinc-finger CAG/glutamine-repeat protein selectively localized at the active zone of presynaptic nerve terminals. J. Cell Biol. *142*, 499–509.

Tomita, S., Chen, L., Kawasaki, Y., Petralia, R.S., Wenthold, R.J., Nicoll, R. a., and Bredt, D.S. (2003). Functional studies and distribution define a family of transmembrane AMPA receptor regulatory proteins. J. Cell Biol. *161*, 805–816.

Tomita, S., Stein, V., Stocker, T.J., Nicoll, R.A., and Bredt, D.S. (2005a). Bidirectional synaptic plasticity regulated by phosphorylation of stargazin-like TARPs. Neuron *45*, 269–277.

Tomita, S., Adesnik, H., Sekiguchi, M., Zhang, W., Wada, K., Howe, J.R., Nicoll, R. a, and Bredt, D.S. (2005b). Stargazin modulates AMPA receptor gating and trafficking by distinct domains. Nature *435*, 1052–1058.

Traynelis, S.F., Wollmuth, L., McBain, C.J., Menniti, F., and Dingledine, R. (2010). Glutamate receptor review. Pharmacol. Rev. *62*, 405–496.

Trussell, L.O., and Fischbach, G.D. (1989). Glutamate receptor desensitization and its role in synaptic transmission. Neuron *3*, 209–218.

Trussell, L.O., Thio, L.L., Zorumski, C.F., and Fischbach, G.D. (1988). Rapid desensitization of glutamate receptors in vertebrate central neurons. Proc. Natl. Acad. Sci. U. S. A. *85*, 4562–4566.

Trussell, L.O., Zhang, S., and Ramant, I.M. (1993). Desensitization of AMPA receptors upon multiquantal neurotransmitter release. Neuron *10*, 1185–1196.

Turecek, R., and Trussell, L.O. (2000). Control of synaptic depression by glutamate transporters. J. Neurosci. *20*, 2054–2063.

Twomey, E.C., Yelshanskaya, M. V., Grassucci, R.A., Frank, J., and Sobolevsky, A.I. (2017). Channel opening and gating mechanism in AMPA-subtype glutamate receptors. Nature.

Waites, C.L., Leal-Ortiz, S.A., Andlauer, T.F.M., Sigrist, S.J., and Garner, C.C. (2011). Piccolo Regulates the Dynamic Assembly of Presynaptic F-Actin. J. Neurosci. *31*, 14250–14263.

Walker, A.S., Neves, G., Grillo, F., Jackson, R.E., Rigby, M., O'Donnell, C., Lowe, A.S., Vizcay-Barrena, G., Fleck, R.A., and Burrone, J. (2017). Distance-dependent gradient in NMDAR-driven spine calcium signals along tapering dendrites. Proc. Natl. Acad. Sci. U. S. A. 201607462.

Wiegert, J.S., and Oertner, T.G. (2013). Long-term depression triggers the selective elimination of weakly integrated synapses. Proc. Natl. Acad. Sci. *110*, E4510–E4519.

Wiesel, T.N., and Hubel, D.H. (1965). Comparison of the effects of unilateral and bilateral eye closure on cortical unit responses in kittens. J. Neurophysiol. *28*, 1029–1040.

Woods, G.F., Oh, W.C., Boudewyn, L.C., Mikula, S.K., and Zito, K. (2011). Loss of PSD-95 enrichment is not a prerequisite for spine retraction. J. Neurosci. *31*, 12129–12138.

Wu, D., Bacaj, T., Morishita, W., Goswami, D., Arendt, K.L., Xu, W., Chen, L., Malenka, R.C., and Südhof, T.C. (2017). Postsynaptic synaptotagmins mediate AMPA receptor exocytosis

during LTP. Nature *544*, 316–321.

Xiao, M.Y., Zhou, Q., and Nicoll, R. a (2001). Metabotropic glutamate receptor activation causes a rapid redistribution of AMPA receptors. Neuropharmacology *41*, 664–671.

Xu-Friedman, M.A., and Regehr, W.G. (2004). Structural Contributions to Short-Term Synaptic Plasticity. Physiol. Rev. *84*, 69–85.

Yamazaki, Y., Fujii, S., Nakamura, T., Miyakawa, H., Kudo, Y., Kato, H., and Ito, K.I. (2002). Changes in [Ca2+]i during adenosine triphosphate-induced synaptic plasticity in hippocampal CA1 neurons of the guinea pig. Neurosci. Lett. *324*, 65–68.

Yan, D., and Tomita, S. (2012). Defined criteria for auxiliary subunits of glutamate receptors. J. Physiol. *590*, 21–31.

Yang, G., Pan, F., and Gan, W.-B. (2009). Stably maintained dendritic spines are associated with lifelong memories. Nature *462*, 920–924.

Yang, Y., Ge, W., Chen, Y., Zhang, Z., Shen, W., Wu, C., Poo, M., and Duan, S. (2003). Contribution of astrocytes to hippocampal long-term potentiation through release of D-serine. Proc. Natl. Acad. Sci. U. S. A. *100*, 15194–15199.

Yi, J., Manna, A., Barr, V.A., Hong, J., Neuman, K.C., and Samelson, L.E. (2016). madSTORM: a superresolution technique for large-scale multiplexing at single-molecule accuracy. Mol. Biol. Cell *27*, 3591–3600.

Zhou, Q., Zhou, P., Wang, A.L., Wu, D., Zhao, M., Südhof, T.C., and Brunger, A.T. (2017a). The primed SNARE–complexin–synaptotagmin complex for neuronal exocytosis. Nature.

Zhou, Y., Lai, B., and Gan, W.-B. (2017b). Monocular deprivation induces dendritic spine elimination in the developing mouse visual cortex. Sci. Rep. *7*, 4977.

Zucker, R.S., and Regehr, W.G. (2002). Short-Term Synaptic Plasticity. Annu. Rev. Physiol. *64*, 355–405.

Zuo, Y., Yang, G., Kwon, E., and Gan, W.-B. (2005). Long-term sensory deprivation prevents dendritic spine loss in primary somatosensory cortex. Nature *436*, 261–265.

ANNEX 1

Article

Neuron

Glutamate-Induced AMPA Receptor Desensitization Increases Their Mobility and Modulates Short-Term Plasticity through Unbinding from Stargazin

Highlights

- Glutamate increases AMPA receptor diffusion in a conformation-dependent manner
- Desensitized AMPAR diffuse faster than closed-resting or open ones
- Preventing AMPAR-stargazin dissociation blocks glutamate-induced AMPAR diffusion
- AMPAR-stargazin unbinding speeds recovery from synaptic short-term depression

Authors

Audrey Constals, Andrew C. Penn, ..., Eric Hosy, Daniel Choquet

Correspondence

eric.hosy@u-bordeaux.fr (E.H.), daniel.choquet@u-bordeaux.fr (D.C.)

In Brief

Constals et al. use single-molecule tracking to show that desensitized AMPA receptors diffuse faster than closed-resting or open ones through unbinding from stargazin. This allows AMPA receptor diffusion to accelerate recovery from short-term synaptic depression.

Constals et al., 2015, Neuron *85*, 1–17
February 18, 2015
http://dx.doi.org/10.1016/j.neuron.2015.01.012

CellPress

Please cite this article in press as: Constals et al., Glutamate-Induced AMPA Receptor Desensitization Increases Their Mobility and Modulates Short-Term Plasticity through Unbinding from Stargazin, Neuron (2015), http://dx.doi.org/10.1016/j.neuron.2015.01.012

Neuron
Article

Glutamate-Induced AMPA Receptor Desensitization Increases Their Mobility and Modulates Short-Term Plasticity through Unbinding from Stargazin

Audrey Constals,[1,2] Andrew C. Penn,[1,2] Benjamin Compans,[1,2] Estelle Toulmé,[1,2] Amandine Phillipat,[1,2] Sébastien Marais,[3] Natacha Retailleau,[1,2] Anne-Sophie Hafner,[1,2] Françoise Coussen,[1,2] Eric Hosy,[1,2,4,*] and Daniel Choquet[1,2,3,4,*]

[1]University of Bordeaux, Interdisciplinary Institute for Neuroscience, UMR 5297, F-33000 Bordeaux, France
[2]CNRS, Interdisciplinary Institute for Neuroscience, UMR 5297, F-33000 Bordeaux, France
[3]Bordeaux Imaging Center, UMS 3420 CNRS, US4 INSERM, University of Bordeaux, F-33000 Bordeaux, France
[4]Co-senior authors
*Correspondence: eric.hosy@u-bordeaux.fr (E.H.), daniel.choquet@u-bordeaux.fr (D.C.)
http://dx.doi.org/10.1016/j.neuron.2015.01.012

SUMMARY

Short-term plasticity of AMPAR currents during high-frequency stimulation depends not only on presynaptic transmitter release and postsynaptic AMPAR recovery from desensitization, but also on fast AMPAR diffusion. How AMPAR diffusion within the synapse regulates synaptic transmission on the millisecond scale remains mysterious. Using single-molecule tracking, we found that, upon glutamate binding, synaptic AMPAR diffuse faster. Using AMPAR stabilized in different conformational states by point mutations and pharmacology, we show that desensitized receptors bind less stargazin and are less stabilized at the synapse than receptors in opened or closed-resting states. AMPAR mobility-mediated regulation of short-term plasticity is abrogated when the glutamate-dependent loss in AMPAR-stargazin interaction is prevented. We propose that transition from the activated to the desensitized state leads to partial loss in AMPAR-stargazin interaction that increases AMPAR mobility and allows faster recovery from desensitization-mediated synaptic depression, without affecting the overall nano-organization of AMPAR in synapses.

INTRODUCTION

The alpha-amino-3-hydroxy-5-methyl-4-isoxazole-propionic acid (AMPA) subtype of glutamate receptors (AMPAR) mediates most of fast excitatory synaptic transmission in the mammalian central nervous system. AMPAR are formed of a core heterotetrameric structure composed of a combination of four subunits, GluA1–GluA4 (Traynelis et al., 2010), surrounded by a variety of auxiliary subunits (Schwenk et al., 2012). AMPAR are largely concentrated in the postsynaptic density (PSD), in front of presynaptic glutamate release sites, where they are stabilized through interactions between the various members of the AMPAR complex with a variety of intracellular and extracellular partners (Jackson and Nicoll, 2011; Shepherd and Huganir, 2007). AMPAR are not all stable in the synapse and around 50% move constantly by Brownian diffusion within the plasma membrane, promoting continuous exchanges between synaptic and extrasynaptic sites. This proportion is highly regulated by neuronal activity and other stimuli (Choquet and Triller, 2013).

The diffusion of AMPAR has long been considered to play a role only in controlling the accumulation of synaptic receptors in time scales ranging from seconds to minutes (Choquet and Triller, 2013; Shepherd and Huganir, 2007). In 2008, we proposed a new physiological role for AMPAR diffusion in the control of fast synaptic transmission over timescales of a few tens of milliseconds (Heine et al., 2008). We demonstrated, using paired-pulse stimulations in electrophysiological recordings and crosslinking of surface AMPAR with antibodies, that the rapid exchange of desensitized receptors by naive ones in the synapse is essential to maintain the fidelity of high-frequency synaptic transmission. In addition, AMPAR stabilization by PSD-95-potentiated frequency-dependent synaptic depression (Opazo et al., 2010). Conversely, accelerating AMPAR movements by removing the extracellular matrix (Frischknecht et al., 2009) accelerated recovery from paired-pulse depression. Altogether, we thus hypothesized that AMPAR diffusion allows synapses to sustain higher frequencies than the rate of AMPAR return from desensitization would normally allow (Choquet, 2010). Upon glutamate release, the postsynaptic area in which AMPAR can be opened does not exceed 100–200 nm in diameter due to their low apparent affinity for glutamate (Lisman et al., 2007). Within this small area, rapidly diffusing receptors can be renewed up to 30% within 10 ms considering a homogeneous distribution of AMPAR at the synapse (Heine et al., 2008). However, as more than 50% of receptors may be immobile in the synapse (Ashby et al., 2006; Heine et al., 2008), this raises questions about the mechanisms through which AMPAR diffusion could allow a fast enough exchange of receptors to allow a measurable impact on high frequency synaptic transmission.

The nanoscale spatial distribution of AMPAR in the synapse is highly heterogeneous (MacGillavry et al., 2013; Masugi-Tokita

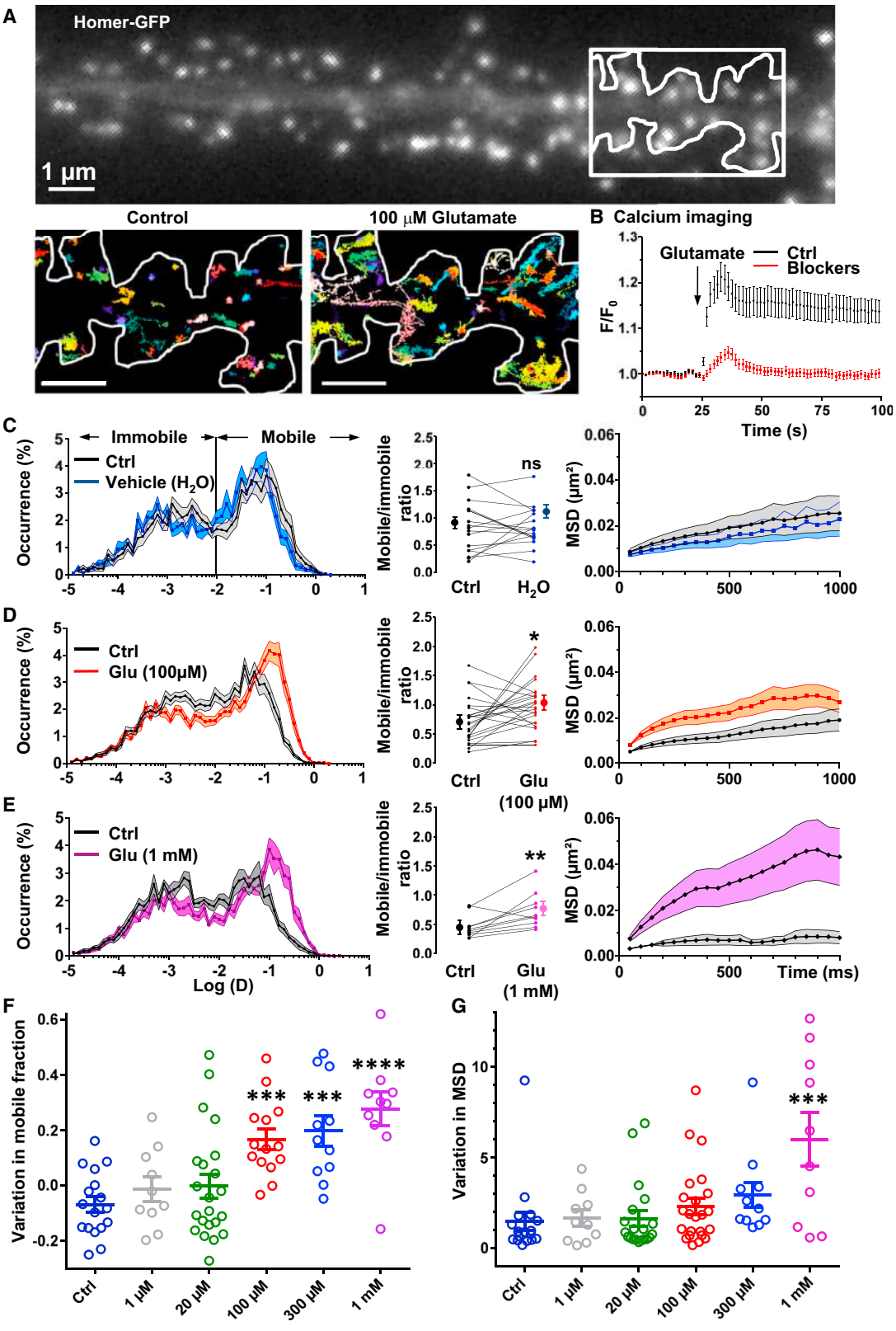

(legend on next page)

and Shigemoto, 2007; Nair et al., 2013). About half of synaptic AMPAR are packed and stabilized in clusters of about 80 nm wide, each comprising about 20 receptors. The other half are mobile in between clusters (Nair et al., 2013). While this could help explain how AMPAR diffusion could contribute to short-term plasticity, the relative stability of AMPAR nanodomains still poses the question of how a large proportion of trapped AMPAR could be exchanged within a few milliseconds.

Several molecular mechanisms are involved in controlling AMPAR stabilization, among which those mediated by the transmembrane AMPAR regulatory proteins (TARPs), and more particularly by stargazin, have been best characterized (Jackson and Nicoll, 2011). Stargazin is involved in stabilizing AMPAR in the PSD via its interaction with scaffolding proteins like PSD-95 (Bats et al., 2007; Opazo et al., 2010; Schnell et al., 2002) which is increased in long-term potentiation (LTP) via a CamKII-dependant phosphorylation of a stretch of serines in the stargazin C-tail (Opazo et al., 2010; Tomita et al., 2005b). Stargazin also modulates receptor pharmacology and controls channel gating: it increases AMPA receptor glutamate affinity, enhances single-channel conductance, slows deactivation and desensitization, and reduces the extent of desensitization (Priel et al., 2005; Tomita et al., 2005a; Turetsky et al., 2005).

The stability of stargazin (TARP)-AMPA receptor complex is controversial. Both the native and recombinantly expressed complexes have been reported to be readily disrupted by exposure to glutamate (Morimoto-Tomita et al., 2009; Tomita et al., 2004). The partial dissociation of the AMPAR/TARP complex within milliseconds after application of glutamate was further suggested using a tandem in which the amino-terminal part of stargazin is fused to the carboxy-tail of the receptor to prevent dissociation of the AMPAR/TARPs complex (Morimoto-Tomita et al., 2009). However, in other studies, rapid agonist-driven dissociation has not been observed (Nakagawa et al., 2005; Semenov et al., 2012).

Now, using single-particle tracking, biochemistry, and electrophysiology, we demonstrate that glutamate impacts AMPA receptor mobility through conformation changes: desensitized receptors being more mobile and less confined than those in the resting state due to specific unbinding of desensitized receptors from stargazin. This allows the desensitized fraction of receptors to move away from the glutamate release site and quickly be replaced by naive functional ones during synaptic transmission. Glutamate-mediated modulation of the mobility state of desensitized AMPAR directly participates to the modulation of frequency-dependent synaptic responses.

RESULTS

Glutamate Increases Mobility of Endogenous GluA2-Containing AMPAR

We first evaluated the impact of various doses of glutamate on the surface mobility of whole cell (see Figures S1A and S1B available online) and synaptic (Figure 1) endogenous GluA2-containing AMPAR in conditions of minimal intracellular signaling by using uPAINT single-molecule tracking of fluorescently labeled antibodies specific to the extracellular domain of GluA2 on dissociated hippocampal Banker cell cultures aged 13–16 days in vitro (DIV) (Giannone et al., 2010). On average, about 1,500 fluorescent AMPAR-bound antibodies were tracked each for at least 0.5 s (median value of trajectory duration in seconds with interquartile range [IQR],: 2.100 IQR 1.513–5.088), during recording periods of 3 min, both before and after application of glutamate (Figure 1A). In these conditions of short recordings, trajectory maps and partial superresolved pictures of the neurons before and after treatment can be reconstructed. Figure 1A represents a stretch of dendrite with synaptic areas identified by eGFP-Homer 1c expression, and shown below are AMPAR trajectories before and after application of 100 μM glutamate on an enlarged view of a dendrite segment. Glutamate application increased AMPAR mobility as evidenced by the larger area covered by AMPAR trajectories.

As previously described (Heine et al., 2008; Tardin et al., 2003), endogenous GluA2-containing AMPAR exhibit a variety of

Figure 1. Glutamate Increases Endogenous GluA2-Containing AMPAR Diffusion in Synapse

(A) Epifluorescence image of a dendritic segment expressing eGFP-Homer1c as a synaptic marker (top) and corresponding synaptic trajectories of endogenous GluA2-containing AMPAR before and after application of 100 μM glutamate (bottom) recorded in the boxed region on the top Homer image. Each trajectory map is obtained by overaccumulation of 2,000 images acquired with uPAINT technique.

(B) Effect of glutamate application on cytoplasmic calcium concentration. Normalized intensity of calcium-sensitive dye Fluo4FF-AM fluorescence is plotted versus time. Neurons preloaded with Fluo4FF-AM dye were imaged every 1.5 s for 2 min in Tyrode's solution (black curve, n = 16 cells) or in Tyrode's solution supplemented with various blockers (see Supplemental Experimental Procedures; red curve, n = 12 cells). After 25 s of recording, 100 μM glutamate was applied. In the absence of the inhibitor cocktail, glutamate triggered a large increase in the intracellular calcium level which was markedly decreased in the presence of the combination of blockers. Unless stated, error bars represent standard error of the mean (SEM).

(C) Absence of modulation of endogenous GluA2-containing AMPAR synaptic mobility upon addition of vehicle (water). GluA2-containing AMPAR were tracked using the uPAINT technique. Left panel shows the average distribution of the logarithm of the diffusion coefficient. Middle panel shows paired ratio of the mobile over the immobile fraction before and after treatment, and averages are represented on the sides (n = 17 cells, paired t test, $p > 0.05$). Right panel is the representation of the synaptic mean square displacement (MSD) as a function of time before and after treatment (n = 17 cells, t test on the under curve area, $p = 0.29$).

(D and E) Modulation of endogenous GluA2-containing AMPAR synaptic mobility by application of glutamate 100 μM (D) and 1 mM (E). From left to right are represented the average distribution of the logarithm of the diffusion coefficient, the paired ratios of the mobile over the immobile fraction (n = 24 cells, paired t test, $p = 0.023$ and n = 10 cells, paired t test, $p < 0.01$), and the plot of the synaptic MSD in function of time before and after treatment (n = 24 cells, t test on the under curve area, $p = 0.038$ and n = 10 cells, paired t test on the under curve area, $p < 0.001$).

(F) Dose-response curve for changes in the paired ratio of mobile over the immobile fraction following addition of varying glutamate concentrations (or vehicle for control). Five glutamate concentrations are tested from 1 μM to 1 mM. A significant increase of the AMPAR mobility is observed for concentrations $\geq$100 μM (mean ± SEM are plotted, statistical test is one-way ANOVA with Dunnet's post test).

(G) Dose-response curve for change in the area under the mean square displacement following addition of various glutamate concentrations (or vehicle control; mean ± SEM are plotted, statistical test is one-way ANOVA with Dunnet's post test).

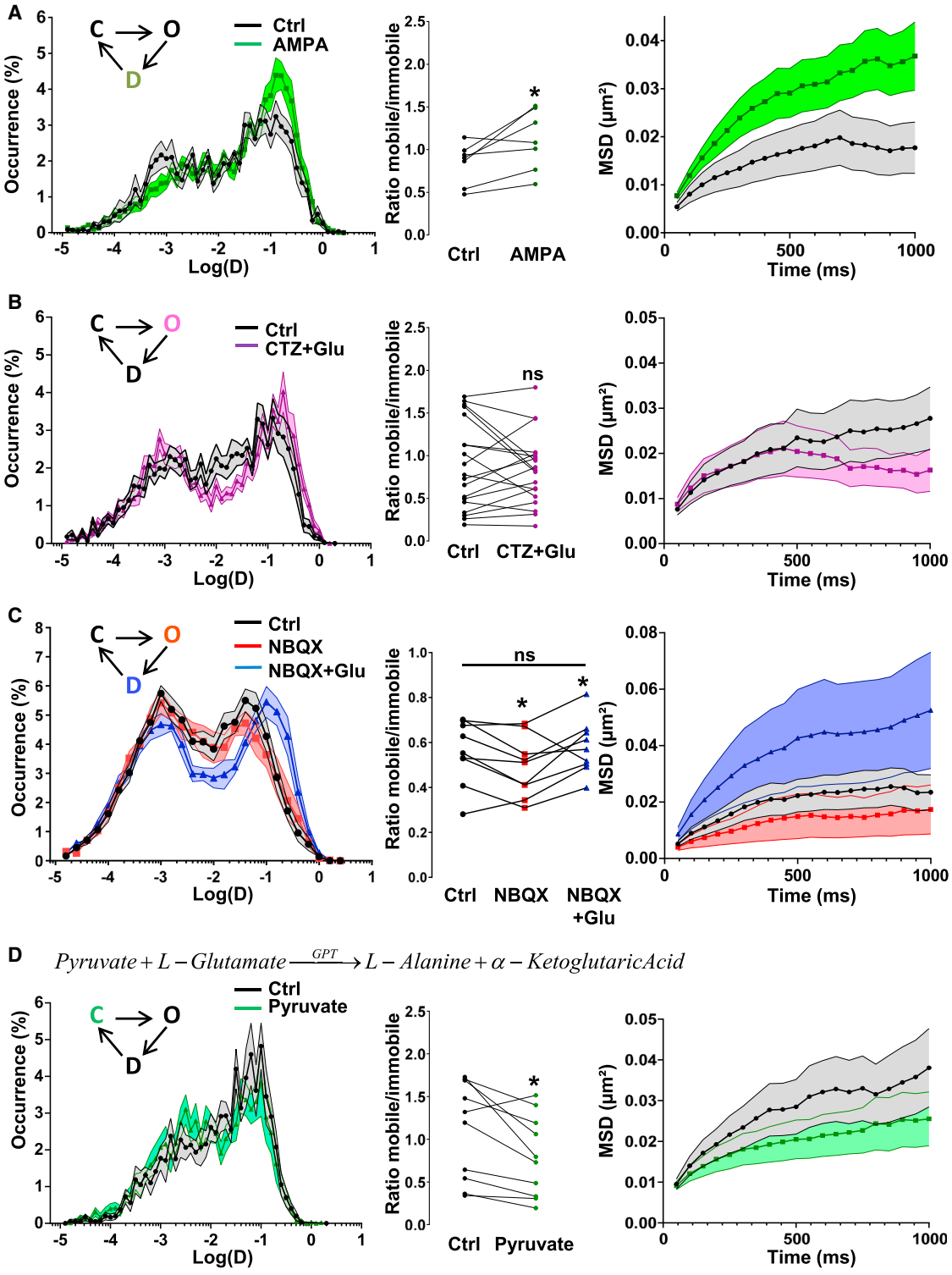

Figure 2. Drug Applications Reveal that Glutamate-Induced Mobility Is Specific of the Desensitized State

(A) Modulation of endogenous GluA2-containing AMPAR synaptic mobility in the presence of AMPA (100 µM) in drug-free Tyrode's solution. From left to right are represented the average distribution of the logarithm of the diffusion coefficient, the paired ratios of the mobile over the immobile fraction (n = 7 cells, paired t test, $p < 0.05$) and the plot of the synaptic MSD in function of time before and after treatment (n = 7 cells, paired t test on the under curve area, p = 0.01). AMPA increase significantly AMPAR mobility.

(legend continued on next page)

diffusion phenotypes ranking from immobile to highly mobile (Figure S1A). The diffusion coefficient (D) distribution can be roughly sorted into two groups. The first group is composed of AMPAR with a D value inferior to 0.008 $\mu m^2.s^{-1}$ and are referred to as "immobile" because they explore an area inferior to the one defined by the image spatial resolution (e.g., 0.08 μm) within one frame, i.e., 50 ms ($D_{threshold}$ = [0.08 μm]^2/[4 × 4 × 0.05 s] ~0.008 $\mu m^2.s^{-1}$). The second group is defined as the mobile part composed of receptors with D values above 0.008 $\mu m^2.s^{-1}$.

To investigate the effect of glutamate binding on AMPAR lateral mobility, independently of downstream intracellular signaling effects, we used acute application of various glutamate concentrations to the recording medium in the presence of a cocktail of inhibitors of (non-AMPA)-glutamate receptors and calcium channels while performing uPAINT acquisition. First, to estimate the effect of glutamate application on global cell signaling in these conditions, we measured the cytoplasmic calcium rise induced by glutamate. Neurons were preloaded with Fluo4FF-AM dye and then imaged every 1.5 s during 2 min in the observation medium. After 25 s of recording, 100 μM of glutamate was added. In the absence of the inhibitors, glutamate triggered a large increase in intracellular calcium level (Figure 1B, black line). The glutamate-induced calcium rise was markedly decreased in the presence of a combination of inhibitors of NMDA receptors, voltage-dependant Na^+ channels, L-type Ca^{2+} channels, mGluR1, mGluR5, and GluA2-subunit lacking AMPAR (Figure 1B). At the peak, in absence of blockers (Figure 1B, black line), the normalized fluorescence F/F_0 increased by 22.2% ± 3.7% compared to baseline level, whereas in presence of all blockers (Figure 1B, red line), this rise was limited to 2.2% ± 1.3%. We performed the recording in the presence of this inhibitors cocktail for all further experiments, unless otherwise stated.

Figures 1C–1G quantifies the effect of glutamate addition. In the presence of 100 μM glutamate, the proportion of mobile AMPAR increased by 30.7% ± 9.4% as compared to control, leading to an increase by 70.6% ± 22.4% of the ratio between the mobile and the immobile fractions of receptors (n = 24 cells, paired t test, p = 0.023) (Figure 1D). In parallel, the MSD, that represents the surface explored by the receptors per unit time, increased by ~70% in the presence of glutamate (Figure 1D, right panel). Application of a lower glutamate concentration (20 μM) or of the vehicle (water) did not induce a significant modification in the mobile/immobile ratio (Figures S1B and 1C and dose response curve, respectively). In contrast, the application of higher glutamate concentration (300 μM and 1 mM) increased the mobile fraction and decreased the confinement of the receptors (Figure 1E and dose response curve, Figures 1F and 1G). Altogether, these experiments suggest that glutamate modifies, in a dose-dependent manner, AMPAR mobility at the synaptic plasma membrane independently of downstream signaling, and possibly directly through changes in receptor conformation.

To confirm that the effect of glutamate on AMPAR mobility was mediated directly by their activation, we applied the AMPAR-specific agonist AMPA (alpha-amino-3-hydroxy-5-methylisoazol-4-propionate) and characterized its effect on diffusion in the absence of the antagonist cocktail present in the other experiments (Figure 2A). Application of AMPA 100 μM leads to a significant increase in GluA2 mobility (44.6% ± 3% for the control and 51.4% ± 3.2% in the presence of AMPA, p = 0.014 paired t test), and an increase of 204% of the initial confinement area.

Glutamate triggers two major changes in AMPAR conformation, first a transition to an open-state and then, within a couple of milliseconds, a transition to a desensitized state (Armstrong et al., 1998; Dürr et al., 2014; Meyerson et al., 2014; Sobolevsky et al., 2009; Sun et al., 2002). To correlate the glutamate-induced increase in AMPAR mobility to one or the other conformational state, we coapplied 100 μM glutamate with 20 μM cyclothiazide (CTZ), which prevents entry in the desensitized state; in this condition most receptors are in the open state (Traynelis et al., 2010) (Figure 2B). Neither the diffusion coefficient nor the MSD of synaptic AMPAR was affected by this treatment. This indicates that AMPAR desensitization, rather than opening, increases its mobility.

In our experiments, ambient glutamate released by neurons in culture could affect the mobility. To test this hypothesis, we first used an AMPAR antagonist (NBQX) to favor the closed-resting state. NBQX (20 μM) significantly decreased the mobile fraction and increased the confinement of AMPAR (Figure 2C). Supplementing 100 μM glutamate to the medium was presumably sufficient to compete out NBQX from enough binding sites to send AMPAR to a desensitized state, since we observed an increase in AMPAR mobility. To confirm the effect of ambient glutamate on AMPAR mobility, we recorded wild-type AMPAR mobility in

(B) Absence of modulation of endogenous GluA2-containing AMPAR synaptic mobility by coapplication of 100 μM glutamate and 20 μM cyclothiazide. From left to right are represented the average distribution of the logarithm of the diffusion coefficient, the paired ratios of the mobile over the immobile fraction (n = 19 cells, paired t test, p = 0.539), and the plot of the synaptic MSD in function of the time before and after treatment (n = 19 cells, paired t test on the under curve area, p = 0.28). Neither the diffusion coefficient nor the MSD of synaptic AMPAR are affected by coapplication of glutamate and cyclothiazide, which stabilized the AMPAR open state.

(C) Modulation of endogenous GluA2 containing AMPAR synaptic mobility by sequential application of NBQX (20 μM) (competitor antagonist), then additionally glutamate (100 μM). From left to right are represented the average distribution of the logarithm of the diffusion coefficient and the paired ratios of the mobile over the immobile fraction (n = 9 cells, p < 0.05). NBQX significantly immobilizes AMPAR by closing the ones desensitized by ambient glutamate, and then addition of extra glutamate reversed the effect on AMPAR mobility, suggesting that high glutamate concentrations are capable of competing with NBQX to send AMPAR into a desensitized state. Right panel is the plot of the synaptic MSD in function of time before and after treatment (n = 9 cells, repeated-measures ANOVA test on the under curve area, p < 0.05).

(D) Average distribution of the logarithm of the diffusion coefficient for synaptic endogenous GluA2-containing AMPAR before and after coapplication of glutamic-pyruvate transminase (GPT) and pyruvate to convert glutamate to L-alanine and α-ketoglutaric acid, thus decreasing the ambient glutamate. The middle panel is the mean ratio of the mobile over the immobile fractions of synaptic receptors before and after application of GPT and pyruvate (n = 10 cells, paired t test, p = 0.015). Scavenging ambient glutamate decreases synaptic AMPAR mobility. The right panel represents the synaptic MSD versus time plot before and after coapplication of GPT.

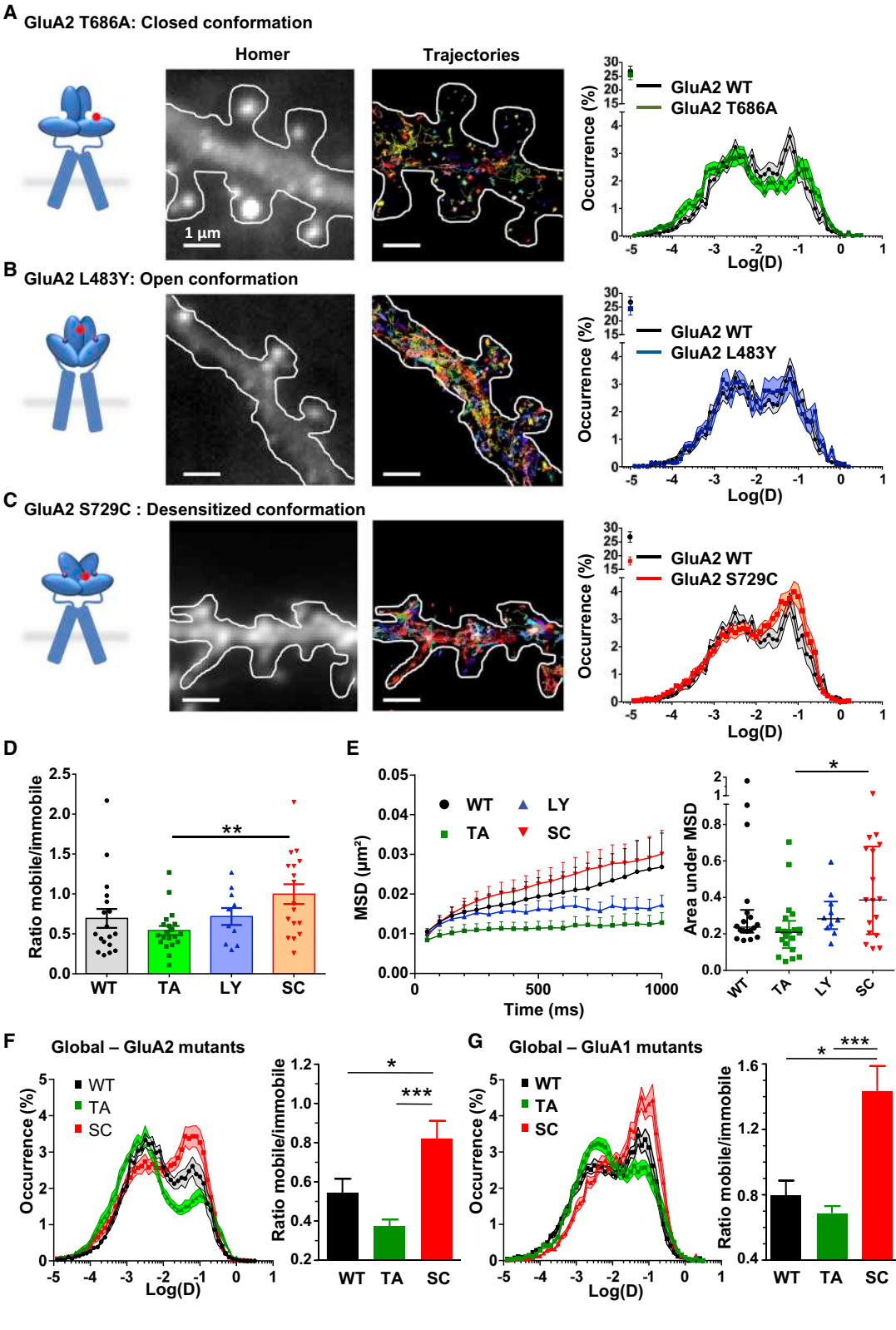

(legend on next page)

the presence of glutamic-pyruvic transaminase (GPT), an enzyme that degrades the ambient glutamate when pyruvate is in excess. Figure 2D shows that acute degradation of ambient glutamate triggers a significant decrease of AMPAR mobility. Finally, in conditions of ambient glutamate, evaluated to be in the micromolar range in hippocampal cultures (Featherstone and Shippy, 2008), a fraction of AMPAR are desensitized (Heine et al., 2008). Application of CTZ in this basal condition, which favors the AMPAR closed state, decreased the fraction of mobile receptors (Figure S1C). Altogether, these experiments demonstrate that basal ambient glutamate is sufficient to significantly increase AMPAR diffusion, likely by increasing the proportion of desensitized receptors, and further suggests that the closed AMPAR are the least mobile.

To analyze the specificity of the glutamate-induced increase mobility for AMPA-type glutamate receptors, we performed uPAINT experiments on kainate receptors (KARs) containing the GluK2 subunit which have similar conformational changes to AMPAR. We expressed Super Ecliptic pHluorin (SEP)-tagged GluK2 to track them with uPAINT using an anti-GFP nanobody. At rest, the diffusion coefficient of GluK2 was lower than that of GluA2 containing AMPAR (median values of the diffusion coefficient D in $\mu m^2.s^{-1}$ with IQR for synaptic GluK2 0.00067 IQR 0.00001–0.01655; for synaptic GluA2 0.00389 IQR 0.000225–0.03900). Application of 100 μM glutamate did not modify the diffusion coefficient nor the MSD over time of GluK2 (Figure S1D). This suggests that although they share common structural properties, the lateral diffusion of KARs and AMPAR is impacted differently by glutamate.

AMPAR Conformation Impacts Its Mobility

To examine if desensitized receptors are indeed more mobile than receptors in other states, we measured the mobility of various AMPAR mutants stabilized in distinct conformational states. We started by mutating the GluA2 subunit, as it is the one we tracked for our experiments on endogenous AMPAR. To measure the mobility of AMPAR largely occupying the closed-resting state, we used the T686A mutation in GluA2 (Robert et al., 2005). In contrast, the L483Y GluA2 mutant is stabilized in an open conformation (Stern-Bach et al., 1998; Sun et al., 2002). Finally, for receptors in a desensitized state, we used the S729C GluA2 mutant, which undergoes spontaneous disulfide bond formation that stabilizes a conformation associated with desensitization (Armstrong et al., 2006; Plested and Mayer, 2009). These mutated receptors were tagged with SEP and tracked with ATTO 647N labeled anti-GFP nanobodies (Figure S2).

As with endogenous AMPAR, exogenous wild-type GluA2 containing AMPAR displays a two-peak synaptic mobility distribution (Figure 3A, right panel, black curve). GluA2 T686A-containing AMPAR, which are mainly in a closed state, displayed a large increase in their immobile fraction correlated with a decrease in the mobile/immobile ratio of ~15% compared with recordings of overexpressed wild-type GluA2 containing AMPAR (Figure 3A right panel; Figure 3D, green curve and bar). Concomitantly, GluA2 T686A displayed an increase in their confinement compared to the nonmutated ones, as evidenced by their lower MSD (Figure 3E, green curve). In parallel, to confirm the insensitivity of GluA2 T686A-containing AMPAR to glutamate, we measured the effect of 100 μM glutamate application on GluA2 T686A mobility. Neither the mobility nor the confinement indexes of GluA2 T686A subunits are affected by glutamate (Figure S3A). This lower mobility and higher confinement of T686A AMPAR compared to wild-type ones (Figures 3D and 3E) is likely due to the partial desensitization of the latter by residual glutamate in the medium and to a couple of outlier cells displaying higher mobility (Figures 3D and 3E, WT).

In contrast to the T686A mutant, mobility of the GluA2 L483Y subunit, which stabilizes the open state in the presence of glutamate, presents similar diffusion properties and confinement values to the wild-type receptor (Figure 3B and Figures 3D and 3E, blue bar and curve). These results confirm the experiments performed when coapplying glutamate and cyclothiazide and

Figure 3. Mutated GluA2 Stabilized in a Desensitized State Are More Mobile than GluA2 Locked in a Closed or Open Conformation

(A–C) The left panels depict schemes representing the tracked AMPAR stabilized in specific conformations using point mutations. On each scheme, only the LBD, linkers, and TMD of a dimer of GluA2 are depicted. Red dots localize the point mutations. Image panels from left to right show the epifluorescence image of DsRed-Homer1c in a sample neuron, a map of the recorded trajectories using the uPAINT technique in the corresponding stretch of dendrite, and the total distribution of the logarithm of the synaptic diffusion coefficient. On each distribution, the dark line represents the control distribution of WT GluA2. (A) Comparison between GluA2 WT and T686A, a mutant stabilized in the closed state. (B) Comparison between GluA2 WT and L483Y, a mutant stabilized in the open state and so cannot desensitize. (C) Comparison between GluA2 WT and S729C, a mutant stabilized in a desensitized state. The mobile fraction of AMPAR is enriched when the receptor is stabilized in a desensitized conformation (red plot) relative to the ones in the closed/resting state (green and blue plots from A and B).

(D) Mean ratio of the mobile over the immobile fractions (±SEM) for synaptic overexpressed SEP-GluA2 and conformational mutants of GluA2 (WT, n = 17 cells; T686A, n = 20 cells; L483Y, n = 10 cells; S729C, n = 17 cells; one-way ANOVA, p = 0.0161, and Sidak's post test p = 0.009, between T686A and S729C). The ratio between the mobile and the immobile fraction is increased when the receptor stays in a desensitized conformation (red bar) compared to when it is in a closed/resting state (green bar).

(E) Plot of the synaptic MSD versus time for overexpressed SEP-GluA2 and the conformational mutants of GluA2 (left panel). Desensitized receptors (red plot) are less confined than closed/resting ones (green plot) (mean ± SEM, one-way ANOVA, p = 0.03, Sidak's post test show that TA/SC is significantly different p = 0.02). Median (±IQR) of the area under MSD are also represented (right panel) to illustrate cell to cell variability.

(F) Average distribution of the logarithm of the diffusion coefficient of pooled dendritic and synaptic overexpressed SEP-GluA2 and conformational mutants of GluA2. The right panel is the mean ratio of the mobile over the immobile fractions of pooled dendritic and synaptic overexpressed SEP-GluA2 and its conformational mutants (WT, n = 18 cells; T686A, n = 20 cells; S729C, n = 17 cells, one-way ANOVA test, and Sidak's post test).

(G) Average distribution of the logarithm of the diffusion coefficient of pooled dendritic and synaptic (left panel) overexpressed SEP GluA1 and its conformational mutants. Mean ratio of the mobile over the immobile fractions for overexpressed SEP GluA1 and its conformational mutants of GluA1 (WT, n = 9 cells; T686A, n = 14 cells; S729C, n = 11 cells; separate one-way ANOVA tests for mutants, with Dunnet's post test).

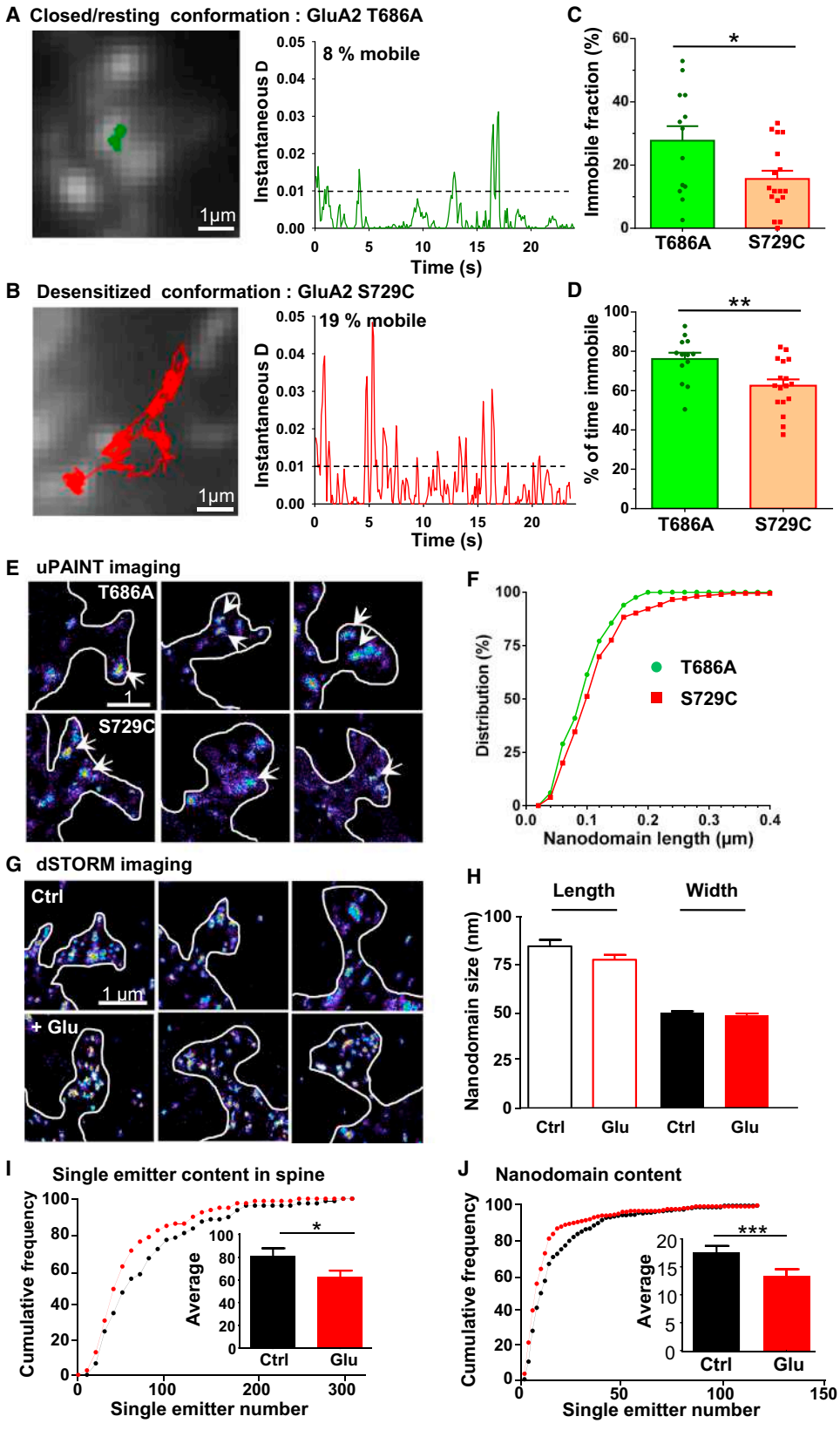

(legend on next page)

indicate the absence of a detectable change in mobility between closed and open receptors.

Finally, we expressed the GluA2 S729C mutant, which is stabilized in a desensitized state. We observed a striking 1.3-fold higher mobility of desensitized synaptic receptors as compared to those in a closed state (median values of the synaptic immobile fraction in % with IQR for GluA2 S729C 53.30 IQR 41.95–64.05; for GluA2 T686A 67.05 IQR 61.65–71.40; unpaired t test p = 0.0016). The mobile/immobile ratio of GluA2 S729C desensitized receptors is significantly higher to that of closed GluA2 T686A or wild-type receptors and similarly, the surface explored by GluA2 S729C is larger than the one explored by wild-type or always closed receptors (Figures 3C–3E). These effects were even more striking when measured on total surface GluA2 receptors (Figure 3F), as expected, since mobile receptors tend to escape from synaptic sites. The three corresponding point mutations in GluA1 induced similar and even more marked modifications in AMPAR mobility, indicating that the conformation dependent AMPAR mobility is largely subunit independent (Figures 3G and S3B).

Altogether, the increase in mobility of wild-type endogenous receptors induced by glutamate and AMPA and the increased mobility of mutants locked in a desensitized conformation indicate that desensitized AMPAR are more mobile than closed or open ones. This suggests that glutamate-induced conformation changes leading to the desensitized state may trigger release of receptors from synapses.

Desensitized AMPAR Are Stabilized for Shorter Durations than Closed-Resting AMPAR

We analyzed individual synaptic trajectories of T686A and S729C mutants lasting at least 2.5 s on neurons. For each time frame, an instantaneous diffusion coefficient was calculated (Figures 4A and 4B). This gives access to the evolution of the mobility of each receptor in function of time, allowing the extraction of two parameters: the percentage of totally immobile trajectories (log(D) < −2.1; Figure 4C) and the fraction of time spent immobile (Figure 4D). The fraction of immobile receptors all along their trajectory is significantly smaller for desensitized than for closed receptors (Figure 4B, unpaired t test, p = 0.023). In parallel, for receptors that alternate between mobile and immobile states, the proportion of time spent immobile is lower for desensitized receptors than for closed ones (Figure 4C, unpaired t test, p = 0.007). Similarly, glutamate significantly decreased the retention time of endogenous synaptic receptors (decrease of 10.5% ± 4.6%, n = 17, paired t test, p = 0.015). Altogether, this indicates that desensitized receptors are trapped less efficiently at synapses, resulting in a diminution in the proportion of immobile receptor in the spine and a corresponding higher exchange rate.

Glutamate-Mediated Increase in AMPAR Mobility Is Not Correlated with a Change in their Nano-organization

We next investigated whether AMPAR nanoscale organization depends on their conformational state. We and others previously demonstrated that wild-type and expressed AMPAR are organized in nanodomains with a full width at half maximum of ~70 nm (MacGillavry et al., 2013; Nair et al., 2013). The T686A and S729C GluA2 mutants formed nanodomains of similar size, as measured by anisotropic Gaussian fitting of presegmented clusters obtained on uPAINT high-resolution intensity images (Nair et al., 2013) (Figures 4E and 4F). This indicates that although desensitized AMPAR spend proportionally less time in the immobile state, their overall nanoscale organization is similar to that of closed receptors.

To confirm this finding, we performed d-STORM experiments on endogenous GluA2 subunits before and after application of glutamate (Figure 4G). The nanodomain size did not vary significantly upon glutamate application (median values of the length (l) and width (w) in nm with IQR in control condition: w = 46.9 IQR 39.9–58.1; l = 75.4 IQR 55.65–104.5 and after glutamate treatment: w = 46.4 IQR 39.19–56.64; l = 67.95 IQR 56.0–88.58; Mann-Whitney test, p = 0.6203 for width, p = 0.1856 for length; Figure 4H). In parallel, we estimated the total number of

Figure 4. Glutamate-Induced Increase in Mobility Is Due to a Remobilization of Trapped Receptors without Affecting Nanodomain Structure

(A and B) Representative synaptic trajectories and the variation of their instantaneous diffusion versus time obtained by tracking GluA2 S729C and GluA2 T686A conformational mutants, respectively. The dark dashed line represents the threshold under which receptors are considered as immobile. S729C mutant are more mobile than the T686A ones. Two parameters can be extracted from these trajectories. The first one is the fraction of receptors which are immobile (C). The second one is the fraction of time AMPAR are immobile measured on trajectories which alternate between mobile and immobile behavior (D).

(C) Fractions of receptors which are immobile (log [D] < −2.1) all along their trajectory duration for GluA2 S729C and GluA2 T686A mutants (mean ± SEM; n = 17 cells for GluA2 S729C, n = 13 cells for GluA2 T686A, unpaired t test, p = 0.023).

(D) Percentage of time AMPAR are immobile on their trajectory when they are partially mobile for GluA2 S729C and GluA2 T686A (mean ± SEM; n = 17 cells for GluA2 S729C, n = 13 cells for GluA2 T686A, unpaired t test, p = 0.007).

(E) Sample superresolved intensity images obtained by uPAINT on neurons expressing GluA2 T686A (top) or GluA2 S729C (bottom). Arrows point to AMPAR nanodomains. Distribution of AMPAR nanodomain length measured for GluA2 S729C and GluA2 T686A (F). Nanodomain sizes are similar for receptors locked in the desensitized or in the closed conformation (S729C, n = 205 nanodomains; T686A, n = 83 nanodomains; Mann-Whitney test, p = 0.086).

(G) Sample superresolution intensity images of spines obtained using d-STORM on neurons live stained for endogenous GluA2. After live incubation with antibodies against GluA2, neurons were incubated for 2 min either in the presence of vehicle (top) or in the presence of 100 μM glutamate (bottom).

(H) Width and length of AMPAR synaptic nanodomains. Nanodomain sizes were measured by anisotropic Gaussian fitting clusters obtained on d-STORM images. Nanodomain length and width (mean ± SEM) in control conditions and after application of 100 μM glutamate are plotted (left, n[ctrl] = 149 and n[Glu] = 174 nanodomains, Mann-Whitney test, p > 0.1 for both width and length). Nanodomain size is not impacted by glutamate application.

(I and J) Cumulative distribution and, in the insert, mean of spine and nanodomain AMPAR content, respectively. The total number of AMPAR inside spines was estimated by counting the single emitters. The cumulative distribution and the average number of single emitters per spines are reported in control and glutamate treated conditions (mean ± SEM; n = 77 and 78 spines, respectively; Mann-Whitney test, p = 0.038). As for the spine level, the number of AMPAR in nanodomains was estimated in control and glutamate treated conditions (mean ± SEM; n = 226 and 189 nanodomains, respectively, Mann-Whitney test, p < 0.0001). Upon glutamate treatment, the number of AMPAR inside both spines and nanodomains significantly decreases.

AMPAR present in spines and in individual nanodomains before and after glutamate treatment by dividing the total number of single-molecule detection events in a spine or a nanodomain by the average number of detection events determined for isolated fluorescent spots that likely represent individual receptors (Nair et al., 2013). Cumulative frequencies of the number of single emitters per spine and nanodomain are represented in Figures 4I and 4J. In both cases, we observed a decrease of ~20% in the number of single emitters when neurons were treated with glutamate (median values of the number of single emitters per spine [s] and per nanodomain [n] with IQR in control condition: s = 58.13 IQR 34.86–102.5, n = 11.02 IQR 6.673–22.01 and after glutamate treatment, s = 46.21 IQR 31.17–75.20, n = 8.337 IQR 5.481–13.40). This represents a loss of ~12 AMPAR per spine (Figure 4I) and three AMPAR per nanodomain upon glutamate application (Figure 4J). Altogether these data indicate that glutamate mediates a mobilization of synaptic AMPAR which leads to a loss of receptors contained in spines and nanodomains. This is not associated with a major change in their subsynaptic organization at the nanoscale level.

Molecular Basis of Glutamate-Induced Increase in AMPAR Mobility

We and others previously demonstrated (Bats et al., 2007; Nair et al., 2013; Opazo et al., 2010; Schnell et al., 2002; Sumioka et al., 2010; Tomita et al., 2005a) that synaptic AMPAR stabilization is mainly based on interactions within a tripartite complex composed of the cytoplasmic scaffold PSD-95, the AMPAR auxiliary protein stargazin, and the AMPAR. To decipher the molecular basis of glutamate-induced increase in AMPAR mobility, we investigated possible modifications in the interaction between stargazin and AMPAR.

Previous work indicated that glutamate induces a dissociation of stargazin from AMPAR (Morimoto-Tomita et al., 2009; Tomita et al., 2004), although this has been debated (Nakagawa et al., 2005; Semenov et al., 2012). We thus investigated whether the glutamate-induced increase in AMPAR mobility could originate from a loss of avidity of stargazin for specific AMPAR conformational states. We coexpressed the various GluA1 mutants locked in the closed and desensitized conformation in HEK cells together with WT GluA2 and stargazin and used coimmunoprecipitation to measure their interaction (Figures 5A and 5B). Strikingly, the S729C desensitized mutant displayed a 60% reduction in binding to stargazin compared to WT and closed forms of GluA1. In order to further test if glutamate-induced stargazin detachment from AMPAR is at the origin of their increased mobility, we measured the effect of glutamate on the mobility of GluA1-stargazin tandems in which the intracellular C terminus of GluA1 is fused to the N terminus of stargazin (Figure 5D), preventing any possible dissociation. This tandem has been previously shown to form functional AMPAR (Morimoto-Tomita et al., 2009). The tandem was tracked by uPAINT using an ATTO 647N tagged anti-GFP nanobody. The tandem presented a decreased mobility compared to WT (compare Figures 5C and 5D), fully compatible with the key role of stargazin in immobilizing AMPAR (Bats et al., 2007). This stabilization was likely mediated through interactions with PSD scaffold proteins, since truncating the PDZ ligand of the chimeric GluA1-stargazin resulted in a construct with very high mobility (data not shown). Bath application of 100 μM glutamate did not increase the mobility nor the mobile/immobile ratio of the GluA1-stargazin tandem, while it increased both when GluA1 was expressed alone (Figures 5C and 5D). Moreover, after application of glutamate, the area explored by the tandem remained unchanged, whereas this area increased for GluA1 (Figures 5C and 5D, right panels). These experiments suggest that the glutamate-induced increase in AMPAR mobility is due to a decreased association of the AMPAR desensitized state with auxiliary proteins.

Acute Stimulation of Synapses by Glutamate Uncaging Mobilizes AMPAR

An important question is to know if the glutamate-induced increase in AMPAR mobility occurs physiologically since AMPAR desensitize even after a brief exposure to glutamate (Colquhoun et al., 1992). As a first step, we refined spatiotemporally the application of glutamate by using two-photon MNI-glutamate uncaging in the presence of the blockers used for bath application of glutamate (Figure 6A). We first verified that 2P glutamate uncaging triggers currents comparable to spontaneous excitatory postsynaptic currents (EPSCs) (Figure 6B). We then compared the mobility of AMPAR before and after uncaging, either at uncaged (Figure 6C) or neighboring synapses (Figure 6D) on the same neuron. Glutamate uncaging induced a specific increase in AMPAR mobility at uncaged synapses, supported both by an increase in the median diffusion and a decrease in the confinement. This increased mobility is more modest that the one observed during bath application of glutamate. This result was expected, since the area over which 2P uncaging is performed is small and the time of glutamate presence very short, while tracking measurements are performed during 0.5 s, a period during which a significant fraction of AMPAR have recovered from desensitization. We performed similar experiments with one-photon uncaging of MNI-glutamate and found similar results (Figure S4). Together, these results corroborate and refine our initial findings with bath application of glutamate: brief application of glutamate increases AMPA receptor mobility at synapses.

Glutamate-Induced Increase in Desensitized AMPAR Mobility Tunes Short-Term Synaptic Plasticity

We have previously shown that AMPAR fast diffusion tunes frequency-dependent synaptic transmission in paired-pulse experiments by allowing desensitized receptors to be replaced by naive ones, thus accelerating recovery from desensitization-induced synaptic depression (Frischknecht et al., 2009; Heine et al., 2008; Opazo et al., 2010). We thus investigated whether the glutamate-induced mobility of desensitized receptors could directly participate in explaining our previous findings that mobile AMPAR are necessary for fast recovery from synaptic depression during high frequency stimulus trains. To this aim, we performed whole-cell patch-clamp measurements of short-term synaptic plasticity in hippocampal neurons expressing SEP-GluA1 either alone or coexpressed with the tandem SEP-GluA1-stargazin. To investigate the impact of mobility, we used the classical antibody-mediated crosslink approach to immobilize expressed receptors and then applied 20 Hz stimulus

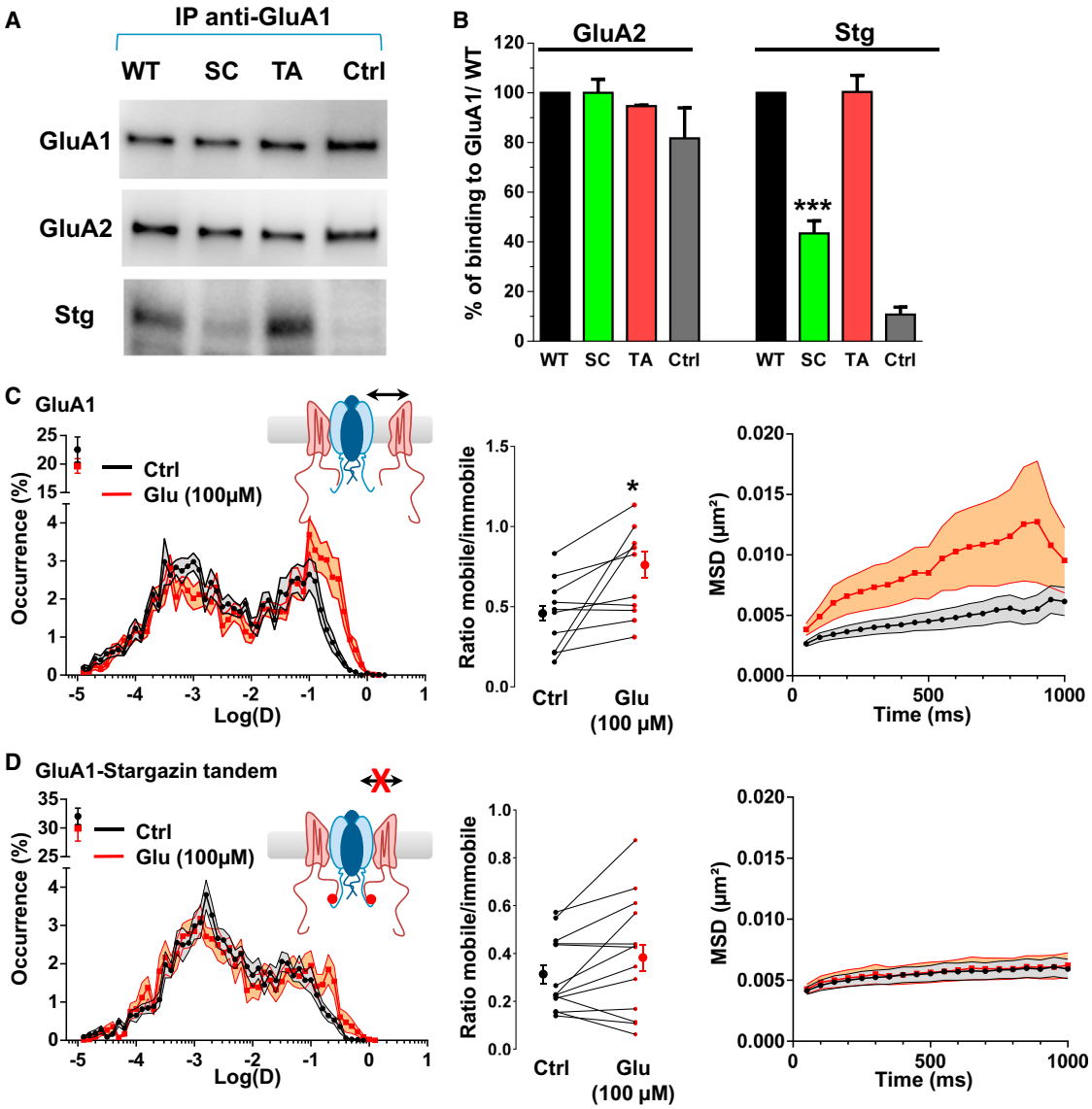

Figure 5. Glutamate-Induced AMPAR Mobility Is Abolished for the Chimera GluA1/Stargazin

(A) Coimmunoprecipitation experiment on extracts from HEK cells coexpressing GluA2 and wild-type, desensitized, or closed mutants of GluA1 with or without (Ctrl) stargazin as indicated in the figure. Immunoprecipitation of GluA1 was performed using an antibody directed against the extracellular domain. The samples were analyzed with anti-GluA1, anti-GluA2, and anti-Stg for each condition.

(B) Quantification of five GluA1/GluA2/stg immunoprecipitation experiments. The Stg binding to desensitized receptor is significantly reduced (mean ± SEM; n = 5 experiments, one-way ANOVA with Dunnet's post test).

(C and D) Left panel insets show schemes representing the hypothetical stargazin and GluA1 interactions and their corresponding mobility before and after glutamate application, in control condition (endogenous stargazin and expressed SEP-GluA1) in (C) and when the two proteins are genetically fused (SEP-GluA1-stargazin chimera) in (D). (Left panels) Distributions of the logarithm of the diffusion coefficients. Middle panels: paired ratio of the mobile over the immobile fraction before and after treatment with 100 μM glutamate (for GluA1: n = 10 cells, paired t test, p = 0.024; for GluA1-stargazin chimera: n = 13 cells, paired t test, p > 0.05). Glutamate mobilizes synaptic GluA1-containing AMPAR but not GluA1-stargazin chimera. Right panels show plots of the synaptic MSD versus time before and after application of glutamate (100 μM).

trains to stimulate presynaptic axons and evoke a series of EPSCs.

In control cells expressing SEP-GluA1, we observed short-term facilitation of the EPSCs. The fifth response was on average increased to 120% of the amplitude of the first EPSC of the train (Figures 7A and S5A). Consistent with what we demonstrated previously for paired-pulse protocols (Heine et al., 2008), cross-linking surface SEP-GluA1-containing AMPAR with an anti-GFP antibody for 5 min caused a marked decrease in the EPSC amplitudes during the train (p = 0.0301, Welch's two-tailed t test), where the fifth EPSC decreased to 78% of the amplitude for the first response of the train (Figure 7A). This short-term

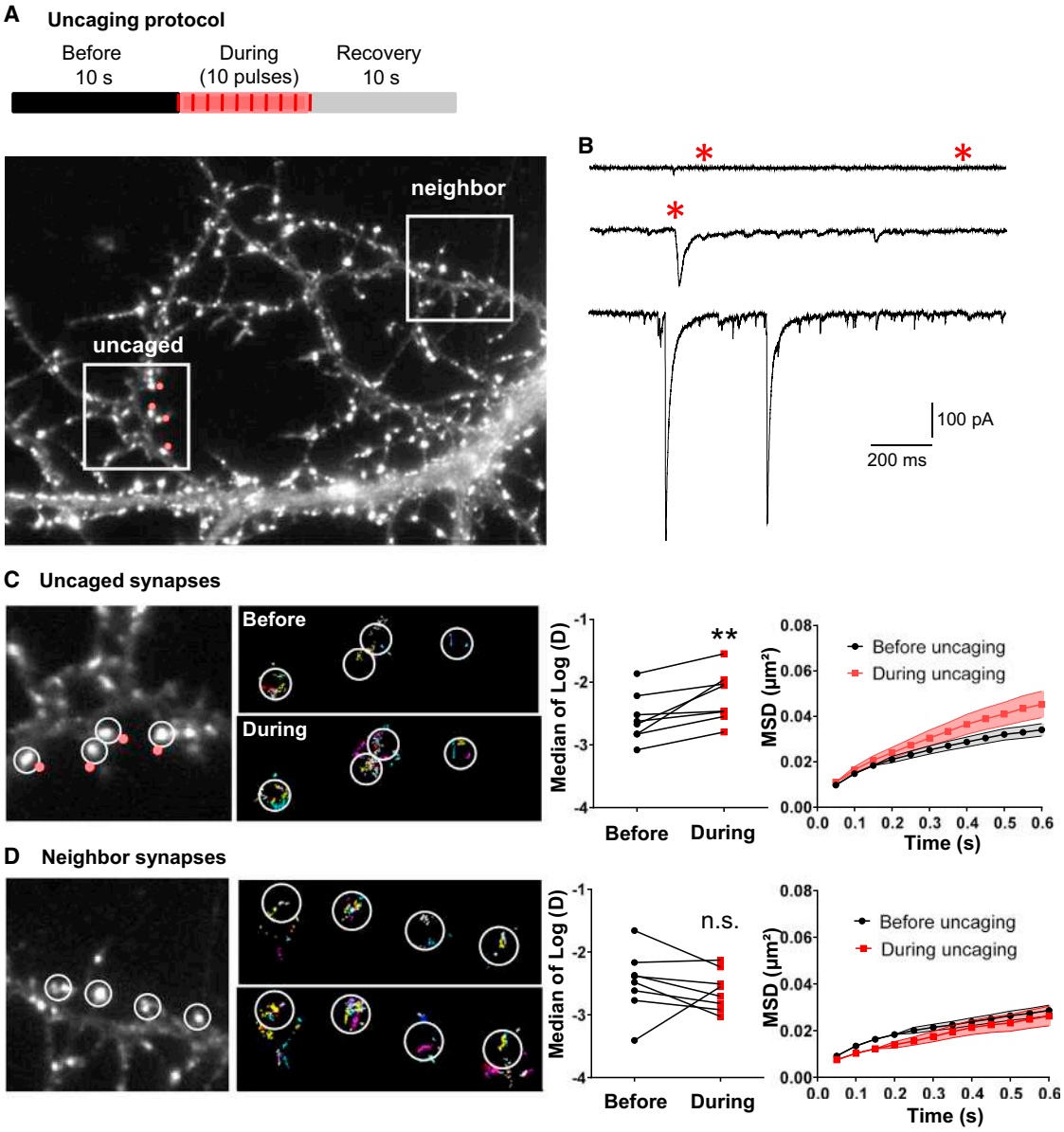

Figure 6. Acute Stimulation of Synaptic AMPAR with Glutamate 2-P Uncaging Mobilizes AMPAR

(A) Top panel shows an illustration of the protocol used for control and glutamate uncaging assays. Lower panel shows an epifluorescence image of a neuron expressing eGFP-Homer 1c as a synaptic marker and the position of uncaging spots indicated with red dots. One protocol round consists of a 10 s baseline recording followed by 10 uncaging laser pulses at 2 Hz, and by 10 s without recording and stimulation to avoid overstimulation. For each cell, five consecutive rounds were recorded.

(B) Examples of electrophysiological currents recorded in the presence of 2.5 mM MNI-glutamate when, from the top to the bottom, the laser is off (no uncaging), laser is on (uncaging) and when synaptic transmission occurred spontaneously and independently of the laser trigger.

(C and D) Left panels show epifluorescence images and synaptic GluA2 trajectories before and during laser pulses at the uncaged synapses (C) and the neighbor synapses (D). Middle and right panels show, respectively, the plots of the median mobility value per cell and the synaptic MSD versus time, before and during laser pulses. AMPAR are less confined after glutamate uncaging (n = 8 cells, paired t test $p < 0.01$ and $p > 0.05$ for uncaged and neighbor synapses, respectively).

depression did not appear to be associated with much larger initial EPSC amplitudes that could otherwise be expected for a higher release probability (Figure 7A). Corroborating the specificity of the antibody crosslink for expressed receptors, a depressive effect on short-term plasticity was not observed when applying the anti-GFP to cells expressing GluA1 without the amino-terminal SEP fusion (Figure S5A). We then performed similar experiments on neurons expressing the GluA1-stargazin tandem. In the control cells (without antibody crosslinking), the ESPCs already depressed during the train (fifth EPSC to 75%),

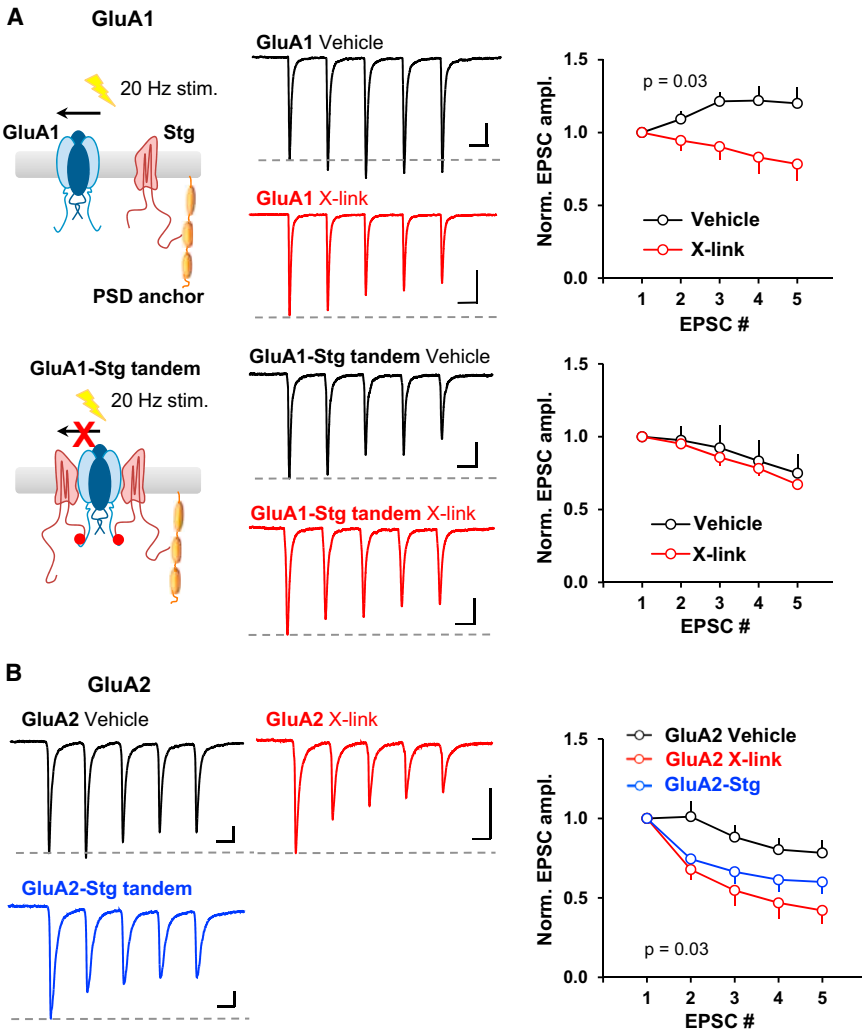

Figure 7. Train Stimulation Triggers Depression in Neurons Expressing the GluA-Stargazin Tandems, which Mimics and Occludes the Effect of AMPAR Crosslinking

(A) The diagrams on the left represent the experimental paradigm: SEP-GluA1 and endogenous stargazin are expressed separately or linked in a SEP-GluA1-stargazin tandem. GluA1 interact with stargazin (maroon, either endogenous or covalently linked) that traps AMPARs at synapses via PDZ interactions. To test the role of AMPAR mobility during a train of stimulation, lateral diffusion was blocked by crosslinking the receptors with an anti-GFP antibody (X-Link). The middle panels represent the average EPSC trains (five pulses at 20 Hz), for example cells in conditions with and without crosslinking. (Right) Plots of the EPSC amplitude normalized to the initial EPSC for stimulations with (n = 5 cells) and without (n = 6 cells) crosslinking. When GluA1 cannot dissociate from stargazin, EPSCs elicited by a train of stimulation already have depressed short-term plasticity, which occludes crosslinking (n = 7 cells, both with and without crosslinking).

(B) The same experiments performed with SEP-GluA2 and SEP-GluA2-Stg tandem (both coexpressed with SEP-GluA1) lead to a similar conclusion. (Left) Average EPSC trains for all cells in each group. (Right) Plots of EPSC amplitude with normalization to the initial EPSC. n = 15, 5, and 8 cells in the vehicle, X-link, and tandem conditions, respectively. (A and B) statistics with Welch's ANOVA test comparing the sum of normalized EPSC amplitudes. Log-transformed initial EPSC amplitudes were not significantly different in (A), top (p = 0.748, Welch's t test), or (B) (p = 0.260, Welch's ANOVA test). Scale bars are 50 pA and 25 ms.

likely as a direct consequence of the lower mobility of this construct (Figures 5D and 7A). We observed a similar effect on short-term plasticity when we coexpressed GluA1 with a GluA2-stargazin tandem (Figure 7B), indicating that the effect was not unique to the GluA1-stargazin tandem. Interestingly, when we tried crosslinking the GluA1-stargazin tandem, we did not observe much further depression during the train (fifth EPSC to 67%), thus demonstrating that fusion of GluA1 to stargazin occludes the depressive effect of crosslinking on short-term synaptic plasticity. Altogether, these experiments establish that preventing GluA1 or GluA2 dissociation from stargazin prevents the positive impact of AMPAR diffusion on recovery from short-term depression.

DISCUSSION

Using high-density single-molecule tracking on live and fixed neurons as well as biochemistry, electrophysiology, and glutamate uncaging, we investigated the impact of changes in AMPAR conformational states on their surface diffusion, confinement, and nanoscale organization. Our results on both wild-type AMPAR and point mutants of GluA1 and GluA2 subunits locked in various conformational states establish that desensitized AMPAR are more mobile than closed or open ones due to less avidity for stargazin. This glutamate-induced increase in AMPAR mobility removes a fraction (~20%–30%) of receptors from nanodomains and synaptic sites but does not modify the overall nanodomain organization of AMPAR. Finally, we show that the increased mobility of desensitized receptors plays a key role in fast synaptic transmission, enabling rapid turnover of AMPAR opposed to glutamate release sites. This allows synapses to recover faster from high-frequency short-term depression consequent to AMPAR desensitization.

Glutamate Binding Induces an Increase in the Proportion of Mobile AMPAR Independent of Intracellular Signaling

The use of single-molecule detection allowed us to obtain the full distribution of AMPAR behavior and detect that ~20%–30% of AMPAR increase their mobility upon glutamate binding in a dose-dependent manner. Glutamate has long been shown to regulate AMPAR traffic. Three main pathways have been

identified in this process. First, glutamate-induced increase in intracellular calcium during high-frequency stimulation triggers AMPAR immobilization and accumulation at synaptic sites (Borgdorff and Choquet, 2002; Heine et al., 2008; Opazo et al., 2010). This effect is largely mediated by CaMKII-induced phosphorylation of the AMPAR auxiliary protein stargazin, which stabilizes AMPAR by increasing binding to PSD-95. Second, the low-frequency stimulation induced increase in AMPAR mobility, which results in AMPAR loss from synaptic sites (Shepherd and Huganir, 2007; Tardin et al., 2003). Both these effects rely on intracellular signaling and have been proposed to underlie long-term synaptic plasticity. Third, and less characterized, activation of AMPAR has been proposed to trigger their endocytosis by a signaling-independent process (Beattie et al., 2000; Lin et al., 2000; Tomita et al., 2004). This is fully consistent with our observation that glutamate and AMPA induce an increase in AMPAR diffusion that does not depend upon intracellular signaling.

AMPAR Conformational Changes Trigger Their Increased Mobility

Glutamate binding triggers major changes in AMPAR conformation that lead to opening of the ion pore and ultimately entry into the desensitized state. Recent work on GluA subunits (Dürr et al., 2014; Meyerson et al., 2014; Nakagawa et al., 2005) indicates that, in the desensitized state, all the extracellular N-terminal domain composed by both the amino-terminal (ATD) and the ligand binding (LBD) domains undergo major rearrangements, resulting in a separation of the four subunits from 25 Å up to complete separation of the ATDs. Our experiments indicate that the AMPAR conformational changes triggered by glutamate are enough to increase their surface diffusion. First, bath glutamate application, glutamate uncaging, and even endogenous ambient glutamate trigger increased AMPAR diffusion. Second, pharmacological manipulations that favor either the AMPAR closed state (NBQX, Figure 2C) or prevent desensitization (CTZ, Figure S1C) slow down AMPAR. Third, point mutants of GluA1 or GluA2 that lock AMPAR in a desensitized conformation display a robust increase in diffusion as compared to wild-type AMPAR, or AMPAR locked in the closed or open conformations. Fourth, coapplication of glutamate and CTZ or expressing the LY mutation suggest that AMPAR in the open state move similarly to the closed ones. We have no certitude as to why the effect is more robust in GluA1 than GluA2 mutants, but this could simply arise from the more physiological expression of GluA1 than GluA2 homomers. In complement, we found that AMPA has a less profound effect on mobility than the physiological agonist, glutamate. Indeed, AMPA is known to trigger not exactly the same conformation changes in AMPAR as glutamate (Jin et al., 2003). Finally, recent results at the *Drosophila* neuromuscular junction also indicate that mutations changing gating properties alter GluR distribution and trafficking, although on a much slower timescale (Petzoldt et al., 2014).

Altogether, these studies and our results indicate that glutamate-induced entry of AMPAR into the desensitized state is associated with major structural rearrangements paralleled by increased receptor surface diffusion. Thus a major question is this: how could changes in the AMPAR ATD and LBD domains lead to their freeing from synaptic anchors?

Molecular Mechanism of Glutamate-Induced AMPAR Diffusion

Among all the protein-protein interactions accounting for AMPAR stabilization in the PSD, only a few are good candidates to be modulated by glutamate-induced AMPAR conformational changes. The GluA C terminus being largely nonstructured, it is hard to conceive how a change in the ATD/LBD organization could transfer into changes in GluA C terminus-scaffold interactions. Alternatively, the TARP family of AMPAR auxiliary subunits plays a central role in regulating AMPAR anchoring at synapses (Bats et al., 2007; Schnell et al., 2002). Stargazin binds AMPAR tightly through a large interface including the AMPAR extracellular domains (Cais et al., 2014; Tomita et al., 2004) and stabilizes the complex in the synapse through binding of its C terminus to PDZ domain-containing scaffolds such as PSD-95. The AMPAR-TARP-PSD-95 complex has been suggested to account in large part for basal and activity-dependent AMPAR immobilization at synapses (Bats et al., 2007; Opazo et al., 2010; Schnell et al., 2002; Tomita et al., 2005b). However, it is hard to conceive how a change in AMPAR conformation could translate into a decrease in TARP/PSD-95 interaction.

An initial biochemical study suggested that AMPAR dissociate rapidly from TARPs upon binding to glutamate and are internalized, whereas TARPs remain stable at the plasma membrane (Tomita et al., 2004), but in other following studies, rapid agonist-driven dissociation has not been observed (Nakagawa et al., 2005; Semenov et al., 2012). Most interestingly, we found now that the TARP-AMPAR interaction depends on AMPAR conformational state, desensitized AMPAR binding less stargazin. Our results thus indicate that increased AMPAR mobility upon glutamate binding is due to the specific dissociation of desensitized AMPAR from stargazin, allowing them to diffuse out of TARP anchoring sites at synapses such as PSD-95 slots (Figure 8). This dissociation could arise from the large structural rearrangement of the extracellular domain occurring upon AMPAR desensitization that likely impacts the normal engagement of both the ATD and LBD of AMPAR in the TARP-AMPAR interface (Cais et al., 2014). This hypothesis is supported by the fact that the GluA-stargazin tandems, which cannot be dissociated by glutamate binding, are less mobile than GluAs alone, and more importantly, that their mobility is not affected by glutamate.

While over 95% of AMPAR become desensitized within a few milliseconds upon glutamate binding (Colquhoun et al., 1992), we observed a change in mobility in only 35% of the receptors at the most. The large interface involved in AMPAR/TARP interaction (Cais et al., 2014; Priel et al., 2005; Tomita et al., 2005a; Turetsky et al., 2005) goes together with the high stability of the resting AMPAR/TARP complex reported in biochemical experiments (Schwenk et al., 2012; Tomita et al., 2004). We suggest that only some desensitized AMPAR have a lower affinity for TARPs, which is compatible with the existence of various desensitized AMPAR conformations (Dürr et al., 2014; Meyerson et al., 2014; Nakagawa et al., 2005). These various conformations would present different levels of mobility, depending on whether they are bound or not to a TARP. This hypothesis is further supported by our biochemical experiments that indicate a lower, but not fully abolished, binding of desensitized AMPAR to stargazin (Figure 5A). In addition, given the high density of

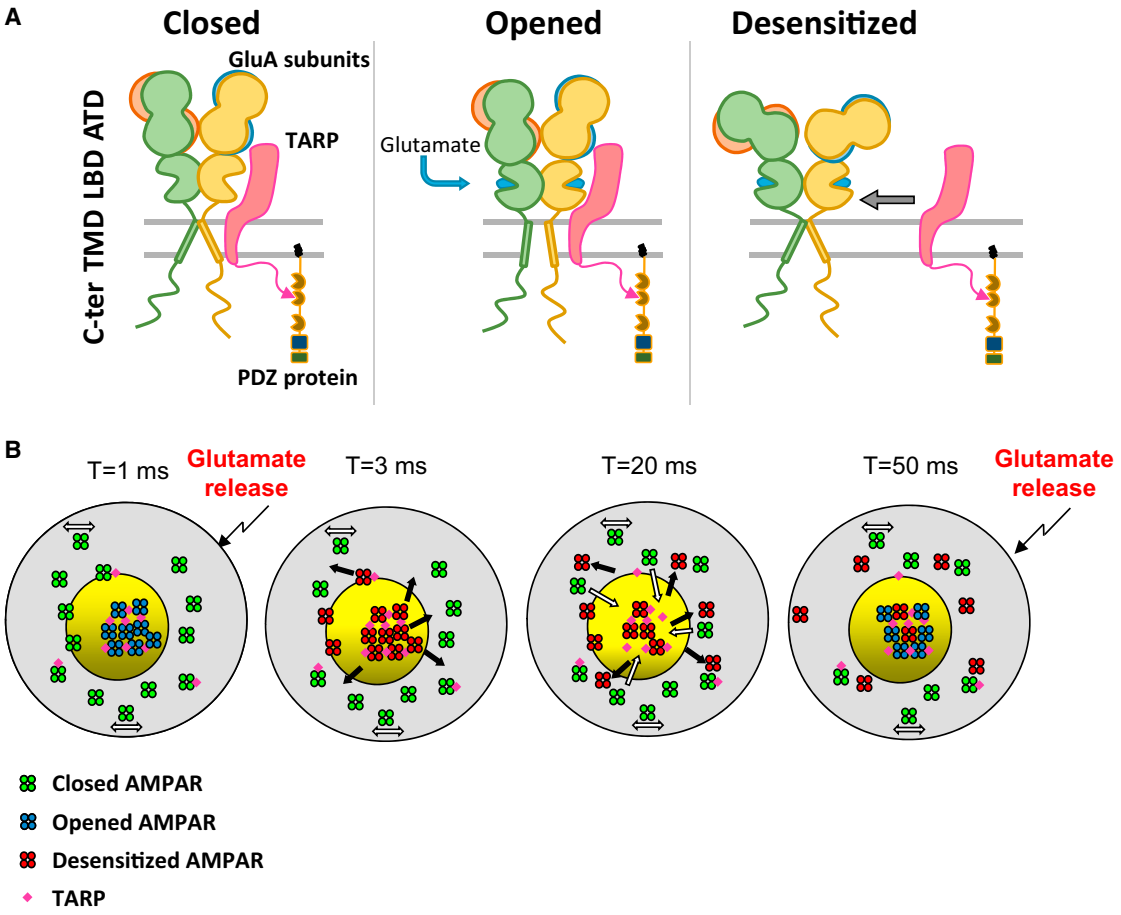

Figure 8. Hypothetical Model of Glutamate-Induced AMPAR Mobility and Effect on Synaptic Organization

(A) AMPAR are tightly coassembled with TARP at least via its transmembrane (TMD) and ligand-binding domain (LBD); the drastic changes operating at the LBD and ATD in the presence of glutamate lead to the desensitization of the AMPAR and to a decrease of its avidity for TARP. This effect could trigger a detrapping of AMPAR and an increase of its mobility.

(B) The schemes represent a top view of a synapse where naive (closed-green) AMPAR are regrouped partly in a nanocluster. The first glutamate release activates AMPAR during the first ms (T = 1 ms, blue, synaptic area covered by glutamate represented by yellow circle), then they quickly desensitize (T = 3 ms, red). This conformational change triggers an increase of AMPAR mobility, freeing TARP immobilization site. Free diffusive closed receptor can be specifically trapped at this free site (T = 20 ms), allowing a renewing of AMPAR in the nanocluster (T = 50 ms). Desensitized receptors are now out of the release site, and closed receptors replace them inside the nanocluster. This specific glutamate-induced mobility of desensitized AMPAR can be at the base of the constant receptor turnover essential for fidelity of fast synaptic transmission.

receptors within each nanodomain, it is conceivable that receptors at the center of the domain resensitize before they have the opportunity to escape the domain due to steric hindrance.

Physiological Consequences of the Enhanced AMPAR Diffusion upon Desensitization

AMPAR fast diffusion in and out of synapses allows faster recovery from desensitization-dependent paired-pulse depression for stimulation frequencies between 10 and 100 Hz (Frischknecht et al., 2009; Heine et al., 2008). All processes accelerating AMPAR diffusion increase recovery from paired-pulse depression by favoring stochastic exchange of desensitized receptors by naive ones. It was tempting to speculate that the mechanism would be even more efficient if desensitized AMPAR would escape faster from the postsynapse than naive ones.

In parallel, recent work (MacGillavry et al., 2013; Nair et al., 2013) demonstrated that around half of AMPAR are stabilized in 80 nm diameter nanoclusters in the postsynaptic density, the other part diffusing rapidly in between them (Nair et al., 2013). Our present experiments indicate that an ~20%–30% fraction of immobile AMPAR become mobile upon glutamate binding. This percentage is similar to the fraction of receptors lost from nanodomains upon glutamate application observed in d-STORM experiments. Interestingly, this loss does not modify the overall organization of AMPAR in nanodomains. We thus postulate that the increased mobility of a fraction of desensitized AMPAR is important to accelerate their exit from immobilization sites such as nanodomains to help synapses recover faster from desensitization-dependent depression. In agreement, we found that expression of the GluA-stargazin tandem, which blocks

glutamate-induced dissociation and maintains receptors immobile, increased short-term depression. In parallel, as found previously, crosslinking wild-type surface GluA1 or GluA2 also increased short-term depression, by preventing the exchange of desensitized receptors for naive ones (Heine et al., 2008).

It was previously proposed that receptor desensitization promotes the transient dissociation of TARP-AMPA receptor complexes within a few milliseconds (Morimoto-Tomita et al., 2009) and that this process accounts for the bell-shaped curve of native AMPAR steady-state glutamate-induced current concentration-response curves, reflecting the autoinactivated concentration-response behavior. The authors postulated further that this dissociation mechanism could contribute to synaptic short-term modulation by promoting paired-pulse depression, given that stargazin tends to decrease desensitization rates (Morimoto-Tomita et al., 2009; Priel et al., 2005). This is at variance with our results with the GluA1 or GluA2 chimera that both display an increased synaptic depression. Interestingly, a recent study (Semenov et al., 2012) found that a fusion protein which links the carboxyl terminus of GluA4i to the N terminus of stargazin shows similar autoinactivation to that observed in the case of separately expressed proteins, which is also in contrast to the previous results (Morimoto-Tomita et al., 2009) where covalent linkage between GluA1 and stargazin was reported to abolish autoinactivation. The reason for these discrepancies is not clear but may originate from the differences in subunits and/or linkers used for the chimera construct.

In conclusion, we propose that the increased mobility of a fraction of desensitized AMPAR is an important process to specifically allow them to diffuse out of individual nanodomains in which they would otherwise remain locked (Figure 8). Our previous simulation work established that AMPAR in nanodomains can account for as much as 70% of EPSCs (Nair et al., 2013). As AMPAR are stable in nanodomains and highly diffusive in between them, freeing desensitized AMPAR from their anchor allows them to quickly diffuse away from the glutamate bathed area in between consecutive vesicle releases. This fast exchange between desensitized and naive receptors allows maintenance of the fidelity of synaptic responses during high-frequency stimulation (Choquet, 2010; Heine et al., 2008). Our results provide a simple explanation to the regulation of synaptic transmission observed through modulation of AMPAR mobility.

EXPERIMENTAL PROCEDURES

Molecular Biology, Biochemistry, Cell Culture, and Transfection

Cloning of plasmids and cultures of rat hippocampal neurons was performed as in Nair et al. (2013) (see Supplemental Experimental Procedures for details).

Direct Stochastic Optical Reconstruction Microscopy, uPAINT Experiments, Receptor Tracking, and Analysis

Single-molecule fluorescent spots were localized in each frame and tracked over time as in Giannone et al. (2010) and Nair et al. (2013) (see Supplemental Experimental Procedures for details).

Glutamate Uncaging and Scavenging Experiments

1-P and 2-P uncaging experiments as well as glutamate scavenging were done using an inverted motorized microscope (Nikon Ti, Japan) equipped with a 100× PL-APO objective (1.49 NA) (see Supplemental Experimental Procedures for details).

Ca^{2+} Imaging, Electrophysiological Recordings, and Crosslinking Experiments

Calcium imaging and electrophysiological recordings and receptor crosslinking were performed following Heine et al. (2008) (see Supplemental Experimental Procedures for details).

Statistics

Statistical values are given as mean ± SEM unless stated otherwise (see Supplemental Experimental Procedures for details).

Ethical Approval

All experiments were approved by the Regional Ethical Committee on Animal Experiments of Bordeaux.

SUPPLEMENTAL INFORMATION

Supplemental Information includes five figures and Supplemental Experimental Procedures and can be found with this article at http://dx.doi.org/10.1016/j.neuron.2015.01.012.

AUTHOR CONTRIBUTIONS

E.H. and D.C. conceived the study, formulated the models, and wrote the manuscript. A.C. performed most single-molecule experiments. E.H. performed part of the single-molecule experiments. A.C.P. designed and performed the electrophysiology experiments for Figures 8 and S5. B.C. performed single-molecule experiments of Figures 1E–1G, S1B, S1C, 2B, and 2C. E.T. and S.M. set up and performed uncaging experiments and associated electrophysiology. N.R. performed most molecular biology constructs. A.-S.H. performed control FRET experiments. A.P. and F.C. performed immunoprecipitation experiments. All authors contributed to the preparation of the manuscript.

ACKNOWLEDGMENTS

We acknowledge C. Mulle, S. Tomita, and S. Okabe for the gift of plasmids; E. Gouaux for the anti-GluA2 antibody; J.-B. Sibarita for providing single-particle analysis software; M. Mondin at the Bordeaux Imaging Center, part of the FranceBioImaging national infrastructure, for support in microscopy; M. Sainlos and I. Gauthereau for anti-GFP nanobody production; and B. Tessier, D. Bouchet, C. Breillat, E. Verdier, and C. Genuer for cell culture and plasmid production. This work was supported by funding from ANR NanoDom and Stim-Traf-Park, Labex BRAIN and ANR-10-INBS-04 FranceBioImaging, Centre National de la Recherche Scientifique, ERC grant nanodyn-syn to D.C. and Marie Curie grant Synapsemap to A.P.

Received: February 10, 2014
Revised: November 30, 2014
Accepted: January 7, 2015
Published: February 5, 2015

REFERENCES

Armstrong, N., Sun, Y., Chen, G.Q., and Gouaux, E. (1998). Structure of a glutamate-receptor ligand-binding core in complex with kainate. Nature *395*, 913–917.

Armstrong, N., Jasti, J., Beich-Frandsen, M., and Gouaux, E. (2006). Measurement of conformational changes accompanying desensitization in an ionotropic glutamate receptor. Cell *127*, 85–97.

Ashby, M.C., Maier, S.R., Nishimune, A., and Henley, J.M. (2006). Lateral diffusion drives constitutive exchange of AMPA receptors at dendritic spines and is regulated by spine morphology. J. Neurosci. *26*, 7046–7055.

Bats, C., Groc, L., and Choquet, D. (2007). The interaction between Stargazin and PSD-95 regulates AMPA receptor surface trafficking. Neuron *53*, 719–734.

Beattie, E.C., Carroll, R.C., Yu, X., Morishita, W., Yasuda, H., von Zastrow, M., and Malenka, R.C. (2000). Regulation of AMPA receptor endocytosis by a signaling mechanism shared with LTD. Nat. Neurosci. *3*, 1291–1300.

Borgdorff, A.J., and Choquet, D. (2002). Regulation of AMPA receptor lateral movements. Nature *417*, 649–653.

Cais, O., Herguedas, B., Krol, K., Cull-Candy, S.G., Farrant, M., and Greger, I.H. (2014). Mapping the interaction sites between AMPA receptors and TARPs reveals a role for the receptor N-terminal domain in channel gating. Cell Rep. *9*, 728–740.

Choquet, D. (2010). Fast AMPAR trafficking for a high-frequency synaptic transmission. Eur. J. Neurosci. *32*, 250–260.

Choquet, D., and Triller, A. (2013). The dynamic synapse. Neuron *80*, 691–703.

Colquhoun, D., Jonas, P., and Sakmann, B. (1992). Action of brief pulses of glutamate on AMPA/kainate receptors in patches from different neurones of rat hippocampal slices. J. Physiol. *458*, 261–287.

Dürr, K.L., Chen, L., Stein, R.A., De Zorzi, R., Folea, I.M., Walz, T., Mchaourab, H.S., and Gouaux, E. (2014). Structure and dynamics of AMPA receptor GluA2 in resting, pre-open, and desensitized states. Cell *158*, 778–792.

Featherstone, D.E., and Shippy, S.A. (2008). Regulation of synaptic transmission by ambient extracellular glutamate. Neuroscientist *14*, 171–181.

Frischknecht, R., Heine, M., Perrais, D., Seidenbecher, C.I., Choquet, D., and Gundelfinger, E.D. (2009). Brain extracellular matrix affects AMPA receptor lateral mobility and short-term synaptic plasticity. Nat. Neurosci. *12*, 897–904.

Giannone, G., Hosy, E., Levet, F., Constals, A., Schulze, K., Sobolevsky, A.I., Rosconi, M.P., Gouaux, E., Tampé, R., Choquet, D., and Cognet, L. (2010). Dynamic superresolution imaging of endogenous proteins on living cells at ultra-high density. Biophys. J. *99*, 1303–1310.

Heine, M., Groc, L., Frischknecht, R., Béïque, J.C., Lounis, B., Rumbaugh, G., Huganir, R.L., Cognet, L., and Choquet, D. (2008). Surface mobility of postsynaptic AMPARs tunes synaptic transmission. Science *320*, 201–205.

Jackson, A.C., and Nicoll, R.A. (2011). The expanding social network of ionotropic glutamate receptors: TARPs and other transmembrane auxiliary subunits. Neuron *70*, 178–199.

Jin, R., Banke, T.G., Mayer, M.L., Traynelis, S.F., and Gouaux, E. (2003). Structural basis for partial agonist action at ionotropic glutamate receptors. Nat. Neurosci. *6*, 803–810.

Lin, J.W., Ju, W., Foster, K., Lee, S.H., Ahmadian, G., Wyszynski, M., Wang, Y.T., and Sheng, M. (2000). Distinct molecular mechanisms and divergent endocytotic pathways of AMPA receptor internalization. Nat. Neurosci. *3*, 1282–1290.

Lisman, J.E., Raghavachari, S., and Tsien, R.W. (2007). The sequence of events that underlie quantal transmission at central glutamatergic synapses. Nat. Rev. Neurosci. *8*, 597–609.

MacGillavry, H.D., Song, Y., Raghavachari, S., and Blanpied, T.A. (2013). Nanoscale scaffolding domains within the postsynaptic density concentrate synaptic AMPA receptors. Neuron *78*, 615–622.

Masugi-Tokita, M., and Shigemoto, R. (2007). High-resolution quantitative visualization of glutamate and GABA receptors at central synapses. Curr. Opin. Neurobiol. *17*, 387–393.

Meyerson, J.R., Kumar, J., Chittori, S., Rao, P., Pierson, J., Bartesaghi, A., Mayer, M.L., and Subramaniam, S. (2014). Structural mechanism of glutamate receptor activation and desensitization. Nature *514*, 328–334.

Morimoto-Tomita, M., Zhang, W., Straub, C., Cho, C.H., Kim, K.S., Howe, J.R., and Tomita, S. (2009). Autoinactivation of neuronal AMPA receptors via glutamate-regulated TARP interaction. Neuron *61*, 101–112.

Nair, D., Hosy, E., Petersen, J.D., Constals, A., Giannone, G., Choquet, D., and Sibarita, J.B. (2013). Super-resolution imaging reveals that AMPA receptors inside synapses are dynamically organized in nanodomains regulated by PSD95. J. Neurosci. *33*, 13204–13224.

Nakagawa, T., Cheng, Y., Ramm, E., Sheng, M., and Walz, T. (2005). Structure and different conformational states of native AMPA receptor complexes. Nature *433*, 545–549.

Opazo, P., Labrecque, S., Tigaret, C.M., Frouin, A., Wiseman, P.W., De Koninck, P., and Choquet, D. (2010). CaMKII triggers the diffusional trapping of surface AMPARs through phosphorylation of stargazin. Neuron *67*, 239–252.

Petzoldt, A.G., Lee, Y.H., Khorramshahi, O., Reynolds, E., Plested, A.J., Herzel, H., and Sigrist, S.J. (2014). Gating characteristics control glutamate receptor distribution and trafficking in vivo. Curr. Biol. *24*, 2059–2065.

Plested, A.J., and Mayer, M.L. (2009). AMPA receptor ligand binding domain mobility revealed by functional cross linking. J. Neurosci. *29*, 11912–11923.

Priel, A., Kolleker, A., Ayalon, G., Gillor, M., Osten, P., and Stern-Bach, Y. (2005). Stargazin reduces desensitization and slows deactivation of the AMPA-type glutamate receptors. J. Neurosci. *25*, 2682–2686.

Robert, A., Armstrong, N., Gouaux, J.E., and Howe, J.R. (2005). AMPA receptor binding cleft mutations that alter affinity, efficacy, and recovery from desensitization. J. Neurosci. *25*, 3752–3762.

Schnell, E., Sizemore, M., Karimzadegan, S., Chen, L., Bredt, D.S., and Nicoll, R.A. (2002). Direct interactions between PSD-95 and stargazin control synaptic AMPA receptor number. Proc. Natl. Acad. Sci. USA *99*, 13902–13907.

Schwenk, J., Harmel, N., Brechet, A., Zolles, G., Berkefeld, H., Müller, C.S., Bildl, W., Baehrens, D., Hüber, B., Kulik, A., et al. (2012). High-resolution proteomics unravel architecture and molecular diversity of native AMPA receptor complexes. Neuron *74*, 621–633.

Semenov, A., Möykkynen, T., Coleman, S.K., Korpi, E.R., and Keinänen, K. (2012). Autoinactivation of the stargazin-AMPA receptor complex: subunit-dependency and independence from physical dissociation. PLoS ONE *7*, e49282.

Shepherd, J.D., and Huganir, R.L. (2007). The cell biology of synaptic plasticity: AMPA receptor trafficking. Annu. Rev. Cell Dev. Biol. *23*, 613–643.

Sobolevsky, A.I., Rosconi, M.P., and Gouaux, E. (2009). X-ray structure, symmetry and mechanism of an AMPA-subtype glutamate receptor. Nature *462*, 745–756.

Stern-Bach, Y., Russo, S., Neuman, M., and Rosenmund, C. (1998). A point mutation in the glutamate binding site blocks desensitization of AMPA receptors. Neuron *21*, 907–918.

Sumioka, A., Yan, D., and Tomita, S. (2010). TARP phosphorylation regulates synaptic AMPA receptors through lipid bilayers. Neuron *66*, 755–767.

Sun, Y., Olson, R., Horning, M., Armstrong, N., Mayer, M., and Gouaux, E. (2002). Mechanism of glutamate receptor desensitization. Nature *417*, 245–253.

Tardin, C., Cognet, L., Bats, C., Lounis, B., and Choquet, D. (2003). Direct imaging of lateral movements of AMPA receptors inside synapses. EMBO J. *22*, 4656–4665.

Tomita, S., Fukata, M., Nicoll, R.A., and Bredt, D.S. (2004). Dynamic interaction of stargazin-like TARPs with cycling AMPA receptors at synapses. Science *303*, 1508–1511.

Tomita, S., Adesnik, H., Sekiguchi, M., Zhang, W., Wada, K., Howe, J.R., Nicoll, R.A., and Bredt, D.S. (2005a). Stargazin modulates AMPA receptor gating and trafficking by distinct domains. Nature *435*, 1052–1058.

Tomita, S., Stein, V., Stocker, T.J., Nicoll, R.A., and Bredt, D.S. (2005b). Bidirectional synaptic plasticity regulated by phosphorylation of stargazin-like TARPs. Neuron *45*, 269–277.

Traynelis, S.F., Wollmuth, L.P., McBain, C.J., Menniti, F.S., Vance, K.M., Ogden, K.K., Hansen, K.B., Yuan, H., Myers, S.J., and Dingledine, R. (2010). Glutamate receptor ion channels: structure, regulation, and function. Pharmacol. Rev. *62*, 405–496.

Turetsky, D., Garringer, E., and Patneau, D.K. (2005). Stargazin modulates native AMPA receptor functional properties by two distinct mechanisms. J. Neurosci. *25*, 7438–7448.

ANNEX 2

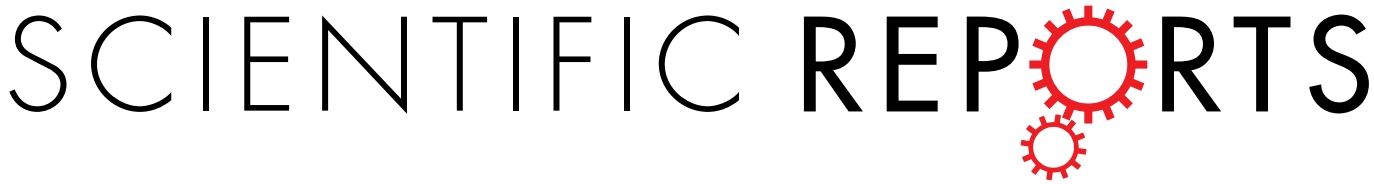

OPEN

Received: 07 April 2016
Accepted: 27 July 2016
Published: 14 September 2016

P2X-mediated AMPA receptor internalization and synaptic depression is controlled by two CaMKII phosphorylation sites on GluA1 in hippocampal neurons

Johan-Till Pougnet[1,2], Benjamin Compans[3,4], Audrey Martinez[1,2], Daniel Choquet[3,4,5], Eric Hosy[3,4] & Eric Boué-Grabot[1,2]

Plasticity at excitatory synapses can be induced either by synaptic release of glutamate or the release of gliotransmitters such as ATP. Recently, we showed that postsynaptic P2X2 receptors activated by ATP released from astrocytes downregulate synaptic AMPAR, providing a novel mechanism by which glial cells modulate synaptic activity. ATP- and lNMDA-induced depression in the CA1 region of the hippocampus are additive, suggesting distinct molecular pathways. AMPARs are homo-or hetero-tetramers composed of GluA1-A4. Here, we first show that P2X2-mediated AMPAR inhibition is dependent on the subunit composition of AMPAR. GluA3 homomers are insensitive and their presence in heteromers alters P2X-mediated inhibition. Using a mutational approach, we demonstrate that the two CaMKII phosphorylation sites S567 and S831 located in the cytoplasmic Loop1 and C-terminal tail of GluA1 subunits, respectively, are critical for P2X2-mediated AMPAR inhibition recorded from co-expressing *Xenopus* oocytes and removal of surface AMPAR at synapses of hippocampal neurons imaged by the super-resolution dSTORM technique. Finally, using phosphorylation site-specific antibodies, we show that P2X-induced depression in hippocampal slices produces a dephosphorylation of the GluA1 subunit at S567, contrary to NMDAR-mediated LTD. These findings indicate that GluA1 phosphorylation of S567 and S831 is critical for P2X2-mediated AMPAR internalization and ATP-driven synaptic depression.

The two major forms of synaptic plasticity in the brain - long term potentiation (LTP) and depression (LTD) - are thought to be involved in information storage and therefore in learning and memory as well as other physiological processes. The main forms of LTP and LTD triggered by either NMDAR or mGluR involve a long-lasting increase or decrease of synaptic strength, respectively resulting mainly from a rapid and long-lasting insertion or removal of AMPARs from the synapses[1].

AMPARs are tetrameric complexes composed of GluA1-A4 subunits[2]. They form complexes with various associated proteins such as transmembrane AMPAR regulatory proteins (TARPs)[3]. These complexes are organized inside synapses by proteins of the post-synaptic density (PSD)[4]. The main AMPARs in the hippocampus are GluA1A2 and GluA2A3 heteromers as well as GluA1 homomers[1,5]. These AMPAR subunits have identified phosphorylation sites in their intracellular C-termini for several protein kinases that are bidirectionnally regulated during activity-dependent plasticity, with LTP increasing phosphorylation and LTD decreasing phosphorylation[4,6,7].

[1]Univ. de Bordeaux, Institut des Maladies Neurodégénératives, UMR 5293, F-33000 Bordeaux, France. [2]CNRS, Institut des Maladies Neurodégénératives, UMR 5293, F-33000 Bordeaux, France. [3]Univ. de Bordeaux, Institut Interdisciplinaire des Neurosciences, UMR 5297, F-33000 Bordeaux, France. [4]CNRS, Institut Interdisciplinaire des Neurosciences, UMR 5297, F-33000 Bordeaux, France. [5]Bordeaux Imaging Center, UMS 3420-US4 CNRS, INSERM, Université de Bordeaux, Bordeaux, France. Correspondence and requests for materials should be addressed to E.B.-G. (email: eric.boue-grabot@u-bordeaux.fr)

Novel forms of plasticity at central synapses require the activation of astrocytes that drives the release of the gliotransmitter ATP and activation of extrasynaptic P2X receptors (P2X)[8–11]. Activation of astrocytic α1-adrenoceptors by noradrenaline (NA) or astrocytic mGluR by afferent activity induces astrocytic ATP release, providing mechanisms by which glial cells can respond to, and modulate synaptic activity[9,10,12,13]. The release of ATP by astrocytes causes a long-lasting increase of glutamatergic synaptic currents in magnocellular neurons, scaling glutamate synapses in a multiplicative manner in the paraventricular nucleus of the hypothalamus. In this case, ATP activates postsynaptic P2X7 which promotes the insertion of AMPAR through a phosphatidylinositol 3-kinase (PI3K)-dependent mechanism[8,9]. However, P2X7 is restricted to specific neuronal populations[14] while P2X2 and P2X4 are widely expressed in the brain[15]. Recently, we showed that an activation of postsynaptic P2X2 by astrocytic release of ATP causes an enduring decrease of postsynaptic AMPAR currents in hippocampal neurons and a depression of field potentials recorded in the CA1 region of mouse brain slices[10]. Ca^{2+} entry through the opening of P2X2 channels triggers internalization of AMPARs, leading to reduced surface AMPARs in dendrites and at synapses[10]. Such a depression of AMPA current and surface GluA1 or GluA1A2 numbers can be reproduced in a heterologous system (*Xenopus* oocytes) following activation of co-expressed P2X2. In addition, NMDA- and ATP-dependent depression are additive in CA1 neurons indicating that P2X- and NMDAR-dependent internalization of AMPAR use distinct signaling pathways[10]. Indeed, P2X-driven synaptic depression and inhibition of AMPAR in oocytes are abolished by a blockade of phosphatase or CaMKII activities, while calcineurin, PKA or PKC inhibitors have no effect[10]. This contrasts with the conventional NMDAR-dependent plasticity model where phosphorylation by CaMKII kinase is associated with LTP and dephosphorylation by calcineurin of AMPAR is required for LTD[4,16]. and suggests that during P2X2 activation a novel form of regulation of AMPAR subunits occurs.

Here, we show that P2X2-mediated AMPAR inhibition is GluA1 or GluA2 subunit specific. We further investigated the differential structural requirement of GluA1 and have identified two critical residues, S831 and S567 phosphorylated by CaMKII, that are crucial for P2X2-mediated inhibition and the removal of surface GluA1-containing AMPAR at the synapses. Finally, we show that S567 of GluA1 is dephosphorylated during P2X-mediated LTD in the hippocampus while no change occurs at S831 and S845, two crucial sites for NMDAR-dependent plasticity[6,16,17].

Results

P2X2-mediated AMPAR inhibition is dependent on GluA subunits. We previously showed that P2X2 activation triggers a dynamin-dependent internalization of homomeric GluA1 or heteromeric GluA1A2 AMPAR, leading to reduced surface AMPAR density and current both in neurons and a recombinant expression system[10]. To evaluate the impact of P2X2 activation on AMPARs, we first examined changes of AMPAR current following P2X2 activation using two electrode voltage clamp recordings from *Xenopus* oocytes co-expressing P2X2 and each GluA1-4 subunit alone or in pair-wise combination (Fig. 1). AMPAR responses were evoked by application of glutamate (Glu 1 mM, 5 s) in the presence of cyclothiazide (CTZ 100 μM, 10 s of preincubation), a blocker of AMPAR desensitization to ensure detection of the whole AMPAR current. Two minutes after a single ATP-evoked current (ATP 100 μM, 5 s), the amplitude of homomeric GluA1 current was drastically reduced from 7.58 ± 0.70 μA (before) to 3.17 ± 0.54 μA (after) ($P < 0.001$, $n = 50$, Fig. 1A,D) as previously described[10]. In contrast to GluA1 receptor inhibition, ATP-evoked P2X2 current did not change homomeric GluA3 responses (3.81 ± 0.87 μA (before), 3.35 ± 0.67 μA (after), $P > 0.05$, $n = 13$, Fig. 1B–D). We superimposed the AMPAR current recorded before and after the ATP-evoked current to visualize directly the P2X-mediated inhibition of AMPAR (Fig. 1C,D). In contrast to the drastic inhibition of GluA1 (by $61.64 \pm 4.11\%$), an inhibitory effect of P2X2 activation on homomeric GluA3 receptors was virtually absent, with the measured residual inhibition of GluA3 ($2.71 \pm 7.39\%$, Fig. 1C,D) being non-significantly different from zero ($P > 0.05$, $n = 13$). However, GluA4 receptors were decreased following P2X2 activation ($19.53 \pm 5.15\%$ of inhibition, $n = 14$). Although this inhibitory effect was significantly smaller ($P < 0.001$) than that observed with GluA1 receptors, it remained significantly different from zero inhibition ($P < 0.05$). P2X-mediated inhibition of GluA2 could not be tested since GluA2 subunits did not form functional homomeric receptors. Since native AMPAR are predominantly heteromers, it was also important to determine the effect of P2X activation on heteromeric AMPAR. As shown in Fig. 1C and as previously reported[10], the inhibition of heteromeric GluA1A2 was similar to that of homomeric GluA1 ($58.17 \pm 2.57\%$, $n = 73$). In contrast, GluA1A3 and GluA2A3 showed significantly less P2X-mediated inhibition ($28.87 \pm 7.72\%$ and $28.25 \pm 6.92\%$ respectively, $n = 15$ for each) and GluA3A4, like homomeric GluA3, displayed a negligible inhibitory influence ($3.44 \pm 7.39\%$, $n = 15$) that was not significantly different from zero ($P > 0.05$). These results thus indicated that P2X2-mediated alteration of AMPAR function and trafficking is a subunit-specific mechanism. GluA3 subunits are insensitive to P2X2 activation and their presence in the receptor complexes alters P2X-inhibition of heteromeric GluA1 or GluA2-containing receptors.

Residues of the CT of GluA1 contribute to the P2X-mediated AMPAR inhibition. GluA subunits display sequence divergence within the C-terminal cytoplasmic domains that have been shown to contain phosphorylation and/or protein interaction sites controlling membrane trafficking (Fig. 2A)[1]. To identify whether AMPA subunit C-terminal domains (CT) confer the subunit specificity of the P2X-mediated inhibition of AMPAR, we first constructed chimeric GluA1 subunits in oocytes in which the CT had been swapped with either GluA2 or GluA3 CT and compared the P2X2-induced AMPAR inhibition (Fig. 2A–C). GluA1CTA2 were inhibited by P2X2 to the same extent as GluA1 ($61.08 \pm 3.99\%$ inhibition, $n = 16$, Fig. 2B,E). In contrast, GluA1CTA3 were partially inhibited following P2X2 activation. Thus, replacing the CT of GluA1 with that of the P2X2-insensitive GluA3 subunits significantly reduced the inhibition to $32.49 \pm 5.34\%$, $P < 0.01$, $n = 35$, Fig. 2C,E). This set of experiments therefore indicates that the CT of GluA1 as well as that of GluA2 subunits contributes to the P2X-mediated inhibition of AMPAR, albeit only partially. Since GluA1, in contrast to GluA2,

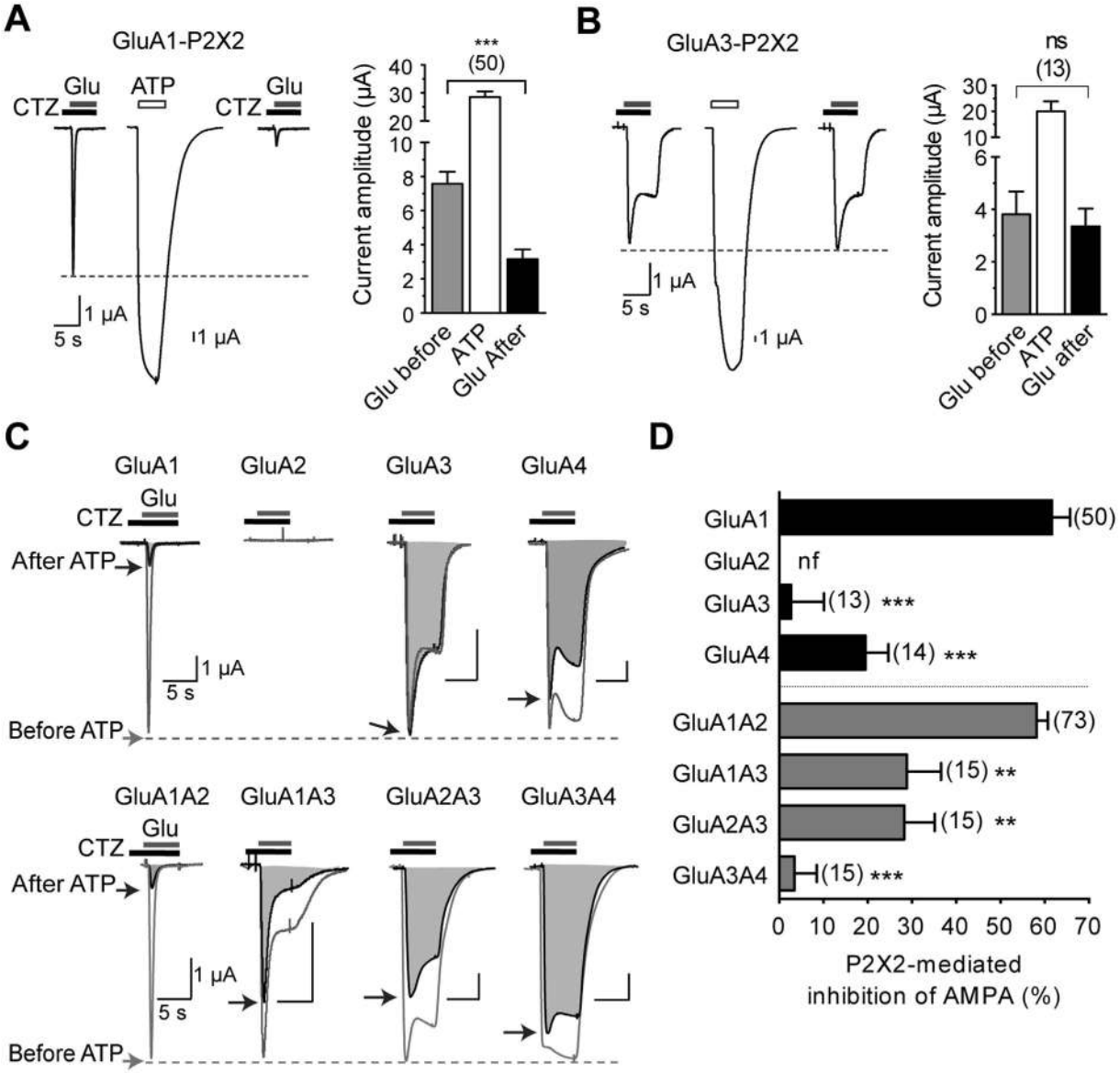

Figure 1. P2X2-mediated inhibition of AMPAR current is dependent upon AMPAR subunit composition. (**A,B**) Representative currents evoked by application of glutamate (Glu 1 mM for 5 s) in the presence of cyclothiazide (CTZ, 100 μM, 10 s of preincubation) before and 2 min after an ATP-induced current (100 μM) in oocytes co-expressing P2X2 and either GluA1 (A) or GluA3 subunits. (**B**) Summary of amplitude averages of AMPAR and P2X2 currents. (**C**) Superimposed AMPAR currents evoked in the same conditions as in A,B before (gray traces, unfilled areas) and 2 min after an ATP-induced current (black traces and shaded areas) for oocytes expressing P2X2R and indicated homomeric or heteromeric AMPARs. (**D**) Bar graphs summarizing the extent of inhibition (expressed as %) of homomeric or heteromeric AMPAR after activation of P2X2R. Statistical differences compared to GluA1 or GluA1A2 are indicated. $^{**}P < 0.01$; $^{***}P < 0.001$; ns, $P > 0.05$; Error bars represent s.e.m.; Numbers of cells are indicated in parentheses. nf, non-functional.

is sufficient to mediate P2X-induced inhibition and form functional homomers, we next focused attention on the structural requirement of GluA1 for this effect. We first tested whether the phosphorylation sites S818, S831 and S845 within the CT of GluA1 are implicated in the P2X2-mediated inhibition by co-expressing mutants of GluA1 with P2X2 in oocytes. Replacement of S818 by an alanine (S818A) or phosphomimetic aspartate (S818D) did not modify the extent of P2X-mediated inhibition of GluA1 ($59.30 \pm 7.34\%$, $n = 12$ and $57.90 \pm 10.08\%$, $n = 13$ respectively, Fig. 2D,E). A similar inhibition of GluA1S845A or S845D was also observed (Fig. 2D,E). Interestingly, the extent of P2X-mediated inhibition of GluA1S831A was significantly smaller compared to that of GluA1 ($25.14 \pm 5.80\%$, $p < 0.01$, $n = 42$) and was similar to the inhibition observed for GluA1CTA3 (Fig. 2C,E). Such a reduction in P2X-mediated inhibition was not expressed by the phosphomimetic mutation S831D (GluA1S831D inhibition was $68.57 \pm 3.74\%$, $n = 20$). Double mutants GluA1S831AS845A or GluA1S831DS845D exhibited the same P2X-mediated change as the single mutant S831A or S831D, respectively. Together these

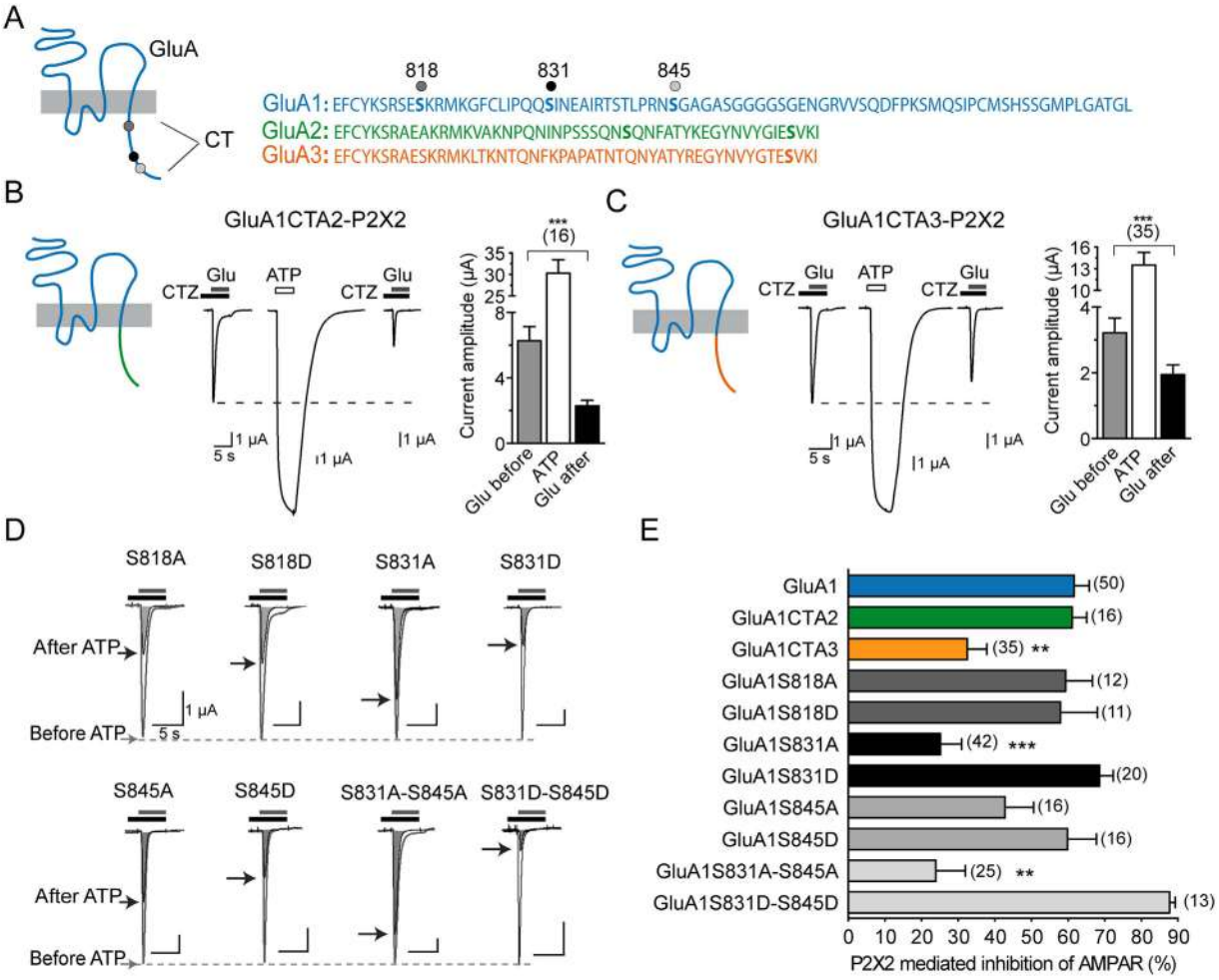

Figure 2. The carboxy tail of the GluA1 and Ser831 residue is necessary but not sufficient for P2X-mediated AMPAR depression. (**A**) Schematic of AMPAR subunit topology and sequence alignment of the intracellular carboxy-terminal tails (CT) of GluA1-A3 subunits. The three main phosphorylation sites on GluA1 known to contribute to synaptic plasticity are indicated by dots. **(B,C)** Chimeric GluA1 receptors with the intracellular CT of either GluA2 (**B**) or GluA3 (C) subunits were designed to determine the region involved in the inhibitory effect of P2X2 activation. Representative currents evoked by applications of glutamate (Glu 1 mM, 5 s) in the presence of cyclothiazide (CTZ, 100 μM, 10 s of preincubation) before and 2 min after an ATP-induced current (100 μM) in oocytes co-expressing P2X2 and chimeric GluA1CTA1 or GluA1CTA3 receptors. The mean amplitudes of currents are also indicated. (**D**) Superimposed glutamate-evoked currents before and after ATP-induced P2X2R current recorded in the same conditions as in (**B**) for point or double GluA1 mutants. Ser818, Ser831 and Ser845 were mutated into alanine (**A**) or phosphomimetic aspartate residues (**D**). Maximal amplitude after ATP-induce currents are indicated by black arrows. (**E**) Summary bar graph representing the percentage of P2X2-mediated AMPAR current inhibition for wild-type, chimeric and mutated GluA1 receptors. Statistical differences compared to GluA1 are indicated. $^{**}p < 0.01$; $^{***}p < 0.001$ number of cells is indicated between brackets.

results point to the S831 residue of the CT as a target for the P2X-mediated regulation of GluA1 receptor trafficking and function, but also suggest that regions other the CT contribute to these processes.

Identification of key residues in the loop1 and the C-tail of GluA1 mediating the P2X2-mediated AMPAR inhibition. We thus explored the possibility that the intracellular loop1 of GluA1 that is critical for AMPAR trafficking[18] plays a role in the P2X-mediated internalization of GluA1-containing receptors. We first compared the P2X-induced inhibition of glutamate-evoked responses of GluA1 to that of GluA1loop1A3 in which the loop1 of GluA1 was swapped with the loop1 of P2X-insensitive GluA3 subunits (Fig. 3A–C). The P2X-mediated inhibition of GluA1loop1A3 ($16.34 \pm 8.64\%$, $n = 35$, Fig. 3A–C) was abolished (i.e., became insignificantly different from zero inhibition) indicating that GluA1loop1A3 currents were not inhibited by ATP currents. S567 is a critical CaMKII site that regulates loop1-dependent AMPAR trafficking as shown by experiments using a non-phosphorylatable S567L mutant[18,19]. We thus examined the implication of S567 by co-expressing the S567L mutant with P2X2 and observed a significant decrease in P2X2-induced inhibition of GluA1S567L ($29.83 \pm 4.43\%$, $n = 17$). However, the inhibition was not abolished ($P < 0.05$ compared to zero inhibition). This

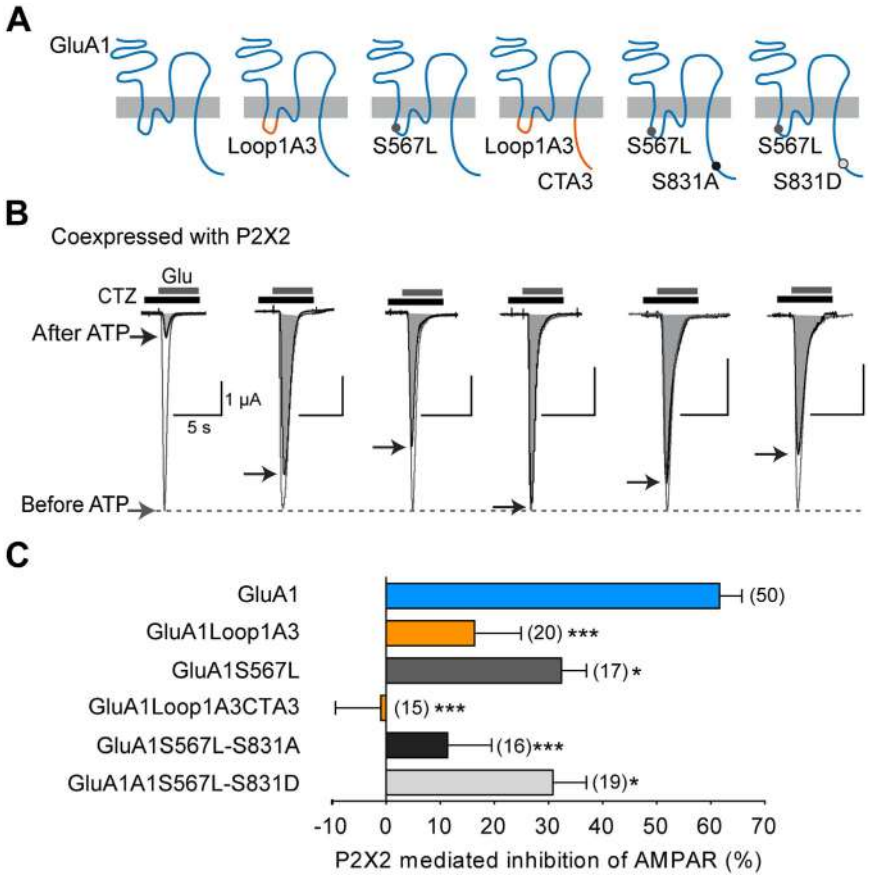

Figure 3. S567 and S831 residues of GluA1 are involved in the P2X2-mediated AMPAR current inhibition. (**A**) Schematic representation of chimeric or mutant GluA1 receptors of the first intracellular loop and CT of GluA1. (**B**) Surimposed glutamate-evoked currents before and after ATP-induced P2X2R current recorded in the same conditions described in Fig. 2 for oocytes co-expressing P2X2R and the corresponding modified GluA1 subunits. Maximal amplitudes of AMPAR currents after ATP (shaded areas) are indicated by black arrows. (**C**) Bar graphs showing the percentage of P2X2-mediated AMPAR current inhibition for wild-type GluA1 and chimeric or mutated GluA1 receptors. Statistical differences compared to GluA1 are indicated. * $p < 0.05$; *** $p < 0.001$; Numbers of cells are indicated in parentheses.

finding therefore shows that loop1 and S567 of GluA1 contributes to the P2X-mediated regulation of AMPAR trafficking. Finally, we replaced both the intracellular loop1 and CT of GluA1 by swapping both domains with the one of the GluA3 subunits. In co-expressing cells, glutamate-evoked current of the GluA1Loop1A3CTA3 were not modified by P2X2 activation ($-0.97 \pm 8.38\%$ of inhibition, $n = 15$). P2X2-induced inhibition was also almost abolished with the double mutant GluA1S567L-S831A ($11.36 \pm 8.13\%$ of inhibition, $n = 16$, not significantly different from zero inhibition), while the extent of GluA1S567LS831D inhibition ($30.81 \pm 6.21\%$, $n = 19$) was similar to that of the single mutant GluA1S567L (Fig. 3A–C), suggesting that both the S567 and S831 residues play a prominent role in the bP2X-induced inhibition of AMPAR.

Could the intracellular domains of GluA1 confer P2X2-mediated inhibition on the insensitive GluA3 receptors? To answer this question, we performed reciprocal experiments by swapping the intracellular loop1 and/or the CT of GluA3 by the homologous domains of GluA1 and measured the effect of P2X activation on glutamate-evoked responses in these constructs (Fig. 4). GluA3CTA1 responses were not significantly inhibited following P2X2 activation. The percentage of inhibition ($15.74 \pm 6.78\%$, $n = 18$) was significantly different ($P < 0.05$) from that of GluA3, but not from zero inhibition ($P > 0.05$). GluA3loop1A1 was partially but significantly inhibited after P2X2 activation ($39.28 \pm 5.69\%$ $n = 15$). Interestingly, GluA3loop1A1CTA1 fully rescued the P2X mediated inhibition that was absent for GluA3 ($62.43 \pm 8.78\%$, $n = 8$), to the same extent as GluA1 receptors, indicating that both domains contribute to the P2X inhibition (Fig. 4B,C). We also mutated the L577 residue of GluA3 into a serine, the residue equivalent to S567 of GluA1. However, GluA3L577S were almost insensitive to P2X2 activation (not shown) as for GluA3, suggesting that a reintroduction of the single serine residue in loop1 is insufficient to rescue the site required for the P2X-mediated inhibition of GluA1.

Together these data show that S567 and S831 are critical residues for the P2X-dependent GluA1-containing AMPAR alteration, supporting the idea that P2X2 induced changes of the phosphorylation state of GluA1 subunits.

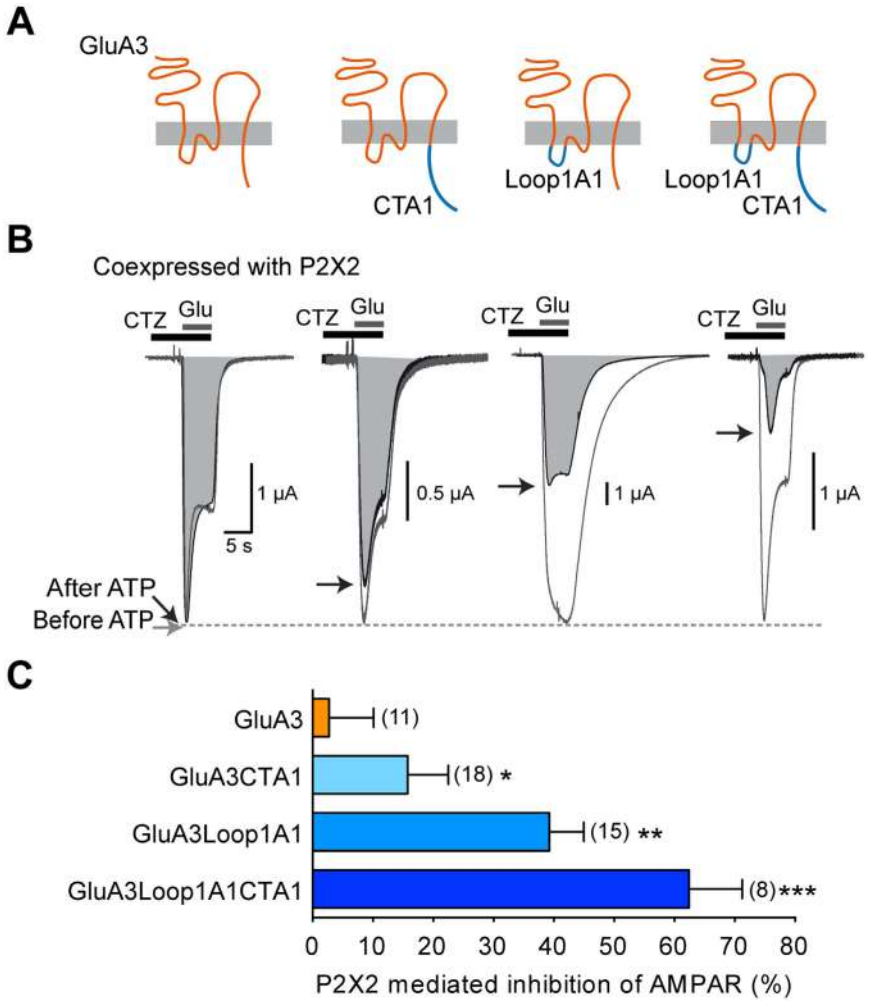

Figure 4. Chimeric GluA3 subunits with intracellular loop1 and CT of GluA1 confers P2X2-mediated inhibition on GluA3 receptors. (**A**) Schematic representation of chimeric GluA3 subunits bearing the first intracellular loop and/or the CT of GluA1. (**B**) Surimposed glutamate-evoked currents before and after ATP-induced P2X2R currents recorded from oocytes co-expressing P2X2R and the corresponding modified GluA3 subunits. Maximal amplitude of AMPAR currents after ATP (shaded areas) are indicated by black arrows. (**C**) Bar graph showing the percentage of P2X2-mediated AMPAR current inhibition for wild-type GluA3 and chimeric GluA3 receptors. Statistical differences compared to GluA3 are indicated. *$p < 0.05$; ***$p < 0.001$; Numbers of cells are indicated in parentheses.

GluA1 S831 and S567 residues are crucial for P2X-mediated internalization in hippocampal neurons. We next examined whether the identified molecular determinants of GluA1 subunits are crucial for an P2X2-mediated removal of surface GluA1-containing AMPAR in hippocampal neurons. Using dSTORM super-resolution imaging, we previously showed that an activation of endogenous P2X receptors reduces the density of native GluA2-containing receptors at the surface of hippocampal dendrites and synapses[10]. Using the same dSTORM imaging technique, we first measured the density of AMPAR on rat hippocampal neurons transfected with super ecliptic pHluorin (SEP)-tagged GluA1 and stained with anti-GFP antibodies coupled to Alexa 647 (Fig. 5A,C). SEP-GluA1 containing AMPARs are clustered at synapses, with a higher number of receptors ($178.5 \pm 6.9/\mu m^2$, $n = 67$) than the dendrites ($58.43 \pm 6.37/\mu m^2$, $n = 13$) as previously shown for endogenous AMPARs[10,20]. Ten minutes after activation of endogenous P2X receptors using 100 µM ATP in the presence of tetrodotoxin (TTX 0.5 µM) and the adenosine receptor antagonist CGS15943 (3 µM), we observed a significant reduction in surface SEP-GluA1 containing receptors in spines and dendrites (after ATP: $125.5 \pm 5.3/\mu m^2$, $n = 73$ and $36.63 \pm 4.69/\mu m^2$, $n = 14$, respectively, Fig. 5A–C) showing that activation of native P2X receptors triggers an internalization of GluA1-containing AMPAR as previously observed for endogenous GluA2-containing receptors[10]. In transfected hippocampal neurons, mutant GluA1S831A, S567L or double mutant S567LS831A exhibited a similar density of AMPAR in both dendrites and spines in control conditions compared to the SEP-GluA1 wild-type. This indicates that these mutations did not significantly alter surface AMPAR trafficking or clustering in spines in basal conditions even though a recurrent small decrease of total AMPAR number could be observed (Fig. 5B,C). However, ATP did not trigger any significant changes in AMPAR numbers in the dendrites and spines

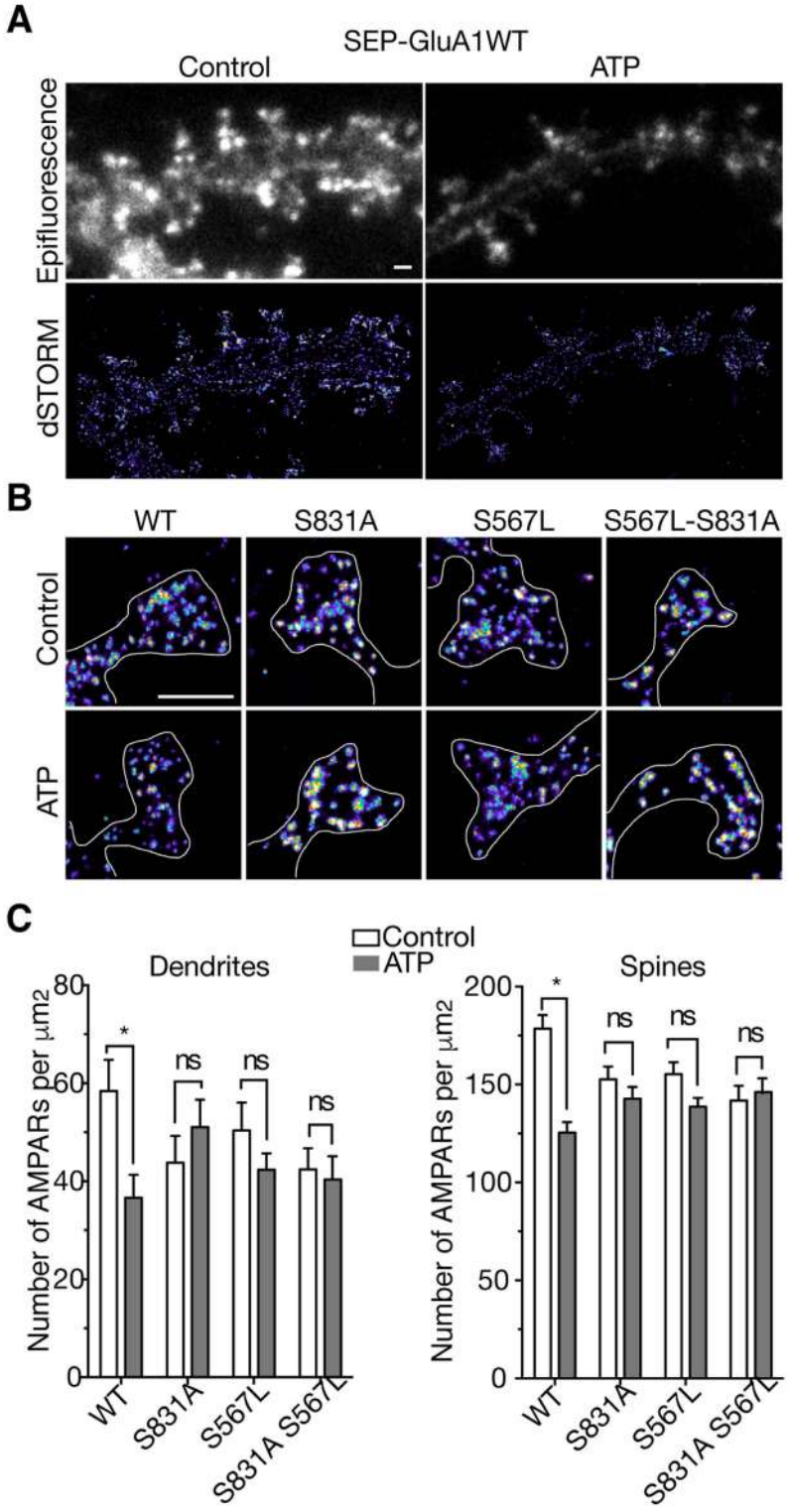

Figure 5. Decrease in number of dendritic and synaptic SEP-tagged GluA1 receptors triggered by activation of native P2XR in transfected hippocampal neurons is mediated by the S831 or S567 GluA1 residues. (**A**) Epifluorescence (upper panels) and super-resolution images (bottom panels) reconstructed from direct Stochastic Optical Reconstruction Microscopy (dSTORM) of wild-type (WT) SEP-tagged GluA1 in transfected hippocampal neurons labeled with surface anti-GFP antibodies before (control, left panel) and after ATP treatments (right panel). (**B**) Representative dSTORM images of spines from neurons expressing wild-type SEP-tagged GluA1 and mutant GluA1 S831A, S567L and double mutant in control conditions or 1a0 min after application of ATP (100 μM, 1 min) in presence of CGS15943 (3 μM) and TTX (0.5 μM). Scale bars, 1 μm. (**C**) Average density values of wild-type and mutant SEP-GluA1-containing AMPAR in synapses and dendrites in control condition (unshaded bars) and after P2XR activation (shaded bars). *$P < 0.05$; ns, $P > 0.05$; Error bars: s.e.m.

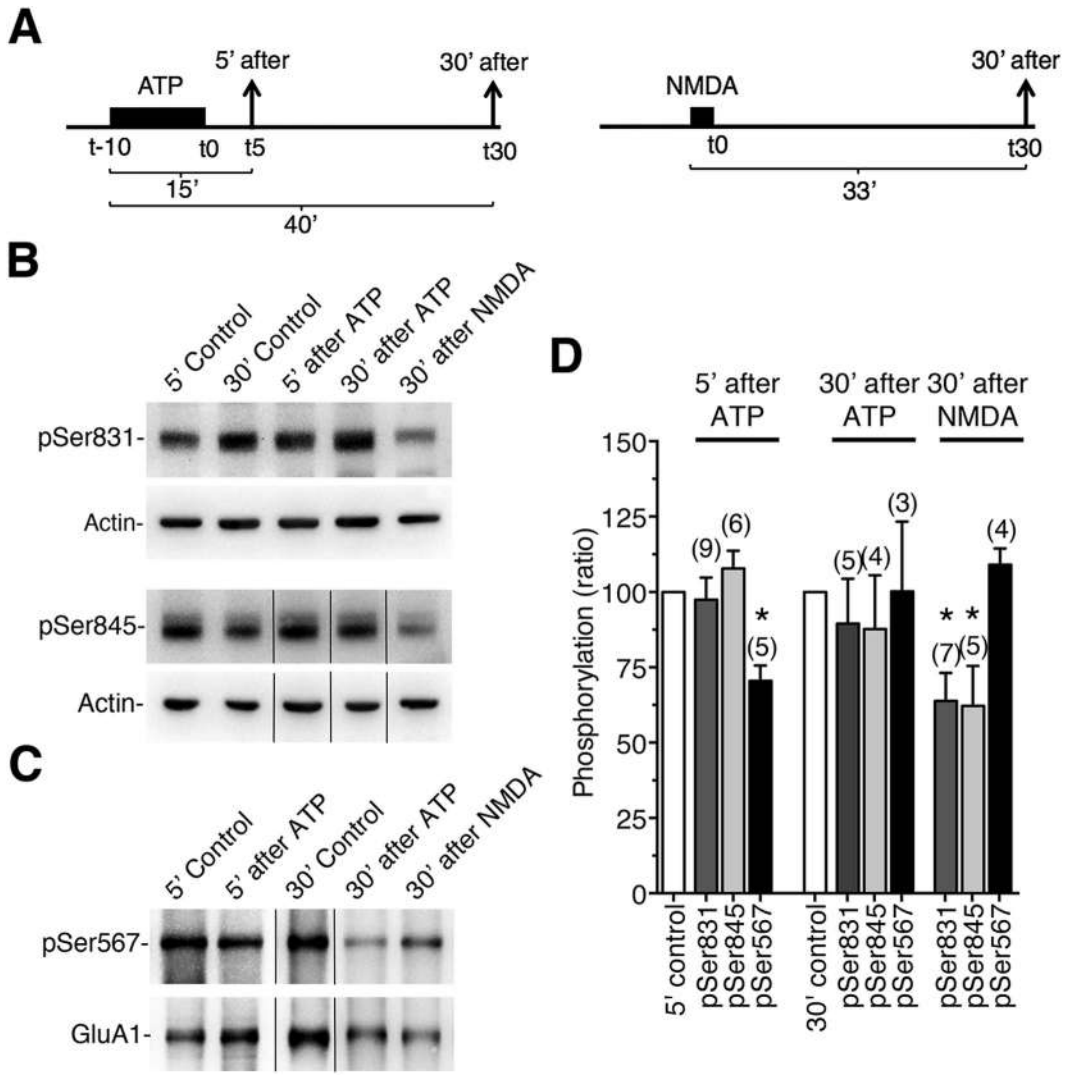

Figure 6. Dephosphorylation of the S567 site of the AMPAR GluA1 subunit during P2XR-mediated synaptic depression in hippocampal slices. (**A**) Experimental design of ATP or NMDA- induced synaptic depression in hippocampal slices. (**B**) Crude membrane fractions from control hippocampal slices and ATP-induced synaptic depression or NMDAR-induced LTD slices taken at indicated times (5′ and/or 30′) after the application of ATP (300 μM for 10 min) or NMDA (20 μM for 3 min) respectively, separated under SDS-PAGE and blotted using antibodies against phospho-S831, phospho-S845 and actin. (**C**) Crude membrane fractions from hippocampal slices treated as described in A, immunoprecipated using anti-GluA1 before separation under SDS-PAGE and blotted using antibodies against anti-phospho S567 and anti-GluA1. Cropped blots are displayed (see Supplementary Fig. 1.) (**D**) Quantification of the relative amounts of phosphorylation of GluA1 on S831, S845 and S567 at indicated time points after ATP or NMDA treatments. Bars represent the ratio of the signals for the anti-phospho site specific antibodies and the actin or the anti-GluA1 normalized to control at each time point. The number of independent experiments is indicated in parentheses. *$P < 0.05$.

of single or double mutants, confirming that both residues are important for P2X-mediated AMPAR internalization in hippocampal neurons.

GluA1 S567 is dephosphorylated during P2X-driven LTD in the hippocampus. We previously showed that perfusion of ATP (300 μM) on acute hippocampal slices from 4–5 week-old mice in the presence of blockers of adenosine and NMDA receptors, consistently produced a long-lasting depression of field excitatory post-synaptic potentials, which was in turn blocked by P2X antagonists[10]. We next sought to determine if the P2X-mediated depression in the hippocampus is associated with a change in the phosphorylation of GluA1 using antibodies against the phosphorylation site-specific of GluA1 subunits. Crude membrane proteins isolated from hippocampal slices at different time points (Fig. 6A) after ATP treatment (300 μM, 10 min) or without treatment were immunoblotted using antibodies against phosphoSer-831, phosphoSer-845 and phosphoSer-567 antibodies (Fig. 6B and Supplementary Fig. 1). For the detection of phosphoSer-567, an immunoprecipitation step using anti-GluA1 antibodies was necessary prior to immunoblotting (see Methods and Supplementary Fig. 2). NMDA

treatment (20 μM, 3 min) was also applied to hippocampal slices to trigger chemical LTD and to determine whether P2X- and NMDA- dependent LTDs involved distinct changes in GluA1 AMPAR (Fig. 6A). Western blotting confirmed that S831, S845 and S567 have a significant level of basal phosphorylation in hippocampal slices (control conditions, Fig. 6B–D)[16,19] and demonstrated that the phosphorylation of Serine 831 or Serine 845 remained unchanged during P2X-mediated LTD. Interestingly, phosphorylation of Serine 567 detected by using anti-phosphoS567 was significantly reduced ($70.49 \pm 5.1\%$ of control, $P < 0.05$, $n = 5$) 5 minutes after ATP treatment (i.e., 15 min after the onset of ATP application, Fig. 6). The dephosphorylation of S567 was not observed 30 min after ATP treatment (i.e., 40 min after ATP application onset), as for the P2X-mediated LTD[10]. In contrast, phosphorylation of S831 and S845 was significantly reduced ($63.85 \pm 9.25\%$ and $62.18 \pm 13.32\%$ of control, respectively; $P < 0.05$, $n = 5–7$) 30 min after NMDA treatment as expected[6,16]. Phosphorylation of S567 after NMDA treatment showed a tendency to increase ($109.1 \pm 5.31\%$ of control, $n = 4$) that was smaller than the increase of phospho-S567 reported during low frequency stimuli-induced LTD[19]. Thus the dephosphorylation of the S567 CaMKII site of GluA1 after ATP treatment strongly correlated with the P2X-mediated depression of synaptic responses both in terms of time course and the blockade by the CaMKII inhibitor KN-93[10].

Discussion

Using a mutational approach, we show here that the two CaMKII phosphorylation sites S567 and S831 located respectively in the cytoplasmic domain Loop1 and the CT of GluA1 subunits are critical for the P2X-mediated internalization and current inhibition of GluA1-containing AMPAR. Our results also suggest that phosphorylation levels of both S567 and S831 is important for P2X-driven depression in the hippocampus. Previously, we described a P2X2-mediated internalization of AMPAR that is critical for the prolonged decrease of hippocampal synaptic strength triggered by an astrocytic release of ATP[10]. Similarly to an NMDA-induced AMPAR internalization[21], the activation of P2X2 or P2X4 triggers AMPAR internalization and AMPAR current inhibition in hippocampal neurons as well as in an heterologous system, and this trafficking event requires primarily a Ca^{2+} influx through the direct opening of P2X2 channels[10]. Because NMDAR- and P2X-dependent synaptic depression are not occlusive in the hippocampus and since P2X-mediated AMPAR internalization and synaptic depression requires, both *in situ* and *in vitro*, phosphatase and CaMKII activities in contrast to NMDAR-dependent internalization and LTD[16,22], we aimed here to explore the signaling mechanism that triggers P2X-induced AMPAR internalization and current inhibition by focusing primarily on the nature of AMPAR itself. We found by co-expressing P2X2 and each GluA1–4 subunit alone or in two subunit combinations in *Xenopus* oocytes that a P2X2-mediated alteration of AMPAR is dependent on the latter's composition. In contrast to homomeric GluA1 or heteromeric GluA1A2 that were strongly inhibited (~60%) (Fig. 1, see also[10]), the inhibition of homomeric GluA4 was less pronounced (~20%) and homomeric GluA3 receptors were completely insensitive to P2X2 activation. In addition, the presence of GluA3 in the receptor complexes significantly reduced the P2X-inhibition of the heteromers GluA1A3 or GluA2A3, indicating a negative impact of GluA3 on the ATP-induced inhibition. These results therefore show the pivotal role played by GluA1 or GluA2 in the P2X-mediated AMPAR alteration and also indicate that P2X may regulate to a varying extent the function and trafficking of the main AMPARs in the hippocampus, which are GluA1A2 or GluA2A3 as well as GluA1 homomers[1,4,5,23]. GluA1–4 subunits have similar extracellular N-terminals and transmembrane domains but differ significantly in their C-terminal (CT) cytoplasmic tail regions which contain multiple regulatory elements that are subject to phosphorylation and/or interaction with scaffold proteins. These latter proteins play a crucial role in the regulation of AMPAR function, trafficking, lateral mobility and synaptic plasticity[4,24]. GluA2 was considered as the primary determinant during NMDAR-dependent internalization of synaptic AMPARs and LTD through modifications of the CT of GluA2 and interaction with scaffolding proteins[4]. However the fact that LTD occurs normally in mice lacking GluA2 and GluA3 in the hippocampus indicated that GluA2 is not essential for hippocampal LTD[25]. Other studies suggested that LTD and AMPAR internalization require calcineurin and dephosphorylation of PSD proteins and/or PKA and PKC sites within the CT of GluA1. In addition knock-in mice containing mutations in the GluA1 CaMKII and PKA phosphorylation sites display significant deficits in expressing LTD[7,16,26–29]. To test whether the signal that confers subunit specificity of P2X-mediated alteration resides within the CT of GluA subunits, we swapped the CT of GluA1 with the CT of GluA2 or GluA3 (Fig. 2). Chimeric receptors showed that replacing the CT of GluA1 with that of GluA2 did not modify the P2X2-induced inhibition of AMPAR. The replacement of GluA1CT with the GluA3CT significantly reduced, but did not abolish, the inhibition. These results therefore indicate that the CT of GluA1 or GluA2 subunits participate, but that regions other than the CT of the AMPAR subunit may also contribute, in the P2X-mediated inhibition of AMPAR. Since GluA2 homomers do not form functional receptors, we focused on GluA1 subunits to identify the molecular determinants of the P2X-mediated inhibition. Interestingly, by single or double mutation of the three serine located within the CT of GluA1 and described as the phosphorylation substrates for alanine or phosphomimetic aspartate (S818, S831 and S845; phosphorylation sites for PKC, PKC/CaMKII and PKA, respectively)[30] we showed that only the substitution of S831 by an alanine significantly reduced the P2X-mediated inhibition. Moreover, this reduction in inhibition was similar to that observed with chimeric GluA1CTA3 receptors. These results excluded a contribution of S818 or S845 in agreement with the previously reported pharmacological insensitivity of the P2X-driven depression to blockade of PKA or PKC activities[10]. In addition, S831D was fully inhibited during P2X2 activation indicating that phosphorylation of S831 is a prerequisite, but not alone sufficient, to produce the observed P2X-mediated AMPAR alteration.

The first intracellular loop1 of GluA1, which was also shown to be critical for AMPAR trafficking and targeting to the synapse, contains a CaMKII site (S567) that is phosphorylated both *in vitro* and *in vivo*[18], and recent work has suggested that CaMKII activities is also required for both hippocampal LTP and LTD[19]. By swapping the Loop1 of GluA1 by the homologous domain of the P2X-insensitive GluA3 subunits (Fig. 3) we showed that such a loop 1 replacement almost abolished the P2X2-mediated inhibition, with the remaining inhibition

(~15%) being insignificantly different from zero. By replacing both loop1 and the CT of GluA1 by the homologous domain of GluA3 or by mutating the two CaMKII sites by nonphosphorylatable residues S567L and S831A, the P2X2-mediated inhibition was completely abolished. Conversely, by replacing both the loop1 and the CT of GluA3 by the homologous domain of GluA1, we fully rescued the P2X-mediated inhibition (~60%) of the insensitive-homomeric GluA3 receptors, thereby confirming that both CaMKII sites located in the intracellular loop1 and CT of the GluA1 subunit are critical for P2X2-mediated inhibition of AMPAR arising from an alteration in the number of surface AMPARs[10]. These data were reinforced with imaging experiments on hippocampal neurons transfected with wild-type or mutant GluA1. Specifically, the use of super-resolution dSTORM imaging showed that activation by ATP of endogenous P2X receptors caused the loss of wild-type SEP-tagged GluA1-containing AMPAR from synapses and dendrites in hippocampal neurons as previously observed for native GluA2-containing receptors[10]. Importantly, as expected, no change in the number of mutant GluA1 following ATP activation of endogenous P2X was observed in hippocampal neurons transfected with the double mutant GluA1S567L-S831A. More surprisingly, the ATP-driven internalization was also completely abolished for both single mutant GluA1S567L and GluS831A. We noted a tendency towards a decrease of total AMPAR number in neurons transfected with mutants compared to wild-type GluA1 but neither S831 nor S567 mutation significantly altered the synaptic targeting of AMPAR in basal conditions, i.e., in the absence of synaptic activity. This is consistent with previous studies showing that the GluA1 CT plays a role in surface delivery of GluA1 and synaptic plasticity and but not in basal synaptic transmission or synaptic trafficking[6,31,32]. Our super-resolution imaging experiments on the S567L mutant contrast with previous colocalization experiments of GluA1 and PSD-95 indicating that GluA1 S567 contributes to the synaptic targeting of AMPAR[18]. These latter experiments were performed by molecular replacement, i.e., expression of GluA1S567 mutant on an AMPAR null background which allowed the specific role of S567 in AMPAR synaptic localization to be defined[18]. This discrepancy may be easily explained but the fact that here we expressed mutant GluA1S567L on a wildtype background, leaving open the possibility that these subunits form complexes with native subunits and/or associated proteins that may ensure proper synaptic localization. These compensatory effects may also explain the differences in the magnitude of the effects on both single mutant GluA1S567L or GluA1S831A observed between the two expression systems. P2X2-mediated inhibition of both single mutants was partially reduced in oocytes, whereas their respective internalizations were fully suppressed in transfected neurons. The association with native wild-type AMPAR subunits such as GluA3 could facilitate P2X-mediated internalization in transfected neurons. In addition, our experiments using phosphorylation site-specific antibodies showed that ATP-induced synaptic depression from hippocampal slices[10] is associated with a fast and reversible dephosphorylation of GluA1 at the CaMKII phosphorylation site S567 without change in the phosphorylation levels of S845 or S831. Furthermore, the kinetics of dephosphorylation were consistent with the duration of the synaptic depression observed by field recordings from hippocampal slices[10]. NMDAR-dependent LTD revealed opposite results with no change in S567 and dephosphorylation of S845 and S831. Although a recent study reported a low level of basal phosphorylation of GluA1 subunits, indicating that the phosphorylation changes of GluA1 during synaptic plasticity may require alternative interpretations[33], NMDAR-dependent or low frequency stimulation (LFS)-induced LTD associated with a persistent dephosphorylation of S845 and a transient dephosphorylation of S831 has been frequently observed[1,7,16,22,26,28].

Together our findings provide evidence that the ATP-mediated internalization of GluA1-containing AMPAR requires two sites, S567 and S831, of GluA1 subunits and that dephosphorylation of GluA1 may contribute to the depression of synaptic activity in the hippocampus. We previously showed that P2X activation depressed naïve synapses as well as synapses already depressed by LFS in the CA1 region[10]. Since high frequency stimulation (HFS)-induced LTP increases phosphorylation of S831[1,6], it will be important to now determine whether P2X activation may dephosphorylate S831 during LTP and thereby contribute to synaptic depotentiation.

Materials and Methods

Constructs. P2X2 subcloned into pcDNA3, wild-type GluA1–4 subunits or super-ecliptic-pHluorin (SEP)-tagged GluA1 or GluA2 subunits subcloned into PrK5 vector have been described previously[10]. Single or double mutations of GluA1 or GluA3 subunits were generated sequentially using the QuikChange site directed mutagenesis method with specific oligonucleotides corresponding to each mutation (Stratagene). GluA1CTA2, GluA1CTA3 chimeras were generated using restriction site addition by PCR and subcloned into pcDNA3. The N-terminal domain of GluA1 was amplified by PCR using pfu polymerase (Fermentas) and primers in order to create 5′ HindIII and 3′ EcoRI restriction site at the junction between TM3 and CT. The EcoRI site naturally present at the same position on GluA2 or GluA3 was used to fuse in-frame the C-term of GluA2 or GluA3 to the N-term of GluA1. The additional EcoRI site present in the CT of GluA2 was first removed by silent mutation using the QuikChange method. Conversely, GluA3CTA1 chimeras were generated by exchange of the C-terminal sequence using the natural EcoRI restriction site on GluA3 and one created by PCR into the same sequence on GluA1. GluA1loop1A3 and Glu3loop1A3 were generated by substitution of the first intracellular loop 1 domain of one GluA subunit by the other one using the Quickchange method and megaprimers. Megaprimers were generated by PCR: for example, the loop1 of GluA3 was first amplified from GluA3 by PCR using primers with flanking regions corresponding to adjacent GluA1 sequences. The PCR product was then used as megaprimers on GluA1 to generate GluA1loop1A3 by the Quikchange method. All constructs were verified by sequencing.

Xenopus oocyte electrophysiology. Oocytes were removed from *Xenopus laevis* as previously described[34,35]. After nuclear injection of cDNAs coding for each wild-type or modified AMPAR subunits (each 50–80 pg) alone or with P2X2 (10–30 pg), oocytes were incubated in Barth's solution containing 1.8 mM $CaCl_2$ and gentamycin (10 mg/ml, Sigma) at 19 °C for 1–3 days before electrophysiological recordings were performed as previously described[10]. Two-electrode voltage-clamp recordings were conducted at room temperature using glass pipettes (tip resistance 1–2 MΩ) filled with 3 M KCl solution to ensure a reliable holding potential. Oocytes

were voltage-clamped at −60 mV, and membrane currents were recorded with an OC-725B amplifier (Warner Instruments) and digitized at 1 kHz on a Power PC Macintosh G4 using Axograph X software (Axograph). Oocytes were superfused at a flow rate of 10-12 ml/min with Ringer solution, pH 7.4, containing in mM: 115 NaCl, 3 NaOH, 2 KCl, 1.8 $CaCl_2$, and 10 HEPES. Agonists and drugs were prepared at their final concentrations in the perfusion solution and applied using a computer- driven valve system (Ala Scientific).

Hippocampal neuron culture and transfection. Primary hippocampal cultures were prepared from E18 Sprague-Dawley rat embryos according to the Banker protocol (Kaech and Banker, 2006). Hippocampi were dissected in Petri dishes filled with HBSS and HEPES, and dissociated by trypsin treatment (0.05%; Gibco) at 37 °C followed by trituration with flame-polished Pasteur pipettes. Cells were electroporated and plated at a density of 250,000 per 60-mm dish, on poly-L-lysine pre-coated 1.5H coverslips (Marienfield, cat. No. 117580), pre-plated with 75,000 non-electroporated cells. After 2 hours, coverslips were transferred to dishes containing an astrocyte feeder layer, plated at a density of 40,000 cells and cultured in MEM (Fisher scientific, cat No. 21090-022) containing 4.5 g/l Glucose, 2 mM L-glutamine and 10% horse serum (Invitrogen) for 14 days. Neuron cultures were maintained in Neurobasal medium supplemented with 2 mM L-glutamine and 1X NeuroCult SM1 Neuronal supplement (STEMCELL technologies) for 14–16 days.

Direct Stochastic Optical Reconstruction Microscopy. Neuronal cultures of 14–16 DIV electroporated with either wildtype or mutant SEP-tagged-GluA1. ATP treatments were conducted in the presence of tetrodotoxin (TTX 0.5 μM) and the adenosine receptor antagonist CGS15943 (3 μM), were incubated with anti-GFP antibodies (1:1000, Roche) in culture medium at 37 °C for 6 minutes and fixed in 4% paraformaldehyde and sucrose in PBS for 10 minutes. After three washes in PBS, they were incubated with NH_4Cl 50 mM for 10 minutes. After three washes in PBS, they were again incubated with PBS containing 2% Bovin Serum Albumin (BSA) (Sigma-Aldrich, St. Louis, MO) for 45 minutes. The Primary antibodies were then revealed by incubating with Alexa647-coupled donkey anti-mouse IgG secondary antibodies (1:500, Jackson lab) for 45 minutes at room temperature. After three washes in PBS containing 2% BSA and 3 washes in PBS, coverslips were again fixed using a previously described protocol and kept in PBS.

The stained coverslips were imaged during the next week at room temperature in a closed chamber (Ludin Chamber, Life Imaging Services, Switzerland) mounted on a Leica SR GSD microscope (Leica Microsystems, Wetzlar, Germany) equipped with a 160 × 1.47 NA objective and an iXon3 EMCCD camera (ANDOR, Belfast, UK). Imaging was performed in an extracellular solution containing a reducing and oxygen scavenging system. For direct Stochastic Optical Reconstruction Microscopy, ensemble fluorescence of Alexa647 were first converted into a dark state using a 642 nm laser 30–50 kw/cm^2. Once the ensemble fluorescence was converted into a desired number of single molecules per frame, the laser power was reduced to 7–15 kw/cm^2 and imaged continuously at 50fps for 90,000 frames. Both the ensemble and single molecule fluorescence was collected by a combination of dichroic and emission filters (D101-R561 and F39-617, respectively, Chroma, USA) and a quad-band dichroic filter (Di01-R405/488/561/635, Semrock, USA). Super-resolution images were reconstructed using a Leica GSD analysis program and corrected for lateral drift using multicolor fluorescent microbeads (Tetraspeck, Invitrogen). The AMPAR density determination was done in two steps. The first consisted of determining the intensity of isolated single particles. The second step was to divide the dendritic and synaptic intensities by the single particle intensity[20].

Hippocampal slice preparation. Horizontal hippocampal slices were prepared from 4–5 -week-old C57BL6 mice as previously described[10]. Animals were anesthetized with isoflurane gas and then decapitated. Brains were rapidly removed and immersed in ice-cold artificial cerebrospinal fluid (ACSF) containing 125 mM NaCl, 2.5 mM KCl, 1.25 mM NaH_2PO_4, 26 mM $NaHCO_3$, 2 mM $CaCl_2$, 1.3 mM $MgCl_2$ and 25 mM glucose saturated with 95% O_2/5% CO_2[36]. Horizontal hippocampus slices (350 μm thick) were obtained from brains using a vibratome (Leica VT 1200 s). The slices were transferred to an interface storage chamber containing ACSF saturated with 95% O_2/5% CO_2 and were left at least 45 min at 35 °C to recover and then were maintained at room temperature for 45 min. Slices were placed into ACSF containing picrotoxin (100 μM, Santa Cruz), D-AP5 (10 μM, Santa Cruz) and CGS 15943 (3 μM, Santa Cruz) to block $GABA_A$, NMDA and adenosine receptors, respectively. For NMDAR-dependent-LTD experiments, D-AP5 was omitted from the bathing ACSF. P2X- or NMDA induced LTD was induced by submerging slices in ATP (300 μM) for 10 min or NMDA (20 μM) for 3 min[10,16]. After agonist treatment, slices were rinsed with ACSF, transferred to another well containing ACSF for 5 or 30 min then quickly placed in cold PBS. Hippocampi were immediately dissected out and placed at −80 °C. Control slices were manipulated in the exact same way but were not subjected to agonist treatment.

Western blotting analysis. Homogenates of two hippocampus slices were prepared by sonicating on ice during 10 s in 10 μl of a homogenization buffer per slice containing a cocktail of 0.1 M Tris pH 8.0, 10 mM EDTA, Halt protease and phosphatase inhibitors (Thermo Scientific) and 1 μM okadaïc acid (Santa Cruz). The protein concentration was determined by the BCA method (Pierce) and 20 μg of proteins per lane were loaded onto an 8% SDS-PAGE gel and then transferred to polyvinylidene difluoride (PVDF) membranes. Western blotting using phospho-S567 revealed no or at most a faint band arising from total proteins (see Supplementary Fig. 2). To quantify the phospho-Ser 567 signals, homogenates were first immunoprecipated using anti-GluA1 antibodies as previously described[18]. 100 μg of homogenates were incubated with 2 μg of anti-GluA1 antibodies (Alomone) and 20 μl of protein G-dynabeads (Pierce) at 4 °C overnight. Beads were washed four times with Homogenization buffer and eluted in an SDS sample buffer. Membranes were saturated for 60 min by incubation with 5% Bovin Serum Albumin (BSA) in a PBS (2 mM KH_2PO_4, 150 mM NaCl, 8 mM $NaH_2PO_4.2H_2O$) containing 0.1% Tween 20 and incubated overnight with the following antibodies: anti-pS831 (1/500, Millipore), anti-pS845

(1/1000, Millipore) or anti p-S567 (1/500, kindly provided by Katherine Roche), anti-actin (1/10,000, Sigma) or anti-GluA1 (1/200, Alomone). Membranes were then incubated for 1 h at room temperature with a secondary anti-mouse or anti-rabbit horseradish peroxidase-coupled antibody (both at 1:5000; Jackson ImmunoResearch) diluted in PBS-Tween 0.1% and supplemented with 5% non-fat milk. Signals were revealed by chemiluminescence (Millipore) and images were acquired on a Chemidoc System (Bio-rad). Quantification of western blots was performed using Image J software (National Institutes of Health), whereby phospho-specific/GluA1 or phospho-specific/actin ratios were determined. (For full length blots see Supplementary Fig. 1).

Statistics. Statistical analysis was performed using the Student's t test, or ANOVA Kruskal-Wallis test with Dunn's *post-hoc* procedure for between-group comparisons (Prism 6.0, Graphpad). Data were considered significantly different when the P value was less than 0.05. Data in Figs 1–4 were also compared to the null hypothesis of the zero inhibition group to determine whether the degree of inhibition (expressed as %) was reduced or abolished (non significantly different from 0% of inhibition). All statistical results are given as the mean ± s.e.m.

Study approval. All experiments were carried out in accordance with the European Communities Council Directive and approval by the ethics committee of the University of Bordeaux (CEEA50).

References

1. Huganir, R. L. & Nicoll, R. A. AMPARs and synaptic plasticity: the last 25 years. *Neuron* **80,** 704–717, doi: 10.1016/j.neuron.2013.10.025 (2013).
2. Traynelis, S. F. *et al.* Glutamate receptor ion channels: structure, regulation, and function. *Pharmacol Rev* **62,** 405–496, doi: 10.1124/pr.109.002451 (2010).
3. Nicoll, R. A., Tomita, S. & Bredt, D. S. Auxiliary subunits assist AMPA-type glutamate receptors. *Science* **311,** 1253–1256, doi: 10.1126/science.1123339 (2006).
4. Anggono, V. & Huganir, R. L. Regulation of AMPA receptor trafficking and synaptic plasticity. *Curr Opin Neurobiol* **22,** 461–469, doi: 10.1016/j.conb.2011.12.006 (2012).
5. Wenthold, R. J., Petralia, R. S., Blahos, J. II. & Niedzielski, A. S. Evidence for multiple AMPA receptor complexes in hippocampal CA1/CA2 neurons. *J Neurosci* **16,** 1982–1989 (1996).
6. Lee, H. K., Barbarosie, M., Kameyama, K., Bear, M. F. & Huganir, R. L. Regulation of distinct AMPA receptor phosphorylation sites during bidirectional synaptic plasticity. *Nature* **405,** 955–959, doi: 10.1038/35016089 (2000).
7. Lee, H. K. *et al.* Phosphorylation of the AMPA receptor GluR1 subunit is required for synaptic plasticity and retention of spatial memory. *Cell* **112,** 631–643 (2003).
8. Gordon, G. R. *et al.* Norepinephrine triggers release of glial ATP to increase postsynaptic efficacy. *Nat Neurosci* **8,** 1078–1086, doi: 10.1038/nn1498 (2005).
9. Gordon, G. R. *et al.* Astrocyte-mediated distributed plasticity at hypothalamic glutamate synapses. *Neuron* **64,** 391–403, doi: 10.1016/j.neuron.2009.10.021 (2009).
10. Pougnet, J. T. *et al.* ATP P2X receptors downregulate AMPA receptor trafficking and postsynaptic efficacy in hippocampal neurons. *Neuron* **83,** 417–430, doi: 10.1016/j.neuron.2014.06.005 (2014).
11. Lalo, U. *et al.* Exocytosis of ATP from astrocytes modulates phasic and tonic inhibition in the neocortex. *PLoS biology* **12,** e1001747, doi: 10.1371/journal.pbio.1001747 (2014).
12. Khakh, B. S. & North, R. A. Neuromodulation by extracellular ATP and P2X receptors in the CNS. *Neuron* **76,** 51–69, doi: 10.1016/j.neuron.2012.09.024 (2012).
13. Pascual, O. *et al.* Astrocytic purinergic signaling coordinates synaptic networks. *Science* **310,** 113–116, doi: 10.1126/science.1116916 (2005).
14. Vavra, V., Bhattacharya, A. & Zemkova, H. Facilitation of glutamate and GABA release by P2X receptor activation in supraoptic neurons from freshly isolated rat brain slices. *Neuroscience* **188,** 1–12, doi: 10.1016/j.neuroscience.2011.04.067 (2011).
15. Rubio, M. E. & Soto, F. Distinct Localization of P2X receptors at excitatory postsynaptic specializations. *J Neurosci* **21,** 641–653 (2001).
16. Lee, H. K., Kameyama, K., Huganir, R. L. & Bear, M. F. NMDA induces long-term synaptic depression and dephosphorylation of the GluR1 subunit of AMPA receptors in hippocampus. *Neuron* **21,** 1151–1162 (1998).
17. Kameyama, K., Lee, H. K., Bear, M. F. & Huganir, R. L. Involvement of a postsynaptic protein kinase A substrate in the expression of homosynaptic long-term depression. *Neuron* **21,** 1163–1175 (1998).
18. Lu, W., Isozaki, K., Roche, K. W. & Nicoll, R. A. Synaptic targeting of AMPA receptors is regulated by a CaMKII site in the first intracellular loop of GluA1. *Proc Natl Acad Sci USA* **107,** 22266–22271, doi: 10.1073/pnas.1016289107 (2010).
19. Coultrap, S. J. *et al.* Autonomous CaMKII mediates both LTP and LTD using a mechanism for differential substrate site selection. *Cell reports* **6,** 431–437, doi: 10.1016/j.celrep.2014.01.005 (2014).
20. Nair, D. *et al.* Super-resolution imaging reveals that AMPA receptors inside synapses are dynamically organized in nanodomains regulated by PSD95. *J Neurosci* **33,** 13204–13224, doi: 10.1523/JNEUROSCI.2381-12.2013 (2013).
21. Beattie, E. C. *et al.* Regulation of AMPA receptor endocytosis by a signaling mechanism shared with LTD. *Nat Neurosci* **3,** 1291–1300, doi: 10.1038/81823 (2000).
22. Collingridge, G. L., Peineau, S., Howland, J. G. & Wang, Y. T. Long-term depression in the CNS. *Nat Rev Neurosci* **11,** 459–473, doi: 10.1038/nrn2867 (2010).
23. Lu, W. *et al.* Subunit composition of synaptic AMPA receptors revealed by a single-cell genetic approach. *Neuron* **62,** 254–268, doi: 10.1016/j.neuron.2009.02.027 (2009).
24. Choquet, D. & Triller, A. The role of receptor diffusion in the organization of the postsynaptic membrane. *Nat Rev Neurosci* **4,** 251–265 (2003).
25. Meng, Y., Zhang, Y. & Jia, Z. Synaptic transmission and plasticity in the absence of AMPA glutamate receptor GluR2 and GluR3. *Neuron* **39,** 163–176 (2003).
26. Lee, H. K., Takamiya, K., He, K., Song, L. & Huganir, R. L. Specific roles of AMPA receptor subunit GluR1 (GluA1) phosphorylation sites in regulating synaptic plasticity in the CA1 region of hippocampus. *J Neurophysiol* **103,** 479–489, doi: 10.1152/jn.00835.2009 (2010).
27. Biou, V., Bhattacharyya, S. & Malenka, R. C. Endocytosis and recycling of AMPA receptors lacking GluR2/3. *Proc Natl Acad Sci USA* **105,** 1038–1043, doi: 10.1073/pnas.0711412105 (2008).
28. Esteban, J. A. AMPA receptor trafficking: a road map for synaptic plasticity. *Molecular interventions* **3,** 375–385, doi: 10.1124/mi.3.7.375 (2003).
29. Ehlers, M. D. Reinsertion or degradation of AMPA receptors determined by activity-dependent endocytic sorting. *Neuron* **28,** 511–525 (2000).

30. Santos, S. D., Carvalho, A. L., Caldeira, M. V. & Duarte, C. B. Regulation of AMPA receptors and synaptic plasticity. *Neuroscience* **158,** 105–125, doi: 10.1016/j.neuroscience.2008.02.037 (2009).
31. Shi, S., Hayashi, Y., Esteban, J. A. & Malinow, R. Subunit-specific rules governing AMPA receptor trafficking to synapses in hippocampal pyramidal neurons. *Cell* **105,** 331–343 (2001).
32. Lin, D. T. *et al.* Regulation of AMPA receptor extrasynaptic insertion by 4.1N, phosphorylation and palmitoylation. *Nat Neurosci* **12,** 879–887, doi: 10.1038/nn.2351 (2009).
33. Hosokawa, T., Mitsushima, D., Kaneko, R. & Hayashi, Y. Stoichiometry and phosphoisotypes of hippocampal AMPA-type glutamate receptor phosphorylation. *Neuron* **85,** 60–67, doi: 10.1016/j.neuron.2014.11.026 (2015).
34. Jo, Y. H. *et al.* Cross-talk between P2X4 and gamma-aminobutyric acid, type A receptors determines synaptic efficacy at a central synapse. *The Journal of biological chemistry* **286,** 19993–20004, doi: 10.1074/jbc.M111.231324 (2011).
35. Toulme, E., Soto, F., Garret, M. & Boue-Grabot, E. Functional properties of internalization-deficient P2X4 receptors reveal a novel mechanism of ligand-gated channel facilitation by ivermectin. *Mol Pharmacol* **69,** 576–587 (2006).
36. Carta, M. *et al.* CaMKII-dependent phosphorylation of GluK5 mediates plasticity of kainate receptors. *The EMBO journal* **32,** 496–510, doi: 10.1038/emboj.2012.334 (2013).

Acknowledgements

We are grateful to Dr. Katherine Roche at the NINDS, NIH (Bethesda) for providing us with anti-phosphoSerine567 antibodies. Microscopy experiments were done at the Bordeaux Imaging Center, a service unit of the CNRS-INSERM and Bordeaux University, member of the national infrastructure France BioImaging. We thank E. Verdier, N. Retailleau and C. Breillat for their technical help. We also thank E. Normand, F. Roguet and A. Le Bris and for help with animal facility. This work was supported by the CNRS, University of Bordeaux and grants from the Conseil Regional Aquitaine and Labex BRAIN ANR-10-LABX-43. The Bordeaux Imaging Center is funded by ANR-10-INSB-04.

Author Contributions

All authors contributed to the interpretation of experiments and commented on the manuscript. J.-T.P., A.M. and E.B.-G. performed molecular biology, electrophysiology and biochemical experiments and data analysis. B.C., D.C. and E.H. performed and analyzed dSTORM experiments. E.B.-G. conceived the study and wrote the manuscript.

Additional Information

Supplementary information accompanies this paper at http://www.nature.com/srep

Competing financial interests: The authors declare no competing financial interests.

How to cite this article: Pougnet, J.-T. *et al.* P2X-mediated AMPA receptor internalization and synaptic depression is controlled by two CaMKII phosphorylation sites on GluA1 in hippocampal neurons. *Sci. Rep.* **6**, 31836; doi: 10.1038/srep31836 (2016).